

Photodynamic Therapy in Head and Neck carcinomas: Clinical and *in vitro* studies

By

Abubakr A. Sharwani
BDS, MMedSci

UCL Eastman Dental Institute
Department of Oral and Maxillofacial Surgery
University College London

2006

Thesis submitted in fulfilment of the
requirements for the degree of PhD in the
University of London

UMI Number: U592372

All rights reserved

INFORMATION TO ALL USERS

The quality of this reproduction is dependent upon the quality of the copy submitted.

In the unlikely event that the author did not send a complete manuscript and there are missing pages, these will be noted. Also, if material had to be removed, a note will indicate the deletion.



UMI U592372

Published by ProQuest LLC 2014. Copyright in the Dissertation held by the Author.
Microform Edition © ProQuest LLC.

All rights reserved. This work is protected against
unauthorized copying under Title 17, United States Code.



ProQuest LLC
789 East Eisenhower Parkway
P.O. Box 1346
Ann Arbor, MI 48106-1346

Declaration

I declare that all the experiments described in this thesis were carried out by myself except the histopathology diagnosis of the surgical biopsies which were performed by the Histopathology department at University College London Hospital.

To my beloved family

Abstract

Despite the advances in diagnostic and therapeutic techniques, the outcome and survival of patients suffering from head and neck cancer has remained poor, primarily due to late detection, and the tendency of the disease to develop loco-regional metastasis. A key to its control is early detection and treatment and prevention of recurrence and metastasis. Tumour metastases can be considered as complex multi-step molecular events which involve the interplay between several processes including changes in cell survival, adhesion, proteolysis, and angiogenesis. Based on these considerations, a positive correlation between tumour invasiveness and expression/suppression of these processes would be expected. Photodynamic Therapy (PDT) is a novel treatment modality for a variety of malignant tumours, including head and neck cancer. The technique is based on the combination of a photosensitive drug and visible light to disrupt cell function and induce cytotoxicity, but there is little agreement on its efficacy. Furthermore, PDT is indicated for early tumour without metastases, yet it is crucial to determine its influence on the metastasis process.

The aims of the study were:

- (i) to explore, using an *in vitro* model, the influence of PDT, alone or in combination with either chemotherapy or small molecules, on cell toxicity, expression of $\alpha 5\beta 1$ and $\alpha v\beta 6$ integrins and epidermal growth factor receptor (EGFR), production of matrix metalloproteinases, MMP-2, MMP-9 and MMP-13, urokinase plasminogen activator (uPA) and vascular endothelial growth factor (VEGF);
- (ii) to clinically evaluate the potential of PDT as a tool for head and neck cancer treatment;
- (iii) to clinically evaluate the ability of an optical system, based on fluorescence and elastic scattering spectroscopy, to distinguish between normal, potentially malignant and malignant tissues and to develop an applicable algorithm that can be used as a standard for the subsequent analysis of “unknown” lesions;
- (iv) to monitor the sensitiser photobleaching during PDT in patients with superficial basal cell carcinoma (BCC), and compare this to clinical outcome.

It was found that, using a series of human oral squamous cell carcinoma cell lines, a marked decrease of tumour invasion and migration is evident after PDT; this was associated with the downregulation of MMP-9, -2 and -13, uPA and VEGF. Moreover, this migratory inhibition was further enhanced when PDT was combined with either cisplatin chemotherapy or tyrosine kinase inhibitors.

Clinically, a complete response with excellent cosmetic results was achieved on patients treated with PDT. Both fluorescence and elastic scattering spectroscopy have shown a great potential to both non-invasively identify dysplastic changes at an early stage and to be used as a screening tool for the detection of subsequent primary lesions.

This thesis has demonstrated that, PDT and its related optical system together are able to detect, treat and reduce invasion and metastasis of head and neck carcinoma.

Acknowledgements

This thesis is the product of several years of effort, none of which would have been possible without the support and encouragement of many people around me. Firstly, I am profoundly indebted to my advisors, Dr Colin Hopper and Dr Vehid Salih, for providing ideas, enthusiasm, encouraging support and unlimited guidance on all aspects of my work.

This work was carried out at the UCL Eastman Dental Institute and Maxillofacial Unit (UCLH NHS Trust). Financial support, for which I wish to express my gratitude, was provided by the Ministry of Higher Education, Kingdom of Saudi Arabia.

Further thanks go to several staff at the National Medical Laser Centre: Prof S G Bown, Dr Sandy MacRobert, Dr Benjamin Clark, Sandy Mosse and Miss Kathryn Dempsey. At the UCL Eastman Dental Institute and the Maxillofacial Unit (UCLH NHS Trust): Prof Irwin Olsen, Dr Mark Lewis, and Dr. Dave Spratt, all played a part in developing ideas and facilitating new developments.

Extra special thanks go to Dr Simon Williams; Miss Helena Zbroinska was responsible for arranging all PDT and optical biopsy clinical appointments and obtaining the necessary drugs, with endless patience. Other members of staff and fellow students within UCL also deserve my gratitude, namely Hesham Khalil, Paul Darkins, Andrea Sinanan, Paul Burkinson, Linda Jones, Navneet Bhadal and Nadia al-Hazmi.

Last, by no means least, I owe a great debt of appreciation to my parents, wife and sons, for their continual emotional support, love and patience.

Contents

| | |
|----------------------------|----|
| DECLARATION | 2 |
| ABSTRACT | 4 |
| ACKNOWLEDGEMENTS..... | 5 |
| CONTENTS | 6 |
| LIST OF TABLES..... | 12 |
| LIST OF FIGURES | 13 |
| LIST OF ABBREVIATIONS..... | 15 |

CHAPTER 1 INTRODUCTION

| | |
|--|----|
| 1.0 OVERVIEW | 18 |
| 1.1 PHOTODYNAMIC THERAPY | 19 |
| 1.1.1 From photodynamic action to photodynamic therapy | 22 |
| 1.1.2 Photosensitisers..... | 23 |
| 1.1.2.1 Photofrin | 23 |
| 1.1.2.2 Foscan | 23 |
| 1.1.2.3 Aminolevulinic acid..... | 24 |
| 1.1.3 Singlet oxygen and the photophysics of PDT..... | 25 |
| 1.1.4 Fluorescence photobleaching..... | 27 |
| 1.2 OPTICAL SPECTROSCOPY..... | 30 |
| 1.2.1 Raman spectroscopy | 32 |
| 1.2.2 Fluorescence spectroscopy | 33 |
| 1.2.3 Elastic scattering spectroscopy | 35 |
| 1.3 CANCER INVASION AND METASTASIS | 37 |
| 1.3.1 Angiogenesis..... | 38 |
| 1.3.2 Cell adhesion | 38 |
| 1.3.2.1 Cadherin..... | 39 |
| 1.3.2.2 Integrins | 39 |
| 1.3.3 Extracellular matrix | 41 |
| 1.3.3.1 Collagens | 41 |
| 1.3.3.2 Fibronectin..... | 41 |
| 1.3.4 Matrix metalloproteinases | 41 |

| | |
|---|----|
| 1.3.4.1 Structure of MMPs | 42 |
| 1.3.4.2 Regulation of MMP activity | 42 |
| 1.3.4.3 Function of MMPs..... | 43 |
| 1.3.5 The Plasminogen activation system..... | 45 |
| 1.3.6 Growth factor receptors | 45 |
| 1.3.6.1 Epidermal growth factor receptor | 45 |
| 1.3.6.2 Hepatocyte growth factor receptor | 46 |
| 1.4 BACKGROUND TO ORAL CANCER..... | 47 |
| 1.5 METASTATIC PROMOTING FACTORS IN ORAL CARCINOMA | 49 |
| 1.5.1 Expression of MMP-2, MMP-9 and MMP-13 | 49 |
| 1.5.2 Expression of uPA | 50 |
| 1.5.3 Expression of VEGF | 50 |
| 1.5.4 Expression of $\alpha\text{v}\beta\text{6}$ and $\alpha\text{5}\beta\text{1}$ integrins | 51 |
| 1.6 METASTATIC PROMOTING FACTORS FOLLOWING PDT IN ORAL CARCINOMA | 52 |
| 1.6.1 PDT and cell adhesion | 52 |
| 1.6.2 PDT and MMPs | 53 |
| 1.6.3 PDT and VEGF..... | 53 |
| 1.7 PDT IN COMBINATION THERAPIES..... | 54 |
| 1.7.1 PDT and chemotherapy | 54 |
| 1.7.2 PDT and small molecules | 55 |
| 1.8 SUMMARY | 56 |
| 1.9 AIMS | 57 |

CHAPTER 2 MATERIALS AND METHODS

| | |
|--|----|
| 2.1 MATERIALS..... | 58 |
| 2.1.1 Chemical reagents and kits | 58 |
| 2.1.2 Antibodies..... | 59 |
| 2.1.3 Drugs..... | 59 |
| 2.2 CELL CULTURE..... | 60 |
| 2.2.1 Routine cell cultures | 60 |
| 2.2.2 Passage of cells | 61 |
| 2.2.3 Cell freezing..... | 61 |
| 2.2.4 Cell thawing..... | 62 |
| 2.2.5 Cell density and viability | 62 |
| 2.2.6 Cell viability assay | 62 |
| 2.3 PHOTODYNAMIC THERAPY | 63 |
| 2.3.1 Photosensitisation | 63 |

| | |
|--|----|
| 2.3.2 Cell irradiation | 63 |
| 2.4 COMBINATION TREATMENT | 64 |
| 2.4.1 PDT and CDDP cytotoxicity assay..... | 64 |
| 2.4.2 PDT and TKI cytotoxicity assay..... | 65 |
| 2.5 CELL DETACHMENT ASSAY | 65 |
| 2.6 CELL ADHESION ASSAY | 66 |
| 2.7 PROTEIN ASSAY..... | 67 |
| 2.7.1 Preparation of supernatants..... | 67 |
| 2.7.2 Determination of total protein | 67 |
| 2.7.3 Zymography..... | 68 |
| 2.7.4 ELISA | 70 |
| 2.8 MIGRATION ASSAY | 71 |
| 2.9 INVASION ASSAY | 73 |
| 2.10 PHOTOMICROGRAPHY | 74 |
| 2.11 FLOW CYTOMETRY..... | 75 |
| 2.11.1 Preparation of Cells for analysis..... | 75 |
| 2.11.2 Data acquisition and processing | 76 |
| 2.12 DETECTION OF ORAL PREMALIGNANCY..... | 77 |
| 2.12.1 Fluorescence spectroscopy (FS) | 77 |
| 2.12.1.1 Patients..... | 77 |
| 2.12.1.2 The system | 78 |
| 2.12.2 Elastic scattering spectroscopy (ESS) | 82 |
| 2.12.2.2 The system | 82 |
| 2.12.2.3 Measurement procedures | 84 |
| 2.13 MONITORING OF PDT | 86 |
| 2.13.1 Patients..... | 86 |
| 2.13.2 The systems | 86 |
| 2.13.3 Monitoring procedures..... | 87 |
| 2.14 STATISTICAL ANALYSIS..... | 87 |
| 2.14.1 <i>In vitro</i> studies | 87 |
| 2.14.2 <i>In vivo</i> studies | 87 |
| 2.14.2.1 Fluorescence spectroscopy | 87 |
| 2.14.2.2 Elastic scattering spectroscopy | 88 |
| 2.14.2.3 Monitoring of PDT | 89 |

CHAPTER 3 RESULT I

PHOTODYNAMIC EFFICACY OF FOSCAN IN OSCC CELLS

| | |
|--|----|
| 3.1 INTRODUCTION | 90 |
| 3.2 FOSCAN-DARK TOXICITY..... | 91 |
| 3.3 EFFECTS OF LASER LIGHT..... | 91 |
| 3.4 PHOTOTOXICITY OF FOSCAN-PDT | 91 |
| 3.5 CELL LINE DEPENDENCE OF FOSCAN-UP TAKE | 97 |
| 3.6 DISCUSSION | 99 |

CHAPTER 4 RESULTS II

THE EFFECTS OF PHOTODYNAMIC THERAPY ON THE EXPRESSIONS OF INVASION PROMOTING FACTORS IN HEAD AND NECK CARCINOMAS

| | |
|---|-----|
| 4.1 INTRODUCTION | 101 |
| 4.2 PDT DECREASES MIGRATION TOWARDS ECM SUBSTRATES..... | 102 |
| 4.3 PDT DECREASES MATRIGEL INVASION | 104 |
| 4.4 PDT DECREASES CELL DETACHMENT..... | 105 |
| 4.5 PDT MODULATES CELL ATTACHMENT | 106 |
| 4.6 PDT REGULATES MMP-2 AND MMP-9 ACTIVITY | 108 |
| 4.7 PDT MODULATES SECRETION OF MMP-13 | 114 |
| 4.8 PDT DECREASES SECRETION OF VEGF | 115 |
| 4.9 PDT DECREASES SECRETION OF UPA..... | 117 |
| 4.10 PDT REGULATES EXPRESSION OF A5B1 AND AVB6..... | 118 |
| 4.11 PDT REGULATES EGFR..... | 123 |
| 4.12 PDT EFFECTS ON THE EXPRESSION OF HGFR | 126 |
| 4.13 DISCUSSION | 129 |

CHAPTER 5 RESULTS III

CHEMICAL THERAPY: ITS IMPLICATION FOR COMBINATION TREATMENT WITH PHOTODYNAMIC THERAPY

| | |
|--|-----|
| 5.1 INTRODUCTION | 133 |
| 5.2 CDDP AUGMENTS PDT ANTI-TUMOUR ACTIVITY | 134 |
| 5.3 IRESSA AUGMENTS PDT ANTI-TUMOUR ACTIVITY | 137 |

| | |
|--|-----|
| 5.4 PD153035 AUGMENTS PDT ANTI-TUMOUR ACTIVITY..... | 140 |
| 5.5 IRESSA AUGMENTS PDT DOWN-REGULATION EFFECT ON VEGF ACTIVITY..... | 143 |
| 5.6 CELL MORPHOLOGY | 145 |
| 5.7 CDDP REGULATES PDT EFFECT ON CELL MIGRATION | 148 |
| 5.8 CDDP AUGMENTS PDT INVASION INHIBITION..... | 151 |
| 5.9 IRESSA AND PD153035 AUGMENT PDT MIGRATION DOWN-REGULATION..... | 153 |
| 5.10 IRESSA AUGMENTS PDT INVASION DOWN-REGULATION | 156 |
| 5.11 DISCUSSION | 159 |

CHAPTER 6 RESULTS IV

PHOTODYNAMIC DIAGNOSIS OF ORAL TUMOURS

| | |
|---|-----|
| 6.1 INTRODUCTION | 163 |
| 6.2 PATIENTS | 164 |
| 6.3 DISTANCE EFFECT ON FLUORESCENCE RATIO | 166 |
| 6.4 RED FLUORESCENCE OF DYSPLASTIC TISSUE | 167 |
| 6.5 DISCUSSION | 172 |

CHAPTER 7 RESULTS V

THE SCATTERING PROPERTIES OF POTENTIALLY MALIGNANT ORAL LESIONS

| | |
|---|-----|
| 7.1 INTRODUCTION..... | 175 |
| 7.2 PATIENTS..... | 175 |
| 7.3 ELASTIC SPECTROSCOPY DETECTS ORAL PREMALIGNANCY | 177 |
| 7.4 DISCUSSION..... | 180 |

CHAPTER 8 RESULTS VI

MONITORING PHOTODYNAMIC THERAPY BY FLUORESCENCE AND ELASTIC SCATTERING SPECTROSCOPY

| | |
|------------------------|-----|
| 8.1 INTRODUCTION | 183 |
| 8.2 PATIENTS | 184 |
| 8.3 ALA-PDT | 186 |

| | |
|---|-----|
| 8.4 PPIX PHOTOBLEACHING MEASURED BY FS..... | 186 |
| 8.5 PPIX PHOTOBLEACHING MEASURED BY ESS | 188 |
| 8.6 DISCUSSION | 191 |

CHAPTER 9 GENERAL DISCUSSION

| | |
|---------------------------------------|-----|
| 9.1 THE <i>IN VITRO</i> STUDIES | 196 |
| 9.2 CLINICAL STUDIES | 199 |
| 9.3 CONCLUSIONS..... | 201 |
| 9.4 FUTURE WORK | 202 |

APPENDIX 1

| | |
|--------------------------|-----|
| MEDIA AND SOLUTIONS..... | 204 |
|--------------------------|-----|

APPENDIX 2

| | |
|---------------------------------|-----|
| DATA FROM RESULTS CHAPTERS..... | 207 |
|---------------------------------|-----|

| | |
|-------------------------|------------|
| REFERENCES | 209 |
|-------------------------|------------|

| | |
|-----------------------------------|------------|
| LIST OF PUBLICATIONS | 232 |
|-----------------------------------|------------|

List of Tables

| | | |
|------------------|---|-----|
| Table 1.1 | List of some ligands of different α - and β -subunits for integrin family. . | 40 |
| Table 1.2 | A list of some tumour associated MMPs and their substrates | 43 |
| Table 2.1 | Clinical features of cell lines..... | 61 |
| Table 3.1 | Approximate sublethal doses of Foscan-PDT..... | 92 |
| Table 6.1 | Number and percentage of surgical biopsies | 165 |
| Table 6.2 | Type and percentage of surgical biopsies with different histology | 165 |
| Table 6.3 | p - values (t -Test) of correlation of red-to-green ratio | 169 |
| Table 6.4 | Classification of oral tissue red-to-green fluorescence ratios | 171 |
| Table 7.1 | The classification of oral tissues in the dataset..... | 176 |
| Table 7.2 | The classification of histological grades in the dataset..... | 176 |
| Table 7.3 | Classification of oral tissue spectra..... | 179 |
| Table 8.1 | Clinical responses to PDT..... | 191 |
| Table 8.2 | PpIX fluorescence as a function of time | 186 |

List of Figures

| | | |
|--------------------|--|-----|
| Figure 1.1 | Clinical pictures showing the cosmetic result following PDT | 21 |
| Figure 1.2 | Representative diagram of haem biosynthetic pathway, | 25 |
| Figure 1.3 | Principles of photodynamic therapy..... | 26 |
| Figure 1.4 | A schematic diagram of the cell death pathways following PDT | 29 |
| Figure 1.5 | Diagrammatic representation of the visible spectrum..... | 32 |
| Figure 1.6 | Optical biopsy using fluorescence spectroscopy..... | 34 |
| Figure 1.7 | Schematic illustration of elastic scattering in human tissue..... | 36 |
| Figure 1.8 | A simplified schematic illustration of tumour cell invasion. | 37 |
| Figure 1.9 | Activation cascade of MMPs.. | 43 |
| Figure 2.1 | Representative picture of gelatin zymography | 69 |
| Figure 2.2 | Schematic illustration of cell migration assay..... | 72 |
| Figure 2.3 | Schematic illustration of cell invasion assay..... | 73 |
| Figure 2.4 | Schematic diagram of the fluorescent ratio imaging apparatus. | 79 |
| Figure 2.5 | Black and white tissue fluorescence image..... | 81 |
| Figure 2.6 | Example of magnified pixel colour fluorescent intensity values. | 81 |
| Figure 2.7 | Schematic illustration of the elastic scattering spectroscopy system. | 83 |
| Figure 2.8 | Schematic diagram of the fibre optic probe | 84 |
| Figure 3.1 | Phototoxicity on KB cells..... | 93 |
| Figure 3.2 | Phototoxicity on UP cells. | 94 |
| Figure 3.3 | Phototoxicity on VB6 cells..... | 95 |
| Figure 3.4 | Phototoxicity on H376 cells | 96 |
| Figure 3.5 | Flow cytometer analysis of Foscan uptake..... | 98 |
| Figure 3.6 | Mean fluorescence of cells shown in Figure 3.5. | 98 |
| Figure 4.1 | Effect of PDT on the migration of UP, VB6 and H376 cells..... | 103 |
| Figure 4.2 | Effect of PDT on the invasion of UP, VB6 and H376 cells..... | 104 |
| Figure 4.3 | Detachment assay of UP, VB6 and H376 cells. | 105 |
| Figure 4.4 | Adhesion assay of UP, VB6 and H376 cells..... | 107 |
| Figure 4.5 | Zymogrm of PDT effect on MMP-2 and -9 expression by UP cells..... | 110 |
| Figure 4.6 | Densitometric analysis of zymogram shown in Figure 4.6.. | 110 |
| Figure 4.7 | Zymogrm of PDT effect on MMP-2 -9 expression by VB6 cells..... | 111 |
| Figure 4.8 | Densitometric analysis of zymogram shown in Figure 4.8..... | 111 |
| Figure 4.9 | Zymogrm of PDT effect on MMP-2 and -9 by H376 cells..... | 112 |
| Figure 4.10 | Densitometric analysis of zymogram shown in Figure 4.10.. | 112 |
| Figure 4.11 | ELISA for MMP-2 (A) and MMP-9 (B). | 113 |
| Figure 4.12 | ELISA for MMP-13.. | 114 |
| Figure 4.13 | ELISA for VEGF..... | 116 |
| Figure 4.14 | Chromogenic assays for uPA. | 117 |
| Figure 4.15 | Histograms analysis of $\alpha 5\beta 1$ by UP, VB6, and H376 cells..... | 119 |
| Figure 4.16 | Mean fluorescence values of $\alpha 5\beta 1$ shown in Figure 4.16.. | 120 |
| Figure 4.17 | Histograms analysis of $\alpha v\beta 6$ by UP, VB6, and H376 cells..... | 121 |
| Figure 4.18 | Mean fluorescence values of $\alpha v\beta 6$ shown in Figure 4.18..... | 122 |

| | | |
|--------------------|--|-----|
| Figure 4.19 | Histogram of EGFR expressions by UP, VB6 and H376 cells. | 124 |
| Figure 4.20 | Mean fluorescence values of EGFR shown in Figure 4.20. | 125 |
| Figure 4.21 | Histogram of expression of HGFR by UP, VB6 and H376 cells. ... | 127 |
| Figure 4.22 | Mean fluorescence values of HGFR shown in Figure 4.22. | 128 |
| Figure 5.1 | Toxicity of CDDP on UP, VB6 and H376 cells. | 135 |
| Figure 5.2 | Toxicity of PDT combined with CDDP on UP, VB6 and H376 cells.. | 136 |
| Figure 5.3 | Toxicity of Iressa on UP, VB6 and H376 cells. | 138 |
| Figure 5.4 | Toxicity of Iressa combined with PDT on UP cells. | 139 |
| Figure 5.5 | Toxicity of PD153035 on UP, VB6 and H376 cells. | 141 |
| Figure 5.6 | Toxicity of PD153035 and PDT on UP (A), VB6 (B) and H376 cells. | 142 |
| Figure 5.7 | ELISA assay of VEGF activity on UP, VB6 and H376 cells. | 144 |
| Figure 5.8 | Morphology and adhesion of UP cells. | 146 |
| Figure 5.9 | Morphology and adhesion of VB6 cells. | 147 |
| Figure 5.10 | Effect of PDT and CDDP on migration towards fibronectin. | 149 |
| Figure 5.11 | Effect of PDT and CDDP on the migration towards collagen type-I. | 150 |
| Figure 5.12 | Effect of PDT and CDDP on the invasion. | 152 |
| Figure 5.13 | Effect of PDT and Iressa on the migration towards fibronectin. | 154 |
| Figure 5.14 | Effect of PDT and PD153035 on the migration towards fibronectin. | 155 |
| Figure 5.15 | Effect of PDT and Iressa on the invasion of cells. | 157 |
| Figure 5.16 | Effect of PDT and PD 153035 on the invasion of the cells. | 158 |
| Figure 6.1 | The distance dependence of the red-to-green ratio signals | 166 |
| Figure 6.2 | Fluorescence intensity versus histopathological stages of oral lesions | 168 |
| Figure 6.3 | Red to green ratio versus histopathological stages of oral lesions | 169 |
| Figure 7.1 | A representative plot of the mean dysplastic and benign spectra. | 178 |
| Figure 7.2 | A ROC Curve of sensitivity and specificity | 178 |
| Figure 8.1 | PpIX photobleaching and reappearance during PDT. | 187 |
| Figure 8.2 | PpIX photobleaching and reappearance during PDT | 187 |
| Figure 8.3 | Acquired spectra as function of time during PDT. | 189 |
| Figure 8.4 | Box-plot analysis of results of the fitted spectra | 190 |

List of Abbreviations

| | |
|----------------------------------|---|
| °C | Degrees Celsius |
| ¹O₂ | Singlet Oxygen species |
| Ab | Antibody |
| AFM | Additive free medium |
| AK | Actinic keratosis |
| ALA | Aminolevulinic acid |
| ANOVA | Analysis of variance |
| APS | Ammonium persulphate |
| BCC | Basal cell carcinoma |
| BSA | Bovine serum albumin |
| CCD | Charged coupled device |
| CDDP | cisplatin, cis-dichlorodiammineplatinum (II) |
| CO₂ | Carbon dioxide |
| DAPI | 4',6-Diamidino-2-phenylindole |
| dH₂O | Distilled water |
| DMEM | Dulbecco's Modified Eagles Medium |
| DMSO | Dimethyl sulfoxide |
| DPX | distyrene, tricresyl phosphate and xylene, medium |
| ECM | Extracellular matrix |
| EDTA | Ethylenediaminetetraacetic acid |
| EGF | Epidermal growth factor |
| EGFR | Epidermal growth factor receptor |
| ELISA | Enzyme linked immunosorbent assay |
| ESS | Elastic scattering spectroscopy |
| FACS | Fluorescence associated cell sorting |
| FAK | Focal adhesion kinase |
| FCM | Flow cytometry |
| FCS | Fetal calf serum |
| FD | Fluorescence diagnosis |
| FI | Fluorescence imaging |
| FITC | Fluorescein isothiocyanate |
| FL1-H | Fluorescence seen through a green filter |
| FL3-H | Fluorescence seen through a red filter |
| FS | Fluorescence spectroscopy |
| FSC | Forward scatter |
| GMF | Geometric mean fluorescence |
| h | Hour, time |

| | |
|-------------------|--|
| HGF | Hepatocyte growth factor |
| HGFR | Hepatocyte growth factor receptor |
| HNSCCs | Head and neck squamous cell carcinomas |
| HPD | Hematoporphyrin derivatives |
| HRP | Horseradish peroxidase |
| ICAM | Intercellular adhesion molecule |
| Ig | Immunoglobulin |
| Iressa | Gefitinib; ZD1839 |
| kDa | Kilodaltons, weight |
| KGM | Keratinocyte growth medium |
| MEM | Minimum essential medium |
| min | Minute, time |
| ul | Microliter, volume |
| ml | Millilitre, volume |
| mm | Millimetre, length |
| MMP | Matrix metalloproteinase |
| mRNA | Messenger RNA |
| m-THPC | meta-tetrahydroxyphenylchlorin |
| ng | Nanogram, weight |
| OSCC | Oral squamous cell carcinoma |
| PA | Plasminogen activator |
| PAI | Plasminogen activator inhibitor |
| PBS | Phosphate buffered saline |
| PDD | Photodynamic diagnosis |
| PDT | Photodynamic therapy |
| PI3-kinase | Phosphatidylinositol-3-OH kinase |
| PpIX | Protoporphyrin IX |
| RGB | Red/Green/Blue |
| RNA | Ribonucleic acid |
| rpm | Revolutions per minute, speed |
| RTK | Receptor tyrosine kinase |
| s | second, time |
| SCC | Squamous cell carcinoma |
| SD | Standard deviation of the mean |
| SDS | Sodium dodecylsulphate |
| SDS-PAGE | SDS-Polyacrylamide gel electrophoresis |
| SFM | Serum free medium |
| SSC | Side scatter |
| TBS | Tris buffered saline |
| TEMED | N,N,N',N'-Tetramethylethylenediamine |

| | |
|-------------|--|
| TIMP | Tissue inhibitor of matrix metalloproteinase |
| TKI | Tyrosine kinase inhibitor |
| tPA | Tissue-type plasminogen activator |
| uPA | Urokinase-type plasminogen activator |
| V | Voltage, power |
| VCAM | Vascular cell adhesion molecule |
| VEGF | Vascular endothelial growth factor |

Chapter 1

Introduction

1.0 Overview

Head and neck cancers are a worldwide problem with different histopathologies, clinical behaviour and response to treatment (Forastiere et al., 2001). In the European Union, there are approximately 85, 000 new cases of head and neck cancer reported every year, and, in the UK alone, around 10.2 per 100,000 males and 5.4 per 100,000 females respectively, are diagnosed every year (Ferley et al., 2000). Globally, there were estimated to be over 500,000 cases of head and neck cancer in 2000. In the US, 40,000 new cases were diagnosed, with approximately 12,500 deaths (Greenlee et al., 2001). Over 90% of the head and neck cancers reported were of a particular type, i.e. squamous cell carcinomas (Vokes et al., 1993). The high infiltrative potential of head and neck tumours, regardless of any prognostic parameters, may result in an early recurrence or regional metastases, with subsequent functional disturbance and aesthetic morbidity (Gath and Brakenhoff, 1999). A key to all forms of cancer control is early detection, treatment and prevention of recurrence and metastasis. Optical techniques offer many advantages in cancer detection and treatment at an early stage.

This thesis is based on both clinical and laboratory-based studies. They are linked by a common goal: to control the cancer by using light based techniques, namely Photodynamic Therapy (PDT) for treatment, and fluorescence and elastic spectroscopy for early diagnosis; two modalities of what is often termed '*optical biopsy*'.

This chapter will present a brief overview of the current state of PDT and related spectroscopy and give a general introduction to each of the areas of investigation to be addressed in the thesis.

1.1 Photodynamic therapy

In efforts to treat cancer, one can make use of a whole armamentarium of therapeutic means. It is in this context that the newly developed treatment known as photodynamic therapy (PDT) appears to offer some hope. PDT has been approved for clinical treatment for various oncologic and non-oncologic indications, including the management of patients with head and neck cancer. PDT can be a selective and curative therapy, with many potential advantages over the available alternative therapies. PDT can be repeated many times with minimal resistance and can be used in combination with other treatment modalities without contraindications. The exposure of adjacent normal tissues to laser light is harmless, with few deleterious consequences. A single treatment can eradicate the disease and also have an excellent cosmetic result (see Figure 1.1), which makes it a viable option for the treatment of skin cancers and other soft tissue tumours. The technique of PDT is based on the use of a light-sensitive dye (photosensitiser) that accumulates in neoplasms and does not affect other tissues and organs. A measured dose of light (mostly from lasers), with a wavelength selected for each photosensitiser in the presence of an adequate concentration of molecular oxygen, activates *in situ* the photosensitiser agent and generates a photochemical reaction. An active molecular species, most probably a singlet oxygen species ($^1\text{O}_2$), is formed during this reaction, which disrupts the cell function and induces cytotoxicity (Dougherty, 2002).

Among numerous types of light sources, lasers are the most convenient and controllable. The laser light is coherent and monochromatic, and can also be directed along fibre optic cables, which allow light to be introduced into hollow organs and deep-seated tumours. Other non-coherent sources include Light Emitting Diodes (LEDs) and xenon lamps and have mostly been developed for dermatological

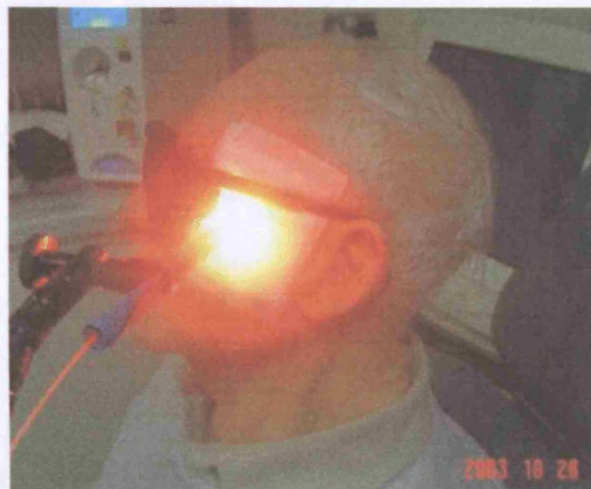
applications. Diode lasers are cost effective, with a light weight that is far less than metal vapour or tuned-dye lasers, and have become alternative light sources. Diode lasers emit light between 660 and 700 nm, and now others of wavelength, 780 -850 nm are available (Brancaleon and Moseley, 2002).

The selective uptake by the hyperproliferating tissues of most photosensitive drugs, together with their intrinsic fluorescence, has expanded their use as minimally invasive tools in the fluorescent detection of cancers, pre-cancers and non-cancerous dysplasias. This procedure is called Fluorescence Diagnosis (FD), Fluorescence Spectroscopy (FS) or Photodynamic Diagnosis (PDD). The term 'PDD' was introduced to indicate its relation to PDT.

Before PDT



During PDT



After PDT



Figure 1.1 Clinical pictures showing the cosmetic result of a lesion of the left temple following PDT (6 months after treatment).

1.1.1 from photodynamic action to photodynamic therapy

The use of photodynamic action or photosensitisation by light has been explored for many years. The civilisations of China, India, Egypt and Greece placed great emphasis on exposure to the sun to cure several diseases and restore health. The earliest photodynamic investigation dated to the late nineteenth century, when Oscar Raab and von Tappeiner (1900) were investigating the toxicity of acridine orange dye in cultures and observed a great increase in acridine killing rate when combined with light. Five years later, von Tappeiner recognised the importance of oxygen in this process, by applying eosin and light for the treatment of basal cell carcinoma (Ackroyd et al., 2001). Then the expression “photodynamic” was coined for this “light effective” phenomenon, and this marked the beginning of PDT (Bonnett, 1999).

Despite the early investigations using PDT, the field was largely neglected until 1960, when investigators at the Mayo Clinic (Boston; USA) found that the injection of hematoporphyrin caused the preferential fluorescence of tumours. This observation stimulated the development of photosensitisers with improved specificity toward tumour cells. Among these was the porphyrin mixture known as hematoporphyrin derivatives (HpD). HpD then underwent some refinement and purification to produce the commercially known sensitiser Photofrin. The first clinical report on the use of HpD in the treatment of cancer appeared in 1976, when Kelly and Snell published results of their trials of early bladder cancer treatment (Kelly and Snell, 1976). Over a 20 year period, several studies into the treatment of cancer were conducted at different centres. The first report on the dermatological application of PDT with 5-aminolevulinic acid (5-ALA) was published in 1990 (Kennedy et al., 1990). Since 1994, various photosensitisers have been developed for clinical use as reviewed in (Detty et al., 2004) or references contained therein.

1.1.2 Photosensitisers

1.1.2.1 Photofrin

Hematoporphyrin derivatives (HpD) are the most frequently clinically used photosensitisers with successful outcomes (Biel, 1998; Allison et al., 2001). Photofrin (profimer sodium) was the first photosensitiser used for a variety of clinical trials (Dougherty, 1996), but the lack of therapeutic selectivity, limited depth effect: (0.5cm), weak absorbance in the red region of the spectrum, where light can penetrate most efficiently into tissues, and prolonged skin sensitivity, which keeps the patient out of daylight for more than 6 weeks after PDT (Gomer et al., 1984; Braichotte et al., 1995), have forced researchers to develop new and improved drugs.

1.1.2.2 Foscan

The second generation meta-tetrahydroxyphenylchlorin (m-THPC; temoporfin, Foscan, Biolitec Pharma, Scotland, U.K.) is a reduced porphyrin of the synthetic chlorins, and is perhaps the most potent second-generation photosensitiser available for use in clinical oncology. Foscan has received approval in Europe for use against head and neck cancer and other cancerous conditions. Foscan has a strong absorption peak in the red part of the spectrum (absorption coefficient 22 400 M/cm at 652 nm) (www.biolitecpharma.com). In animal studies, no significant correlation between tumour Foscan levels and PDT response has been found, which suggests that Foscan-PDT effects are most likely to be associated with vascular damage (Cramers et al., 2003). Many trials work with some degree of success to improve drug selectivity by conjugating Foscan to other structures, such as poly (ethylene glycol) conjugates eg. PEG-mTHPC (Krueger et al., 2003). Foscan is currently being evaluated in phase III clinical trials for a wide variety of cutaneous lesions, including head and neck tumours (Dilkes et al., 2003; Copper et al., 2003).

The major side effect of Foscan is skin photosensitivity, and this can last up to 4 weeks post treatment. The drug now is used in multicentre trials for the treatment of

early or recurrent cancer and the palliative control of resistant oral tumours. All of the released results have shown promising tumour response rates (Hopper et al., 2004a; Kubler et al., 2001). A clinical study on 128 patients with advanced squamous cell carcinoma who were treated with Foscan-PDT demonstrated that 43% of all patients achieved 100% tumour mass reduction, while 53% experienced a significant quality of life benefit (D'Cruz et al., 2004).

1.1.2.3 Aminolevulinic acid

Aminolevulinic Acid (ALA) is another photosensitiser that shows promise in the treatment and detection of early and advanced malignant lesions, including head and neck cancer tumours. ALA is an endogenous precursor of the biosynthetic pathway of haem. Following exogenous administration, ALA is transformed enzymatically by ferrochelatase into fluorescing protoporphyrin IX (PpIX). A simplified scheme of this biosynthetic pathway is shown in Figure 1.2. The administration of exogenous ALA can overload the haem biosynthesis pathway and the normal feedback control mechanism is then bypassed, leading to the transient accumulation of PpIX to levels more than those normally present in the body.

Since the first successful clinical application of ALA, various publications have subsequently demonstrated that the accumulation of PpIX is increased in tumours relative to the surrounding normal tissues and it has been suggested that this is due to the increased permeability of tumorous vasculature and the reduced ferrochelatase concentrations in tumour tissue (el-Sharabasy, 1992; Rittenhouse-Diakun et al., 1995; Ackermann et al., 1998; Detty et al., 2004). ALA-PDT has received approval in Europe for the treatment of superficial cutaneous lesions (www.photocure.com) such as actinic keratosis (AK) and basal cell carcinoma (BCC), with a high complete response rate (Dolmans et al., 2003).

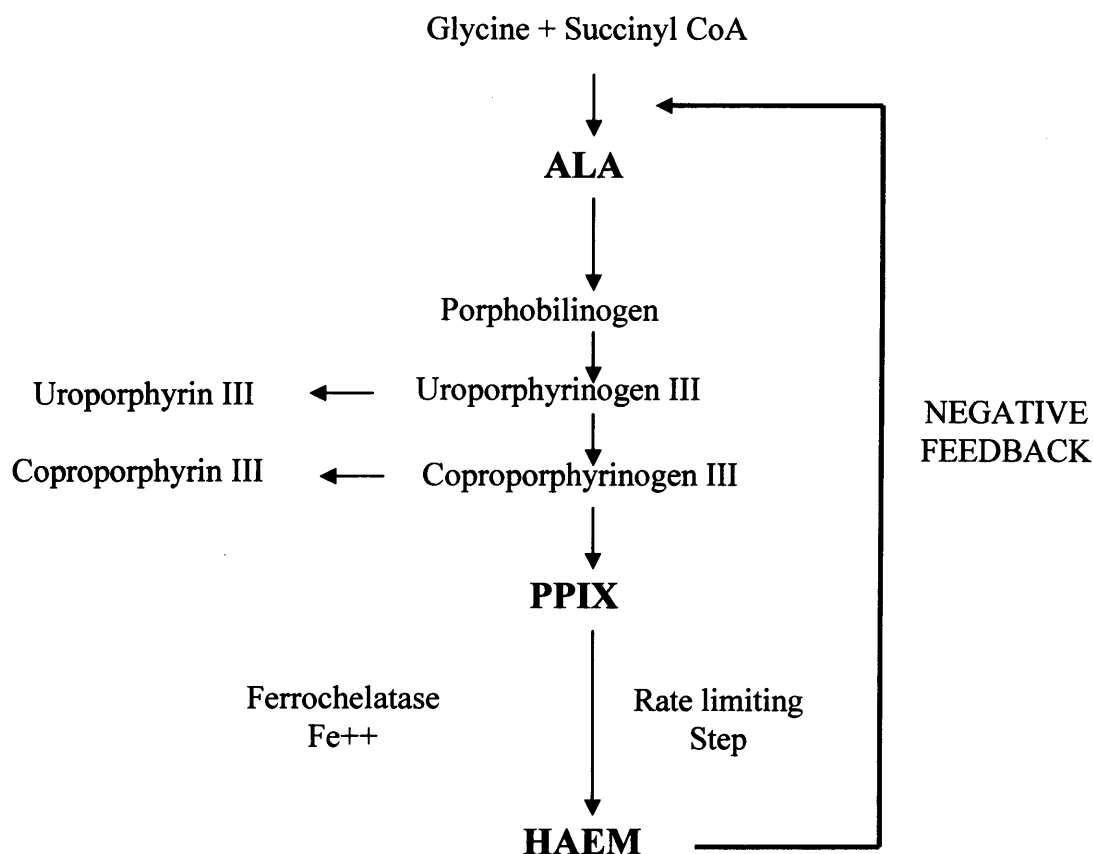


Figure 1.2 Representative diagram of haem biosynthetic pathway, adapted from (Peng et al., 1997)

1.1.3 Singlet oxygen and the photophysics of PDT

The destruction mechanism of malignant tissue following PDT mostly takes place through two reactions, type I and II. This photooxidation process requires photosensitiser drugs, a light source, and oxygen. Each photosensitiser absorbs light with specific wavelengths to produce an excited electronic state (Figure 1.3).

After the successful absorption of the light photons by the photosensitiser, chemical reactions are initiated and proceed when the photosensitiser electrons are elevated from a ground low energy state to an excited high energy singlet state. This state is short lived and can subsequently dissipate directly to a ground state with the release

of fluorescence, but without photodynamic action. This phenomenon forms the basis of light-induced fluorescence, a method used to detect cancer at an early stage with the help of an imaging device. Other relatively long-lived states are formed when the photosensitiser is further excited to a first triplet state (T_1), where electrons can be lost and radical cations (RC) are formed. These radicals can either react with the adjacent cellular membranes or endogenous alcohols (type I photoreaction) or transfer their energy to molecular, triplet-state oxygen, producing singlet-state oxygen (1O_2) (type II photoreaction) and returning the sensitiser back to the ground state, where it can absorb another photon (Dougherty et al., 1998). This 1O_2 is highly cytotoxic to all cells hosting the photosensitiser, including normal cells. The short lifetime ($<0.04 \mu s$) and short radius of action ($<0.02 \mu m$) of 1O_2 can result in limiting the action to the irradiated tissue loaded with sufficient concentration of photosensitiser and oxygen. In addition, the relative preferential uptake of the photosensitiser in cancerous tissue also provides the basis for selective cancer treatment (Moan and Berg, 1991; Niedere et al., 2003).

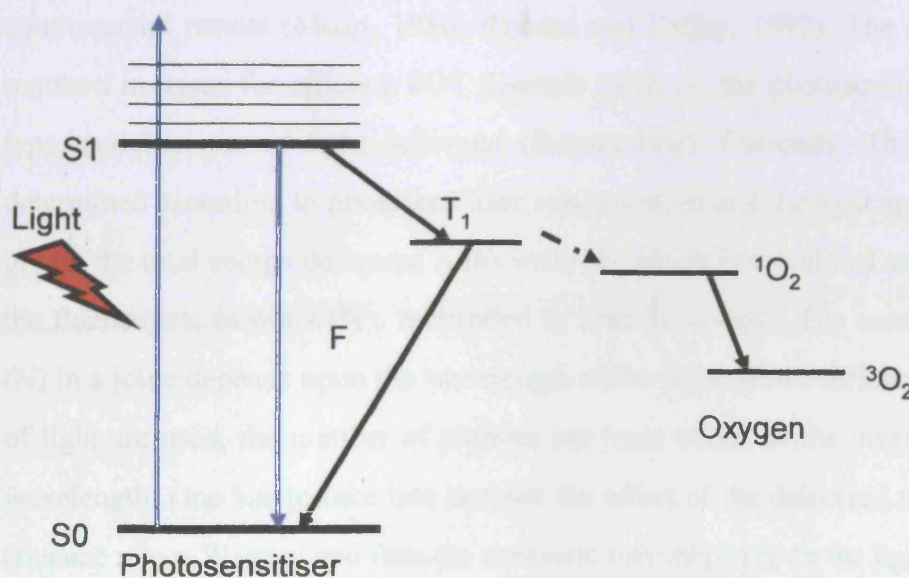


Figure 1.3 Principles of photodynamic therapy. S0: ground state, S1 excited singlet state, F: fluorescence emission, T1: excited triplet state of the photosensitiser, 1O_2 singlet state, 3O_2 triplet state

1.1.4 Fluorescence photobleaching

Photobleaching occurs when the transient species reacts with the photosensitiser, resulting in the production of photoproducts that deplete the concentration of photosensitiser during treatment and consequently reduce the PDT efficiency. This photoproduct has different characteristics from the photosensitiser (Georgakoudi and Foster, 1998). Generally, photobleaching is measured as the decrease in fluorescence over time, since the concentration of photosensitiser and fluorescence intensity are proportional (Mang et al., 1987). Once the photosensitiser has been used up, any further irradiation has no extra effect. This seems to prevent overdosage (Taber et al., 1998). The monitoring of the sensitiser photobleaching via fluorescence measurement can, therefore, provide a means of real time dosimetry in order to solve some of the problems encountered by clinicians due to insufficient PDT dose (Wilson et al., 1997).

Researchers have attempted to measure photobleaching fluorescence *in vivo* with controversial results (Moan, 1986; Rhodes and Diffey, 1997). The amount of $^1\text{O}_2$ required in tissue for efficient PDT depends partly on the photosensitiser, the tissue type, and the rate of light delivered (fluence rate). Currently, The PDT dose is determined according to photosensitiser concentration and the light applied. The unit giving the total energy delivered is the joule (J), which is calculated as the product of the fluence rate in watts (W), multiplied by time in seconds. The number of photons (N) in a joule depends upon the wavelength of the light. If two different wavelengths of light are used, the number of photons per joule varies as the inverse ratio of the wavelength. One has to take into account the effect of the delivered rate of the light (fluence rate = W/area) and thus the treatment time depends on the light source used. If the light is delivered at a high rate, significant heating of the molecule and its surrounding area may take place.

Many researchers have evaluated what is termed the “*on-and-off*” protocol, which is based on the concept that the re-oxygenation of the areas where the oxygen was

depleted by photochemistry is probably the most important effect (Messmann et al., 1997; Babilas et al., 2003). *In vivo*, re-oxygenation is partly due to the diffusion of oxygen from the capillaries and partly to the relaxation of the vasculature that has been subject to vasoconstriction (Pogue et al., 2002). In a normal rat colon sensitised with ALA-induced PpIX, the introduction of a break of approximately 150 s was found to increase markedly the volume of necrosis, with a reduction of the total delivered light dose (Curnow et al., 2000). The use of hyperbaric oxygen to compensate for the depletion of oxygen has also been reported, with encouraging results (Maier et al., 2000; Tomaselli et al., 2001; Huang et al., 2003). According to the discussion from the previous papers, it seems that dependence on sensitiser and light dose are insufficient to predict treatment outcome. Chapter 8 of this thesis presents the clinical results of photobleaching of the ALA-induced PpIX.

1.1.5 Biological considerations

Necrosis was considered the only cell death mechanism caused by PDT until an apoptotic response to PDT was reported in 1991 (Agarwal et al., 1991). Since then, apoptosis has been observed in a variety of tumour cell lines (Figure 1.4). *In vitro*, the primary cellular target of photodynamic therapy is clearly determined by the subcellular location of a given photosensitiser. Photosensitisers localizing in the plasma membrane usually exert their destruction either by inactivation of membrane bound apparatus, endoplasmic reticulum and cytoplasm are usually involved in signal transduction enzymes or by direct photoperoxidation of the membrane itself, which causes (i) loss of membrane integrity and favours necrotic cell death; (ii) while photosensitisers accumulated in mitochondria lead to disruption of their function which causes the release of cytochrome C, several events are initiated which result in an apoptotic mode of cell death (Almeida et al., 2004; Oleinick et al., 2002; Marchal et al., 2005).

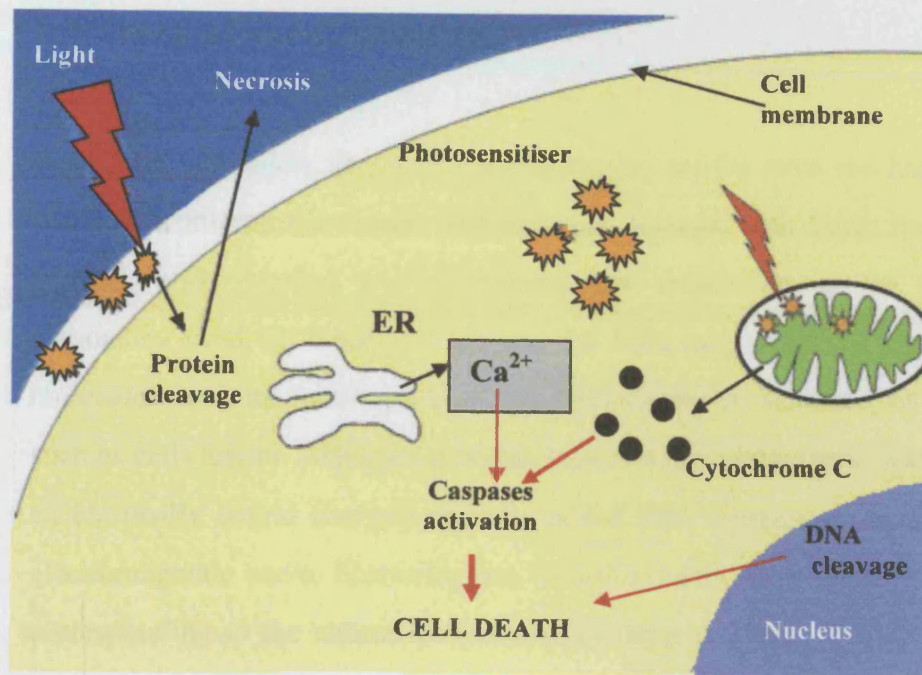


Figure 1.4 A schematic diagram of the extrinsic and the mitochondria-mediated cell death pathways following exposure to PDT leading to cell death. Adapted from (Almeida et al., 2004)

1.2 Optical spectroscopy

Reflection, refraction, absorption and scattering are the main mechanisms that occur when light migrates in tissue. The light can interact with tissue by photochemical, thermal, photoablation, and photodisruption, depending on the tissue and light parameters used. In biological tissues, the light may either be absorbed by tissue molecules such as water proteins and hemoglobin or scattered by tissue particles such as cells nuclei. Absorption occurs when an electromagnetic wave interacts with an elastically bound charged particle, which then vibrates at the frequency of the electromagnetic wave. Scattering, on the other hand, takes place at frequencies not corresponding to the natural frequencies of these particles. For wavelengths >850-900 nm, the photons may not have sufficient energy to participate in a photochemical reaction. Therefore, the wavelength range between 600 and 800 nm has been determined as the practical therapeutic window (Richards-Kortum and Sevick-Muraca, 1996).

The term spectroscopy refers to the study of the interaction of electromagnetic radiation with matter. There are three aspects to a spectroscopic measurement: irradiation of a sample with electromagnetic radiation; measurement of the absorption, spontaneous emission (fluorescence, phosphorescence) and/or scattering (Rayleigh elastic scattering, Raman inelastic scattering) from the sample; and analysis and interpretation of these measurements. Clinically, the term describes the process of evaluation of the tissue optical properties with subsequent spectral analysis of the acquired data by using an *in vivo* system. A diagnosis or monitoring of tissue status is then attempted, based on *in situ* optical measurement which can be performed non-invasively, without the need for surgical biopsy (Hammes, 2005). It has become universally known that early detection of premalignant and malignant lesions can substantially reduce the risk or improve the prognosis in oral cancer. Clinical differentiation of lesions is usually based on morphological changes in tissues; this technique is quite difficult to implement and experience usually is considered to be a major factor in its success. However it can be found to be less

sensitive in differentiating between lesions with similar clinical and morphological characteristics, i.e. dysplasia and carcinoma *in situ*.

There is always a risk of a premalignant lesion transforming into a malignant one if certain factors or conditions lead to its excitation; these usually require continuous monitoring, which can sometimes be difficult since it might require multiple biopsies to be taken from the patient, which can be uncomfortable, time consuming and costly. Moreover, it is difficult to screen a large number of the population who are at high risk of developing the disease. Several diagnostic and alternative methods have been employed to increase the detection of mucosal lesions, such as histopathology, radiology, biological markers or application of certain dyes, including iodine solution, Lugol's iodine, and Toluidine blue; combining two or more techniques together has been shown to increase the sensitivity and specificity (Kurita and Kurashina, 1996; Onizawa et al., 1999; Onizawa et al., 1996). Caution must be exercised, as the vital staining is only appropriate for dysplastic changes that appear on the surface and has no value if there is underlying infiltrating carcinoma that does not produce surface dysplasia. Moreover, some of these medical techniques are costly and only available to a limited number of populations. Screening and detection of cancer at an early stage may be improved by optical techniques which are now under scientific investigation.

The main techniques currently utilised in the detection of oral dysplasia and malignancies are Fluorescence, Raman and Elastic Scattering spectroscopy. This thesis, however, concentrates on fluorescence and elastic scattering spectroscopy. All three types utilise light within, or just outside, the visible range of electromagnetic radiation (Figure 1.5).

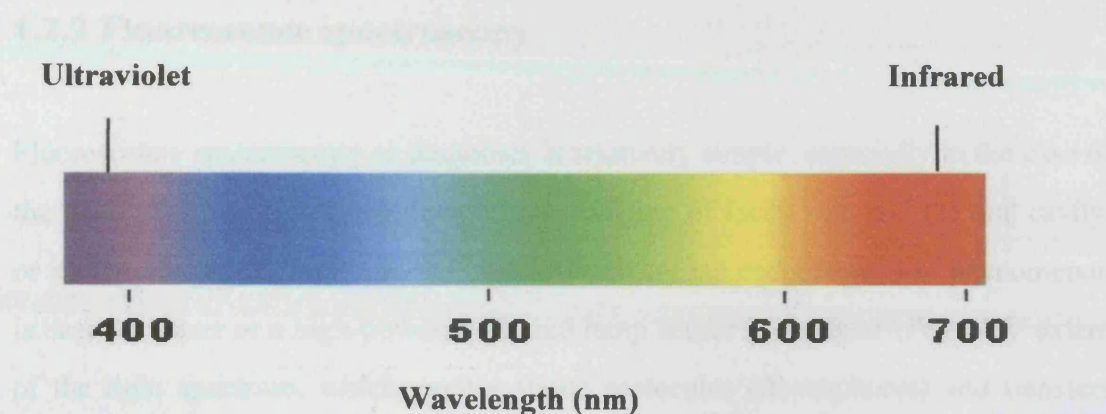


Figure 1.5 Diagrammatic representation of the visible spectrum demonstrating colour versus wavelength

1.2.1 Raman spectroscopy

Raman spectroscopy is an optical method based on inelastic light scattering. A Raman spectrum is a plot of scattered intensity as a function of energy difference between incident and scattered photons, i.e. Raman effects are produced when incident light excites sample molecules and scatter them at different wavelengths. This inelastically scattered light is called the Raman scatter. From the energy level point of view, the process of Raman scattering can be viewed as the transition of a molecule from its ground state to an excited vibration state, accompanied by the simultaneous absorption of an incident photon and emission of a Raman scattered photon. Recent developments in fibre-optic probe technology have enabled its application as an *in vivo* technique to study the structure and dynamic function of important molecules (Hanlon et al., 2000).

Many studies have shown that high quality Raman spectra can be interpreted from a biochemical viewpoint for the possibility of diagnosing the pre-cancerous tissues (Stone et al., 2000; de et al., 2005).

1.2.2 Fluorescence spectroscopy

Fluorescence spectroscopy or diagnosis is relatively simple, especially in the case of the photosensitiser-enhanced fluorescence imaging of facial skin and the oral cavity, or it may be more complex in the case of fluorescence endoscopy. The phenomenon is based on laser or a high-powered filtered lamp source in the near-UV or UV extent of the light spectrum, which excites tissue molecules (fluorophores) and transfers them into an excited state that rapidly reverts to a more stable and less energetic state after the emission of fluorescent light (Figure 1.6).

The fluorescence can either occur as autofluorescence (induced by UV light), or as a laser-induced phenomenon and may also be enhanced by either topical or systemic application of 5-aminolevulinic acid (5-ALA) and can be used for single-point or imaging measurements. 5-ALA is a precursor of the fluorescent photosensitiser, protoporphyrin IX (PpIX), and can be administered systemically or applied topically to the oral mucosa and facial skin. The main characteristic of tissue fluorescence used for medical diagnostics are that one may see (i) an obvious difference in the emission spectrum at a set excitation wavelength between diseased and healthy tissue; (ii) differences in the excitation spectrum, the fluorescence lifetime and polarization (Andersson-Engels et al., 1997). Fluorescence diagnostics offers several clinical benefits and has therefore been extensively studied in preclinical and clinical studies since 1990 as reviewed in (Sokolov et al., 2002). The use of native tissue fluorescence for the early detection of malignant tissues was investigated. The results were encouraging but varied greatly between some patients and appeared inappropriate for others (Betz et al., 1999). In addition, there are a high percentage of false-positive and false-negative results, which may be attributed to insufficient number of patients, whereas fluorescence spectroscopy of exogenous fluorophores has shown high sensitivity and specificity.

Dysplastic and malignant tissues, as well as having different spectral characteristics, tend to have increased red fluorescence and decreased green fluorescence, with

significant increase of the red/green fluorescence ratio (Rhodes and Diffey, 1997; Leunig et al., 2001; Zheng et al., 2002a). Chapter 6 of this thesis presents the clinical results of fluorescence imaging of the ALA-induced PpIX for early detection of tissue dysplasia.

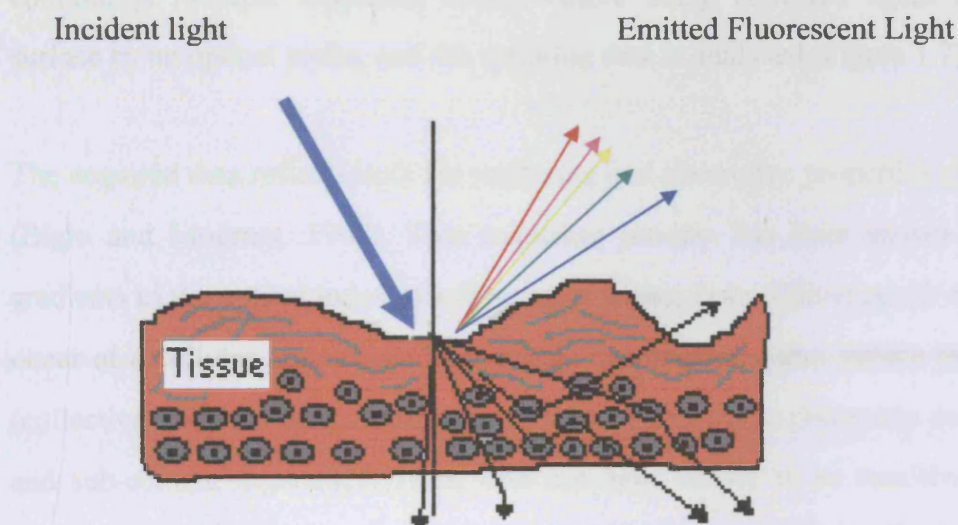


Figure 1.6 Optical biopsy using fluorescence spectroscopy. Emitted fluorescence light of different wavelengths to incident light

1.2.3 Elastic scattering spectroscopy

Elastic Scattering Spectroscopy (ESS) is an emerging technique that generates a wave-length dependant spectrum that reflects structural and morphological change within tissues. Elastic scattering implies that the light returns with the same kinetic energy as the incident photons. The incident light can undergo single, or more commonly, multiple scattering events before being collected again at the same surface by an optical probe, and the resulting data is analysed (Figure 1.7).

The acquired data reflects both the scattering and absorptive properties of that tissue. (Bigio and Mourant, 1997). This scattering process has been shown to occur at gradients in the optical index of refraction resulting from differences in densities that occur at a cellular and sub-cellular level. The structures that induce the scattering (collectively known as scattering centres) are the nucleus, chromatin concentration, and sub-cellular organelles. Thus, ESS has been shown to be sensitive to nuclear size, chromatin content and nuclear/cytoplasmic ratio, which are all criteria that the histopathologist looks for when establishing malignancy within a tissue (Perelman et al., 1997; Wallace et al., 2000; Mourant et al., 2000; Drezek et al., 2003).

ESS has the advantage of being fast, reliable and cost effective and potentially offers a non-invasive diagnosis in-situ, and in real time. The technique has not been used only in the diagnosis of dysplasia and malignancy, but can be used to monitor chemotherapy levels and possibly free-flap oxygenation levels. It can also enable guided rather than random biopsies, and assess surgical margins and regional lymph nodes intra-operatively (Gollnick et al., 2001; Mourant et al., 2000; Nordstrom et al., 2001; Jerjes et al., 2005). ESS has, in a number of studies, been combined with extracted intrinsic fluorescence and diffused reflectance, forming a “tri-modal spectroscopy” device which has been shown to have a higher sensitivity and specificity when examining premalignant and malignant lesions (Georgakoudi et al., 2001). Chapter 7 of this thesis presents the clinical results of ESS for an early detection of tissue dysplasia.

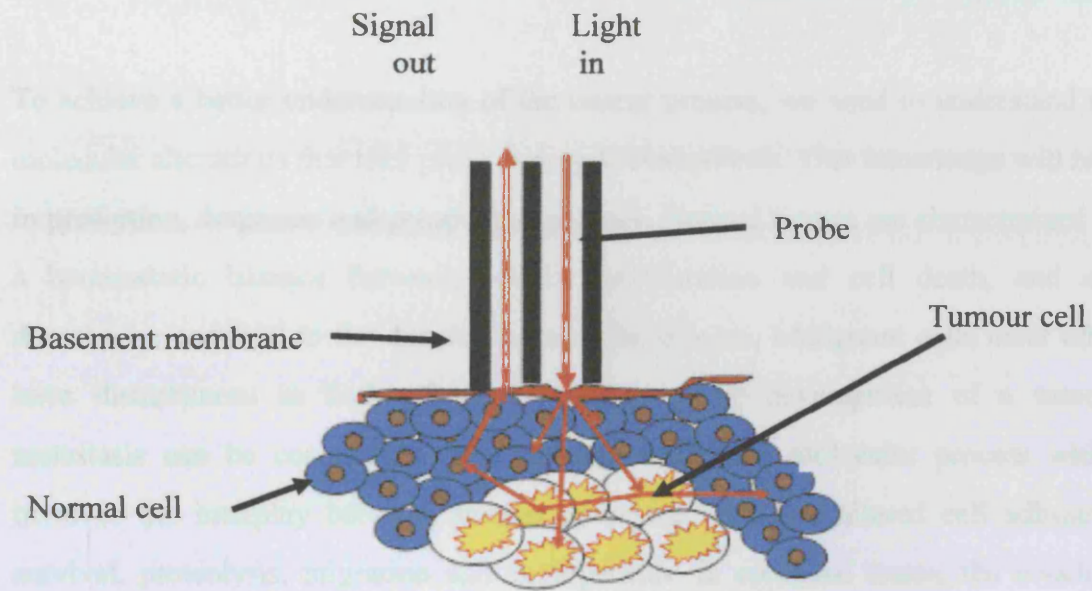


Figure 1.7 Schematic illustration of elastic scattering in human tissue.

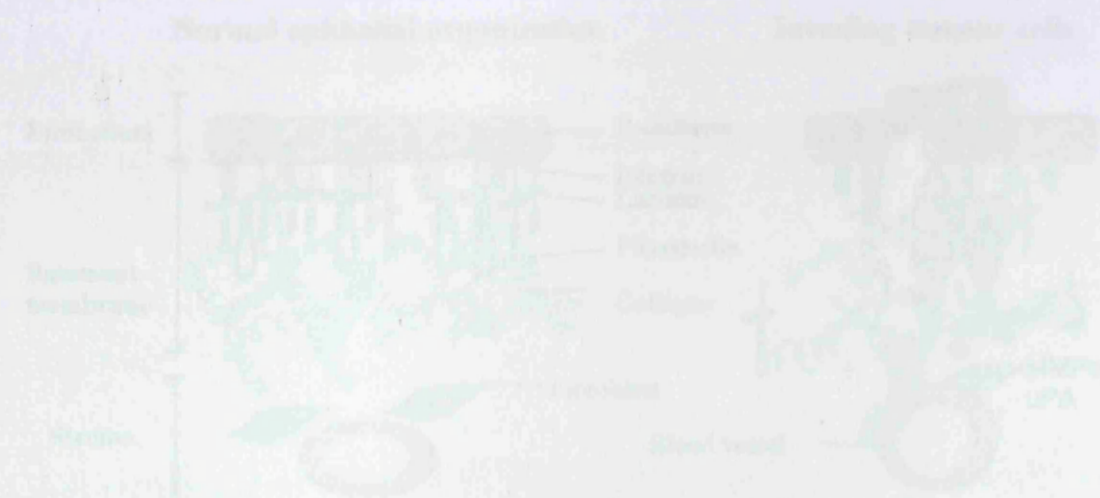


Figure 1.8 A simplified schematic illustration of events during cancer cell invasion.

1.3 Cancer invasion and metastasis

To achieve a better understanding of the cancer process, we need to understand the molecular alterations that take place during carcinogenesis. This knowledge will help in prediction, diagnosis and prospective therapy. Normal tissues are characterized by a homeostatic balance between cellular proliferation and cell death, and any disturbance can lead to the development of the disease. Malignant cells most often have disturbances in both of these processes. The development of a tumour metastasis can be considered as a complex multi-step molecular process which involves the interplay between several processes including altered cell adhesion, survival, proteolysis, migration and angiogenesis. In epithelial tissue, the invading cells should be able (i) to induce the development of blood vessels by expressing a gene for blood vessel growth factors; (ii) to pass through a basement membrane by altered interactions of the invading cells with extracellular matrix (ECM) components such as laminin, collagen type I and -IV and fibronectin. Adhesion molecules, such as integrins and cadherins, are also involved in both cell-to-cell and cell-to-ECM interactions (Hanahan and Weinberg, 2000), as illustrated in Figure 1.8.

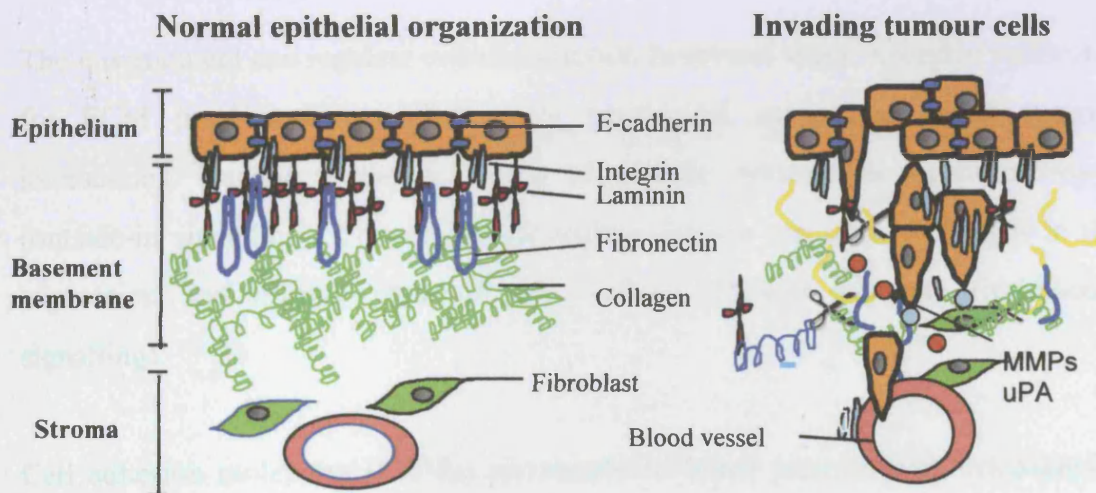


Figure 1.8 A simplified schematic illustration of events during tumour cell invasion.

1.3.1 Angiogenesis

The formation of new capillary blood vessels (angiogenesis) represents an essential requirement for the continued growth and invasion of solid tumour cells, including those found in head and neck squamous cell carcinoma. This process is regulated by a balance between proangiogenic factors, such as the vascular endothelial growth factor (VEGF) and its family, and the antiangiogenic factors (Laughner et al., 2001).

Angiogenesis is a sequential process emanating from the microvascular endothelial cells, when proangiogenic factors bind to cell receptors and stimulate growth. As a consequence, more proteases are secreted from the endothelial cells. These proteases can digest the extracellular matrix proteins, which also results in the further release of proangiogenic factors. Following digestion, the cells start to move toward the sources of the stimulus (tumour cells) and undergo morphological changes to form new blood vessels which contribute to solid tumour feeding (Bhushan et al., 2002).

1.3.2 Cell adhesion

The environment can regulate cellular function in several ways: Receptor molecules for ECM proteins can mediate both mechanical stress and ligand specific interactions, leading to the activation of specific intracellular signal pathways (outside-in signalling). Conversely, intracellular events can lead to changes in the expression and affinity state of cell surface adhesion receptors (inside-out-signalling).

Cell adhesion molecules (CAMs) are membrane-based proteins with cytoplasmic, transmembrane and extracellular domains. The cytoplasmic tail often interacts with the cytoskeletal proteins that serve as the actual anchor within the cell. The extracellular domains extend from the cell and binds to adjacent cells or to an extracellular matrix through homophilic, heterophilic or an intermediary linker.

CAMs are divided into four major families: cadherins, the immunoglobulin super family, integrins and selectins (Juliano, 2002). This thesis, however, concentrates on a subset of integrins.

1.3.2.1 Cadherin

E-Cadherin is the main adhesion molecule of epithelia and is sometimes called 'molecular glue'. It is a transmembrane glycoprotein which mediates calcium dependent intracellular adhesion proteins in the epithelial tissues through its extracellular domain. The cytoplasmic domain of E-cadherin can play a role in transmission of anti-growth signals (Christofori and Semb, 1999). Over-expression of these molecules may result in an inverse relationship with the metastatic capacity of the tumour cells (Luo et al., 1999).

1.3.2.2 Integrins

Integrins are a large family of transmembrane cell surface receptor proteins which play a crucial role in cellular stability by providing adhesive function in cell-to-cell and cell-to-ECM interactions, and mediate numerous intra-cellular pathways that regulate many cell functions, such as proliferation, differentiation, migration, invasion, apoptosis, and gene expression (Mizejewski, 1999). Functional integrins consist of heterodimeric complexes of noncovalently linked α - and β -chains and serve as a link between the ECM and the cytoskeleton of the cell (Hynes, 2002). At present, 18 different α subunits and 8 β subunits are known to combine to form more than 24 integrins, each has a distinct ligand binding specificity (Mizejewski, 1999), as illustrated in Table 1.1. Following binding to ligand, integrins undergo a set of dynamic changes. Integrin expression is dependent on anatomy and tissue condition, e.g. in normal epithelia, $\alpha 3\beta 1$, $\alpha 2\beta 1$ and $\alpha 6\beta 4$ integrin receptors are generally expressed, while in oral squamous cell carcinoma, $\alpha 5\beta 1$ and $\alpha v\beta 6$ expression are more obvious; this may correlate with the downregulation of $\alpha v\beta 5$ subunits (Giannelli et al., 2001; Maragou et al., 1999).

Table 1.1 List of currently known ligands of different α - and β -subunits for integrin family (Mizejewski, 1999).

| α subunit | β subunit | Known Ligands substrate |
|------------------|-----------------|--|
| $\alpha 1$ | $\beta 1$ | Collagens, Laminins |
| $\alpha 2$ | $\beta 1$ | Collagens, Laminins |
| $\alpha 3$ | $\beta 1$ | Laminins, Fibronectin, Thrombospondin |
| $\alpha 4$ | $\beta 1$ | Fibronectin, VCAM |
| $\alpha 4$ | $\beta 7$ | Fibronectin, VCAM, |
| $\alpha 5$ | $\beta 1$ | Fibronectin |
| $\alpha 6$ | $\beta 1$ | Laminins |
| $\alpha 6$ | $\beta 4$ | Laminins |
| $\alpha 7$ | $\beta 1$ | Laminins |
| $\alpha 8$ | $\beta 1$ | Fibronectin, Tenascin |
| $\alpha 9$ | $\beta 1$ | Tenascin |
| $\alpha 10$ | $\beta 1$ | Collagens |
| $\alpha 11$ | $\beta 1$ | Collagens |
| αD | $\beta 2$ | VCAM, ICAMs |
| αE | $\beta 7$ | E-cadherin |
| αL | $\beta 1$ | ICAMs |
| αM | $\beta 1$ | Fibrinogen, ICAMS |
| αX | $\beta 2$ | Fibrinogen |
| αv | $\beta 1$ | Fibronectin, Vitronectin |
| αv | $\beta 3$ | Fibronectin, Vitronectin, Fibrinogen, von Willebrand's factor, Thrombospondin |
| αv | $\beta 5$ | Vitronectin |
| αv | $\beta 6$ | Fibronectin, Tenascin |
| αv | $\beta 8$ | Collagens, Laminins, Fibronectin |
| αIIb | $\beta 3$ | Collagens, Fibronectin, Vitronectin, Fibrinogen, Von Willebrand's factor, Thrombospondin |

1.3.3 Extracellular matrix

The extracellular matrix (ECM), the network of proteins surrounding cells, is a highly organized fibrillar meshwork, consisting mainly of collagens, fibronectin, vitronectin and laminins, which serve as substratum for cell adhesion and migration.

1.3.3.1 Collagens

Collagens represent the major protein comprising the ECM with more than 20 different collagen types identified so far (Gelse et al., 2003). Collagen types I, II and III are the most abundant fibrils of similar structure. Types IV and VII collagen form a two-dimensional reticulum, which represents the major component of the basal lamina. Collagens are secreted inactive into the extracellular space and require activation by the extracellular enzymes. This is implicated in both the normal physiological processes, such as embryogenesis and wound healing, and carcinogenesis (O'Toole, 2001).

1.3.3.2 Fibronectin

Fibronectin is a large, multidomain glycoprotein of high molecular weight found on cell surfaces, extracellular matrix and in plasma. It interacts with several molecules found within the extracellular matrix, basement membranes and cell-surface receptors. Integrin molecules mediate its binding to the cell surface and serve to trigger cellular signalling. Fibronectin plays special roles in cell adhesion, migration, differentiation and cytoskeletal organization (Pankov and Yamada, 2002).

1.3.4 Matrix metalloproteinases

Cell function and fate are dictated by both the intrinsic cellular signalling pathways and the external microenvironment. The microenvironment signals may regulate cell adhesion, differentiation, division, and apoptosis. Limited proteolysis via

components known as matrix metalloproteinases (MMPs), allow cells to move through modified matrix. This movement involves continuous ECM attachments and detachments by invading cells.

1.3.4.1 Structure of MMPs

MMPs are a family of more than 24 zinc and calcium-dependent members of metalloenzymes (Table 1.2). MMPs are numbered according to their order of discovery, and divided according to their substrate specificity into interstitial collagenases (MMPs -1, -8 and -13), stromelysins (MMPs -3, -10 and -11), gelatinases (MMPs -2, and -9), and other membrane types (MT)-MMPs (Kleiner and Stetler-Stevenson, 1999). MMPs are also divided into subclasses according to their shared functional domains into eight distinct classes: five are secreted and three are membrane-bound (Kerkela and Saarialho-Kere, 2003).

1.3.4.2 Regulation of MMPs activity

The synthesis of MMPs is regulated by several factors, including growth factors and cytokines secreted by lymphocytes, stromal cells, tumour cells and ECM proteins. All MMPs are produced in a pro-form, which needs extracellular activation through the removal of their propeptide domains. The soluble types of MMPs, such as gelatinases and collagenases, are activated mainly by other MMPs or plasmin (Figure 1.9), while the activation of membrane type MMPs is a more complex process (Curran and Murray, 1999). The four members of the tissue inhibitor MPs (TIMP-1, -2, -3 and -4) can bind to MMPs and reversibly inhibit their activity (Fassina et al., 2000).

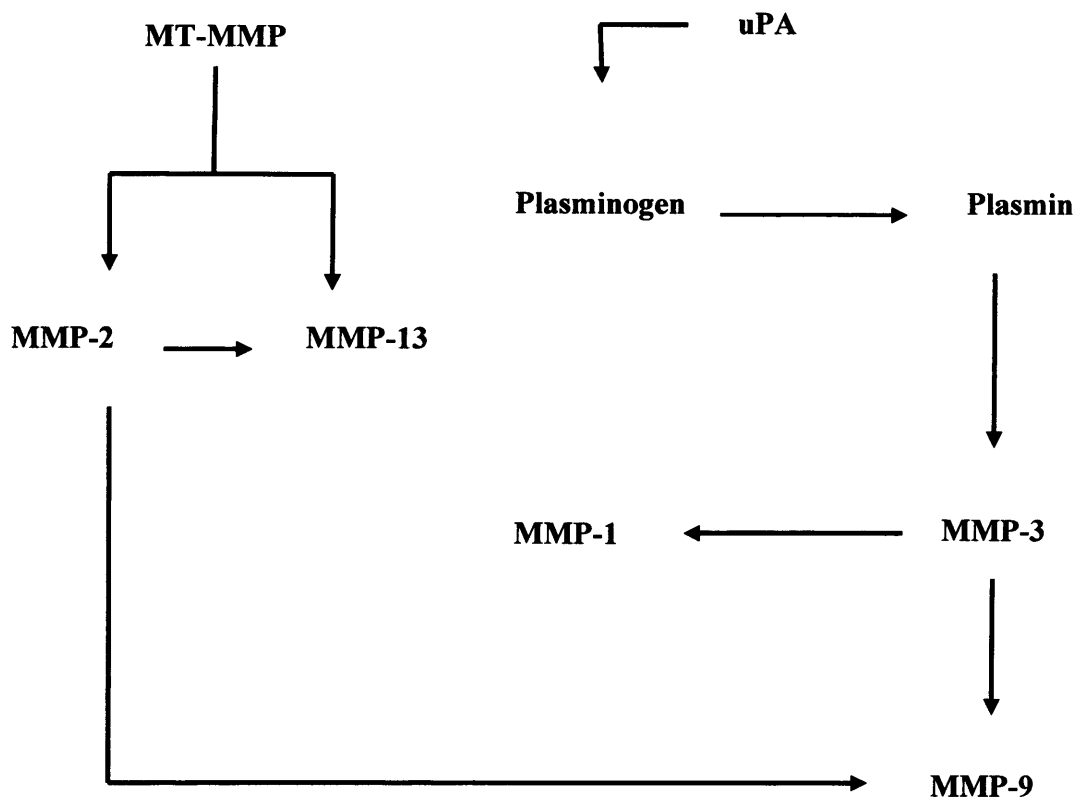


Figure 1.9 Activation cascade of MMPs. Adapted from (Curran and Murray, 1999).

1.3.4.3 Function of MMPs

MMPs have a role in the normal development of the tissues and organs during embryogenesis. This function however, is altered in malignant tissues. MMPs have a dual role in tumour growth and metastasis. They promote tumour growth by degrading most of the ECM components, and enhancing angiogenesis (Rundhaug, 2005). They also provide cells with directional information by modifying the environment in front of the cell (Bogenrieder and Herlyn, 2003; Kramer et al., 2005).

Table 1.2 A list of some tumour associated MMPs and their substrates (Kerkela and Saarialho-Kere, 2003)

| Enzyme | MMP number | Matrix substrates |
|-----------------|-------------------|--|
| Collagenases-1 | MMP-1 | Collagens I, II, III, VII, VIII, X and XI, gelatin, entactin, tenascin, aggrecan, fibronectin, vitronectin, casein. |
| Collagenases-2 | MMP-8 | Collagens I, II and III, aggrecan. |
| Collagenase-3 | MMP-13 | Collagens I, II, III, IV, IX, X, XIV, gelatin, fibronectin, aggrecan, casein. |
| Gelatinase A | MMP-2 | Collagens I, II, III, IV, V, VII and X, gelatin, fibronectin, laminin, aggrecan, elastin, vitronectin, tenascin. |
| Gelatinase B | MMP-9 | Collagens IV, V, XI, XIV, elastin, aggrecan, decorin, laminin, fibronectin. |
| Stromelysin-1 | MMP-3 | Collagens III, IV, V, IX, X, and XI, gelatin, aggrecan, elastin, fibronectin, vitronectin, laminin, entactin, tenascin, decorin. |
| Stromelysin-2 | MMP-10 | Collagens III, IV and V, gelatin, fibronectin, elastin, aggrecan, casein, pro-MMP-1, pro-MMP-2, pro-MMP-9, pro-TNF- α . |
| Stromelysin 3 | MMP-11 | Ealstin, collagen IV, gelatin, fibronectin, vitronectin, laminin, entactin, |
| Metalloelastase | MMP-12 | |
| MT1-MMP | MMP-14 | ProMMP-2, proMMP-13, collagens I, II and III, gelatin, fibronectin, vitronectin, laminin-1 and -5. |
| MT2-MMP | MMP-15 | |
| MT3-MMP | MMP-16 | ProMMP-2, laminin, fibronectin, tenascin, entactin, aggrecan, perlecan. |
| MT4-MMP | MMP-17 | Fibrinogen, fibrin, pro-TNF- α . |
| MT6-MMP | MMP-25 | Collagen IV, gelatin, fibrinogen, fibronectin. |

1.3.5 The Plasminogen activation system

The Plasminogen Activator System (PA), which consists of two types, is involved in the conversion of plasminogen to active plasmin. It can be classified according to its immunologic or biological characteristics, namely: tissue-type plasminogen (t-PA) and urokinase-type plasminogen activator (u-PA). There are also plasminogen activator inhibitors (PAIs) which are divided into three groups, namely: PAI-1, -2 and -3). In addition, there are the protease nexins, which also inhibit PA. Under normal physiological conditions, the activation of plasminogen into active enzyme occurs to numerous processes, e.g. during fibrinolysis, cell migration, wound healing, trophoblast invasion, angiogenesis, tissue destruction, and the activation of growth factors and other proteolytic enzymes (Figure 1.9). Many of the roles of the PAs in normal physiology are equally important in cancer progression (Dano et al., 2005).

1.3.6 Growth factor receptors

The growth factor receptors play an influential role in signalling that direct the behaviour of normal and tumour cells. Therapies targeting these receptors are the main focus of recent research, attempting to control replication, or tumourigenesis or cytotoxic effects on tumours.

1.3.6.1 Epidermal growth factor receptor

The epidermal growth factor receptor (EGFR) is a transmembrane glycoprotein present in many human tissues. EGFR is one of four membrane growth factor receptor proteins that share similarities in structure and function making together the c-erbB family of receptor tyrosine kinases. EGFR is a 170-kDa glycoprotein, which also known as c-erbB-1, is composed of three major domains: a cysteine rich extracellular ligand-binding domain connected to an intracellular protein tyrosine kinase domain with tyrosine kinase function (Yarden, 2001).

Multiple ligands bind to and activate the EGFR, including epidermal growth factor (EGF), transforming growth factor- α (TGF- α), and amphiregulin (Salomon et al., 1995). EGFR become activated by binding to its ligands, leads to autophosphorylation of receptor tyrosine kinase and subsequent activation of signal transduction pathways, which played an important role in cell growth, differentiation, angiogenesis, adhesion, metastasis and the inhibition of apoptosis (Herbst, 2004). In addition to ligand binding, EGFR can also be activated by additional EGFR activation mechanisms, such as metalloproteinase-mediated cleavage of precursor membrane-bound EGF ligands (Prenzel et al., 1999), and uP receptors (Liu et al., 2002). Over the past decade, work has been directed at developing anticancer agents that able to stop or reduce the EGFR activity. The most common studied to date approaches consist of monoclonal antibodies, such as C-225 (cetuximab, Erbitux[®]), directed to block ligand binding to the extracellular domain, and small molecules inhibitors, such as ZD1839 (Iressa, Gefitinib), which interfere with intracellular tyrosine kinase activity.

1.3.6.2 Hepatocyte growth factor receptor

The receptor for the hepatocyte growth factor (HGF), also known as the scatter factor (SF), is a transmembrane tyrosine kinase receptor, c-met protein, which is predominantly expressed on endothelial cells, whereas the mesenchymal cells generally express their ligand, which tends to act in a paracrine manner. The activation of c-met by interaction with its ligand, HGF, has been shown to induce a variety of cellular responses, including epithelial cell proliferation, survival, tumour angiogenesis, invasion and metastasis (Maulik et al., 2002).

1.4 Background to oral cancer

Oral cancer remains a disfiguring disease associated with high mortality rate. It is the sixth most common cancer diagnosed in world (Ferley et al., 2000). Squamous cell carcinoma is the most common type of oral cancer, and associated with environmental exposure to carcinogens, particularly smoking tobacco and betel nut chewing, which represent the major risk factors for oral cancer (Zavras et al., 2001). There is also association with alcohol consumption and possibly viral infection, particularly Human papilloma viruses (Smith et al., 2004).

Squamous cell carcinoma is a heterogeneous disease with distinct presentation. Clinically, the appearance of the lesion will be easier if the clinician follows a systemic and logical sequence, including full history and physical examination of all regions. The lesion arises from the surface mucosa lining the oral cavity, and can readily be detected by visual inspection and palpation. At an early stage, it may appear as an ulcer, with or without central necrosis and exophytic margins, or as mucosal erosion.

Currently, Computerised Tomography (CT), Magnetic Resonance Imaging (MRI), and Ultrasound Scans (US) are still the most vital tools being used for the assessment of advanced tumours and to determine the stage of the disease. Much promise has been also shown by the use of the newer imaging tools, such as lymphoscintigraphy for identification of sentinel nodes (Payoux et al., 2005; Kovacs et al., 2005). Other emerging non-invasive optical methods, including fluorescence spectroscopy, elastic light scattering and Raman spectroscopy are still under investigation, as discussed in Chapters 6 and 7 of this thesis.

At present, the genetic factors that contribute to the development of squamous cell carcinoma are still not clearly defined, and data showed differences in genetic aberrations in different nations, which may be due to different etiological factors (Jeon et al., 2004; Ginos et al., 2004). One example is the *p53* gene, a tumour

suppressor gene, whose detection may be used as a prognostic indicator, since the risk of oral cancer is increased as the gene expression decreased (Greenblatt et al., 2003).

In the management of cancer of the oral cavity, surgical resection and radiation with or without adjuvant chemotherapy, are the basic treatment for early disease (Forastiere et al., 2001). Isolated tumours in young patients may be best treated with an excision operation, to avoid the risk of long-term radiotherapy complications, while an elderly or frail patient may well be referred for radiotherapy, even for lesions that could easily be treated by surgery. For many patients, surgery is simply not an option because of general poor health or perhaps because of previous surgery to the head and neck region. Radiation therapy is effective in the treatment of loco-regional disease.

The debilitating effect of neck dissection on its function is reduced by the use of selective and super-selective neck dissection which involves only removal of affected lymph nodes, and the improvement in reconstruction methods of tissue defects caused by surgery (Robbins et al., 2005).

1.5 Metastatic promoting factors in oral carcinoma

The prognosis of patients with OSCC is still poor due to the high rate of invasion and metastasis. This process requires efficient ECM digestion and nutrient supply, which is accomplished through the activity of several proteolytic and growth promoting factors, including MMPs, plasmin system, adhesion receptors and growth factors. Based on these considerations, a positive correlation between malignancy and expression/suppression of these factors would be expected (Myoung et al., 2002). This thesis, however, concentrates on ECM proteinases; MMP-2, -9 and -13 and uPA, proangiogenic factor; VEGF and $\alpha v\beta 6$ and $\alpha 5\beta 1$ integrin receptors.

1.5.1 Expression of MMP-2, MMP-9 and MMP-13

MMPs play a dual role in tumour growth and metastasis. They promote tumour growth by digesting the matrix barrier and enhancing angiogenesis. Numerous *in vitro* studies have suggested a positive correlation between invasion and metastasis and the expression of MMP-2 and MMP-9 (Sundelin et al., 2005; Robinson et al., 2003; Nyberg et al., 2002; Kawahara et al., 1993; Bennett et al., 2000). *In vivo*, a study of the presence of MMPs in human surgical biopsy specimens of oral squamous cell carcinoma demonstrated a marked expression of MMP-2 and MMP-9; this was significantly associated with invasion and lymph node metastasis (Kurahara et al., 1999). In 91 head and neck squamous cell carcinoma samples, the presence of MMP-2 and MMP-9 was investigated using immunohistochemistry, and a close relationship between the expression of MMP-2 and MMP -9 and clinical stages, nodal metastases and tumour-stages was found (Do et al., 2004). In a recent study by de Vicente and his group using immunohistochemistry examination, MMP-2 and MMP-9 were detected only in 19 (28%) and 12 (17.6%) cases, respectively, of 68 primary OSCC samples (de Vicente et al., 2005). Also, MMP-13 *in vivo* is found in invasive head and neck carcinomas. In a study of 78 patients with head and neck squamous cell carcinoma, using immunohistochemical techniques, 44 (56.4%) tumours were found to significantly express MMP-13, whereas none of the normal

tissues examined was found to express this protein. Moreover, these high levels of MMP-13, in highly invasive tumours were noted regardless of patient age, sex or tumour site (Culhaci et al., 2004). More recently, Using β 6-transfected OSCC cells, the MMP-13 expression at both mRNA and protein level was recently observed (Ylipalosaari et al., 2005).

1.5.2 Expression of uPA

According to its function, the uPA is believed to influence the progress of tumour dissemination and metastasis. The contribution of uPA to the invasive process of OSCC was clearly demonstrated, in which invasion was substantially reduced when the catalytic site of urokinase was blocked (Clayman et al., 1993). It was demonstrated that OSCC was able to activate plasminogen and produce significant u-PA levels *in vitro*, higher than those of controls (Ghosh et al., 2002). In human tumour specimens, expression of uPA found to correlates with the mode of invasion and secondary regional lymph node metastasis of OSCC (Yasuda et al., 1997; Nozaki et al., 2005). Furthermore, it was also found that patients suffering from oral cavity tumour recurrence had statistically significant higher levels of uPA in the tumour tissue as well as in tumour positive lymph nodes (Zemzoum et al., 2003; Hundsdorfer et al., 2005).

1.5.3 Expression of VEGF

VEGF is one of the main regulators of angiogenesis, which is now accepted to play a vital role in the continued growth and metastasis of solid tumours (Sauter et al., 1999). Based on these considerations, a positive correlation between malignancy and expression /suppression of these factors would be expected. However, few studies have reported the correlation between VEGF expression and prognosis of OSCC. Immunohistochemistry studies using antibodies to the VEGF from tumour specimens obtained from 45 patients with oral squamous cell carcinoma revealed a minority of tumours expressed VEGF. Thus, 19 carcinomas (42.2%) were VEGF

positive and 26 (57.8%) were negative (Maeda et al., 1998). The relationship between VEGF expression value, prognosis and regional lymph node metastasis was evaluated clinically in 63 patients with oral squamous cell carcinoma. It was found that values of VEGF expression were significantly higher for patients with poor prognosis than for those with good prognosis, but regarding lymph node metastasis, no significant correlation was found, since the average percentage of VEGF immunopositive area was 19.4% in patients with regional lymph node metastasis, and 24.0% in patients without a metastatic lymph node (Uehara et al., 2004).

1.5.4 Expression of $\alpha v\beta 6$ and $\alpha 5\beta 1$ integrins

The pattern of integrin expression in oral squamous cell carcinoma varied between each malignant lesion, but $\alpha v\beta 6$ is one of the most commonly unregulated in oral carcinomas and is found to correlate with tumour progression and invasiveness (Regezi et al., 2002; Thomas et al., 1997; Li et al., 2003). The adhesion of oral squamous cell carcinoma cells to fibronectin in the presence of neutralizing antibodies to both $\alpha v\beta 6$ and $\alpha 5\beta 1$ was tested *in vitro*. It was found that blocking of $\alpha 5\beta 1$ alone reduced the adhesion to 70%, whereas if both $\alpha v\beta 6$ and $\alpha 5\beta 1$ integrins were blocked, adhesion was completely lost. In addition, an 81% reduction in migration was achieved when $\alpha v\beta 6$ was blocked (Xue et al., 2001). A significant increase in OSCC invasiveness was observed when non-invasive C1 line was retrovirally infected with $\beta 6$ cDNA to produce highly invasive VB6 cell line (Thomas et al., 2001a). Using similar approach, Ramos et al. showed that $\alpha v\beta 6$ expression correlated with OSCC invasion and tumour growth *in vitro* and *in vivo* when poorly invasive SCC9 cell line was transfected with $\beta 6$ cDNA (Ramos et al., 2002).

1.6 Metastatic promoting factors following PDT in oral carcinoma

PDT is currently under clinical investigation for the treatment of early cancer. The biological effects of PDT are primarily mediated by the generation of reactive oxygen species that result in cytotoxic effects on treated cells. The oxidative stress produced by PDT has been shown to induce the expression or activity of several proteins and initiation of numerous signal transduction pathways that control motility, growth and metastasis (Mitra et al., 2003).

1.6.1 PDT and cell adhesion

Prevention of cell adhesiveness represents an important parameter in cancer metastasis. Most sensitisers used in PDT accumulate in cellular membranes where the obvious cell destruction is initiated. This results in alterations in tumour cell adhesiveness with a possible distant spread. Only few studies have demonstrated the effect of PDT on adhesion. It was suggested earlier that PDT is a safe treatment when considering metastases (Foultier et al., 1994). Vonarx (1995) found an increased adhesiveness rate of some colonic cancer cells on plastic substratum, while, on ECM, the adhesion was decreased and this was correlated with a decreased metastatic potential *in vivo* (Vonarx et al., 1995). Rousset et al (1999) demonstrated a transient decrease in the expression of ICAM-I, MHC-I and CD44V6 surface adhesion molecules after Photofrin-PDT (Rousset et al., 1999). In brain tumours, a significant inhibitory effect on the ability of the cells to migrate through an artificial basement membrane was observed following a sublethal dose of Photofrin-PDT (Jiang et al., 2002).

1.6.2 PDT and MMPs

Photosensitisation of mouse mammary tumour cells with Photofrin-PDT increased MMP-9 protein levels (Ferrario et al., 2004). *In vitro* studies using the 5-ALA sensitizer also showed an increase in MMP-1 and MMP-3 mRNA transcription and in protein levels in scleroderma fibroblasts cells subjected to PDT (Karrer et al., 2003). Interestingly, no change in MMP-1 and MMP-3 levels was observed in keratinocyte cells (Karrer et al., 2004).

1.6.3 PDT and VEGF

To date, there is, however, little information about the *in vivo* effects of PDT on VEGF. Most previous studies on VEGF have been done *in vitro* (Lisnjak et al., 2005; Togashi et al., 2006a). It was found that treatment of BALB/c mice transplanted with fibrosarcoma BFS1 tumour with PDT had reduced the levels of VEGF in mice sera and by 46% (the concentrations of control group after 24 h did not exceed 70.8 pg/ml whereas in tumourbearing, untreated mice, VEGF concentration was over 150pg/ml (Osiecka et al., 2003). Using immunohistochemical staining, The PDT treated mice cells expressed a transient elevation of VEGF for up to 6 h, which subsequently returned to normal levels at 24 h after PDT (Uehara et al., 2001). *In vivo* studies have revealed that VEGF levels were higher in tumour surrounding tissues of rat brain (Jiang et al., 2004). In a recent study using human oral squamous cell carcinoma xenograft, a significant difference of VEGF expression between the control and experimental groups at 6 h after PDT ($p = 0.0436$) whereas no significant differences between the control and experimental groups at 0, 3, 24, 48, and 72 h after PDT was demonstrated (Togashi et al., 2006b).

1.7 PDT in combination therapies

The excellent cosmetic results, the low toxicity of the modern photosensitiser, the absence of significant morbidity, and the low cost of PDT compared to traditional modalities make PDT a competitive treatment choice (Hopper et al., 2004b). However, and importantly, there are several side effects to PDT, such as prolonged photosensitization and limited target depth, which, at times, cause the long-term follow-up results to be worse than their conventional treatments. At the cellular level, the anti-tumour efficiency of any drug can be measured by the apoptosis cascades initiated. Regardless of the numerous apoptotic factors, other factors have been identified to prevent cell death (anti-apoptotic), such as growth factors and cytokine ligands; all can lead us to consider ways to improve PDT cancer treatment. Therefore, a combination of more than one treatment may increase the therapeutic outcome and reduce the side effects of each treatment used in isolation.

1.7.1 PDT and chemotherapy

The combination of PDT with chemotherapy may result in enhanced clinical results. At sub-toxic doses of PDT, the further addition of cytotoxic drugs may produce an additive effect (no more than the addition of the efficiency of each modality alone). This does not mean that there are no clinical benefits, since the adverse effect profile of the two modalities may combine to give a greater therapeutic ratio. Alternatively, the two modalities may produce a synergistic effect that exceeds the value of each modality. Many researchers have studied the effect of PDT combined with cytotoxic chemotherapeutic agents, and some suggest that the two modalities are synergistic with supra-additive effects (Dima et al., 1990; Ma et al., 1993; Ma et al., 1992; Gantchev et al., 1996). Others also suggest that the cytotoxic effects are stronger if the chemotherapy is applied before the PDT (Datta et al., 1997). Thus, clinical studies based on the combination of two treatment modalities are needed in order to optimise and establish this approach. Chapter 5 of this thesis presents the results of combination of PDT with chemotherapy.

1.7.2 PDT and small molecules

One approach to enhancing the effects of PDT and reduce limitations is to add PDT either simultaneously or concurrently to other antitumour agents. The EGFR is considered to enhance cell proliferation, motility, adhesion, invasion and angiogenesis, (Almeida et al., 2004). Several approaches have been designed to diminish EGFR function. One of these is the development of a family of tyrosine kinase inhibitors (TKIs) that block the adenosine triphosphate (ATP) site in the EGFR tyrosine kinase domain and abrogate the receptor autophosphorylation and inhibit cell proliferation. The first small molecule found to have the ability to inhibit the tyrosine kinase pathways is Gefitinib (Iressa; ZD1839), which been licensed in many countries for non-small-cell lung cancer. Pre-clinical evaluation of different tumour types has shown that an enhanced cytotoxicity has been observed when ZD1839 is used in combination with a number of conventional therapeutic agents, including cisplatin and radiation (Al-Hazzaa et al., 2005; Magne et al., 2002), but no report, at the time of writing, could be found regarding the combination of Iressa with PDT.

It has previously been reported earlier that treatment of epidermoid carcinoma A431 cells with hypericin-PDT irreversibly inhibited the tyrosine kinase activity of the epidermal growth factor (EGF) and insulin growth factor (IGF) receptors (Agostinis et al., 1995). This was also increased in the mouse lymphoma L5178Y-R cells when sensitised with silicon phthalocyanine (Xue et al., 1997) and murine mastocytoma P815 cells sensitised with benzoporphyrin derivative monoacid ring A and subjected to PDT (Granville et al., 1998). This increase in phosphorylation was later suggested as being, at least in part, secondary to Ca^{2+} ion release (Pereira et al., 2003). Recently, there has been reported evidence that intraperitoneal administration of C225, a monoclonal antibody that inhibits the EGFR and benzoporphyrin derivative monoacid-A (BPD) - based PDT acts synergistically to prevent or inhibit tumour cell growth and extend survival in a murine model of ovarian cancer peritoneal metastasis. The survival rate was approximately threefold greater than controls (no-

treatment) and 33% and 10% greater than treatment with only C225 or PDT, respectively (del Carmen et al., 2005).

1.8 Summary

Despite the advances in diagnostics and therapeutic techniques, the outcome and survival of patients suffering from head and neck carcinomas has remained poor, primarily due to late detection, and the tendency of the disease to develop loco-regional metastases. A key to its control is early detection and treatment and prevention of recurrence and metastasis. Invasion and metastasis represent complex multistage processes which require migration, invasion, angiogenesis and proteolysis. The invasion of tumour cells is associated with the secretion of various types of degrading enzymes. Several studies have identified the roles of MMPs, VEGF and uPA in this process (Yoshizaki et al., 2001; Franchi et al., 2002; Werner et al., 2002; Pacheco et al., 2002). Many methods were applied to the control of invasion using growth factor antagonists and signal transduction inhibitors, all of which have resulted in varied results and limited success.

PDT is a recent treatment modality for a variety of malignant tumours, including head and neck cancer. The technique is based on the combination of a photosensitive drug and visible light which result in cytotoxic effects on treated cells. The selective uptake by the hyperproliferating tissues of most photosensitive drugs, together with their intrinsic fluorescence and negligible dark toxicity, has expanded also their use as minimally invasive tools in the early detection of cancers and non-cancerous dysplasias.

In recent years, the use of PDT for treatment, and fluorescence and elastic light spectroscopy for early diagnosis, have been studied extensively, resulting in numerous publications, but there is little agreement on their efficacy. Furthermore, PDT is indicated for early tumour without metastasis, yet it is crucial to determine the influence of PDT on the metastatic process. Thus, this thesis hypothesises that

exposure of head and neck cancer tumour cells to PDT will affect particular cellular functions or processes that might reduce metastasis.

1.9 Aims

The aims of the study were:

- (i) to explore, using *in vitro* models, the influence of PDT, alone or in combination with either chemotherapy or small molecules, on cell toxicity, expression of $\alpha 5\beta 1$ and $\alpha v\beta 6$ integrins and growth receptors and expression of MMP-2, -9 and -13, uPA and VEGF in OSCC;
- (ii) to clinically evaluate the ability of an optical system, based on fluorescence and elastic scattering spectroscopy, to distinguish between normal, potentially malignant and malignant tissues and to develop an applicable algorithm that can be used as a standard for the subsequent analysis of “unknown” lesions;
- (iii) to clinically evaluate the potential of PDT as a tool for head and neck cancer treatment, using ALA sensitiser and red laser light;
- (iv) to clinically monitor the sensitiser photobleaching pre-, peri- and post-PDT in facial lesions, and compare this to clinical outcome.

Chapter 2

Materials and Methods

2.1 Materials

2.1.1 Chemical reagents and kits

| | |
|-----------------------------------|--------------------------------------|
| Bromophenol blue | Sigma Chemical Co., Poole, UK. |
| BSA | Sigma Chemical Co., Poole, UK. |
| Chromogenic substrates | Sigma Chemical Co., Poole, UK. |
| Cisplatin | Sigma Chemical Co., Poole, UK. |
| Collagen type-1 (rat tail) | BD Biosciences, Oxford, UK, |
| Coomassie brilliant blue R250 | Sigma Chemical Co., Poole, UK |
| DMEM | GIBCO/Invitrogen Corp., Paisley, UK. |
| DMF | Sigma Chemical Co., Poole, UK. |
| DMSO | Sigma Chemical Co., Poole, UK. |
| EGF | Sigma Chemical Co., Poole, UK. |
| FCS | PAA Laboratories, Somerset, UK. |
| Fibronectin (human) | Sigma Chemical Co., Poole, UK |
| Formalin. | Sigma Chemical Co., Poole, UK. |
| Foscan (m-THPC; temoporfin) | Biolitec Pharma. Ltd, Edinburgh, UK. |
| Glycerol | Sigma Chemical Co., Poole, UK. |
| Glycine | Sigma Chemical Co., Poole, UK. |
| Hydrochloric acid | VWR International, |
| Iressa Gefitinib ;ZD1839; | AstraZeneca, UK. |
| Isopropanol | VWR International, |
| Kaleidoscope prestained standards | Bio-Rad, Herts,UK, |
| Matrigel | Becton Dickinson (Oxford, UK). |
| MTT | Chemicon int., Temecula, CA |
| PBS (non-sterile tablets) | Oxoid, Hampshire, UK, |
| PBS (sterile) | GIBCO/Invitrogen Corp., |
| PD153035 | Calbiochem; UK |

| | |
|--|-------------------------------|
| Penicillin/streptomycin | GIBCO/Invitrogen Corp., |
| Plasminogen | Sigma, UK, |
| Protein assay reagent kit BCA | Pierce & Wariner, UK, |
| Quantikine ELISA kits (MMP-2 and-9 and VEGF) | R&D Systems, Oxfordshire, UK, |
| Scion image software | Scion Corp; USA, |
| SDS | VWR International, |
| TEMED | Sigma Chemical Co., |
| Triton X-100 | Sigma Chemical Co., |
| Trizma Base | Sigma Chemical Co., |
| Trizma Hydrochloride | Sigma Chemical Co., |
| Trypsin-EDTA | GIBCO/Invitrogen Corp., |
| Tween 80 | Sigma Chemical Co., |
| UVP Image store 5000 | Ultra-Violet Products, UK, |

2.1.2 Antibodies

All primary antibodies were monoclonal mouse anti-human.

| | |
|---|------------------------------|
| $\alpha 5\beta 1$, clone P1D6 | Chemicon International Inc., |
| $\alpha v\beta 6$, clone 10D5 | Chemicon International Inc., |
| EGFR, clone 102618 | R&D systems, |
| HGFR, clone 35309 | R&D systems, |
| FITC. F(ab') ₂ Rabbit anti-mouse | Dako, |

2.1.3 Drugs

The photosensitive drug, meta-tetrahydroxyphenyl chlorin (m-THPC; temoporfin; Foscan) 4 mg/ml stock was kindly provided as gift by Biolitec Pharma Ltd. (Edinburgh, UK). Foscan was stored according to the manufacturer's instructions. Cisplatin (cis-dichlorodiammineplatinum (II); CDDP; Sigma, UK), was prepared by

dissolving 100mg powder in 5ml dimethyl formamide (DMF) to give 20mg/ml stock. The tyrosine kinase inhibitors (TKIs), Gefitinib (Iressa; ZD1839) provided by AstraZeneca Pharmaceuticals (London, UK) and PD153035 (Calbiochem; UK) were dissolved in dimethylsulfoxide (DMSO) at stock concentration 10 mM and stored at -20°C . Further dilution of all drugs was performed in serum free medium (SFM; Appendix I). Control cells were treated with the medium containing an equal concentration of DMSO.

2.2 Cell culture

All cells were grown in a humidified atmosphere at 37°C and 5% CO_2 /95% air.

Solutions and media used can be found in the Appendix I.

2.2.1 Routine cell cultures

A series of keratinocyte cell lines were used as PDT targets in this study. They were H376-human oral squamous cell carcinoma cell line (Prime et al., 1990); VB6- β 6 transformed oral SCC cell line (Thomas et al., 2001a) and KB-human cervical cancer cell line (gifts from Professor O. Irwin; UCL Eastman Dental Institute, UK) and UP-human benign skin keratinocytes cell line (papilloma 16 virus-transformed), served as a control (Pei et al., 1991). Table 2.1 shows the origin and characteristics of each cell line.

Cells were retrieved from liquid nitrogen by thawing and cultured to confluence in keratinocyte growth medium (KGM; Appendix I). The cultures then were maintained in a humidified incubator at 37°C with 5% CO_2 /95% air atmosphere. All cells were allowed to attach for 24 h before replacing the medium with fresh culture medium. The medium was changed every 2-3 days until cells were reaching the end of log phase (semi-confluent).

Table 2.1 Clinical features of cell lines used in studies.

| Cell Line | Site of Tumour | Pathology of Primary Tumour |
|------------------|-----------------------|------------------------------------|
| UP | Skin | Well differentiated |
| KB | Cervix | Poorly differentiated |
| VB6 | Tongue | Well differentiated |
| H376 | Floor of the mouth | Well differentiated |

2.2.2 Passage of cells

Once the cells became confluent, the culture medium was removed and the monolayer was washed twice with phosphate buffered saline (PBS). The cells were then removed using 0.25% (w/v) trypsin with 0.05M ethylenediaminetetraacetic acid (EDTA). The cells were kept in a humidified incubator at 37°C with 5% CO₂ for 5 min or until cells were detached. Four times the volume of KGM was then added to each flask to inhibit further trypsin activity. The cell suspension was collected in a sterile 15ml tube and centrifuged at 1100rpm for 5 min. The medium was discarded and the cell pellet was re-suspended in fresh culture medium. The cells were seeded at 3×10^5 cells per 80 cm² Falcon tissue culture flask.

2.2.3 Cell freezing

The cells were examined under a phase light microscope to rule out any microbial contamination and then washed with PBS, trypsinized and centrifuged for 5 min at 1100rpm. Supernatant was discarded and the pellet was washed in 1ml of fresh KGM prior to cell counting (section 2.6.1). Approximately 2×10^6 cells were re-suspended in 900μl of culture medium containing 100μl dimethyl sulfoxide (DMSO). The 1 ml solution was transferred into a cryovial, labelled and transferred to an insulated container containing isopropyl alcohol and stored at -80°C overnight before being transferred to a liquid nitrogen tank for long term storage.

2.2.4 Cell thawing

The vials of frozen cells from liquid nitrogen were quickly thawed in a water bath set at 37°C. The thawed cell suspension was rapidly re-suspended in a pre-warmed culture medium in a sterile 15 ml tube and centrifuged at 1100rpm for 3 min. The medium was discarded and the cell pellet was re-suspended in 1ml of fresh culture medium and transferred to an 80 cm² flask containing 10ml of culture medium. The flask was maintained in the incubator, as described in section 2.1.

2.2.5 Cell density and viability

Cell density was determined using an improved haemocytometer (Assistant, Germany) viewed under a phase-contrast light microscope at X10 magnification. Cells were trypsinized and re-suspended in 1ml growth medium. 10µl of the cell suspension was placed at the edge of the haemocytometer glass coverslip. The cells were counted within the four major squares and the average value was calculated. The viable cells were determined under the light microscope, at the same time of each passage by mixing 10µl of cells suspension with an equal volume of 0.4% trypan blue (prepared in 0.81% sodium chloride and 0.06% potassium phosphate). Unstained cells were counted and considered viable and cell viability percentage was determined by the ratio of viable cells to the total number of cells.

2.2.6 Cell viability assay

Cell viability was determined both by the trypan blue dye exclusion test (section 2.1.4) and MTT colorimetric assay. MTT is based on cellular conversion of the tetrazolium compound (3-(4, 5-dimethylthiazol-2-yl)-2,5-diphenyl-2H-tetrazolium bromide; MTT) into a purple formazan product. Optical readings were performed at 570 nm using a microplate reader (Multiscan, MCC/340; Flow Laboratories, Herts,

UK). Appropriate blanks were subtracted from the test absorbance figures. As results for the two methods were well correlated for all cell lines, the MTT assay was subsequently used routinely.

2.2.7 Cell growth assays

Cell lines were trypsinized, counted and re-suspended in KGM and seeded into 96-well plates at a cell concentration of 2×10^3 cells per well. Cells were allowed to attach for 24 h in a humidified incubator at 37°C with 5% CO₂. MTT solution was added to wells and the total number of cells was calculated from the standard curve (previously prepared from a known number of cells). Readings were taken every 24 h for 7 days.

2.3 Photodynamic therapy

2.3.1 Photosensitisation

Sub-confluent cells were harvested, counted and seeded into 96-well plates in KGM at cell concentration of 3×10^4 cells per well. Cells were allowed to attach for 24 h at 37°C before Foscan was added at concentrations of 0.25, 0.5, 1, 2 and 4 µg/ml in serum free KGM. The cells were incubated with Foscan in darkness at 37°C in 5% CO₂ for 3 h and 24 h unless otherwise stated. Cells not exposed to Foscan were used as controls.

2.3.2 Cell irradiation

Cells were washed three times in PBS and new serum free KGM was added. Cells were then exposed to 652 nm diode red laser (Diomed Ltd, Cambridge, UK). The laser beam was transmitted through a microlens fibre, giving a fluence (energy) rate of 25 mW/cm². The distance from the distal end of the fibre to the bottom of the well and the exposure time were automatically adjusted by the laser machine

microprocessor to obtain various energy densities (fluence) of 0.25, 0.5, 1, 2, 3 and 4 J/cm². Percentage phototoxicity was determined by the MTT assay after 3 and 24 h.

2.4 Combination treatment

2.4.1 PDT and CDDP cytotoxicity assay

Cytotoxicity of CDDP combined with PDT was also determined by MTT assay. The UP, VB6 and H376 cells were seeded into 96-well plates at a cell concentration of 3x10⁴ cells per well and allowed to attach for 24 h at 37°C before KGM was replaced with serum free KGM containing CDDP (2, 4 and 8 µg/ml) and Foscan (0.5 µg/ml). After 24 h of incubation at 37°C, cells were washed with PBS and new serum free KGM was added. Cells then were exposed to 0.5 J/cm² (20 s) of red light. Cytotoxicity for each cell line was then determined by MTT assay after 24 h. Cells not exposed to treatment were used as controls.

Cytotoxicity of CDDP and PDT, each alone was also determined by MTT assay. For CDDP alone, the UP, VB6 and H376 cells were seeded into 96-well plates at a cell concentration of 3x10⁴ cells per well and allowed to attach for 24 h at 37°C. A range of concentrations between 2 and 40 µg/ml of CDDP in serum free KGM were added for 24 h before cytotoxicity by MTT assay was determined. Cells not exposed to CDDP were used as controls. For PDT alone, cells were incubated with Foscan at 0.5 µg/ml. After 24 h of incubation at 37°C, new Foscan free culture medium was added before exposure of the cells to red light at 0.5 J/cm² (20 s). Cytotoxicity for each cell line was then determined by MTT assay after 24 h. Cells not exposed to PDT were used as controls.

2.4.2 PDT and TKI cytotoxicity assay

Cytotoxicity of Iressa or PD153035 combined with PDT was determined by MTT assay. The UP, VB6 and H376 cell lines were harvested, counted and seeded into 96-well plates at a cell concentration of 3×10^4 cells per well and for 24 h at 37°C. After attachment, KGM was replaced with serum free KGM contained Iressa between 0.05 and 10 μ M or PD153035 between 0.5 and 20 μ M and 2 doses of Foscan (0.25 μ g/ml; PDT-1) or (0.5 μ g/ml; PDT-2) were added for 24 h at 37°C. After incubation, new drugs free medium was added and cells then exposed to 0.5 J/cm² of red light. Cytotoxicity for each cell line was then determined by MTT assay after 24 h. Cells not exposed to treatment were used as controls.

Cytotoxicity of Iressa and PD153035, each alone, was also determined by MTT. For Iressa or PD153035, the UP, VB6 and H376 cell lines were harvested, counted and seeded into 96-well plates at a cell concentration of 3×10^4 cells per well for 24 h at 37°C. Following attachment, KGM was replaced with serum free KGM contained Iressa between 0.05, and 50 μ M or PD153035 between 0.5 and 20 μ M was added. After 24 h of incubation at 37°C, Iressa and PD153035 cytotoxicity was determined by MTT assay. Cells not exposed to any treatment were used as controls. For PDT alone, Foscan at (0.25 μ g/ml; PDT-1) or (0.5 μ g/ml; PDT-2) was added for 24 h cells then were exposed to 0.5 J/cm² of red light. Cytotoxicity for each cell line was then determined by MTT assay after 24 h. Cells not exposed to PDT were used as controls.

2.5 Cell detachment assay

The detachment assays of control and treated cells were studied on 24-well culture plates (Falcon; Becton Dickinson, UK). Cells were seeded at a density of 1×10^5 cells/well in 1ml of KGM. The cells were allowed to attach and grow until confluent. The medium was aspirated and the cultures were then washed twice in PBS. Thereafter 0.1ml of trypsin/EDTA was added. The cells were then re-incubated at 37°C for 5 min. The number of detached cells was counted using a haemocytometer. The results were expressed as the ratio of treated cells that had detached compared to the untreated control.

2.6 Cell adhesion assay

The adhesion assays of control and treated cells to fibronectin, collagen type I or Matrigel were studied on 96-well microtiter plates (Falcon; Becton Dickinson, UK). Wells were coated with 50 μl of 10 $\mu\text{g/ml}$ of fibronectin, collagen type I, or Matrigel and allowed to dry for 1 h in a humidified incubator at 37°C in 5% CO_2 /95% air atmosphere. The wells were subsequently washed with PBS containing 10% FCS and then blocked by incubation in PBS containing 0.5% (w/v) bovine serum albumin (BSA; Sigma, UK). The wells were then returned to the humidified incubator for 30 min before being washed with PBS containing 10% FCS. Treated and control cells were harvested and plated into the coated wells at a concentration of 4×10^4 cells per well in 100 μl of SFM. Plates were incubated for 1 h to allow cells to adhere.

Following incubation, the medium and non-adherent cells were removed by immersion the plate gently twice in PBS supplemented with 1mM CaCl_2 and 0.5mM MgCl_2 . To each well, 100 μl of SFM was then added and allowed to equilibrate for 1 h at 37°C with 5% CO_2 . Thereafter 10 μl of MTT solution was added to each well and cells were incubated for 4 h. The relative absorbance of the coloured product of MTT was measured at 570 nm and the relative number of cells in each well was calculated from a standard curve prepared by measuring the optical density of known

number of cells. The non-specific adhesion (Adhesion to BSA coated wells) reading was subtracted and the results were expressed as mean percentage of attached cells in each well compared to the number of original seeded cells, which was expressed as 100%.

2.7 Protein assay

2.7.1 Preparation of supernatants

The treated and control cells were detached with trypsin/EDTA and seeded into 24-well tissue culture plates, at a concentration of 1×10^5 cells per well in 0.5ml of additive free medium (AFM; Appendix I) supplemented with 10% FCS for 24 h at 37°C. Culture medium in each well then was replaced with new 0.5ml of serum free AFM and supernatant of each cell line sampled after 24 h, at which time conditioned medium was cleared of cells and debris by centrifugation at 4000 g for 10 min, followed by protein estimation using the colorimetric BCA protein assay reagent (Pierce Warriner, UK). Cell media of non-treated cultures was considered as controls.

2.7.2 Determination of total protein

The amount of total protein concentration within each cell sample in conditioned medium was determined using a colorimetric BCA. Briefly, a series of protein concentrations for a standard curve was prepared by dilution of BSA at 1:2, 1:5, 1:10, 1:100 or 1:1000 v/v in PBS. Working reagent was prepared by mixing 50 parts of Reagent A with 1 part of Reagent B. Then 10µl of conditioned medium samples or standard were added into each well of a 96-well microtiter plate, followed by 200µl of working reagent. The plate was then incubated at 37°C for 30 min. The relative absorbance at 652 nm was determined using a plate reader (Multiscan, MCC/340; Flow Laboratories, Herts, UK). The standard curve was created by

plotting the protein concentrations versus absorbance, and the protein concentrations of test samples were calculated from this.

2.7.3 Zymography

Introduction

Zymography is a simple, sensitive, quantifiable, and functional approach used to investigate and quantify the expression of matrix-degrading metalloproteinases (MMPs). The standard method for zymography is based on the use of SDS-polyacrylamide gels co-polymerized with a protein substrate, in particular gelatin, or casein. Proteases that have the ability to renature after removal of SDS and to exert proteolytic activity on a co-polymerized substrate can be analyzed with this method. MMP-2 (gelatinase A, 72 kD) and MMP-9 (gelatinase B, 92 kD) can be detected on gelatin zymograms and MMP-7 on casein gels. Staining of the gel with commassie blue allows the bands of proteolytic activity to be detected as clear bands of lysis against a blue background (Figure 2.1). Based on the molecular weights, these bands reflect inactive and active MMP-2 and inactive and active MMP-9, and the band intensity is related to the amount of protein loaded.

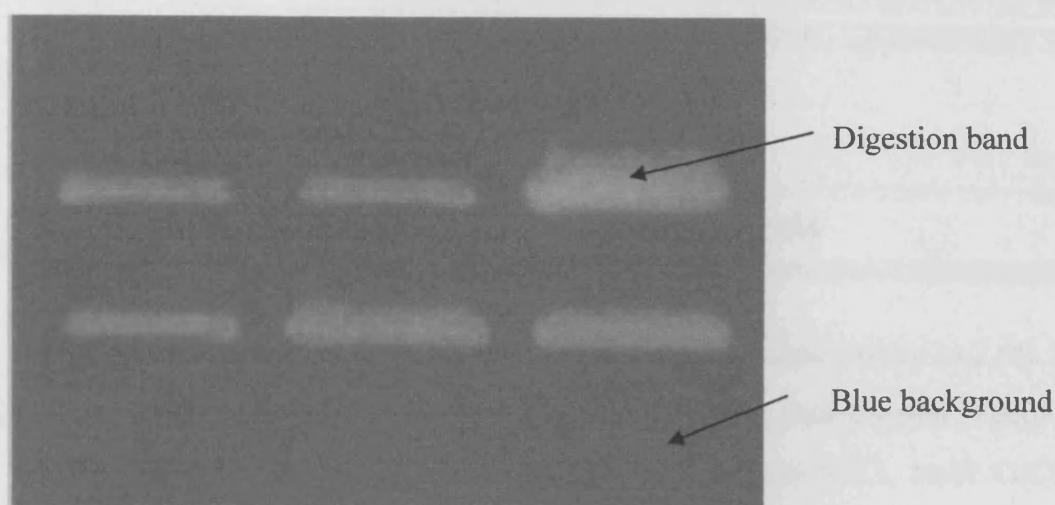


Figure 2.1 Representative picture of gelatin zymography (clear area represent areas of enzymatic digestion of gelatin gel).

Electrophoresis of supernatant samples

In the present study, MMP-9 and MMP-2 activities were analysed using SDS-PAGE substrate gels. Gelatin (BLOOM 300, Sigma, UK) was added to 12% acrylamide separating gel at a final concentration of 1mg/ml, and poured using a pre-assembled vertical gel electrophoresis apparatus (Mini-PROTEAN[®] II cell; Bio-Rad). The gel was immediately overlaid with isopropanol to inhibit the air interface, and allowed to set for about 30 min at room temperature. After checking the setting of the gels, the isopropanol was discarded and the tops of gels were rinsed with distilled water and dried with filter paper. The stacking gels (Appendix 1) were poured into the top of the resolving layer. Again, the stacking gels were poured and the proper comb was seated before being allowed to set for 20-30 min. The comb was removed and the gels were fitted into the electrophoresis tank before an appropriate amount of SDS-running buffer (Appendix 1) was added. The supernatant samples with equal protein were diluted 1:1 in non-reducing sample buffer (Appendix 1) and loaded into the wells using capillary disposable pipette tips. The molecular weight marker (Kaleidoscope pre-stained standards) was prepared according to the manufacture's

instructions and loaded into one well. Samples were run at 100V through the stacking gel stage and the current then elevated to 120V for approximately 2 h or until the samples approached the resolving bottom gel.

Renaturing, developing and staining of gels

The gels were separated from the plates with care and washed twice in 2.5% Triton X-100 for 30 min at 37°C to remove SDS. The gels were then allowed to equilibrate in developing buffer containing 50mM Tris-HCL, 0.2mM NaCl, 5mM CaCl₂ and 0.02% Triton X-100. The buffer was discarded and changed with fresh developing buffer and incubated overnight at 37°C. Following development, the gels were gently immersed in Coomassie Blue stain (Appendix 1) for 30 min at room temperature before being de-stained with Coomassie de-stain (Appendix 1) for 3-4 h until the enzyme activity bands were obviously clear as white bands against a blue background. Stained gels were captured under illumination using the UVP Image store 5000 (Ultra-Violet Products, UK) and obtained Images saved on a personal computer (PC). The images were analysed quantitatively using the Scion image software (Scion, USA). The intensity bands was measured by densitometric analysis, and comparisons were made within each gel to determine the relative changes in MMP activity. Data for each zymogram were expressed as a relative change in MMP activity, and these relative changes were compared with repeat experiments. Direct comparison between separate gels was not made as the intensity of background staining was variables.

2.7.4 ELISA

To quantify the amount of specific protein in cell culture supernatants, commercial ELISA kits for human MMP-2 (total) , MMP-9 (total) , pro MMP-13 and VEGF (R&D Systems, Inc. Europe) were used. The assay is based on a two site ELISA 'sandwich' format and performed according to the manufacturer's instructions. Briefly, cell supernatants were prepared as for zymography, and 100µl sample was

added to each well and immobilized MMP or VEGF detected by the horseradish peroxidase labelled Fab' antibody directed to MMP-9, MMP-2, MMP-13 or VEGF. The reaction was stopped by addition of an acid solution (2 N H₂SO₄) and the intensity of the resultant colour change read at 450 nm on a spectrophotometer (Multiscan, MCC/340; Flow Laboratories, Herts, UK). The concentration was determined by interpolation from a standard curve using known concentration of MMP-9, MMP-2, MMP-13 or VEGF standards as supplied.

2.7.5 Assay of plasminogen activator (PA)

The activity of PA in 50µl of cell supernatants (prepared as for zymography) was indirectly estimated by hydrolysis of a specific chromogenic substrate H-D-Val-Leu-Lys-paranitroanilide 2HCl (2.5mg/ml; Cs -2251; Chromogenix, UK) in the presence of Human Glu-plasminogen (15µM; Enzyme Research Labs, UK) in Tris-HCl buffer, 150 mM, pH 7.4) at 37°C for 2 h. The intensity of formed H-D-Val-Leu-Lys-OH + pNA was measured spectrophotometrically at 405 nm using a microplate reader (Multiscan, MCC/340; Flow Laboratories, Herts, UK). The concentration of uPA (This assay measure both tPA and uPA, However, since monolayer cells were tested, this experiment assumed that most of secreted PA was uPA) was estimated by interpolation from standard curve using known concentrations of uPA standards.

2.8 Migration assay

The haptotactic assay of malignant cells, which implicates the liability of migrating cells to move towards a gradient of coated ligand, was studied using a modified Boyden chamber assay system. The two clamberers were divided by a tissue culture treated poly carbonate filter with 8-µm pore size, 6.5 mm diameter and 10µm thickness (Transwell®; Costa). The lower surface of the filter was coated with fibronectin (10µg/ml) or collagen type I (40µg/ml), both diluted in PBS, and left to dry for 1 h at 37°C. Non-specific sites on the filter of each chamber were blocked by adding 100µl of migration buffer (DMEM, F12 3:1 and 5% BSA) into the upper

chamber and 600µl of migration buffer into the lower chamber for 1 h at 37°C. The buffer in the upper chamber of triplicate wells was replaced with 100µl of migration buffer containing 1×10^5 of treated cells. The untreated cells were used as controls. The lower chamber had migration buffer replaced with fresh buffer. The chambers were incubated for 3 h at 37°C with 5% CO₂. Following this incubation period, the filters were fixed for 10 min in 10% neutral buffered formalin. The filters were then stained with 0.5% crystal violet in ethanol (w/v) for 10 min and washed in deionised water. The cells on the upper surfaces of the filters were wiped off with cotton swabs and the filters left overnight to air-dry. The filters were cut and mounted in DPX on glass slides for microscopy. The number of remaining cells was counted in random high powered fields (X40) (at least 6 random positions per filter, as determined by cumulative frequency analysis). The results were expressed as mean values per microscope field \pm standard deviation.

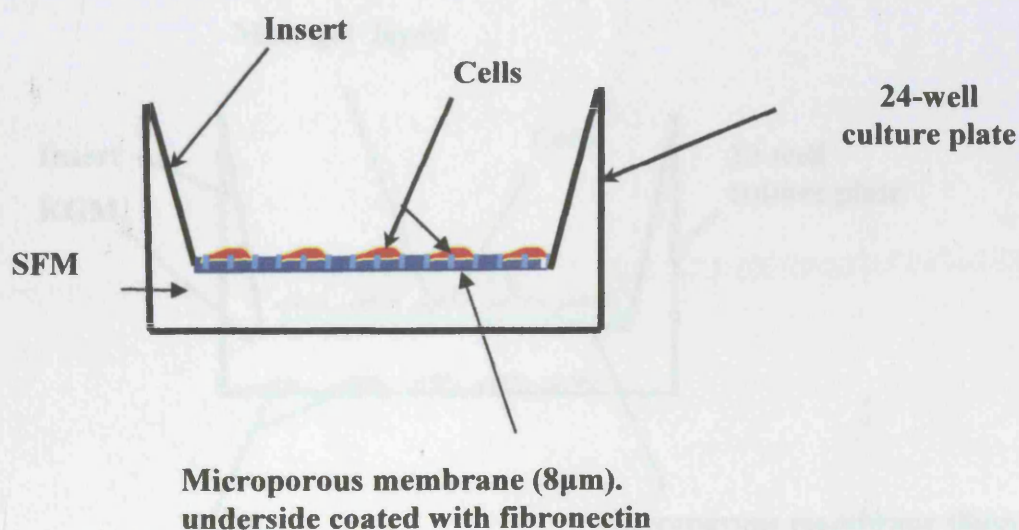


Figure 2.2 Schematic illustration of cell migration assay. SFM=serum free medium

2.9 Invasion assay

Chemotaxis assay of tumour cells, which implies cell movement toward a soluble chemo-attractant gradient, was studied using poly carbonate membranes with 8- μm pore size, 6.5mm diameter and 10 μm thickness (Transwell®; Costa). The inserts were coated with 40 $\mu\text{g}/\text{cm}^2$ of Matrigel diluted in PBS. The gel was allowed to polymerize for 1 h at 37°C. The treated and control cells were trypsinised and counted. 1×10^5 cells in 200 μl of SFM were added to the upper chamber of triplicate wells. The lower chambers were filled with KGM, which would behave as a chemo-attractant. Cells then were incubated for 72 h at 37°C in 5% CO_2 atmosphere. Cells that had invaded the lower chamber, including those bound to the under-surface of the filter, were trypsinised and counted. To ensure that the reduction of invasion of PDT treated cells was not due to the loss of initial cell attachment, the cell adhesion assays on Matrigel were carried out at the same time as the invasion assays.

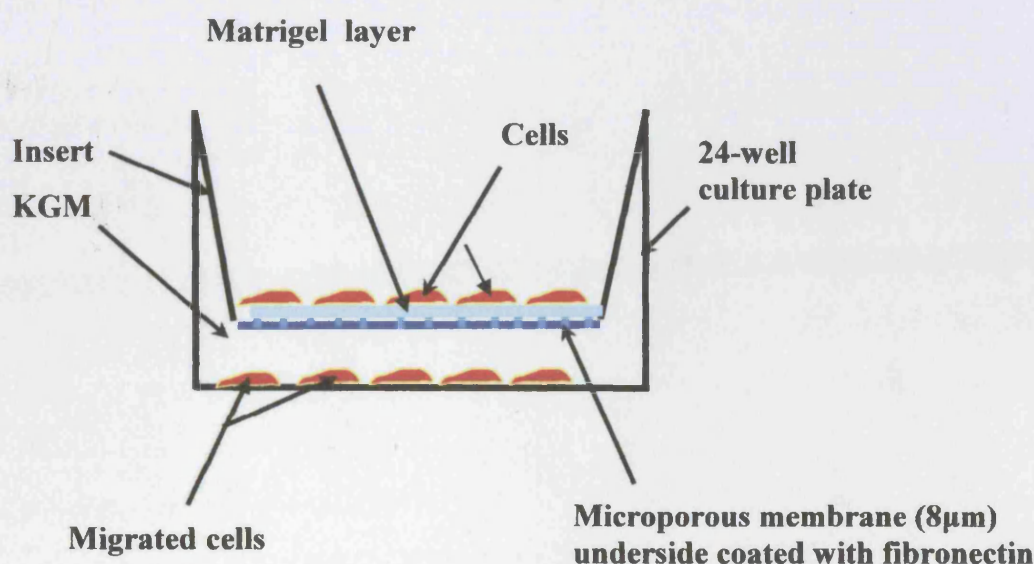


Figure 2.3 Schematic illustration of cell invasion assay

2.10 Photomicrography

The UP, VB6 and H376 cells were washed with PBS, trypsinized and counted. The cells were then added to a 25cm² tissue culture flasks at a concentration of 2×10^5 cells per flask. The flasks were incubated at 37°C with 5% CO₂ until confluent. The morphology of control and treated cells was determined by viewing the cultured cells under a phase-contrast-microscope (Olympus CK2) at a magnification of X20. The pictures were taken by digital camera (Nikon Coolpix 4500) at 0, 24 and 48 h post treatment. Untreated cells served as controls and photographed at the same time points as the test cells.

2.11 Flow cytometry

Flow cytometry uses the principles of light scattering, excitation, and emission of fluorescent light from molecules in or attached to cells. Cells are focused in a sheath of PBS before intercepting an optimally focused laser light source. The cells are excited with light with a specific wavelength. Following excitation, the light photons can be emitted as fluorescence or scattered either in a forward direction (FSC) with low angle ($<2^\circ$) to the light axis (proportional to cell size), or at scatter angle (90°) known as 'side scatter' (SSC) (proportional to cell granularity). The released light from the cells is then converted into electrical pulses and processed by a series of linear and log amplifiers. Logarithmic amplification is most often used to measure fluorescence signals in cells, which is considered to be proportional to the amount of target antigen attached via the fluorophores (Mandy et al., 1995). The data were then stored on computer for future analysis.

2.11.1 Preparation of cells for analysis

Treated and control cells from confluent or late log-phase cultures were washed twice with PBS and released by trypsin/EDTA (0.25% w: v, 5 mM EDTA) used to reduce the proteolytic breakdown of the extracellular domain of surface proteins. The cells were then centrifuged, counted and washed once in washing buffer (PBS solution supplemented with 10% v/v FCS) at 1100rpm for 5 min. The cells were pelleted into round bottom polystyrene fluorescence activated cell sorting (FACS) tubes (Becton Dickinson) in 100 μ l washing buffer at a concentration of 1×10^5 cells per tube. Cells were incubated with primary antibodies to EGF, HGF, $\alpha 5\beta 1$ and $\alpha v\beta 6$ cell receptors (1:200 dilution) for 40 min at 4°C , control cells were incubated with washing buffer only. Following incubation, cells were washed twice with washing-buffer. Fluorescein isothiocyanate (FITC)-conjugated rabbit anti-mouse anti-sera secondary antibody (1:250 dilution) was added to the cells for 30 minutes at 4°C . The cells were then washed twice in washing-buffer and resuspended immediately in 0.5 ml of washing-buffer. The size, granularity and fluorescence intensity of 10,000

individual cells were analysed using the FACScan flow cytometer (Becton Dickinson) for duplicate samples from three separate experiments.

2.11.2 Data acquisition and processing

Labelled cells were passed through the flow chamber and each individual cell was then subjected to the laser beam of a specific wavelength that matched the excitation wave length of the attached label. Emitted signals (FCS, SCC and fluorescence) were transmitted from the flow cytometer and the scatter-window was set to eliminate dead cells (usually about 6% in control cells and up to 20% for PDT-treated cells). Foscan fluorescence intensity in FL3-H and the expression of $\alpha 5\beta 1$ and $\alpha v\beta 6$ integrins, EGF and HGF receptors in FL1-H were analysed and stored digitally on the attached computer (Quadra 650, Apple Macintosh). For each cell label, two separate tubes were analysed. A dot plot was created and FSC versus SCC was produced following manual gating, the arbitrary units obtained by the software programme. The intensity of sample-emitted fluorescence in FL1-H and FL3-H was represented by a frequency distribution histogram and gated in accordance with negative controls. The mean fluorescence value was calculated.

2.12 Detection of oral premalignancy

It has become universally known that early detection of premalignant/ malignant lesions can substantially reduce the risk or improve the prognosis in oral cancer.

2.12.1 Fluorescence spectroscopy (FS)

2.12.1.1 Patients

Seventy-one patients (mean age 59 years, range 37-81 years) with clinically suspicious oral leukoplakia took part in this study in the Maxillofacial Unit, University College Hospital (UCH), London. The trial protocol was approved by the UCH Joint Research and Ethics Committee. An information sheet explaining the aim of our study in simple non-scientific terms was given to each patient and those who then consented were examined. FS was then used to examine the suspicious area for each of those patients prior to surgical biopsy. Inclusion criteria were patients over 18 years of age who presented with suspicious oral leukoplakia, while the exclusion criteria were women who were or might have been pregnant. However, there are no known teratogenic effects that FS might induce. The main reason behind this is the anxiety that might be triggered during the examination.

Two hours prior to examination, a topical application of 0.4% (w/v) 5-ALA (supplied by the UCH pharmacy) has applied to the oral mucosa via an oral rinse. This was prepared by dissolving 200mg 5-ALA in 50ml of mineral water. The patient is required to rinse the mouth for 15 min, and maintain 3 x 5 min of continuous contact to achieve the maximum saturation of the mucosa with the solution. The solution was prepared shortly before application to avoid unwanted effects reported from the instability of such solutions (Novo et al., 1996). Following this, the patients were allowed to rinse with mineral water prior to examination but they were warned to avoid illumination and brushing of teeth. We have considered this relatively short incubation period to be applicable for routine clinical diagnosis;

Leunig A et al. found that the absolute fluorescence intensities in tumour tissue decreased 3 h following the 5-ALA application and this could lead to the reduction of contrast between pre-malignant/malignant and healthy tissue (Leunig et al., 1996).

2.12.1.2 The system

The apparatus (Figure 2.4) consisted of a light optical power output light delivery system that includes a xenon-arc lamp (Medical Light Technologies Ltd, UK) whose output was filtered by a long pass filter (BG12, Schott Glass, Germany) and a bandpass filter centred at 425(\pm 17) nm (Corion Corp., MA, USA). An optical endoscope was used for both illumination and detection of the tissue fluorescence. The fluorescence image of the tissue was acquired by a high sensitivity single chip charge-coupled device (CCD) colour camera (Sensicam, Personal Computer Optics, Germany) integrated with red/green/blue (RGB) mosaic filter and coupled to the endoscope to facilitate examination of all tissues. The images were captured by a frame-grabber (0.6 s integration time) fitted with an analogue/digital converter (ADC) and analysed and displayed by personal computer loaded with software (Sensicam, Personal Computer Optics, Germany). This allowed fast computation and analysing times. In addition, the RGB system provides wavelength separation allowing only red and green detection for ratio imaging. The output power of the blue light at the endoscope tip was kept to approximately 2mW/cm²; this was found to minimise the photobleaching of the photosensitiser (Scott et al., 2000).

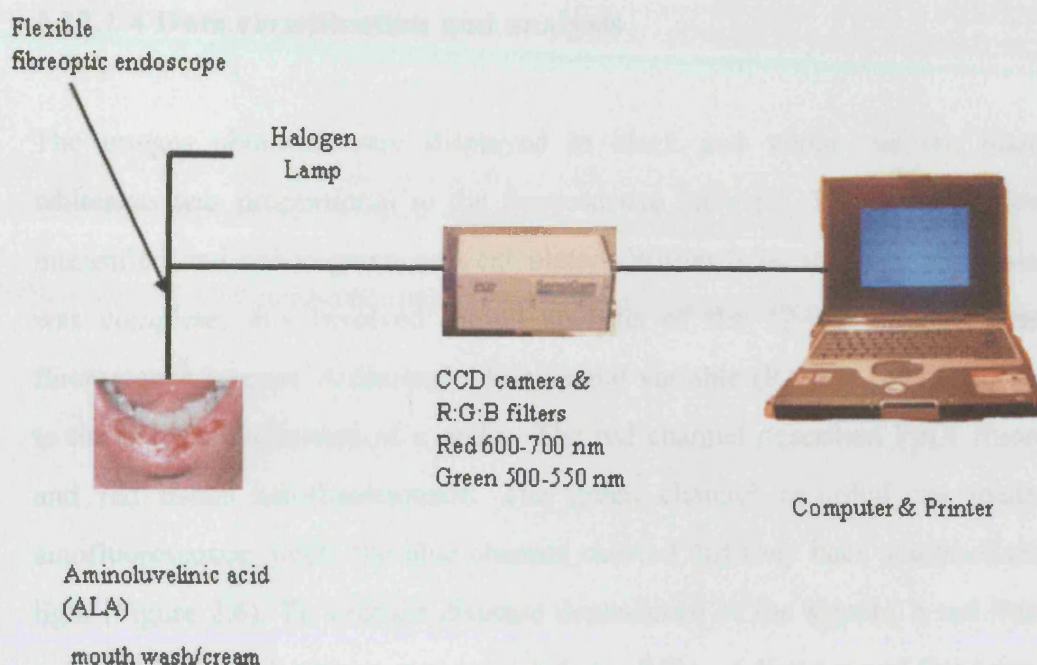


Figure 2.4 Schematic diagram of the fluorescence spectroscopy system.

2.12.1.3 Measurement procedures

All measurements were taken at the Maxillofacial Surgery Unit, UCH. All histopathological samples were examined by the Histopathology department at UCH, London. The premalignant/malignant and normal tissue accumulated PpIX was excited via an endoscope with a blue light generated by a filtered high optical power output xenon-arc lamp, following excitation, PpIX and tissue autofluorescence were detected by a sensitive single chip CCD colour camera connected to a personal computer. Following examination, the images produced (Figure 2.5) were analysed by the computer to identify the area of the highest fluorescence signal. Then this area was marked with blue ink in a diamond pattern. Subsequently, the area was subjected three times to fluorescence spectroscopy in order to reduce the error and ensure the reproducibility at each biopsy site by quick calculation of red-to-green intensity ratio. To prevent any optical interference, care was taken not to capture any fluorescence image after marking.

2.12.1.4 Data classification and analysis

The images obtained were displayed in black and white and the intensity of whiteness was proportional to the fluorescence intensity. The captured image was intensified and red-to-green was calculated. Within 0.2s, the data processing stage was complete; this involved digital analysis of the 12-bit red, green and blue fluorescence images. A dimensionless spatial variable (R) was calculated according to the pixel coordination of x and y. The red channel described PpIX fluorescence and red tissue autofluorescence. The green channel recorded the green tissue autofluorescence, while the blue channel showed diffusely back scattered excitation light (Figure 2.6). To exclude distance dependence of the signals, a red fluorescent spot within normal mucosa was recorded at a different distance and fixed integration time.

Following fluorescence imaging, 71 acquired biopsies (from 71 patients) were obtained from various oral sites and sent for histopathology studies. These biopsies were examined histopathologically and were found to be either normal (normal, inflammatory or hyperkeratotic) or potentially malignant (mild, moderate or severe dysplastic). To allow the correlation of fluorescence images and histology, the red PpIX fluorescence and green tissue autofluorescence for each site were calculated. Histopathological reports were considered as standard and correlated with red to green ratios measured in terms of oral changes. The ratios (red/green) were set at 1.2 and 1.3 as the threshold values for demarcation between normal and dysplastic.

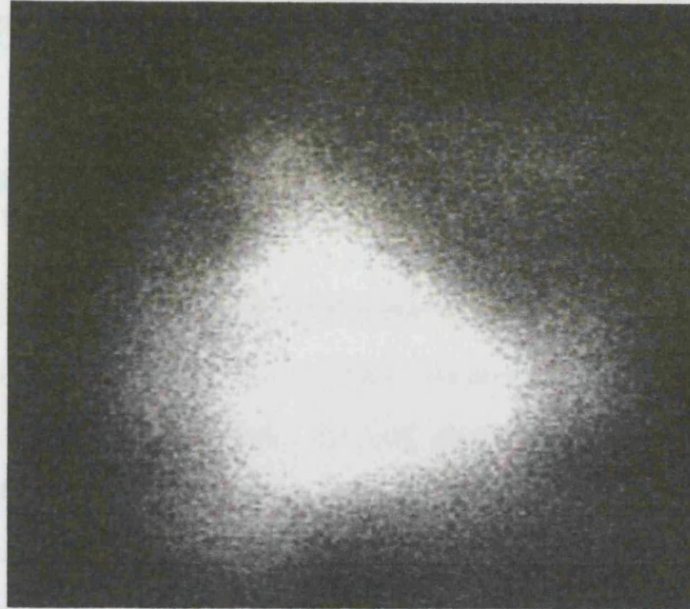


Figure 2.5 Black and white tissue fluorescence image. Bright area represent the highest fluorescence intensity whereas low intensity in black area

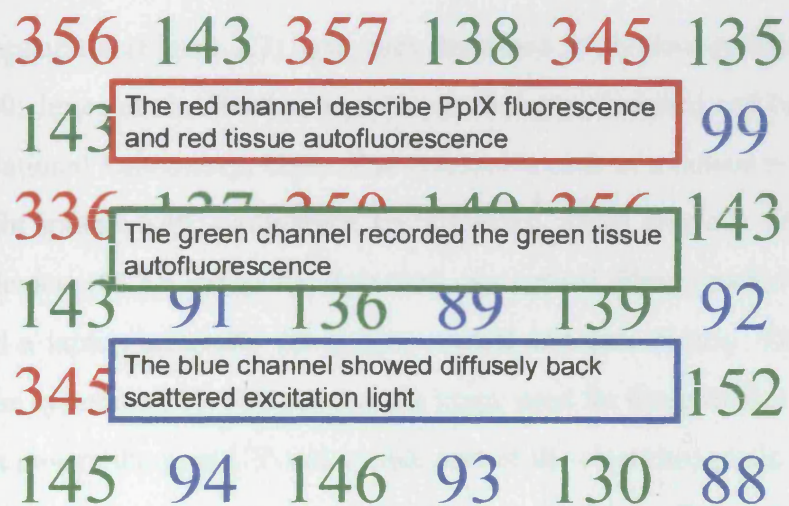


Figure 2.6 Example of magnified pixel colour fluorescent intensity values.

2.12.2 Elastic scattering spectroscopy (ESS)

2.12.2.1 Patients

Twenty-five patients (13 male and 12 female), mean age 52 years, age range 41–67 years, with clinically suspicious oral leukoplakia took part in this study in the Maxillofacial Unit, UCH, London. The trial protocol was approved by the Joint Research and Ethics Committee of UCH. An information sheet explaining the aim of the study in simple non-scientific terms was given to each patient, and those who consented were further examined. ESS was used to examine the suspicious area of each of those patients prior to surgical biopsy. Inclusion criteria were patients over 18 years of age who presented with one or more suspicious oral lesions; while the exclusion criteria were women who were pregnant, since this group of patients are usually more anxious when attending hospitals.

2.12.2.2 The system

The ESS apparatus (Figure 2.7) have been described in previous publications, (Bigio et al., 2000; Jerjes et al., 2004) is a prototype that was designed and built at the Los Alamos National Laboratory, USA. The system consists of a pulsed xenon-arc lamp for the light source, a PC-compatible spectrometer, which employs a linear charged coupled device (CCD) array for detection, an optical fibre (graded-index) based probe, and a laptop computer for system control and data display. The wavelength range of the system is 300–900 nm, but the range used for these studies was 330–750 nm, which covers the near UV and visible part of the electromagnetic spectrum; the range of the spectrum usually covers the light emitted by cellular and sub-cellular organelles. The output of the arc lamp is coupled to the illumination fibre, which has a core diameter of 400µm. A second, 200µm diameter fibre alongside the illuminating fibre, collects the scattered light from the tissue and guides it to the spectrometer where an optical spectrum is generated for further processing; centre-

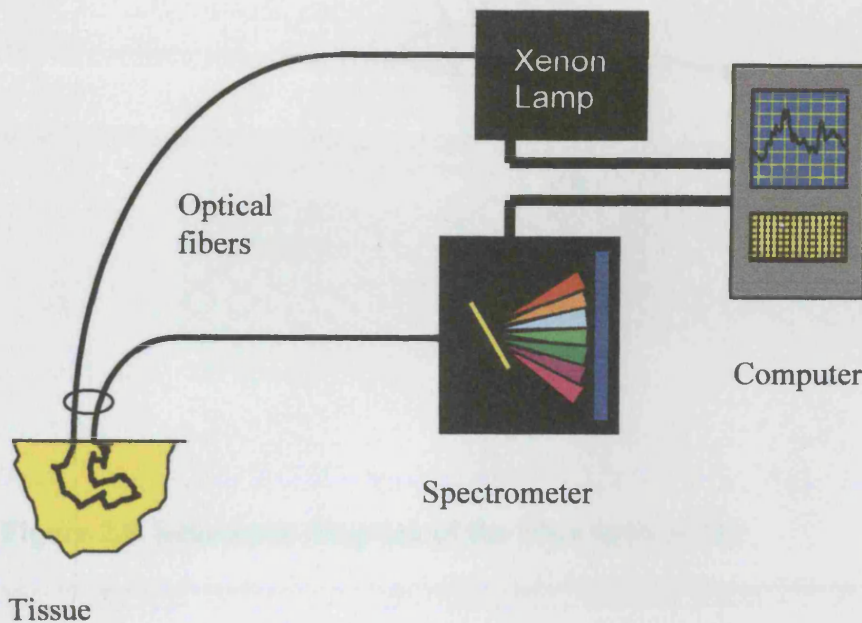


Figure 2.7 Schematic illustration of the elastic scattering spectroscopy system.

The system probe (Figure 2.8) was designed to be used in (gentle) optical contact with tissues, and incorporates two optical fibres, one to transmit the light into the tissue and the other one for collecting the scattered light from tissue; the two probes are built-in one bigger probe so the viewer can see only the latter. Placement of the probe in direct contact with the tissue avoids interference with specularly reflected light. With this probe geometry, the volume of tissue visited by the collected photons occupies $\approx 1\text{mm}^3$. This has been determined from computational simulations using Monte Carlo code, which incorporates Mie theory for the details of the scattering events.

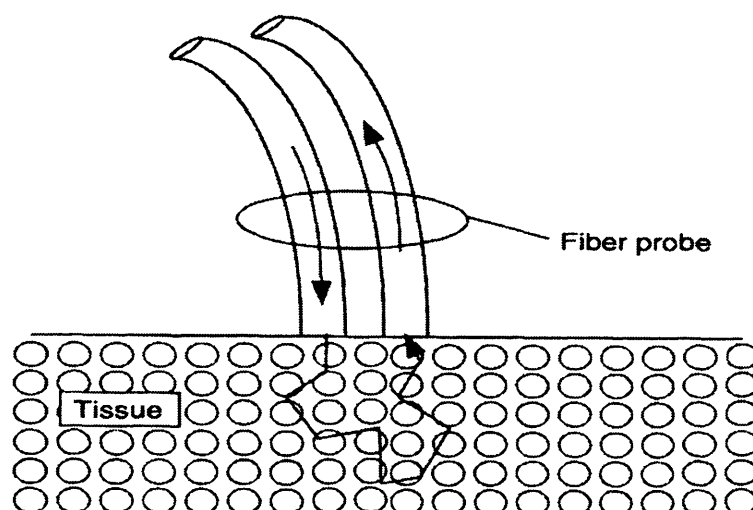


Figure 2.8 Schematic diagram of the fibre optic probe

2.12.2.3 Measurement procedures

In clinical use, the suspected tissue areas were marked and the tip of the fibre probe was momentarily placed in direct contact with the suspected lesion. The measurement then was activated at the keyboard. The system automatically takes a background measurement without firing the lamp, followed immediately (within-100 ms) by an ESS measurement with the pulsed lamp was been triggered, and then subtracts the background spectrum from the ESS spectrum. The entire measurement processes (activating the spectrometer, triggering the arc lamp, reading the detector array with an analogue/digital (A/D) converter etc.) were computer controlled by a laptop PC. This allowed both accurate and reproducible measurements within the clinical setting. It provides also the clinician with the advantage of rapid data acquisition and a display time of less than 1 s for each site measured. Three optical measurements were acquired from each of the suspected lesions; 1st measurement from the centre, 2nd from the periphery of the lesion and in between the two measurements the 3rd was acquired.

Following the optical readings, a surgical biopsy was taken, preserved in formalin, processed in H&E stain and examined by the histopathologist; digital pictures have been taken and sketches have been made for all the suspected sites to ensure that all sites are easily identified by the pathologist and hence reduce any chance of false results. The tissue samples (25 biopsies in total) were graded as normal, hyperkeratotic, mild dysplastic, moderate dysplastic, severe dysplastic and carcinoma in situ. The elastic spectrum of each lesion was correlated to its histology.

In this study, spectra were combined together although they originated from histologically different oral sites (floor of mouth, tongue, cheek); before doing this, each acquired spectrum from a particular site was compared to a spectrum acquired from a histology-similar normal oral site; the intention here was to reduce discrepancies in the readings.

2.13 Monitoring of PDT

2.13.1 Patients

Fourteen patients (mean age 66 years, range 39-78 years) treated with ALA-PDT for superficial BCC of the scalp and the face took part in this study at the Maxillofacial Unit, UCH, London. The trial protocol was approved by the Joint Research and Ethics Committee of UCH. An information sheet explaining the aim of the study in simple non-scientific terms was given to each patient who was then consented prior to examination. Inclusion criteria were patients over 18 years of age diagnosed with superficial BCC. Excluded from the study were pregnant or breastfeeding women. A full written informed consent was obtained from each patient who entered the trial.

Prior to PDT, a freshly prepared cream containing 20% ALA (prepared locally at UCLH pharmacy) was applied with a margin of approximately 1cm beyond the skin tumours and then covered with plastic adhesive dressing. The ALA was left on the skin and the patients were instructed not to expose the creamed area to direct sunlight for 3 h. The plastic adhesive was removed, cream was then wiped-off, and the tumour demarcated with 5 mm margins of macroscopically normal skin. This shielded all normal surrounding skin and allowed optimal tumour illumination. All lesions were illuminated through a fixed perpendicular coupled lens fibre to deliver 100 J/cm^2 at a fluence rate of 150 mW/cm^2 , generated from 635 nm diode red laser (Diomed Ltd, Cambridge, UK) at a distance to cover the whole target area.

2.13.2 The systems

PDT was monitored by FS and ESS systems (previously described in sections 2.12.1.2 and 2.12.2.2).

2.13.3 Monitoring procedures

Three fluorescence readings and ESS spectra were acquired from each patient: “pre-PDT” (5 min before the PDT), “peri-PDT” (333 s after starting PDT), “peri-PDT” (660 s after starting PDT, marks the end of treatment) and “post-PDT” (15 min after PDT). The primary treatment outcome was evaluated by visual inspection and palpation when patients returned for their follow-up visit at 6 weeks and later at approximately 6 months. Complete response was defined as the disappearance of the disease (i.e. treatment site was macroscopically normal with no evidence of tumour). Partial response was defined as a decrease of at least 50% in the total tumour size relative to pre-treatment size

2.14 Statistical analysis

2.14.1 *In vitro* studies

Data were entered into the Microsoft Office Excel 2003 database, and expressed as the mean of observation \pm standard deviation (SD). The difference in values between groups was determined by analysis of variance (ANOVA) and Student *t*-test unless otherwise stated. Results were considered significant when the value of $p \leq 0.05$.

2.14.2 *In vivo* studies

2.14.2.1 Fluorescence spectroscopy

The red-to-green values of the suspected areas were calculated and correlated with the histopathology. A Student's *t*-test was used to test the viability of the ratios regarding its ability to discriminate between different disease stages. Sensitivity and specificity determination, histopathological reports (normal, inflammation, hyperkeratosis, mild dysplasia, moderate dysplasia, severe dysplasia and carcinoma in situ) were considered as standard and correlated with red-to-green ratios measured

in terms of oral changes in this clinical trial. Results were considered significant when the value of $p \leq 0.05$.

2.14.2.2 Elastic scattering spectroscopy

The number of dimensions in the data (wavelengths) greatly exceeded the number of observations (spectra), and so a naive analysis of the raw data would result in a model that was vastly over-fitted and would be much more sensitive to noise in the training data set. To avoid this problem, the data was cropped between 340 and 800 nm to remove those parts of the spectrum with low signal-to-noise ratio. Spectra were smoothed using a Savitsky–Golay linear filter (to remove the noise) with a smoothing width of 30 points (10 nm), and normalised so that each spectra had a mean intensity of zero and a standard deviation of unity with virtually no loss of information; by doing this we were able to compare and analyse spectra with different intensities.

In this clinical trial, to test the system, all types of dysplasia were classified as ‘malignant’ whereas all other reports (normal, inflammation, and hyperkeratosis) were considered “non-malignant or benign” changes. A linear discriminant analysis was used to find a transformation that maximised the difference between the data belonging to the dysplastic and the benign groups. In order to determine how successful this algorithm was at discriminating between the novel benign and dysplastic spectra, leave-one-out (or “jacksnipe”) validation was used. All analyses were performed in R (R Development Core Team, 2005), using software libraries from (Venables and Ripley, 2002).

2.14.2.3 Monitoring of PDT

For the fluorescence data, the image obtained was intensified and PpIX and red tissue autofluorescence intensity was calculated. For the ESS data, the acquired spectra were first smoothed with a Savitzky-Golay linear filter with a smoothing width of 30 points (10 nm). Then the spectra taken during, at the end of, and after PDT were each log-ratioed against the mean spectra taken from that patient prior to PDT. The relative change in the absorbance of ALA was estimated by calculating the area under a peak centred at 408 nm with a width of 10 nm. To test whether the ESS instrument detected significant differences in the relative absorbance over time, ANOVA was used where the integrated area under the curve was explained by time period (a factor with three levels: “during”, “at the end of” and “after”, depending on when the measurement was taken).

Chapter 3

Results I

Photodynamic Efficacy in OSCC Cells

3.1 Introduction

The relationship between the degree of photodamage occurring in tumour tissue and photosensitiser uptake and light dose is controversial. Early studies indicated a reciprocal relationship between the photosensitiser and light, but this balance can be lost when using an excessive amount of the photosensitiser, which suggests shielding of the delivered light (Bown et al., 1986; Barr et al., 1990). In contrast, Teiten et al. showed that there is no significant correlation between tumour drug levels and PDT response *in vitro*, when measuring the amount of drug in human breast cancer cells (Teiten et al., 2001). In addition to photosensitiser and light, other groups have suggested the rule of tissue threshold (Lilge and Wilson, 1998); the same group also suggested that doses below the lethal level can repair cell damage caused by PDT. However, it is important to deliver the proper drug and light dose to the target area in order to initiate the photochemical reaction. Thus, minimum drug and power light, sufficient to achieve tumour ablation without causing side effects, i.e. long-term toxicity and thermal damage, are required.

The purpose of the experiments described in this chapter was to investigate, using various doses of both Foscan and light, in an attempt to determine whether treatment could potentially improve the outcome. A further purpose was to determine the sublethal PDT dose for each cell line to be used for subsequent chapters.

3.2 Foscan-dark toxicity

To determine the safety of Foscan on cell viability, cells were incubated with concentrations of the Foscan (0, 1, 5, 10, and 15 μ g/ml) for 72 h prior to analysis by MTT assay. It was noted that sensitisation of KB, UP, VB6 and H376 cells with 5 μ g/ml of Foscan for up to 5 days in the dark had no significant effect on the viability of the cells. At higher dose concentrations, the cell viability was decreased slightly in a dose and time dependant manner. For example, at 15 μ g/ml, which represents a 15- fold increase of the normal *in vitro* dose, the percentage survival in VB6 cells was 97% \pm 1.2 and 90% \pm 2.7 by day 1 and day 3, respectively, compared to the untreated controls (data not shown).

3.3 Effects of laser light

To determine the safety of red light on cell viability, cells were illuminated with doses of the 652 nm red light (0, 1, 5, 10 and 15J/cm²), and incubated for 72 h prior to analysis by MTT assay. It was noted that exposure of cell lines up to 5J/cm² of red laser had no effect on cell survival. At the higher doses (\geq 10J/cm²), the proliferation of cells was increased slightly. For example, in H376 cells, the proliferation was 10% \pm 2 higher than controls when cells were exposed to 10J/cm² of red light (data not shown).

3.4 Phototoxicity of Foscan-PDT

To analyse Foscan-PDT induced cytotoxicity, KB, UP, VB6 and H376 cells were subjected to various doses of PDT. Thus, when cell lines were subjected to Foscan at concentrations of 0.25, 0.5, 1, 2, and 4 μ g/ml for 3 h and 24 h, and then illuminated with 0.5, 1, 2 and 4J/cm² of red light, the levels of phototoxicity were induced in dose-dependant manner by both the drug and light and time of incubation (Figures 3.1-4). Compared to untreated control, the results showed a very significant ($p < 0.001$) phototoxicity was found for all cell lines sensitised with 4 μ g/ml of Foscan for

24 h and then illuminated with $4\text{J}/\text{cm}^2$ light. When cell lines were incubated with $2\mu\text{g}/\text{ml}$ Foscan for 24 h and illuminated with $2\text{J}/\text{cm}^2$, the phototoxicity was maximal in KB cells and lesser in UP cells resulted in $11\% \pm 1.2$ and $66.3\% \pm 6.4$ cell survivals, respectively. These cell survivals were reduced to $8.3\% \pm 6.3$ and $58.3\% \pm 3.4$, respectively when cells incubated with Foscan for 24 h only. Control experiments show that both drug and light were required for any significant cytotoxicity to any of the cell lines. The sublethal doses causing approximately not more than 15% cell death in UP, VB6 and H376 cells are summarized in Tables 3.1. In order to determine the effects of PDT on metastasis, each cell line was subjected to this subtoxic dose, as reported in Chapter 4.

Table 3.1 Approximate sublethal doses of Foscan-PDT

| | Incubation time (h) | Foscan ($\mu\text{g}/\text{ml}$) | Fluence (J/cm^2) | Fluence rate mW/cm^2 | Exposure time (s) | Survival (%) |
|----------------|------------------------|---------------------------------------|---------------------------------------|---|----------------------|----------------------|
| UP | 24 | 1.0 | 0.5 | 25 | 20 | 88 ± 3 |
| VB6 | 24 | 0.5 | 0.5 | 25 | 20 | 87 ± 2 |
| H376 | 24 | 0.25 | 0.5 | 25 | 20 | 85 ± 3 |
| Control | 24 | 0.0 | 0.0 | 0.0 | 0 | Normalized to 100 |

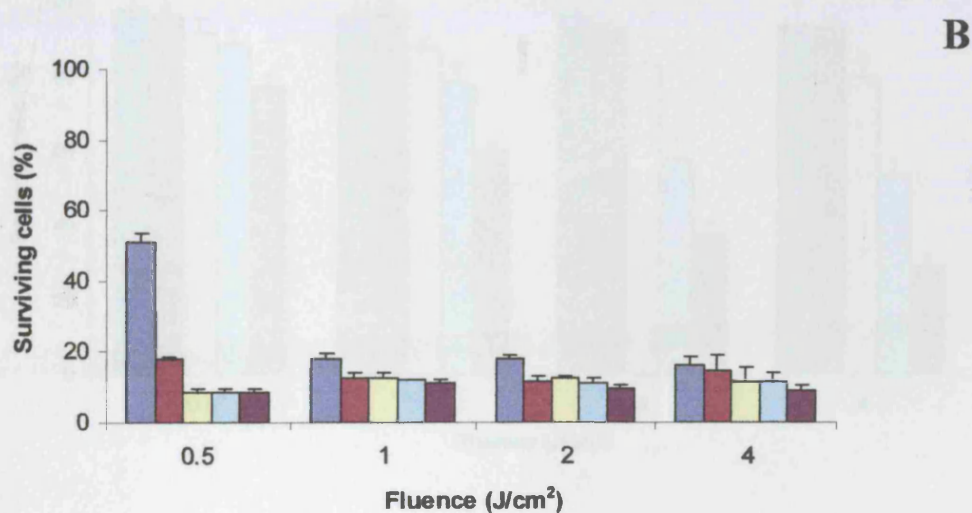
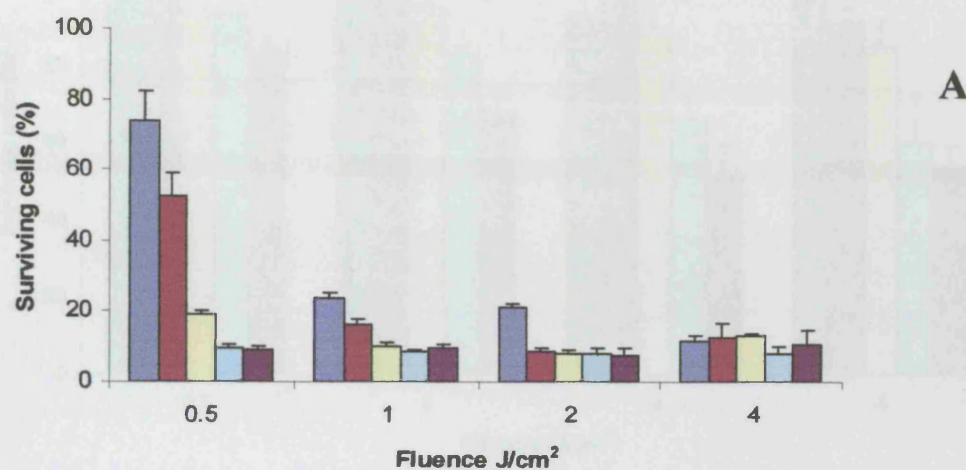


Figure 3.1 Phototoxicity on KB cells treated with various concentration of Foscan 0.25 (■), 0.5 (■), 1 (■), 2 (■) and 4 (■) $\mu\text{g}/\text{ml}$ for 3 h (A) and 24 h (B). The cells were exposed to 652 nm red light at 0.5, 1, 2, or 4 J/cm^2 . Controls were cells without treatment. Data represent the % of surviving cells relative to controls (= 100). Error bar represent standard deviation of triplicate wells. The experiment was repeated twice with similar results.

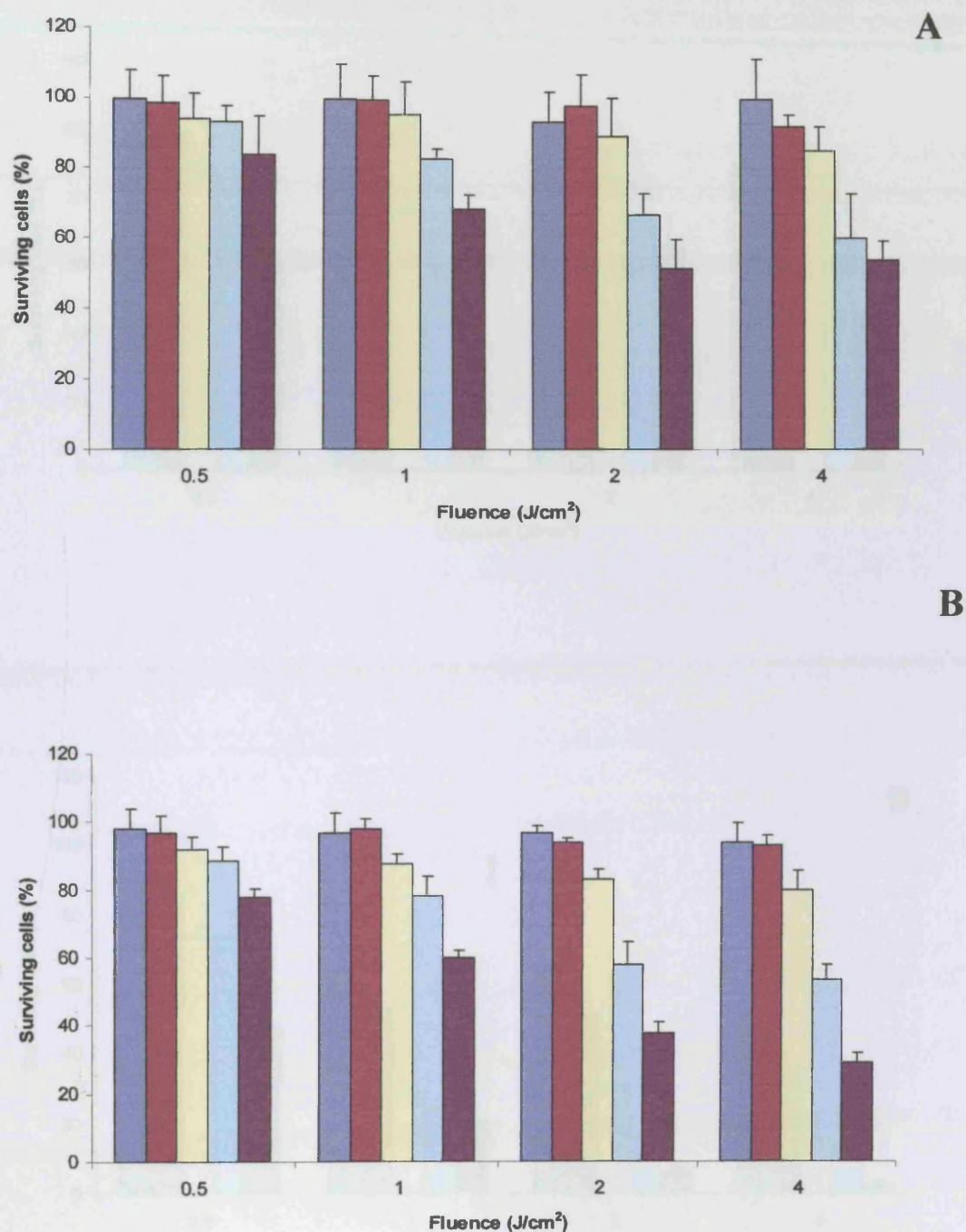


Figure 3.2 Phototoxicity on UP cells treated with various concentration of Foscan 0.25 (■), 0.5 (■), 1 (■), 2 (■) and 4 (■) µg/ml for 3 h (A) and 24 h (B). The cells were exposed to 652 nm red light at 0.5, 1, 2, or 4 J/cm². Controls were cells without treatment. Data represent the % of surviving cells relative to controls (= 100). Error bar represent standard deviation of triplicate wells. The experiment was repeated twice with similar results.

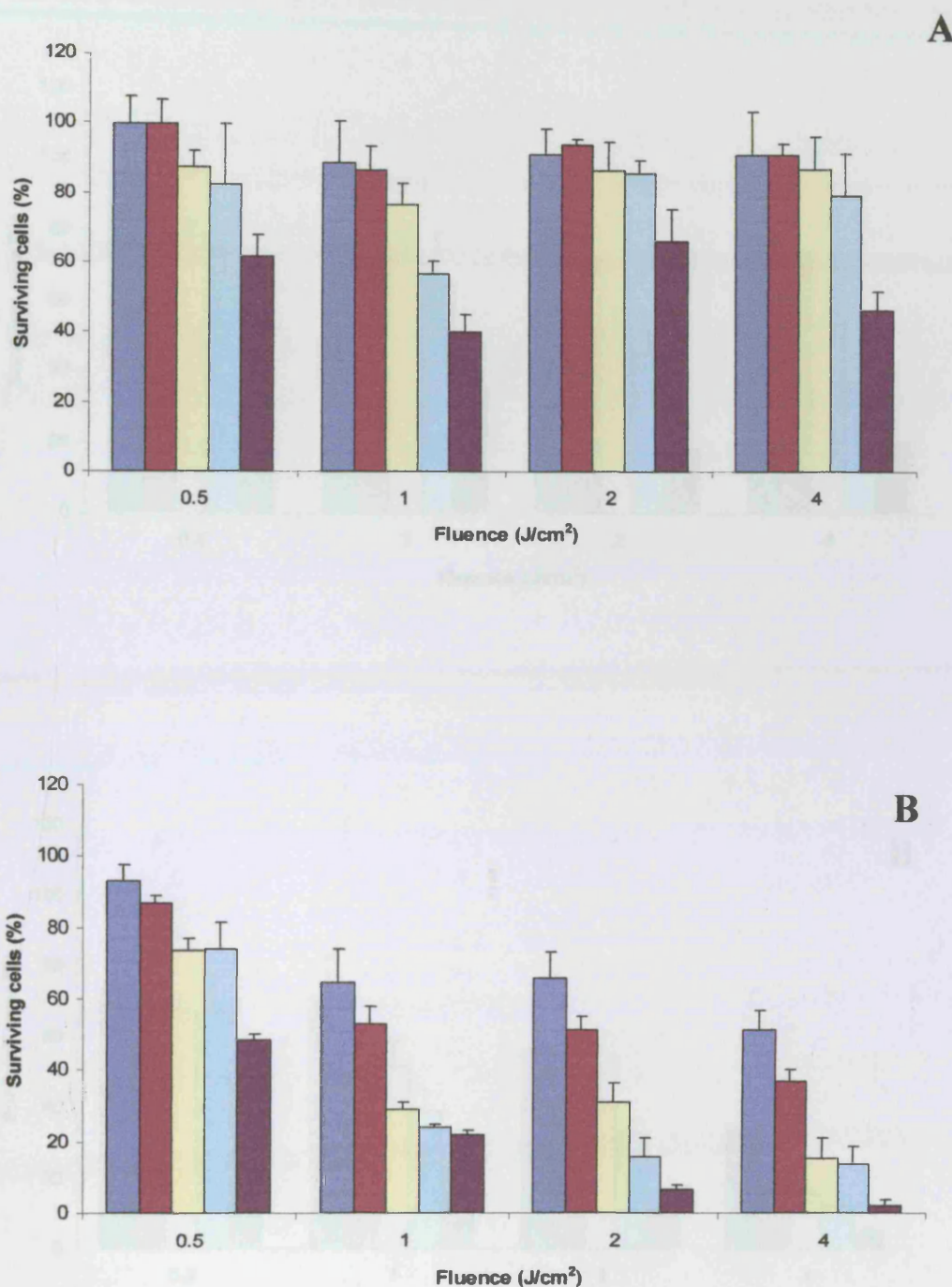


Figure 3.3 Phototoxicity on VB6 cells treated with various concentration of Foscan 0.25 (■), 0.5 (■), 1 (■), 2 (■) or 4 (■) µg/ml for 3 h (A) or 24 h (B). The cells were exposed to 652 nm red light at 0.5, 1, 2, or 4 J/cm². Controls were cells without treatment. Data represent the % of surviving cells relative to controls (= 100). Error bar represent standard deviation of triplicate wells. The experiment was repeated twice with similar results.

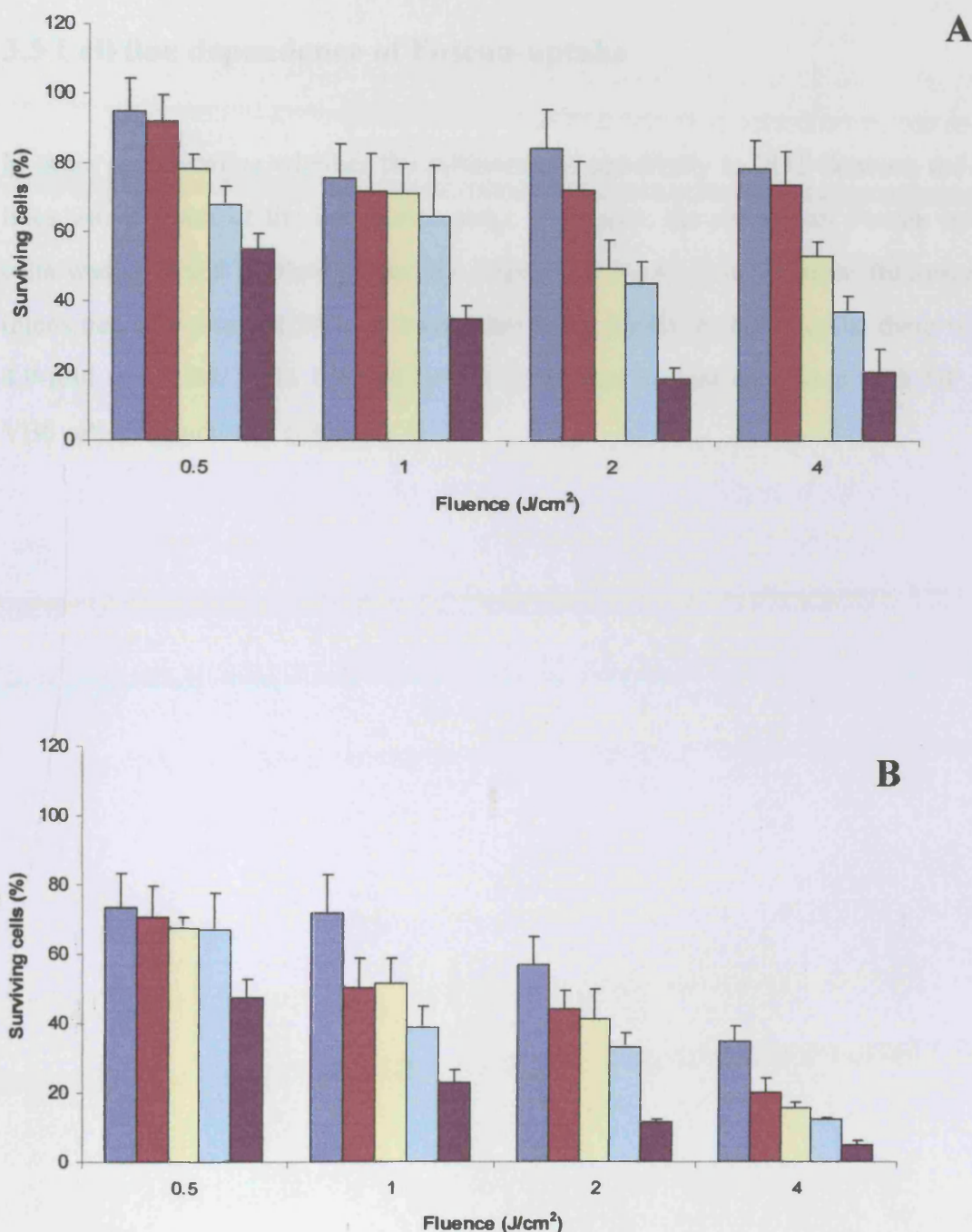


Figure 3.4 Phototoxicity on H376 cells treated with various concentration of Foscan 0.25 (■), 0.5 (■), 1 (■), 2 (■) or 4 (■) $\mu\text{g}/\text{ml}$ for 3 h (A) or 24 h (B). The cells were exposed to 652 nm red light at 0.5, 1, 2, or 4 J/cm^2 . Controls were cells without treatment. Data represent the % of surviving cells relative to controls (= 100). Error bar represent standard deviation of triplicate wells. The experiment was repeated twice with similar results.

3.5 Cell line dependence of Foscan-uptake

In order to determine whether the difference in sensitivity to PDT between the cell lines was a result of the increased uptake of Foscan, the amount of Foscan within cells was analysed by flow cytometry. Figure 3.5 shows that the mean fluorescence intensities of Foscan at 24 h of incubation were varied. In H376 cells, there was a 4.9-fold ($p < 0.001$) and 1.7-fold ($p < 0.05$) higher content compared with UP and VB6 cells, respectively (Figure 3.6).

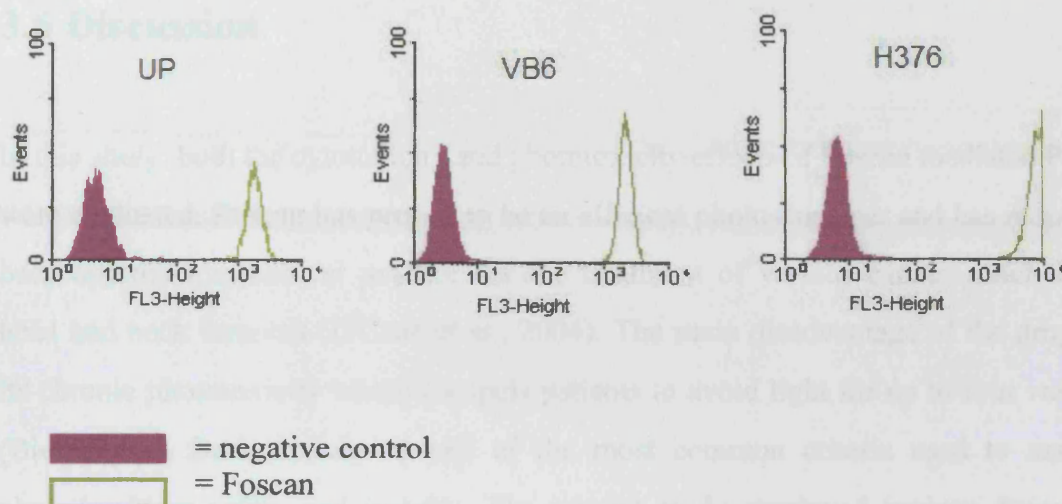


Figure 3.5 Flow cytometer analysis of Foscan uptake by UP, VB6 and H376 cells. Cells were incubated with 0.5 μ g/ml of Foscan for 24 h. Cells were then released by trypsin/EDTA. Foscan was detected by measuring its red fluorescence in FL3-H. Negative controls of all cells (first left solid histogram) had no treatment. Figure represents results for one experiment run in duplicate.

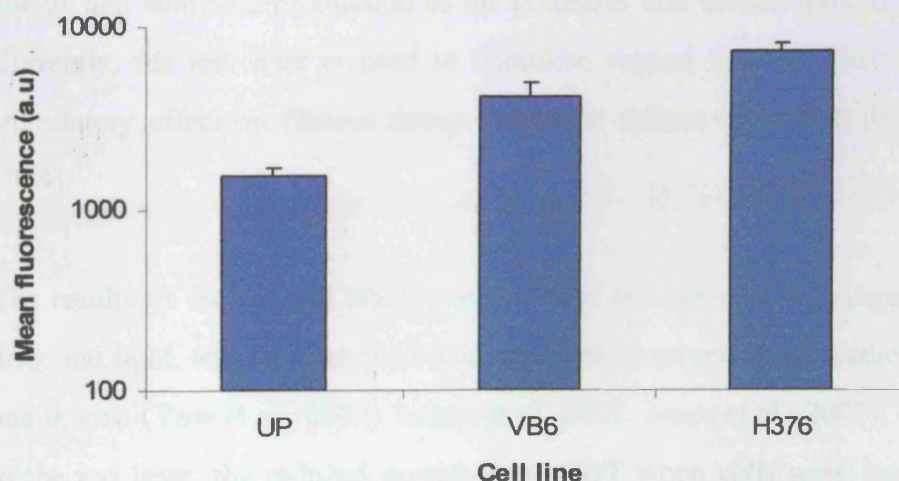


Figure 3.6 Mean fluorescence of cells shown in Figure 3.5. The values were calculated by subtracting the mean fluorescence of the peaks of untreated cells from mean fluorescence of the peaks of Foscan treated cells. Fluorescence is measured in arbitrary units (a.u). Error bars represent standard deviation.

3.6 Discussion

In this study, both the cytotoxicity and phototoxicity effects of Foscan mediated PDT were evaluated. Foscan has proved to be an efficient photosensitiser and has recently been approved in clinical practice for the treatment of various cancers, including head and neck tumours (D'Cruz et al., 2004). The main disadvantage of the drug is its chronic phototoxicity which compels patients to avoid light for up to four weeks (Biel, 1995). Dark toxicity is one of the most common criteria used to assess photosensitiser safety and activity. The present study employed various doses of both light and drug to series of established cancer cell lines. Foscan, in this study, showed no toxicity and the illumination of the cell lines to red light alone (no photosensitiser) resulted in slight stimulation of growth. This is consistent with other authors who found that a stimulatory effect is produced by low intensity laser light (Pe et al., 1994). The increased growth was explained as an increase in mitochondrial transmembrane electrochemical proton gradient, which in turn enhanced calcium release in cytoplasm, while excess light can deplete cellular energy and stimulate production of the proteases and lipases (Hornung et al., 1997). Currently, the red laser is used to stimulate wound healing. This is based on its stimulatory effect on fibrous tissue to initiate release of growth factors (Pe et al., 1994).

The results of the present study revealed that cell survival was dependent on both drug and light, and this has been demonstrated in several other studies, both *in vitro* and *in vivo* (Yow et al., 2000; Teiten et al., 2001; Jones et al., 2003). Upon exposure to the red laser, the reduced sensitivity to PDT when cells were incubated for 3 h indicates either a reduction of the intracellular Foscan concentration, or the possibility that the drug is not effectively distributed in the cell, as has been reported (Melnikova et al., 1999).

Flow cytometry was used in this study to quantify the intracellular concentration of Foscan, which indicated that Foscan was taken by all investigated cells. UP, VB6 and H376 cells showed different drug uptakes and were inversely proportional to their size and positively related to their sensitivity to PDT. This difference in response to PDT could be explained in part by their Foscan uptake. This is contrasted Moan et al. who indicated that normal cells and cells of varying malignancy potential take up similar levels of photosensitiser (Moan et al., 1992). Another explanation for different sensitivity to PDT could be the result of their degree of differentiation. The poorly differentiated cells (KB) were the most sensitive line to PDT. This was in contrast with another report concerning erythroleukemia cells, where reduction in HpD sensitiser uptake by differentiated cells was reduced, but without changes in sensitivity to PDT (Lejbkiewicz and Salzberg, 1992). Furthermore, UP cells are keratinocyte-like (papilloma virus transformed cells) and not an established cancer cell line, which may explain their low response in spite of their large size compared to the other cell lines used in the study. This is in agreement with other study on human colon carcinoma cells which were divided into sensitive and resistant according to the cell volume (West and Moore, 1992).

Many studies have shown a relationship between photosensitiser localization and uptake and the killing effects of PDT (Sharman et al., 2004; Endlicher et al., 2001; Teiten et al., 2003; Fabris et al., 2001; Biel, 1995). The modulation of the sensitiser or light dose could lead to an enhanced killing effect, for example, decreasing the Foscan dose or incubation time and increasing the light dose could result in fewer adverse effects, therefore improving the outcome. Clinically, this protocol has now been partially applied with promising results here at UCLH.

Chapter 4

Results II

The Effects of Photodynamic Therapy on the Expressions of Invasion Promoting Factors in Head and Neck Carcinomas

4.1 Introduction

PDT is currently under clinical investigation for the treatment of early cancer. The biological effects of PDT are primarily mediated by the generation of reactive oxygen species, such as singlet oxygen, which result in cytotoxic effects on treated cells with the initiation of signal transduction pathways (Margaron et al., 1997; Runnels et al., 1999; Almeida et al., 2004). *In vitro*, cell death is mainly due to the singlet oxygen reactions with the cellular organelles and membranes (direct killing), while *in vivo*, in addition to the direct effect, there is also significant microvascular damage which greatly contributes to tumour cell destruction (Fingar et al., 1999; Triesscheijn et al., 2005). Apart from a death response, cells can also undergo a rescue response after PDT and restore their activities (Kessel and Luo, 1999; Mitra et al., 2003). PDT is mainly used for treatment of early cancer without metastases, yet it is crucial to determine the influence of PDT on the metastatic process.

The purpose of the experiments in this chapter was to describe the results of PDT on migration and invasion capacity including its effect on the secretion of MMP-2, MMP-9, MMP-13, uPA, VEGF and expression of $\alpha v\beta 1$ and $\alpha v\beta 6$ integrin receptors by human oral carcinoma.

4.2 PDT decreases migration towards ECM substrates

The effect of PDT on the migration of UP, VB6 and H376 cells was investigated using modified Boyden chamber assays. Cells were allowed to migrate for 4 h on membranes precoated with one of two ECM proteins, fibronectin or type I collagen. The obtained data (Figure 4.1) shows that the migratory activity of all cells was varied, depending on the cell line and coated matrix proteins. Overall, both fibronectin and type I collagen promoted the migration of all lines. VB6 cells showed a relatively higher migratory affinity towards fibronectin, approximately 2-fold, compared to the UP or H376 cells.

Compared to the untreated control, treatment of cell lines with PDT (Figure 4.1-A) had down reduced the affinity of UP, VB6 and H376 cells to migration toward fibronectin by 5.8, 8.5, and 18-fold, respectively ($p < 0.001$ for all). Migration toward type I collagen, (Figure 4.1-B) was approximately equally reduced by all cell lines; 3.4, 3.6 and 3.4-fold by the UP, VB6 and H376 cells, respectively ($p < 0.001$ for all).

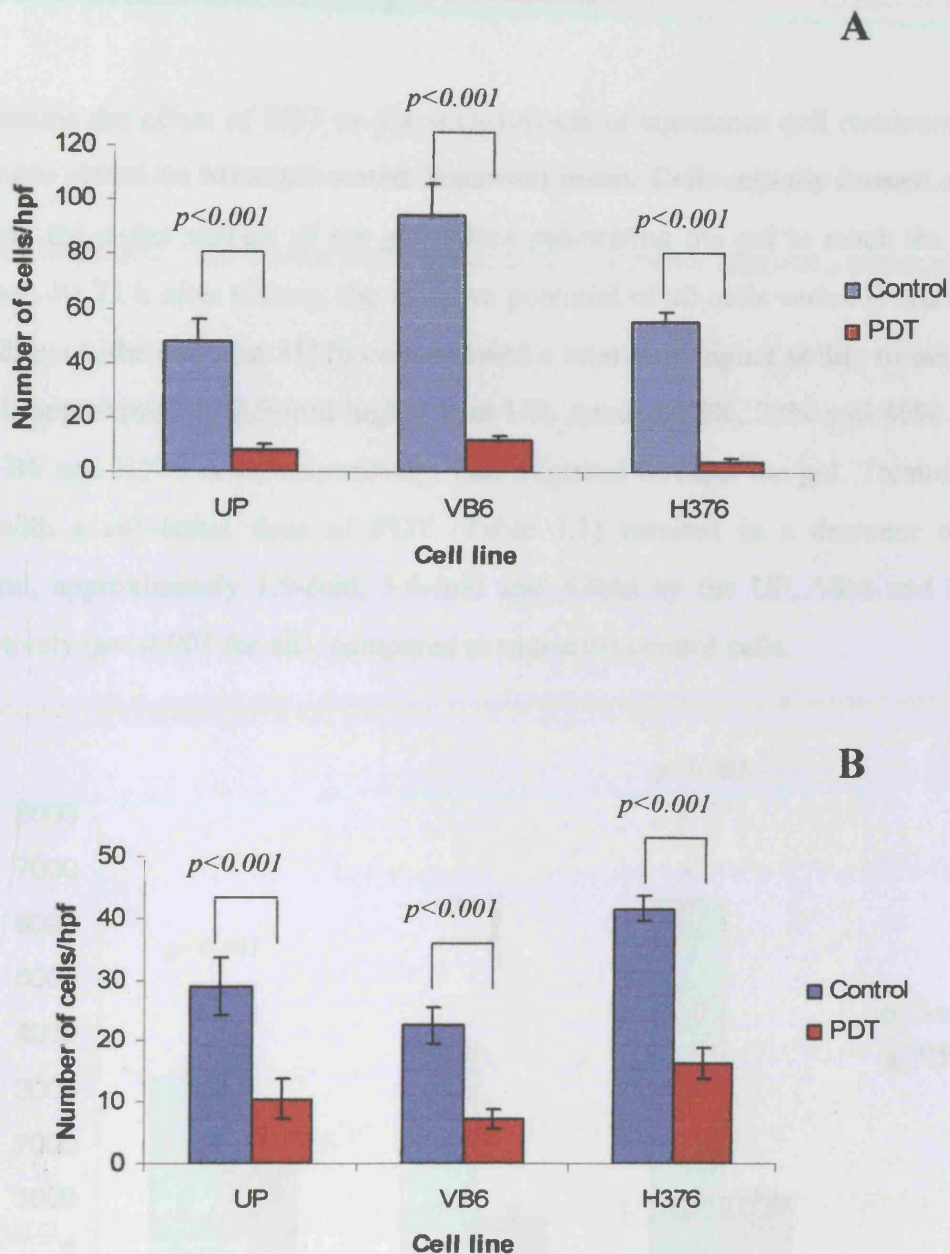


Figure 4.1 The Effect of PDT on the migration of UP, VB6 and H376 cells towards fibronectin (A) or collagen type I (B). Following sublethal dose of PDT, cells were plated on Transwell membranes coated with 10 μ g/ml of collagen type I and allowed to migrate for 3 h. The cells that migrated and bound to the undersurface of the filter were stained and counted by light microscopy using X40 objective. Data is expressed as the mean number of migrating cells per high power field (hpf) in each membrane. Error bars represent the standard deviation of three assays. The experiment was repeated twice with similar results.

4.3 PDT decreases Matrigel invasion

To examine the effect of PDT on the invasiveness of squamous cell carcinoma, the cells were plated on Matrigel-coated Transwell insert. Cells initially formed a layer covering the entire surface of the gel before penetrating the gel to reach the lower chamber. At 72 h after plating, the invasive potential of all cells varied (Figure 4.2), depending on the cell line. H376 cells showed a relatively higher ability to penetrate the gel, approximately 2.5-fold higher than UP. Around 15%, 22% and 46% of the UP, VB6 and H376 cells, respectively, had migrated through the gel. Treatment of cells with a sub-lethal dose of PDT (Table 3.1) resulted in a decrease of cell invasion, approximately 1.9-fold, 5.6-fold and 6-fold by the UP, VB6 and H376, respectively ($p < 0.001$ for all), compared to untreated control cells.

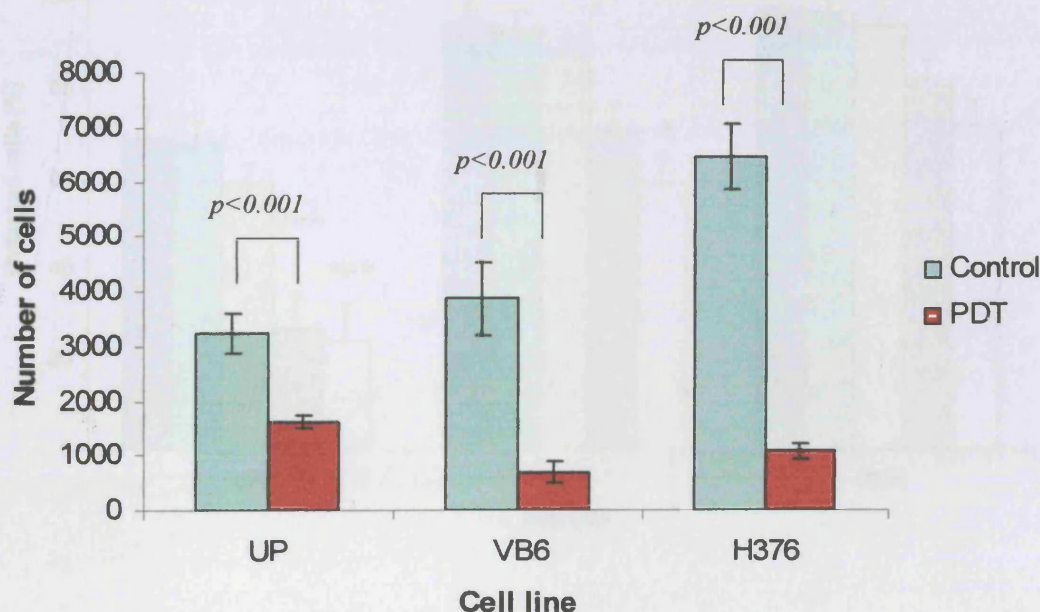
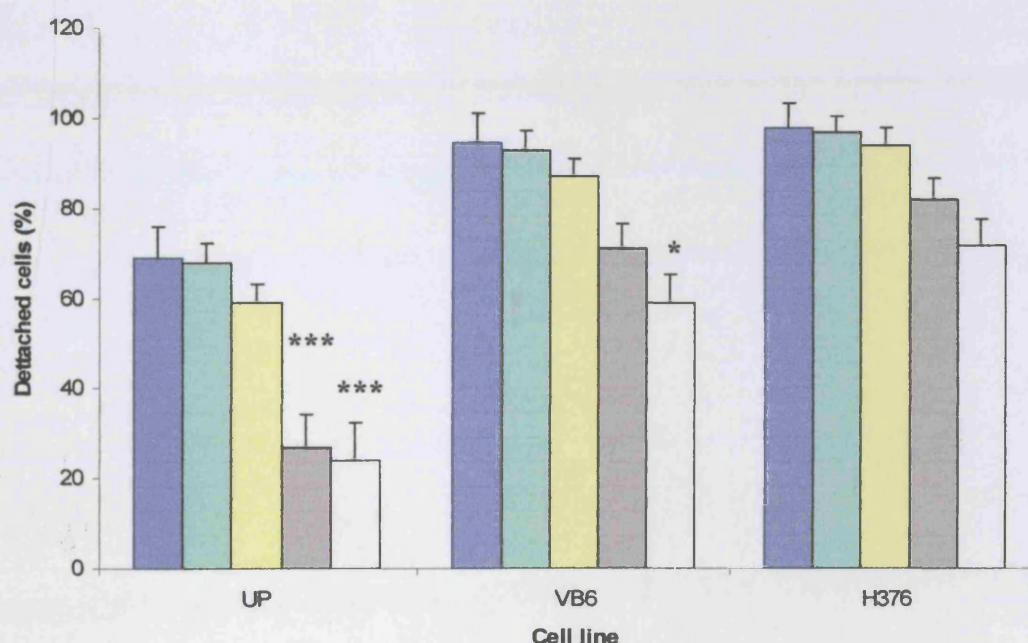


Figure 4.2 Effect of PDT on the invasion of UP, VB6 and H376 cells. Following treatment with sublethal dose of PDT (Table 3.1), cells were plated on Transwell membranes coated with $40\mu\text{g}/\text{cm}^2$ of Matrigel diluted in PBS and allowed to invade for 72 h. Cells that invaded the lower chamber, including those bound to the under-surface of the filter, were trypsinized and counted using light microscopy. Data is expressed as the number of invading cells per well and represent a mean \pm standard deviation of three wells. The experiment was repeated twice with similar results.

4.4 PDT decreases cell detachment.

There was no significant effect from either Foscan or red light treatment alone on the detachment of cells from the plastic substratum (data not shown). When the cells were treated with PDT, the percentage of detached UP, VB6 and H376 cells was significantly reduced (Figure 4.3). For example, at 24 h post-PDT, the number of detached cells was reduced by 73% ($p < 0.001$), 29% ($p < 0.05$) and 18% by UP, VB6 and H376 cells, respectively, in comparison to untreated controls (100%).



* $p \leq 0.05$ (compared with corresponding control)

*** $p \leq 0.001$ (compared with corresponding control)

Figure 4.3 A representative bar chart showing detachment assay of UP, VB6 and H376 cells. Following treatment with sublethal dose of PDT (Table 3.1), cells were detached by trypsin/EDTA over a variable time; 0 (■), 1 (■), 3 (■), 24 (■) or 48 (■) h, and the number of detached cells was counted. Data represent the % of detached cells relative to the untreated control (=100). Error bars represent standard deviation of triplicate wells from one of three similar independent experiments.

4.5 PDT modulates cell attachment

The effect of PDT on the attachment properties of UP, VB6 and H376 was examined in short-term adhesion assays. The extracellular matrix proteins fibronectin and collagen type I, Matrigel or plastic substrate were used. Figure 4.4 shows no significant difference in the adhesion of UP, VB6 and H376 to any of the ECM proteins except to Matrigel by H376 cells ($p < 0.05$). In contrast, the adhesion to the plastic substratum was significantly reduced by approximately 2.4-fold, 3.5-fold and 2.7-fold by the UP, VB6 and H376 cells, respectively, following PDT ($p < 0.05$ for all).

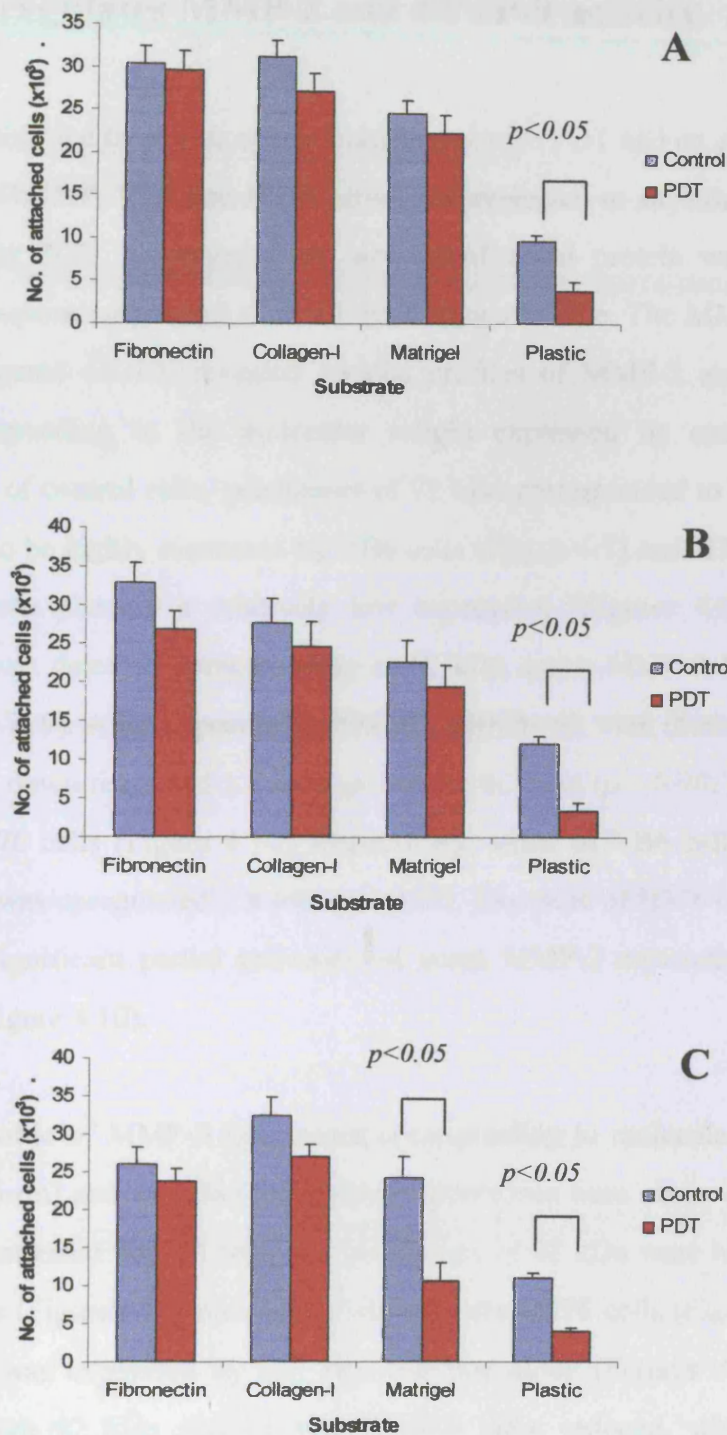


Figure 4.4 Adhesion assay of UP (A), VB6 (B) and H376 cells (C). Following treatment with PDT, cells were plated to fibronectin, collagen type I, Matrigel coated and plain wells. Data is expressed as the number of attached cells determined by the growth curve of each cell line, as determined by MTT assay. Error Bars represent standard deviations of triplicate wells. The experiment was repeated twice with similar results.

4.6 PDT regulates MMP-2 and MMP-9 activity

To find whether the treatment of oral carcinomas with PDT had an effect on MMP-2 production, The UP, VB6 and H376 cells were subjected to sublethal dose of PDT. At 24 h post PDT, the supernatant samples of equal protein were run in 12% acrylamide separating gel and stained with Coomassie blue. The MMP-2 and MMP-9 bands (Figures 4.5-10) revealed various profiles of MMP-2 and MMP-9 lysis zones corresponding to the molecular weight expressed by each cell line. In supernatants of control cells, gelatinases of 72 kDa corresponded to the pro-MMP-2 were found to be highly expressed by VB6 cells (Figure 4.7) and H376 (Figure 4.9), while UP cells showed a relatively low expression (Figures 4.6). No band of gelatinases was detected corresponding to 62 kDa active-MMP-2 for all cell lines (Figures 4.5, 7, 9). After exposure to PDT, the activity of total (both pro and active) MMP-2 was down-regulated 1.8-fold ($p < 0.05$), 4.3-fold ($p < 0.001$) by UP (Figure 4.6) and H376 cells (Figure 4.10), respectively, while in VB6 cells, total MMP-2 (Figure 4.9) was upregulated 1.8-fold ($p < 0.05$). Exposure of H376 cells to PDT had resulted in significant partial activation of latent MMP-2 approximately 14.3-fold ($p < 0.001$; Figure 4.10).

A similar profile of MMP-9 lysis zones corresponding to molecular weights of 92 kDa (latent form) and 84 kDa (active form) gelatinases were observed (Figures 4.5-10). In the untreated control samples, gelatinases of 92 kDa were highly expressed by VB6 cells (Figures 4.7) and only slightly by the H376 cells (Figures 4.9), while the 84 kDa was expressed by the VB6 cell line alone (Figures 4.7). After PDT treatment, both 92 kDa and 84 kDa MMP-9 were reduced, with a significant decrease in expression by VB6 cells ($p < 0.001$; Figures 4.7).

In order to support zymography results, ELISA kit against MMP-2 and MMP-9 was used, taking care to ensure that the same protein loading concentrations were used as in the zymography. The results showed that, following PDT treatment, the levels of total MMP-2 proteins (Figure 4.11A) were reduced by 9.6-fold only by the H376

($p < 0.001$) compared to the control. For UP and VB6 cells, no significant differences between control and PDT treated samples were evident. For MMP-9, the total MMP-9 levels (Figure 411B) were 5.4 times less in VB6 cells compared to the control ($p < 0.001$). No significant differences between the control and PDT treated samples of UP cells were evident.

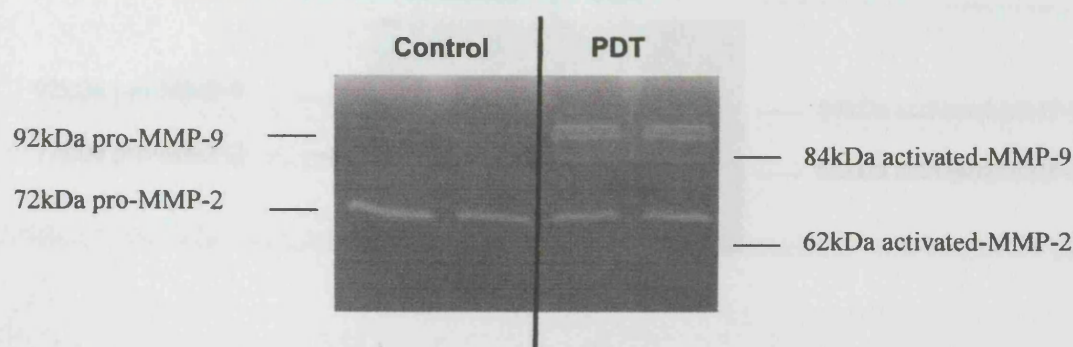


Figure 4.5 Zymogram showing PDT effect on MMP-2 and MMP-9 expression by UP cells. After treatment with sublethal doses of PDT (Table 3.1), cells were grown for 24 h before supernatant sampling and cell counting. Samples containing equal protein were run on each gel with m.w markers. Control samples were supernatants of the untreated cells. The intensity of the bands was measured by densitometric analysis, as shown in Figure 4.6.

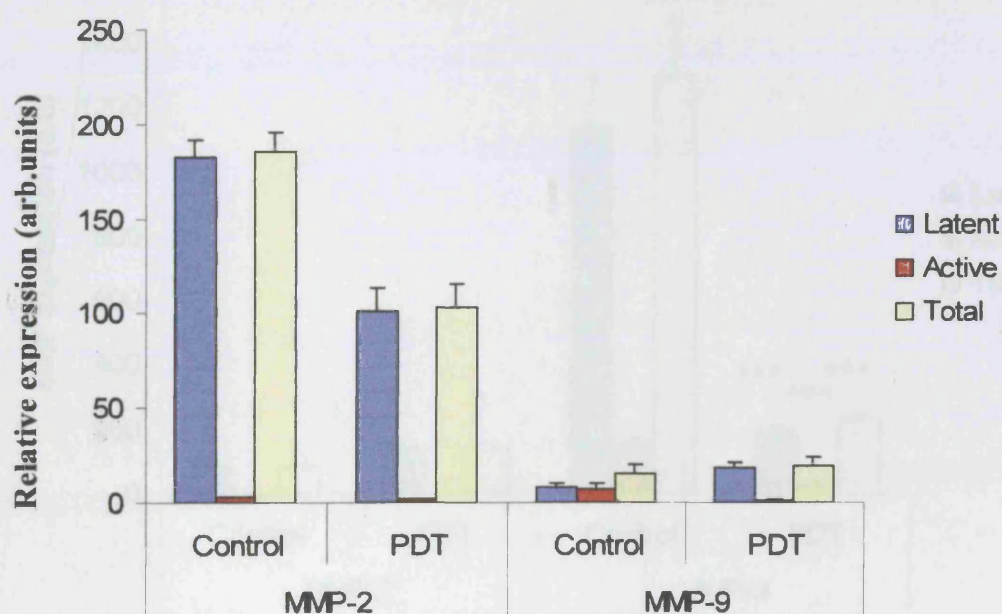


Figure 4.6 Representative chart of densitometric analysis of zymogram shown in Figure 4.5. Comparisons were made within each gel to determine relative changes in MMP-2 and MMP-9 activity measured in arbitrary units (a.u). Data represents the mean of relative activity in 2 lanes. Error bars = \pm standard deviations. Comparison between zymograms should not be made due to variation in intensity of background staining.

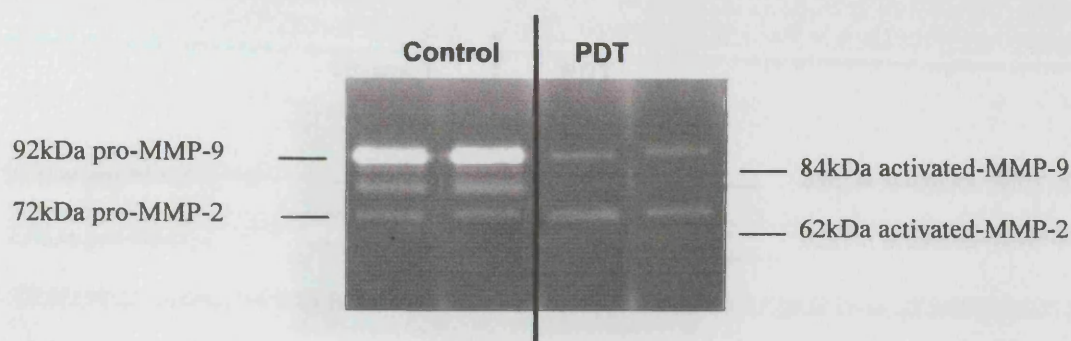
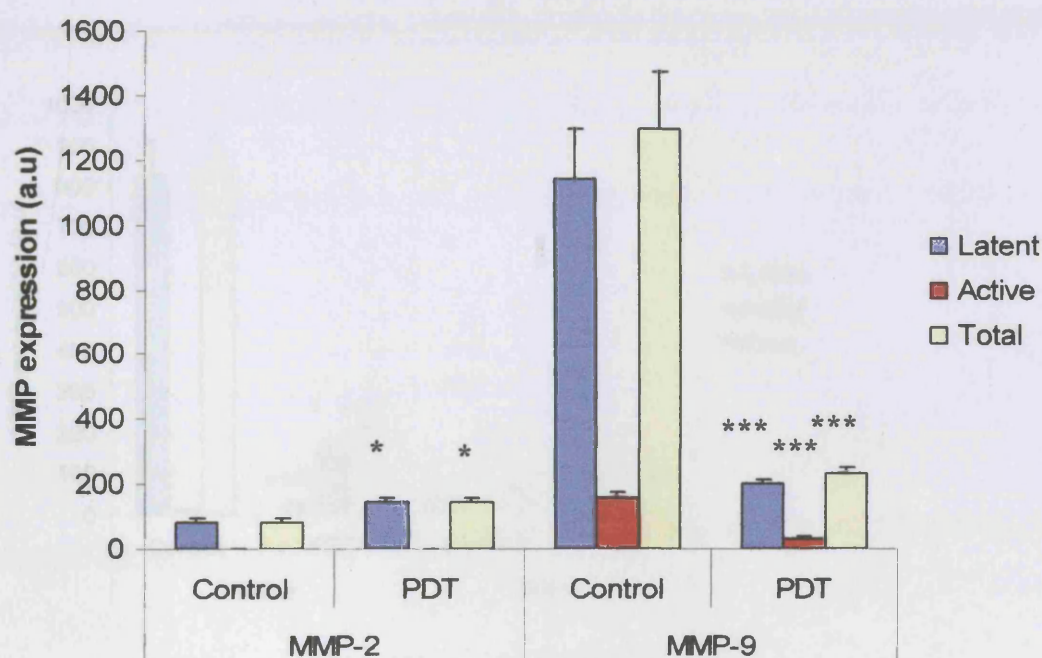


Figure 4.7 Zymogram showing PDT effect on MMP-2 and MMP-9 expression by VB6 cells. After treatment with sublethal doses of PDT (Table 3.1), cells were grown for 24 h before supernatant sampling and cell counting. Samples containing equal protein were run on each gel with m.w markers. Control samples were supernatants of the untreated cells. The intensity of the bands was measured by densitometric analysis, as shown in Figure 4.8.



* $p \leq 0.05$ (compared with corresponding control)

*** $p \leq 0.001$ (compared with corresponding control)

Figure 4.8 Representative chart of densitometric analysis of zymogram shown in Figure 4.7. Comparisons were made within each gel to determine relative changes in MMP-2 and MMP-9 activity measured in arbitrary units (a.u). Data represents the mean of relative activity in 2 lanes. Error bars = \pm standard deviations. Comparison between zymograms should not be made due to variation in intensity of background staining.

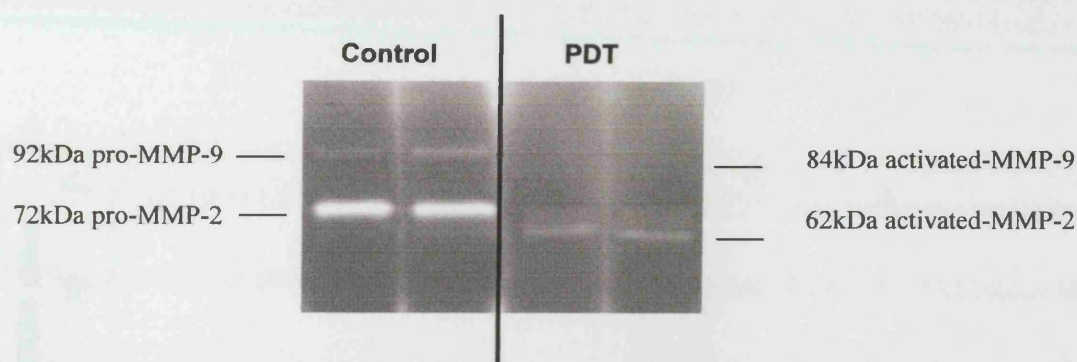
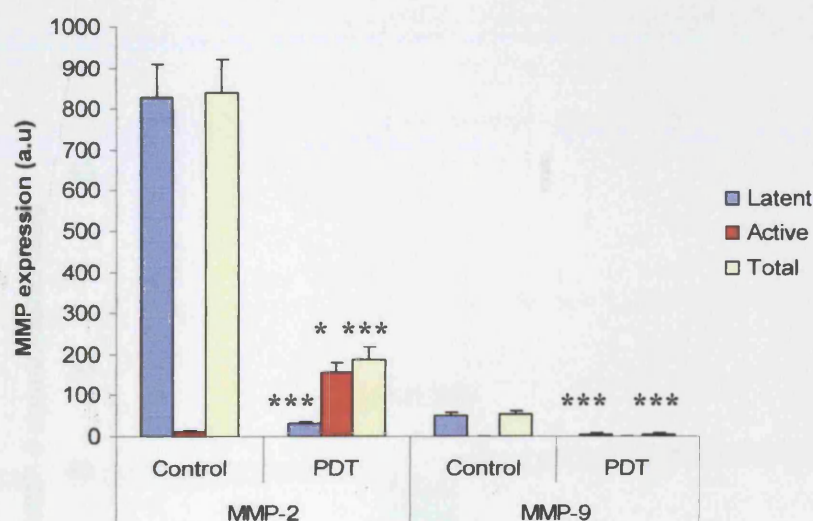


Figure 4.9 Zymogram showing PDT effect on MMP-2 and MMP-9 expression by H376 cells. After treatment with sublethal doses of PDT (Table 3.1), cells were grown for 24 h before supernatant sampling and cell counting. Samples containing equal protein were run on each gel with m.w markers. Control samples were supernatants of the untreated cells. The intensity of the bands was measured by densitometric analysis, as shown in Figure 4.10.



* $p \leq 0.05$ (compared with corresponding control)

*** $p \leq 0.001$ (compared with corresponding control)

Figure 4.10 Representative chart of densitometric analysis of zymogram shown in Figure 4.9. Comparisons were made within each gel to determine relative changes in MMP-2 and MMP-9 activity measured in arbitrary units (a.u). Data represents the mean of relative activity in 2 lanes. Error bars = \pm standard deviations. Comparison between zymograms should not be made due to variation in intensity of background staining.

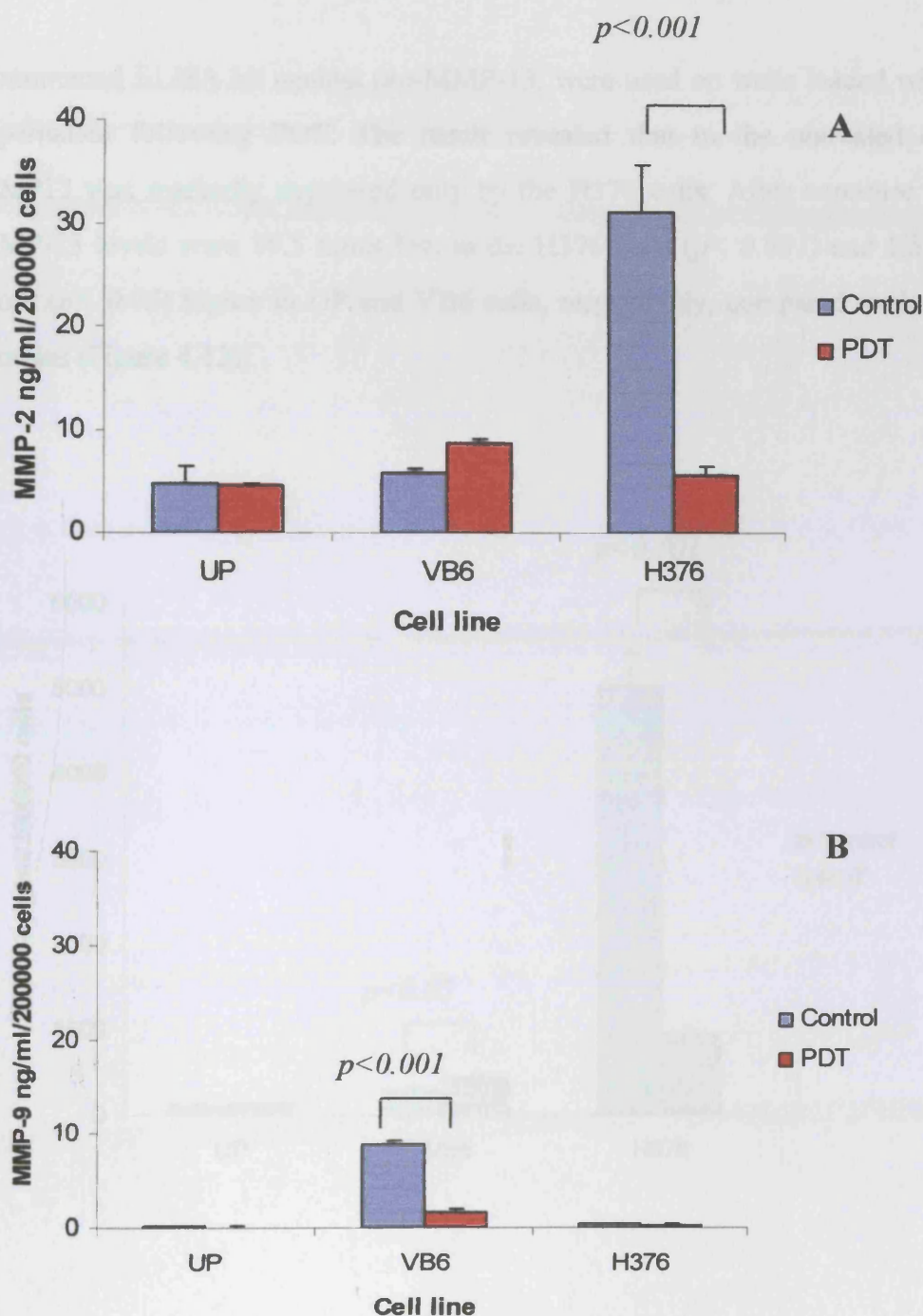


Figure 4.11 ELISA for MMP-2 (A) and MMP-9 (B). Following treatment with sublethal doses of PDT (Table 3.1), cell supernatants were prepared as for zymography. Sample (100 μ l) was added to each well and the concentration determined by interpolation from standard curve using known concentrations of MMP standards. Control samples were supernatants of the untreated cells. Figures show representative experiments. Error Bars represent standard deviations of triplicate samples. Experiments were repeated twice with similar results.

4.7 PDT modulates secretion of MMP-13

Commercial ELISA kit against pro-MMP-13, were used on wells loaded with cells' supernatant following PDT. The result revealed that in the untreated controls, MMP13 was markedly expressed only by the H376 cells. After exposure to PDT, MMP-13 levels were 19.5 times less in the H376 cells ($p < 0.001$) and 1.5 and 1.6 times ($p < 0.05$) higher in UP and VB6 cells, respectively, compared to the control samples (Figure 4.12).

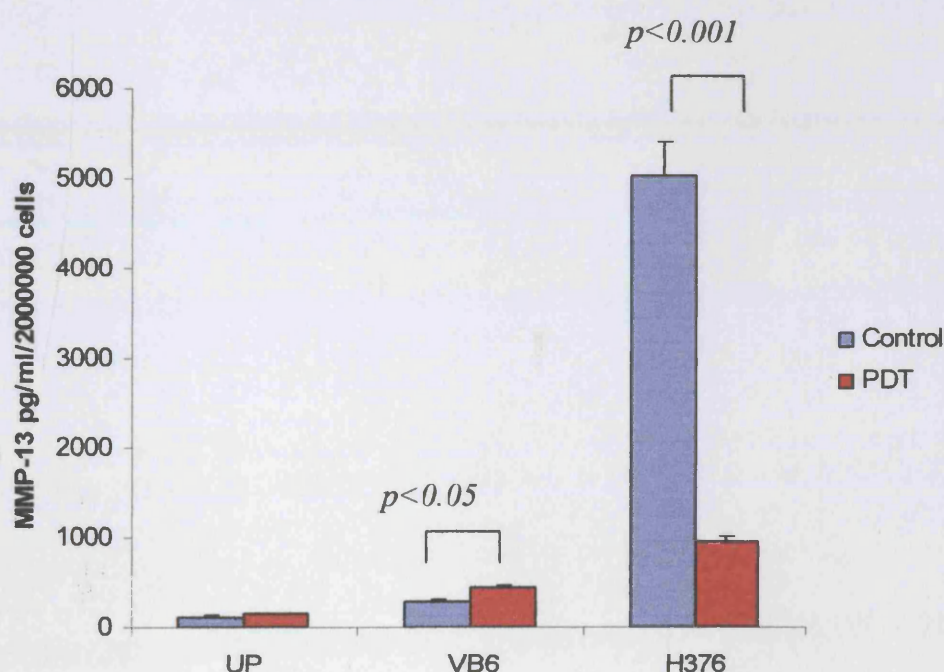


Figure 4.12 ELISA for MMP-13. Following treatment with sublethal doses of PDT (Table 3.1), cell supernatants were prepared as for zymography. Sample (100 μ l) was added to each well and the concentration determined by interpolation from standard curve using known concentrations of MMP standards. Control samples were supernatants of the untreated cells. Figure show representative experiment. Error Bars represent standard deviations of triplicate samples. Experiment was repeated twice with similar results.

4.8 PDT decreases secretion of VEGF

The effect of PDT on VEGF levels in the conditioned medium was determined by an ELISA assay. The results showed that the level of VEGF in the medium of PDT treated cells, compared to the untreated controls over the 24 h culture period (Figure 4.13A), were 3.3 and 3.8 times less in VB6 and H376 cells, respectively ($p < 0.05$ for both). This was reduced to 2.4-fold and 4-fold ($p < 0.01$ for both) when the cells were cultured for 48 h (Figure 4.13B). For UP cells, no significant difference in VEGF expression over any of the experiment times was found (Figure 4.13A-B).

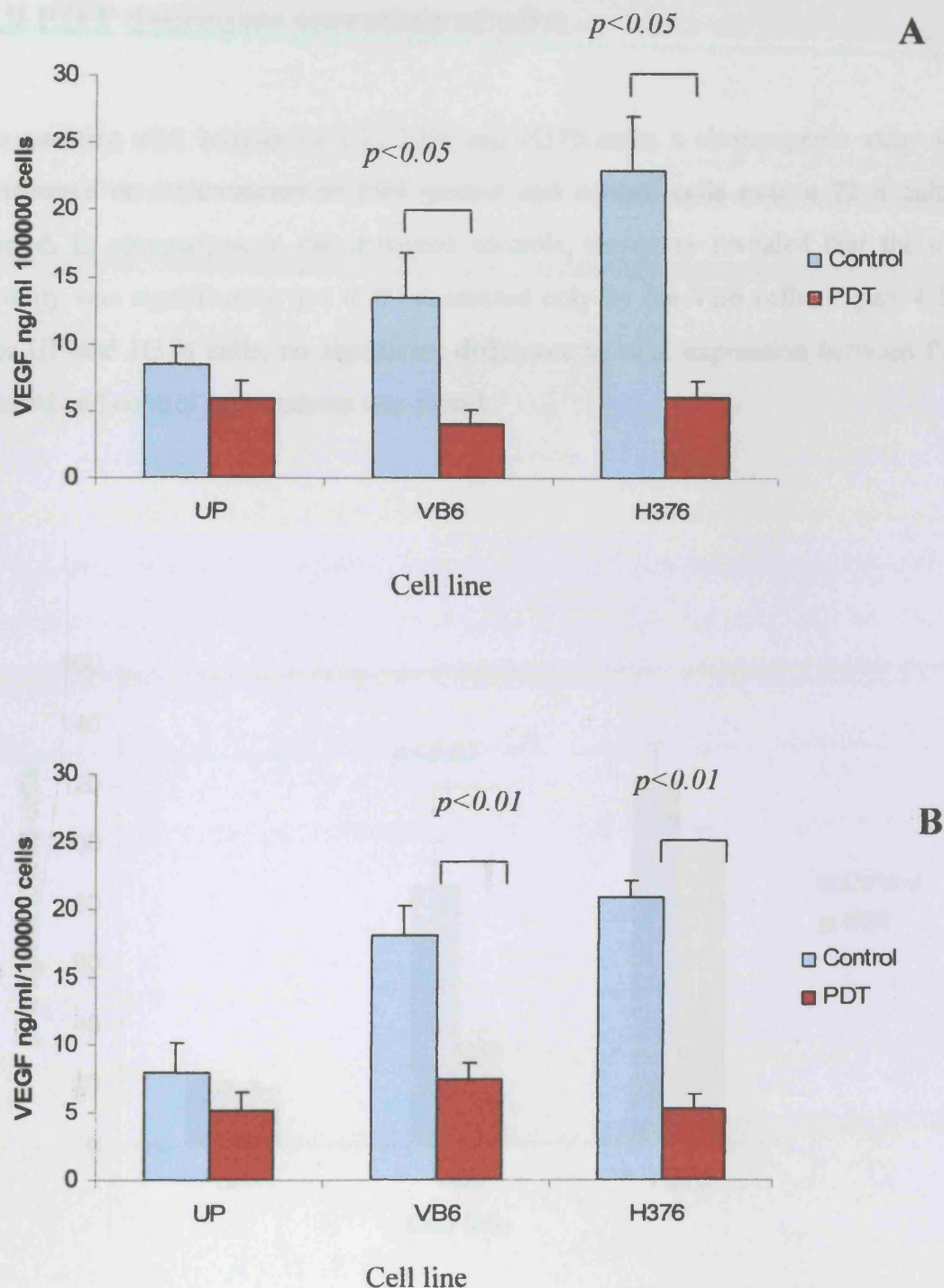


Figure 4.13 ELISA for VEGF. After treatment with sublethal doses of PDT, UP, VB6 and H376 cells were grown for 24 h (A) and 48 h (B) before supernatant sampling and cell counting. Cell supernatants were prepared as for zymography. Sample (100 μ l) was added to each well and the concentration determined by interpolation from standard curve using known concentrations of VEGF standards. Control samples were supernatants of the untreated cells. Figures show representative experiments. Error Bars represent standard deviations of triplicate samples. Experiments were repeated twice with similar results.

4.9 PDT decreases secretion of uPA

To quantify uPA activity by UP, VB6 and H376 cells, a chromogenic assay was performed on supernatants of PDT treated and control cells over a 72 h culture period. In comparison to the untreated controls, the assay revealed that the uPA activity was significantly ($p < 0.05$) decreased only by the VB6 cells (Figure 4.14). For UP and H376 cells, no significant difference in uPA expression between PDT treated and control supernatants was found.

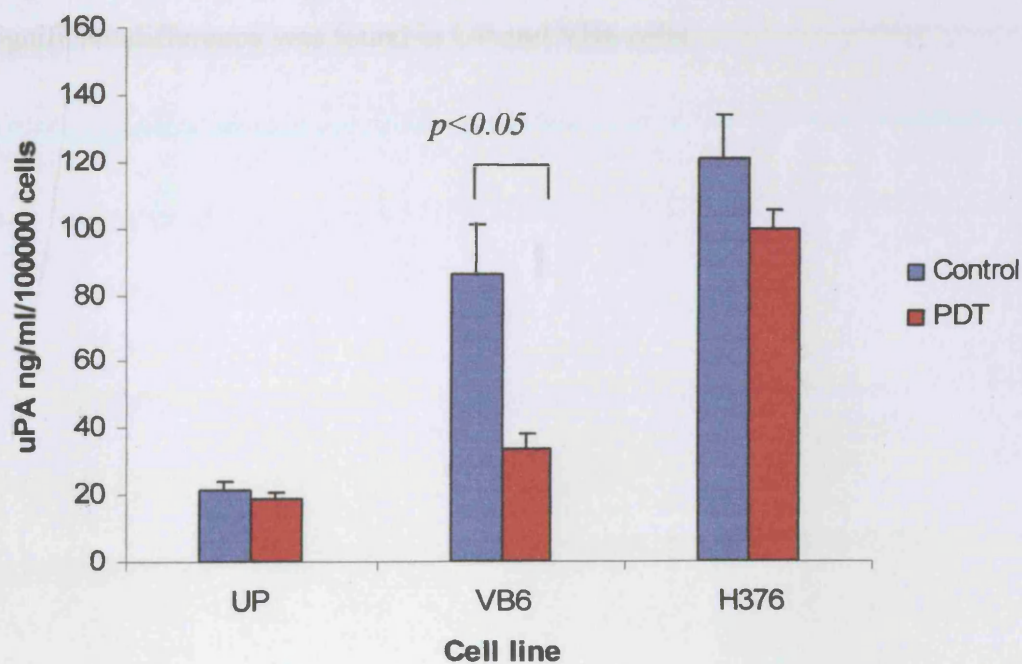


Figure 4.14 Chromogenic assays for uPA. Cells were grown for 24 h before being exposed to a sublethal dose of PDT. Cell supernatants were prepared as for zymography. Sample (50 μ l) was added to each well and the concentration determined by interpolation from the constructed standard curve prepared using range of human uPA substrate standards. Figure show representative experiment. Error Bars represent standard deviations of triplicate samples. Experiment was repeated twice with similar results.

4.10 PDT regulates expression of $\alpha 5\beta 1$ and $\alpha v\beta 6$

As the expression of adhesion receptors is an important event in the metastasis process, it was decided to investigate whether treatment of keratinocytes with PDT had an effect on the expression of $\alpha 5\beta 1$ integrin receptor. An analysis flow cytometry data indicated that exposure of the cells to sublethal doses of PDT caused an enhancement of $\alpha 5\beta 1$ receptor (Figures 4.15-4.16). The receptor was enhanced by 6.54 fold and 5.6 fold by the UP and H376 cells, respectively ($p < 0.01$ for both). For VB6 cells, no significant change in $\alpha 5\beta 1$ receptor expression following PDT was found. Similarly in $\alpha v\beta 6$ receptor (Figure 4.17-4.18), data indicated that exposure of the cells to sublethal doses of PDT caused an enhancement of $\alpha v\beta 6$. The receptor was significantly enhanced 10 fold ($p < 0.001$) by H376 cell line only, whereas no significant difference was found in UP and VB6 cells.

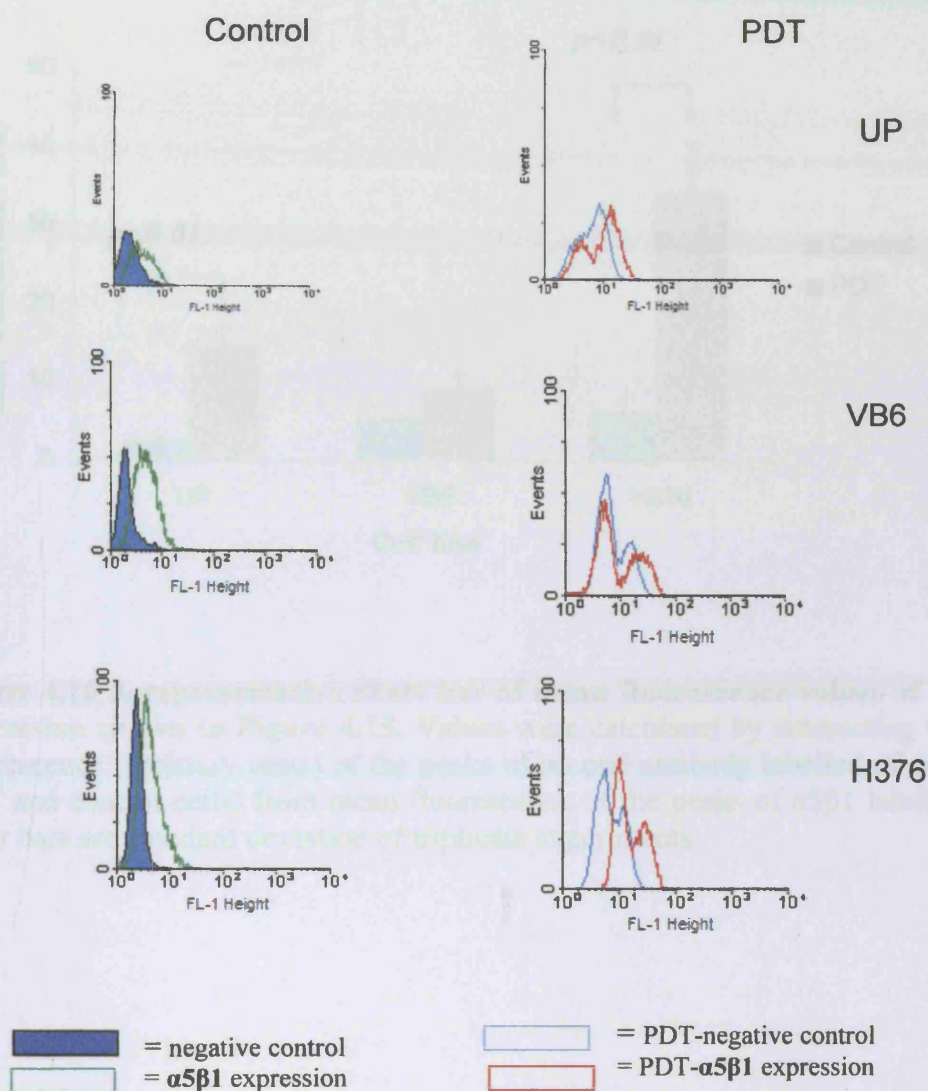


Figure 4.15 Histograms analysis of $\alpha 5 \beta 1$ by UP, VB6, and H376 cells. Cells were released by trypsin/EDTA and labelled with $\alpha 5 \beta 1$ (P1D6). Bound $\alpha 5 \beta 1$ was detected by FITC-conjugated rabbit anti-mouse anti-sera. Negative controls of both untreated and PDT treated cells (first left histogram of each) had secondary antibody only. The X-axis represents fluorescence intensity in log scale and the Y-axis represents cell counts (no. of events).

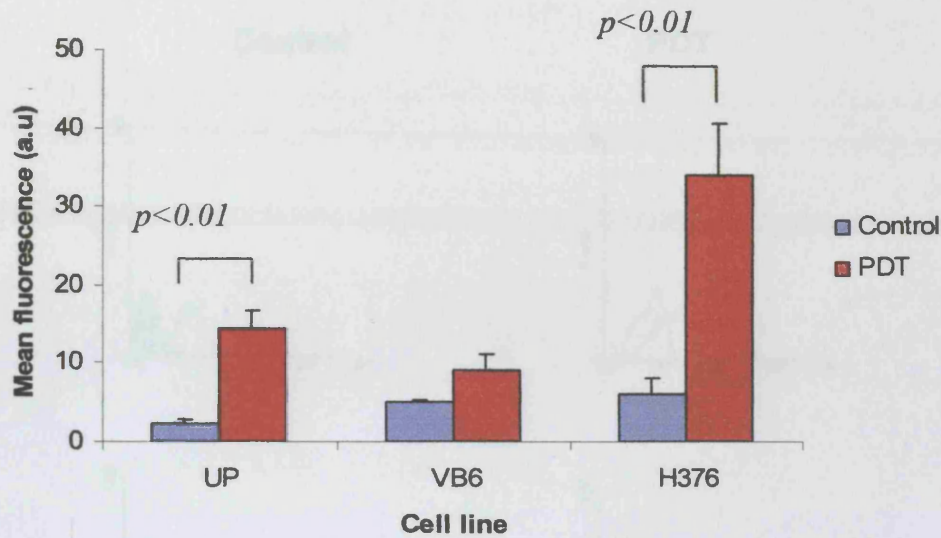


Figure 4.16 A representative chart bar of mean fluorescence values of receptor expression shown in Figure 4.15. Values were calculated by subtracting the mean fluorescence (arbitrary units) of the peaks of second antibody labelled of cells (both PDT and control cells) from mean fluorescence of the peaks of $\alpha 5\beta 1$ labelled cells. Error bars are standard deviation of triplicate experiments.

Figure 4.17 Histograms analysis of cells by UP, VB6, and H376 cells. Cells were stained by trypan blue and labelled with anti-CD45. Bound cells were stained by FITC-conjugated anti-CD45 antibody. Negative controls of both untreated and PDT treated cells were not stained with secondary antibody only. The X-axis represents the intensity of the signal and the Y-axis represents the number of cells.

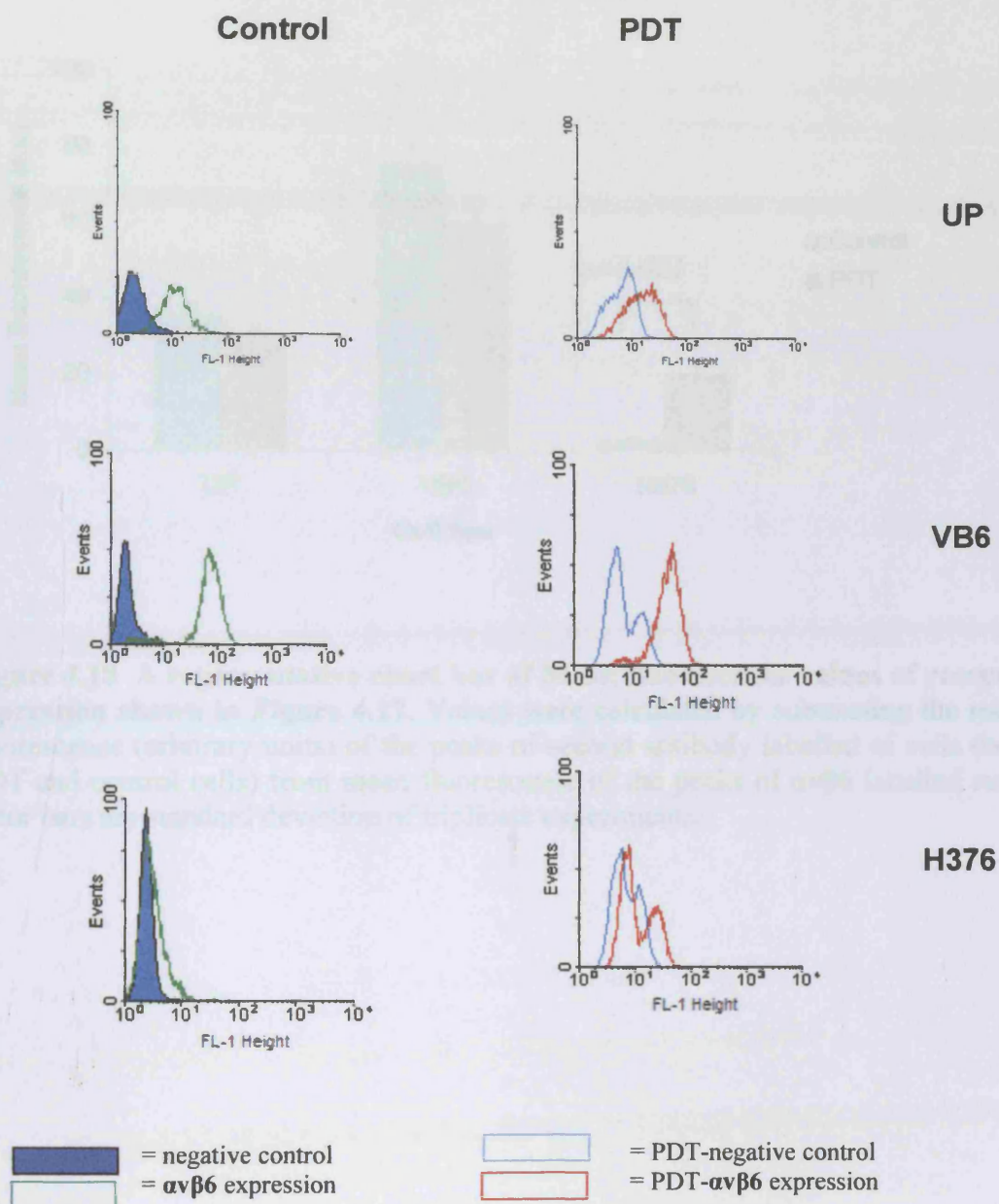


Figure 4.17 Histograms analysis of $\alpha v \beta 6$ by UP, VB6, and H376 cells. Cells were released by trypsin/EDTA and labelled with $\alpha v \beta 6$ (E7P6). Bound $\alpha v \beta 6$ was detected by FITC-conjugated rabbit anti-mouse anti-sera. Negative controls of both untreated and PDT treated cells (first left histogram) had secondary antibody only. The X-axis represents fluorescence intensity in log scale and the Y-axis represents cell counts (no. of events).

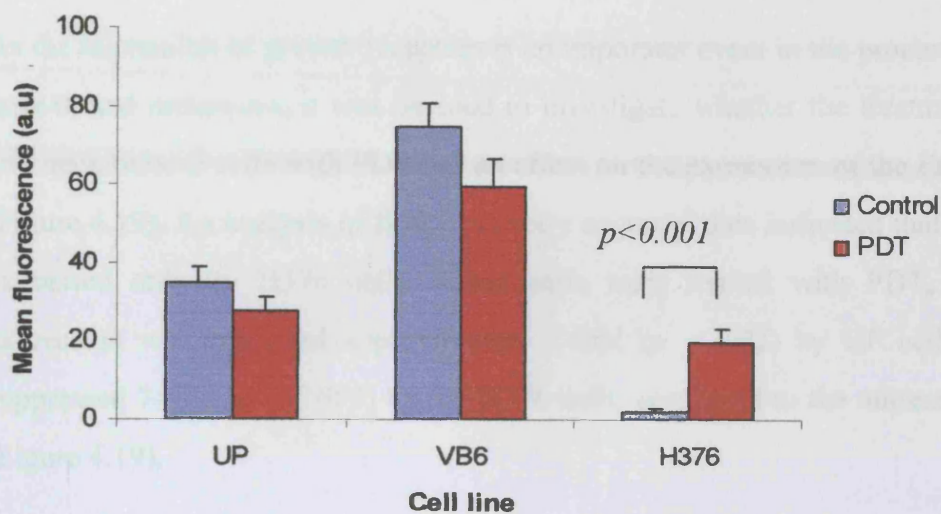


Figure 4.18 A representative chart bar of Mean fluorescence values of receptor expression shown in Figure 4.17. Values were calculated by subtracting the mean fluorescence (arbitrary units) of the peaks of second antibody labelled of cells (both PDT and control cells) from mean fluorescence of the peaks of $\alpha v\beta 6$ labelled cells. Error bars are standard deviation of triplicate experiments.

4.11 PDT regulates EGFR

As the expression of growth receptors is an important event in the process of tumour growth and metastasis, it was decided to investigate whether the treatment of head and neck tumour cells with PDT has an effect on the expression of the EGF receptor (Figure 4.19). An analysis of flow cytometry acquired data indicated that EGFR was expressed only by H376 cells. When cells were treated with PDT, the EGFR expression was enhanced approximately 3-fold ($p < 0.01$) by UP cells only and suppressed 7-fold ($p < 0.001$) by the H376 cells, compared to the untreated controls (Figure 4.19).

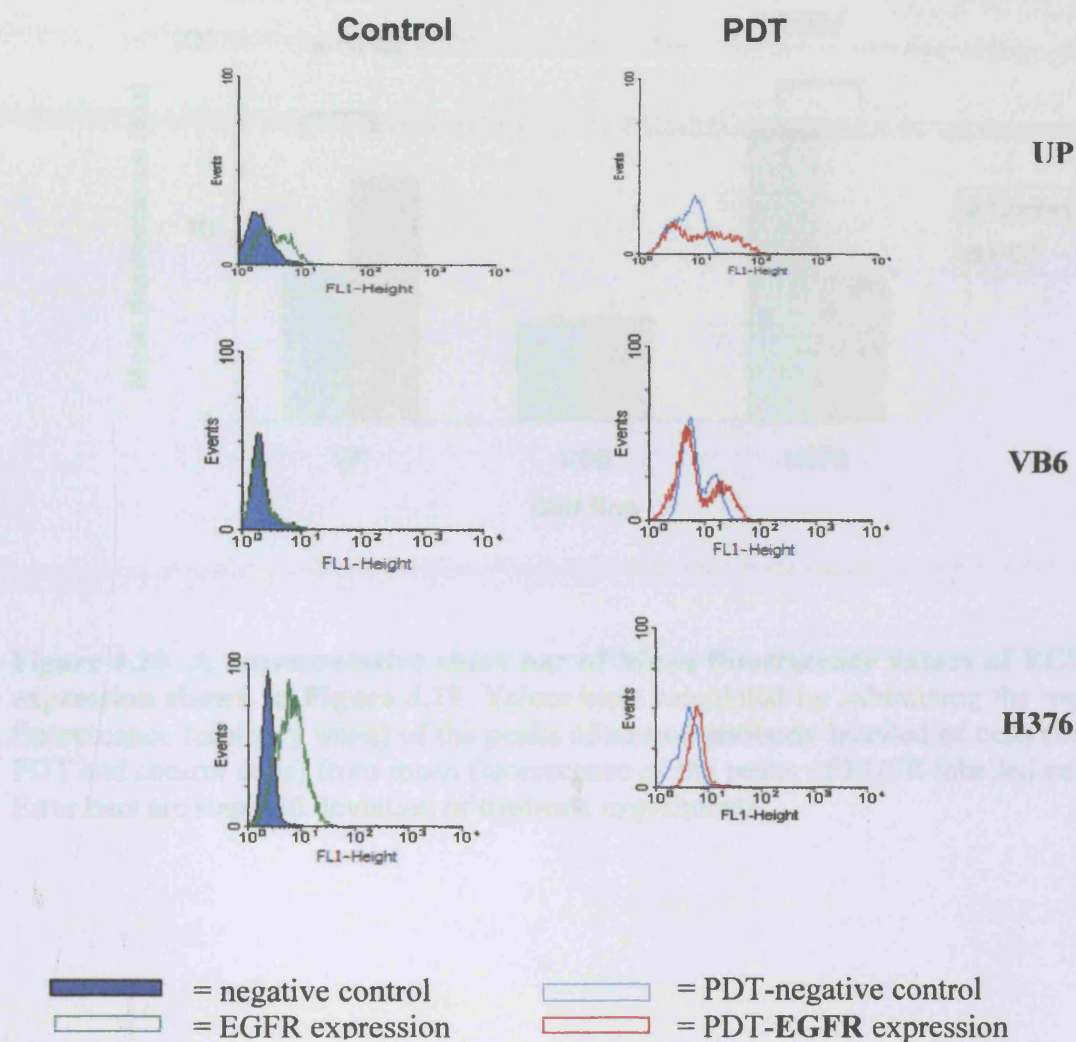


Figure 4.19 Histogram of EGFR expressions by UP, VB6 and H376 cells. Cells were either given no treatment (control) or treated with sublethal dose of PDT (Table 3.1). Cells were released and labelled with EGFR (102618). Bound EGFR was detected by FITC-conjugated rabbit anti-mouse anti-sera. Negative controls of both untreated cells and PDT treated cells (first left histogram) had secondary antibodies only. The X-axis represents fluorescence intensity in log scale and the Y-axis represents cell counts (no. of events).

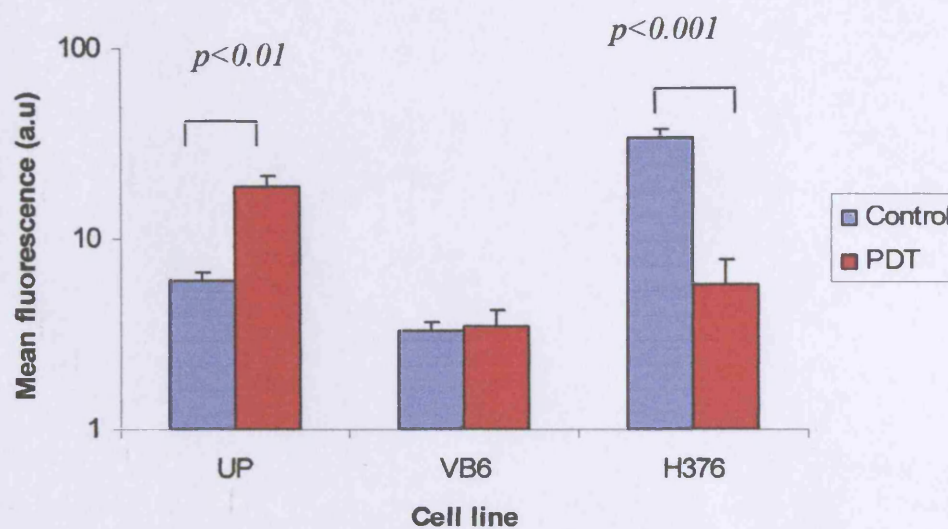


Figure 4.20 A representative chart bar of Mean fluorescence values of EGFR expression shown in Figure 4.19. Values were calculated by subtracting the mean fluorescence (arbitrary units) of the peaks of second antibody labelled of cells (both PDT and control cells) from mean fluorescence of the peaks of EGFR labelled cells. Error bars are standard deviation of triplicate experiments.

4.12 PDT effects on the expression of HGFR

It was also decided to investigate whether the combined treatment has any effect on the expression of HGF receptors (Figure 4.21). An analysis of flow cytometry results indicated that HGFR was not expressed by any of the cell lines, nor were any significant changes observed following treatment with sub-lethal doses of PDT (Figure 4.22).

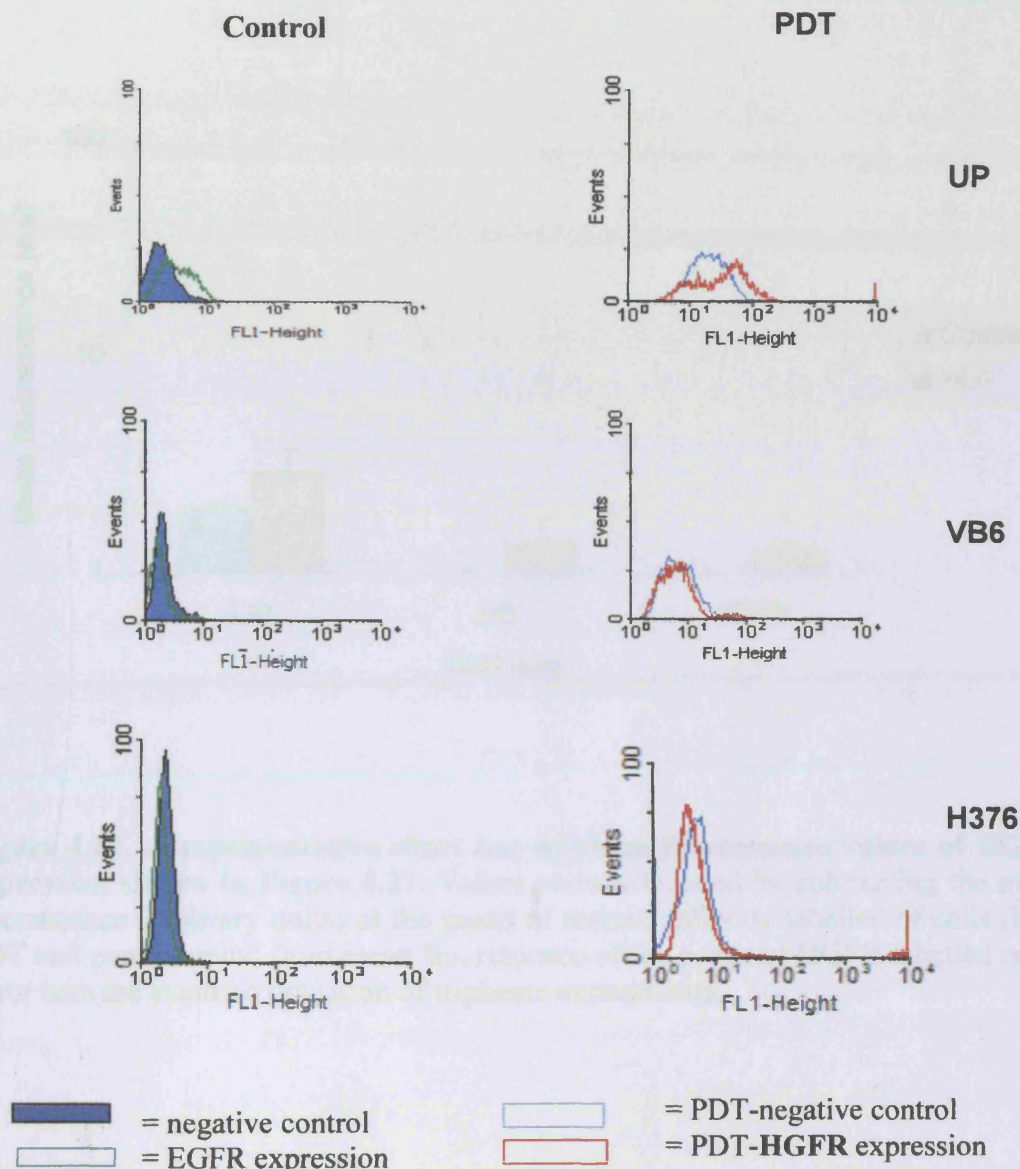


Figure 4.21 Histogram of expression of HGFR by UP, VB6 and H376 cells. Cells were either given no treatment (control) or treated with sublethal dose of PDT (Table 3.1). Cells were released and labelled with HGFR (35309). Bound GFR was detected by FITC-conjugated rabbit anti-mouse anti-sera. Negative controls of both untreated cells and PDT treated cells (first left histogram) had secondary antibodies only. The X-axis represents fluorescence intensity in log scale and the Y-axis represents cell counts (no. of events).

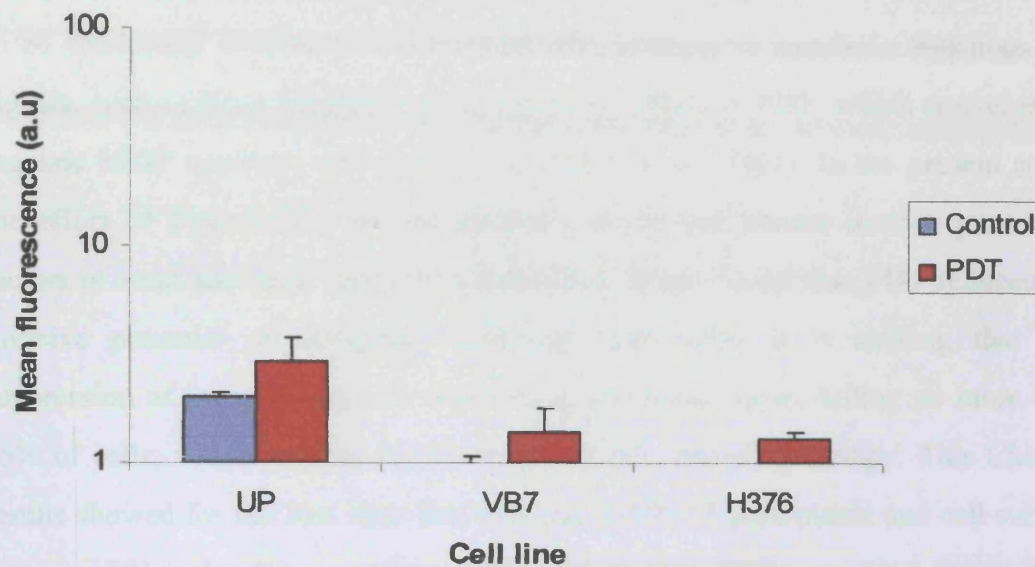


Figure 4.22 A representative chart bar of Mean fluorescence values of HGFR expression shown in Figure 4.21. Values were calculated by subtracting the mean fluorescence (arbitrary units) of the peaks of second antibody labelled of cells (both PDT and control cells) from mean fluorescence of the peaks of HGFR labelled cells. Error bars are standard deviation of triplicate experiments.

4.13 Discussion

The precise mechanism by which PDT interferes with the metastatic process has yet to be elucidated. This may be associated with changes in metabolic functions and signals, such as those triggered by the apoptotic effect of PDT, which converges to regulate MMP synthesis and activity (Agostinis et al., 2004). In the present study, the effect of Foscan-PDT on the synthesis of several known tumour promoting factors in head and neck cancer was examined. It was found that PDT reduced the invasive potential of malignant head and neck cells. It is striking that this suppression of invasiveness was observed at sub-lethal doses, killing no more than 15% of cells, which implies the feasibility of this emerging therapy. This Chapter results showed for the first time that uPA and MMP-13 proteinases and cell surface integrin $\alpha 5\beta 1$ and $\alpha v\beta 6$ expression can be modulated by PDT.

In this study, invasiveness reduction was associated with the decreased activity of MMP-2 and MMP-9 in most of the cell models used. This conflicts with the findings of other researchers (Ferrario et al., 2004) who have explored the effect of PDT on the expression and/or activity of MMP-2 and MMP-9 and found that exposure of mouse mammary tumour to Photofrin-mediated PDT has increased the MMP-9 activity, but without significant changes in MMP-2 profiles. One potential explanation for this enhancement of MMP-9 activity could relate to the different protocol applied, i.e. the use of broad spectrum fluorescence bulbs to initiate the photochemical reaction, which might included UVB bands, and has been shown to stimulate the expression and secretion of different MMPs (Ramos et al., 2004; Brenneisen et al., 2002). In a recent *in vitro* report, it was demonstrated that when fibroblast cells were treated with ALA-PDT, no change in MMP2 secretion was observed, while the levels of MMP-1 and MMP-3 proteins increased up to 3-fold, suggesting that MMP-1 and MMP-3 are produced by fibroblasts in response to photodynamic therapy (PDT) and may be involved in the antisclerotic effects of ALA-PDT (Karrer et al., 2003). This effect was not obvious on keratinocytes, since neither enzyme, MMP-1 nor MMP-3, was altered significantly (Karrer et al., 2004).

Du et al. have analysed the effect of hypericin-based photodynamic therapy (hypericin-PDT) on MMP-1 expression in two nasopharyngeal cancer (NPC) cell lines and in an animal tumour model (Du et al., 2004). They found MMP-1 was increased at both mRNA and protein levels in well differentiated HK1 and poorly differentiated CNE-2 NPC cells.

On gelatinase zymography, MMP-2 and MMP-9 activity is occasionally seen as a doublet, reflecting the inactive, higher molecular weight and the active, lower molecular weight of the enzyme. Here, both the decrease and increase in intensity of both bands were noted. An increase of the higher weight inactive form by non-malignant UP cells and lowers molecular weight active form by H376 cell line following PDT suggests that PDT could have an effect on local factors, e.g. an imbalance between MMPs and their inhibitors, while the decrease in the upper band could be due to a reduction in the synthesis or secretion of the matrix protein. Also, the low secretion of MMP-13 by VB6 cells may be explained by recent findings on $\beta 6$ -transfected OSCC cells, that $\alpha v\beta 6$ integrin has caused downregulation of MMP-13 expression at both mRNA and protein level (Ylipalosaari et al., 2005).

In the present study, the levels of uPA and VEGF were reduced by invasive cell lines. This agrees with the findings of Uehra et al., who reported a decrease in VEGF expression 24 h after PDT, and attributed this reduction to tumour re-oxygenation (Uehara et al., 2001). It was also demonstrated that following exposure to PDT, the VEGF expression in healthy tissue surrounding rat brain tumour was highly expressed in comparison to the tumour tissue (Jiang et al., 2004).

A sub-lethal dose of PDT markedly reduced cell attachment to collagen, fibronectin, Matrigel and plastic tissue culture with a reduction of cell migration. The reaction of cells with their surrounding matrices has been shown to promote cell migration, proliferation and the digestion of ECM (Kramer et al., 2005). It was demonstrated previously that the prevention of cancer metastasis can be achieved by the

prevention of tumour adhesion and migration (Liotta et al., 1982), and agents that inhibit cell attachment *in vitro* decrease the invasiveness and metastatic potential of cancer cells *in vivo* (Vollmers et al., 1984; Humphries et al., 1986). This study demonstrated that the attachment of transformed and malignant cells to the type I collagen, fibronectin, Matrigel and plastic substratum decreased following pre-treatment with a sub-lethal dose of PDT, and this depended on cell type and matrix proteins. This is in agreement with Vonarx (1995), who found that treatment of colonic cancer cells with hematoporphyrin photosensitiser caused a decrease in the adhesion of cells to the ECM proteins with subsequent reduction of their metastatic potential (Vonarx et al., 1995). A similar result is reported in another study (Foultier et al., 1994). In addition, a recent report demonstrated that ALA-PDT resulted in a slowing down the cell attachment process at both toxic and non-toxic PDT application (Uzdensky et al., 2004).

Trypsin acts by digesting the bonds between the cell surface proteins and the substratum and leads to cell detachment. In the present study, it was demonstrated that the suppression effects of Foscan-PDT on trypsin-induced cell detachment and the reduction in enzyme activity showed differential effects in relation to cell lines and time after PDT treatment. These observations are in agreement with Uzdensky [2004], who demonstrated that the trypsin releasing efficiency is lost when adenocarcinoma cells were grown on plastic substratum and treated with a sub-lethal dose of PDT using 5-aminolevulinic acid (ALA), disulfonated tetraphenylporphyrine (TPPS2a), or a MitoTracker Red (MTR) as photosensitiser (Uzdensky et al., 2004). However, this was in contrast to Ball [2001], who reported no resistance to trypsin in fibroblast cells when m-THPC was used as a photosensitiser but a significant resistance with pyridinium zinc(II) phthalocyanine (PPC), suggesting that the role of tissue transglutaminase may cause this resistance (Ball et al., 2001).

The role of integrins in the regulation of the adhesion of cells to the ECM is well established. Integrin-mediated cell adhesion can trigger Ca^{2+} influx, activate and

deactivate protein tyrosine kinases (e.g. focal adhesion kinase (FAK) and Src tyrosine kinase), serine/threonine protein kinases, e.g. MAP kinases, protein kinase C (Giancotti and Ruoslahti, 1999; Cordes and Meineke, 2004; Danen, 2005). In this study, the two subunits, $\alpha 5 \beta 1$ and $\alpha v \beta 6$ integrins were examined. The data showed for the first time that cell surface integrin $\alpha 5 \beta 1$ and $\alpha v \beta 6$ expression can be modulated by Foscan-PDT. This was clear in $\alpha v \beta 6$ positive cell line (VB6), which was reduced by PDT.

The results demonstrated that Foscan based PDT markedly reduces the ability of UP, VB6 and H376 cells to migrate and invade through artificial membrane. The mechanism by which PDT extensively suppresses cell migration and inhibits the invasive process is unclear. Invading cells must pass through an extracellular matrix, a process that involves attachment/detachment and enzymatic degradation of the components of the ECM. The results of this study shown that secretion of MMP-2, MMP-9, MMP-13, uPA and VEGF was reduced following PDT, which could explain the reduction of cells invasive potential. Many studies revealed that the enhanced production of MMPs, uPA and VEGF correlates with the invasion, metastasis and angiogenesis of the tumour cells (Franchi et al., 2002; Werner et al., 2002; Culhaci et al., 2004; Pacheco et al., 2002; Chin et al., 2005; Benefield et al., 1996).

Chapter 5

Results III

Chemical Therapy: Its Implication for Combination Treatment with Photodynamic Therapy.

5.1 Introduction

Combination therapies have been shown to improve the treatment outcomes in many human cancers, including head and neck squamous cell carcinoma. Using this approach, drug resistance and limitation can be overcome. The most commonly used combinations are chemotherapy regimens whereby different agents are given concurrently, i.e. cisplatin/5-fluorouracil and combinations of chemotherapy with radiotherapy (Bradley et al., 2002), and more recently with tyrosine kinase inhibitors (Ciardiello et al., 2000; Raben et al., 2005; Zhu et al., 2005). PDT is characterised by low toxicity and cost, excellent cosmetic results and absence of significant morbidity (D'Cruz et al., 2004; Hopper et al., 2004b) but at the same time there are several side effects, such as prolonged photosensitization, limited depth and others, which occasionally cause long-term follow-up results to be worse than for its conventional counterparts.

Nevertheless, at the time of writing, there has been no work on combinations of PDT with either ZD1839 or PD153035 TKIs. Therefore, the effects of small molecules (ZD1839 and PD153035) or CDDP chemotherapy combined with Foscan mediated-PDT on the toxicity and anti-metastatic effects of PDT, were evaluated using oral squamous carcinoma cell lines as ‘‘targets’’.

5.2 CDDP augments PDT anti-tumour activity

To evaluate the effects of CDDP combined with PDT on cell toxicity, the cells were treated with combination doses of PDT and CDDP. Firstly, the effect of CDDP on the viability of transformed and malignant cells as a single treatment was evaluated. Compared to the untreated controls, cell growth (Figure 5.1) as evaluated by MTT assay revealed that CDDP suppressed the proliferation of UP, VB6 and H376 cells in a dose-dependent manner, with IC_{50} ranging between 6 and 12 $\mu\text{g/ml}$. Approximately 90% inhibition of growth was observed at a dose of 4 $\mu\text{g/ml}$ in UP cells and 2 $\mu\text{g/ml}$ in both VB6 and H376.

Subsequently, the effect of the addition of CDDP to PDT was determined. Figure 5.2 shows that additive (no more than the addition of the efficiency of each treatment modality alone) and synergistic (exceeds the value of each modality) inhibitory effects on growth were achieved when PDT was combined with CDDP. This was dependent on cell line and CDDP dose. In UP cells, only an additive inhibition effect was produced following combination of PDT with any of CDDP dose used (Figure 5.2A-C).

In H376 cells, a synergistic inhibitory effect (Figure 5.2A-B) was produced at 4 $\mu\text{g/ml}$ of CDDP, since a single treatment with CDDP or PDT reduces the cell survival to $57 \pm 7.3\%$ and $71 \pm 1\%$, respectively, whereas exposure to both treatments reduced cell survival to $8 \pm 2\%$. When PDT was combined with 8 $\mu\text{g/ml}$ of CDDP, an additive inhibitory effect on H376 cells was observed (Figure 5. 2C).

For VB6 line, an additive inhibitory effect (Figure 5.2A-B) was produced only when cells were treated with PDT combined with 8 $\mu\text{g/ml}$ of CDDP, since a single treatment with CDDP or PDT reduces the cell survival to $39 \pm 3.8\%$ and $83 \pm 6\%$, respectively and exposure to both treatments reduced cell survival to $14 \pm 2.5\%$.

Exposure of VB6 cells to combined doses of PDT and CDDP (2 and 4 $\mu\text{g/ml}$) caused a synergetic effect on cell survival.

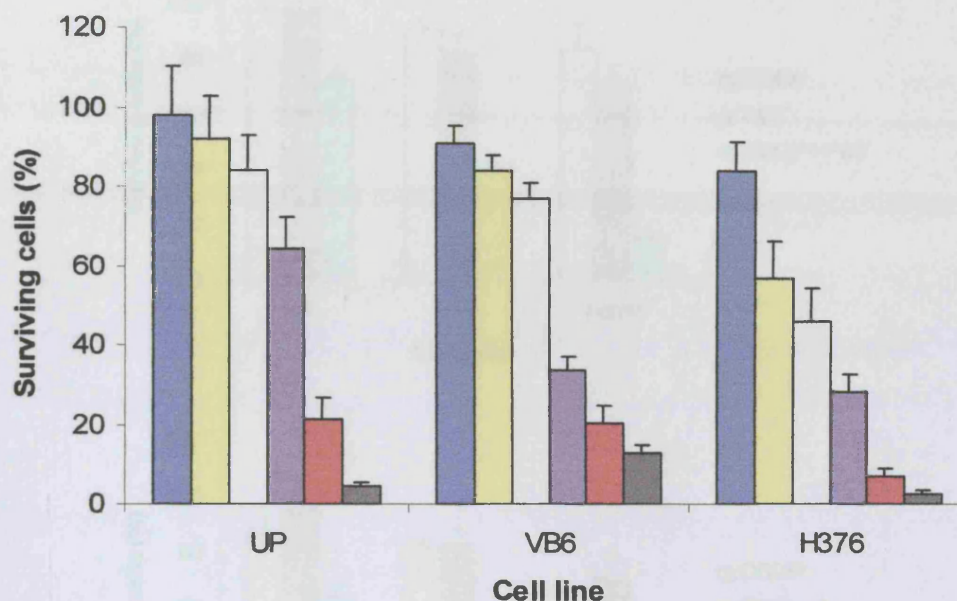


Figure 5.1 Toxicity of CDDP on UP, VB6 and H376 cells. Cells were incubated with CDDP at 2 (■), 4 (■), 6 (□), 10 (■), 20 (■), and 40 (■) µg/ml for 24 h. Cells were then released and counted using MTT assay. The data represents the % of surviving cells 24 h after the treatment relative to the untreated controls (=100). Error Bars represent standard deviations of triplicate wells. The experiment was repeated twice with similar results.

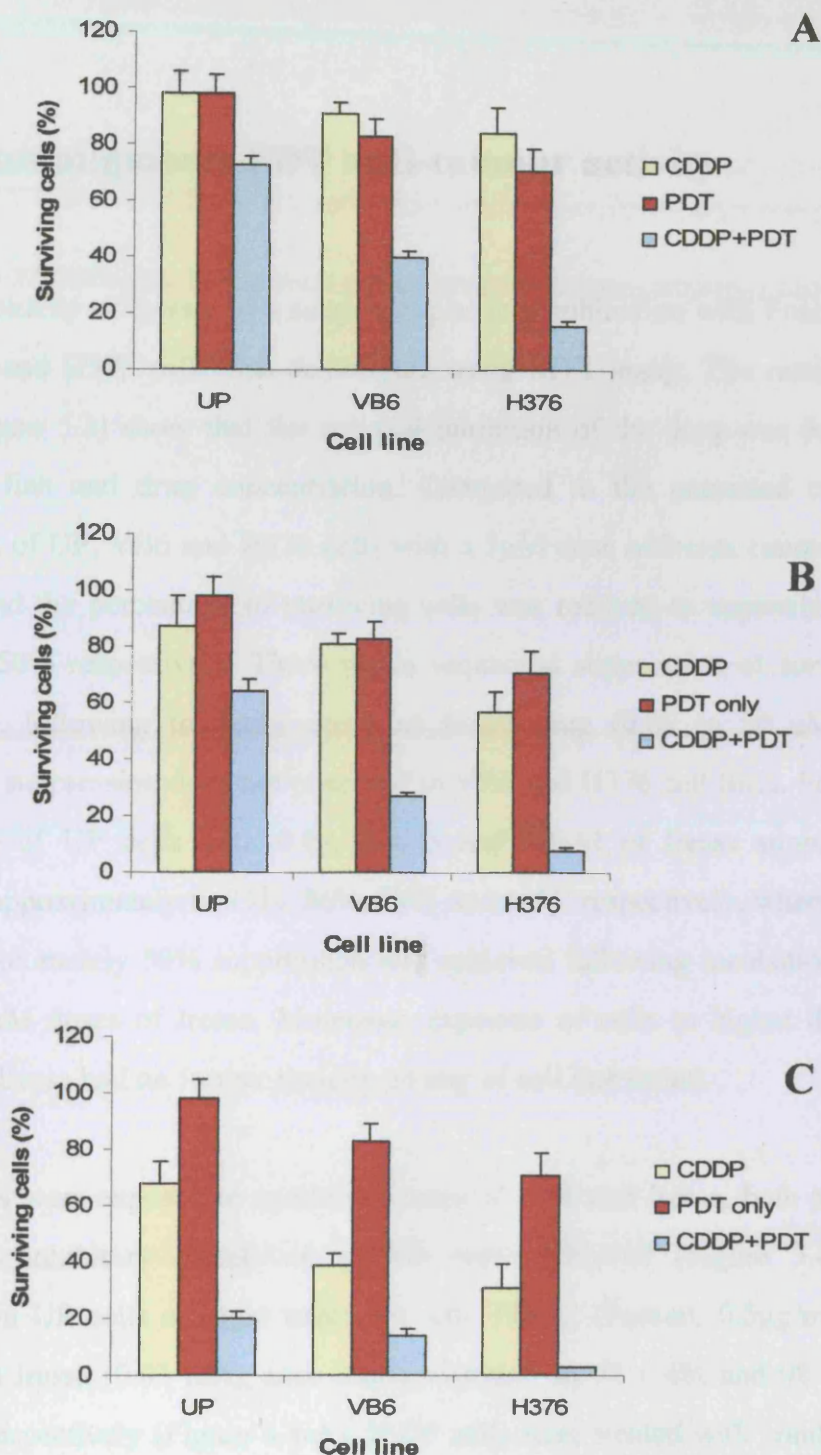


Figure 5.2 Toxicity of PDT combined with CDDP on UP, VB6 and H376 cells. Cells were incubated with CDDP at 2 (A), 4 (B) or 8 µg/ml (C) for 24 h. Cells were treated with small dose of PDT (0.5 µg/ml Foscan; 0.5 J/cm² light) before being released and counted using MTT assay. The data represents the % of cells that survived 24 h after the treatment in comparison to the untreated controls (=100). Figure represents results for one experiment run in triplicate. Error bar represent standard deviation of triplicate wells. The experiment was repeated twice with similar results.

5.3 Iressa augments PDT anti-tumour activity

The cytotoxicity of Iressa, as a single drug or in combination with Foscan-PDT, on UP, VB6 and H376 cells was determined using MTT assay. The results of Iressa alone (Figure 5.3) show that the survival inhibition of the drug was dependent on both cell line and drug concentration. Compared to the untreated controls, the incubation of UP, VB6 and H376 cells with a 5 μ M dose of Iressa caused maximum toxicity and the percentage of surviving cells was reduced to approximately 79%, 72% and 50% respectively. There was a sequential suppression of survival in UP cells only, following increases doses of Iressa drug (0.05 to 50 μ M), but this sequential suppression does not observed in VB6 and H376 cell lines. Fore example incubation of UP cells with 0.05, 0.5, 5 and 50 μ M of Iressa suppressed their survivals approximately to 93%, 86%, 79% and 63%, respectively, whereas in H376 cells, approximately 50% suppression was achieved following incubation with 0.5, 5 and 50 μ M doses of Iressa. Moreover, exposure of cells to higher doses (up to 50 μ M) of Iressa had no further toxicity on any of cell line tested.

When cells were exposed to combined doses of PDT and Iressa, both additive and synergistic inhibitory effects on growth were achieved (Figure 5.4A-C). For example, in UP cells a single treatment with PDT-2 (Foscan, 0.5 μ g/ml; light 0.5 J/cm²) and Iressa (0.05 μ M), each alone, resulted in $97 \pm 4\%$ and $98 \pm 11\%$ cell survival, respectively (Figure 5.4-A). If UP cells were treated with combined doses of PDT-2 (Foscan, 0.5 μ g/ml; light 0.5 J/cm²) and Iressa (0.05 μ M), the cell survival was reduced (synergistically) to $73 \% \pm 6\%$. In VB6 cells (Figure 5.4-B), a single treatment with PDT (Foscan, 0.5 μ g/ml; light 0.5J/cm²) or Iressa (0.05 μ M) reduced cell survival approximately to $87 \pm 2\%$ and 85% respectively in comparison to the untreated controls (100%). Exposure of cells to combined doses of PDT and Iressa

reduced the cell survivals to 35%. Similarly in H376 cells, combined treatment had synergistically reduced the cell survivals to 25% (Figure 5.4-C).

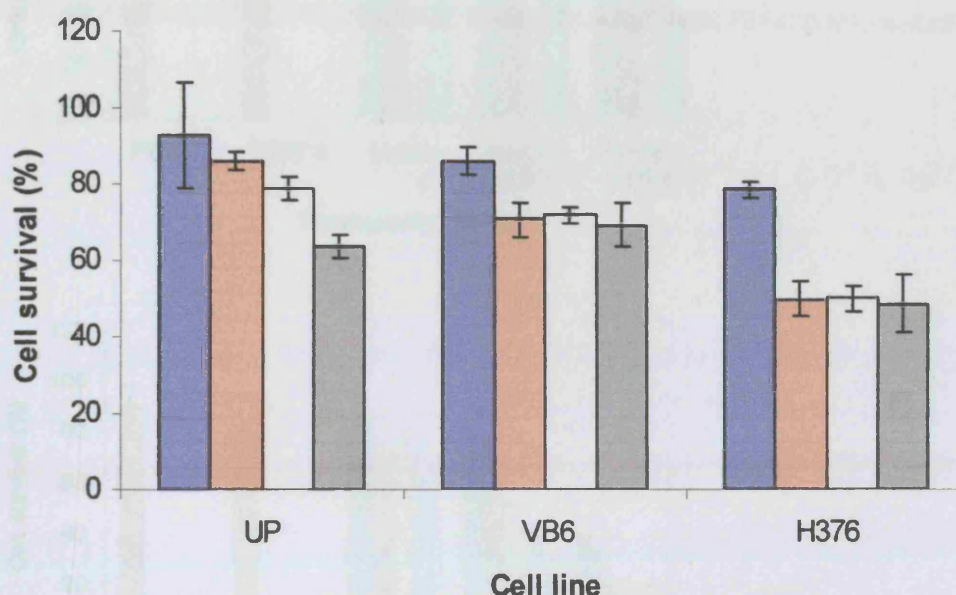


Figure 5.3 Toxicity of Iressa on UP, VB6 and H376 cells. Cells were incubated with Iressa at 0.05 (■), 0.5 (■), 5 (□) or 50 (■) μ M. After 24 h, cells were released and counted using MTT assay. The data represents the % of surviving cells in comparison to the untreated controls (= 100). Error bar represent standard deviation of triplicate wells. The experiment was repeated twice with similar results.

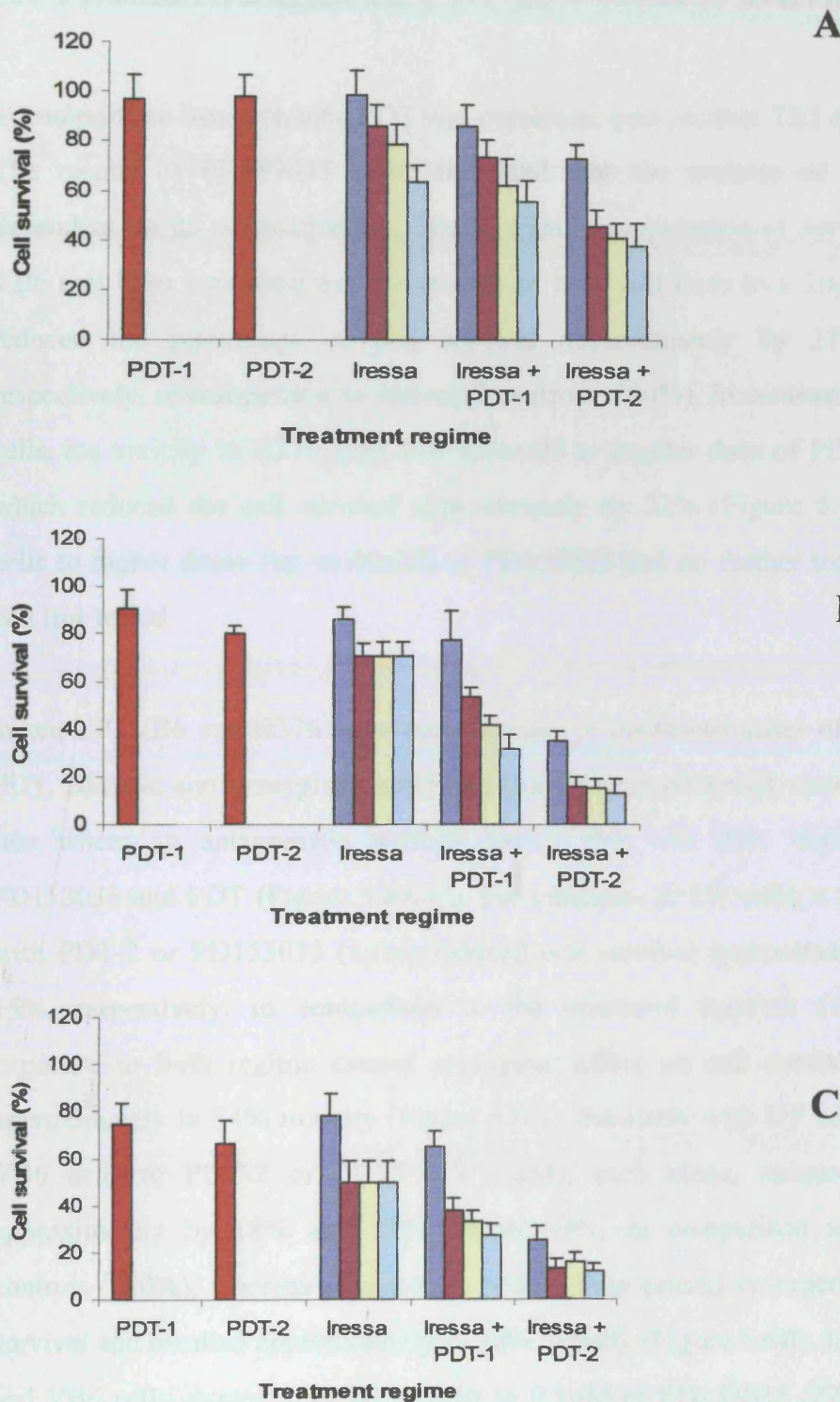


Figure 5.4 Toxicity of Iressa combined with PDT on UP (A), VB6 (B) and H376 cells (C). Cells were incubated with 0.05, (■), 0.1 (■), 1 (■), and 10 μM (■) of Iressa and PDT-1 (Foscan, 0.25 μg/ml; light 0.5 J/cm²) and PDT-2 (Foscan, 0.5 μg/ml; light 0.5 J/cm²) doses. The data represents the % of surviving cells compared to the untreated controls (=100). Error bar represent standard deviation of triplicate wells. The experiment was repeated twice with similar results.

5.4 PD153035 augments PDT anti-tumour activity

To support the Iressa results, PDT was combined with another TKI drug, PD153035. The results of PD153035 alone indicated that the toxicity of PD153035 was dependent on its concentrations. The maximum suppression of survival in UP and VB6 cell lines was obtained at exposure of both cell lines to a 20 μ M dose, which reduced the percentage of cell survival approximately by 27 % and 26%, respectively, in comparison to untreated controls (100%). In contrast to UP and VB6 cells, the toxicity in H376 cells was observed at smaller dose of PD153035 (1 μ M), which reduced the cell survival approximately by 52% (Figure 5.5). Exposure of cells to higher doses (up to 40 μ M) of PD153035 had no further toxicity on any of cell line tested.

When UP, VB6 and H376 cells were exposed to combined doses of PD153035 and PDT, additive and synergistic inhibitory effects were observed, except in H376 cell line where an antagonistic toxicity found; this was dose dependant of both PD153035 and PDT (Figure 5.6A-C). For example, In UP cells, a single treatment with PDT-2 or PD153035 (1 μ M) reduced cell survival approximately by 3% and 15%, respectively, in comparison to the untreated controls (100%), whereas exposure to both regime caused synergetic effect on cell survival and resulted approximately in 54% toxicity (Figure 5.6A). Similarly with UP cells, exposure of VB6 cells to PDT-2 or PD153035 (1 μ M), each alone, reduced cell survival approximately by 18% and 21%, respectively, in comparison to the untreated controls (100%), whereas exposure to both regime caused synergetic effect on cell survival and resulted approximately in 76% toxicity (Figure 5.6B). In contrast to UP and VB6 cells, exposure of H376 cells to 0.5 μ M of PD153035 (27% toxicity) and PDT-1 (26% toxicity), resulted in an antagonist effect on cell toxicity (41% toxicity). This antagonist effect become synergetic if PD153035 was combined with PDT-2 dose (31% toxicity), which increases the toxicity approximately to 70% (Figure 5.6C).

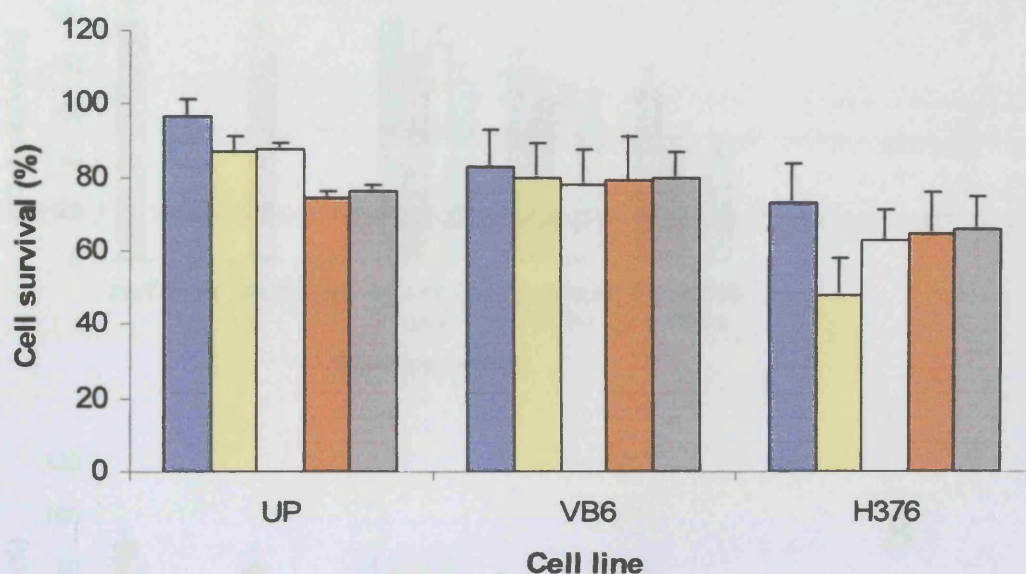


Figure 5.5 Toxicity of PD153035 on UP, VB6 and H376 cells. Cells were incubated with Iressa at, 0.5 (\blacksquare), 1 (\blacksquare), 5 (\square), 10 (\blacksquare) and 20 μ M (\blacksquare). After 24 h, cells were released and counted using MTT assay. The data represents the % of surviving cells in comparison to the untreated controls (=100). Error bar represent standard deviation of triplicate wells. The experiment was repeated twice with similar results.

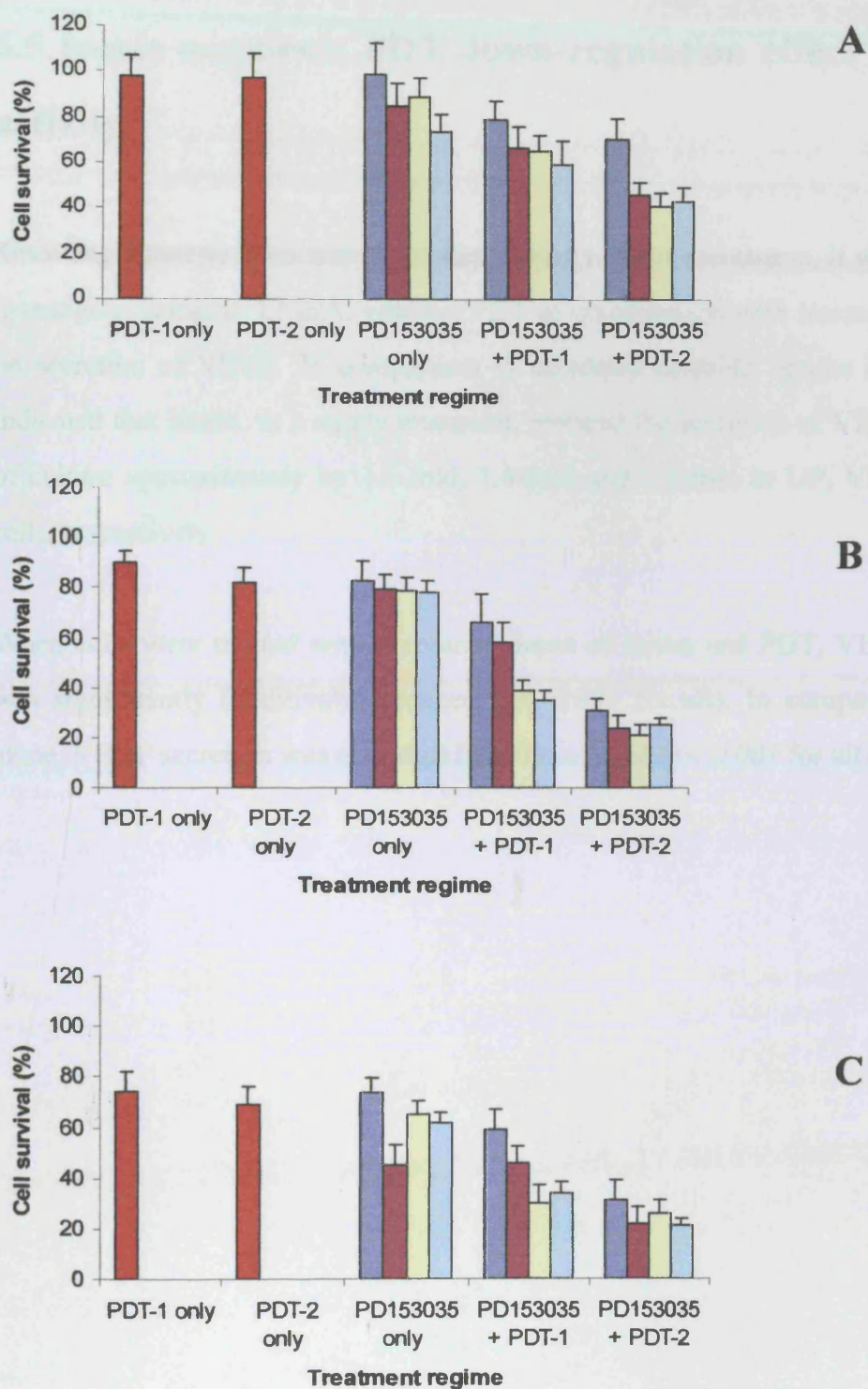


Figure 5.6 Toxicity of PD153035 combined with PDT on UP (A), VB6 (B) and H376 cells (C). Cells were either incubated with 0.5, 1, 5, and 20 μ M of PD153035 and then treated with PDT-1 and PDT-2. The data represents the % of surviving cells in comparison to the untreated controls (=100). Error bar represent standard deviation of triplicate wells. The experiment was repeated twice with similar results.

5.5 Iressa augments PDT down-regulation effect on VEGF activity

Since angiogenesis is an important step during tumour metastasis, it was decided to investigate, using an ELISA, whether PDT in combination with Iressa had an effect on secretion of VEGF. In comparison to untreated controls, results (Figure 5.7A) indicated that Iressa, as a single treatment, reduced the secretion of VEGF over 48 h of culture approximately by 1.1-fold, 1.4-fold and 1.5-fold in UP, VB6 and H376 cells, respectively.

When cells were treated with combined doses of Iressa and PDT, VEGF secretion was significantly (additively) reduced ($p < 0.001$ for all). In comparison to PDT alone, VEGF secretion was also significantly reduced ($p < 0.001$ for all).

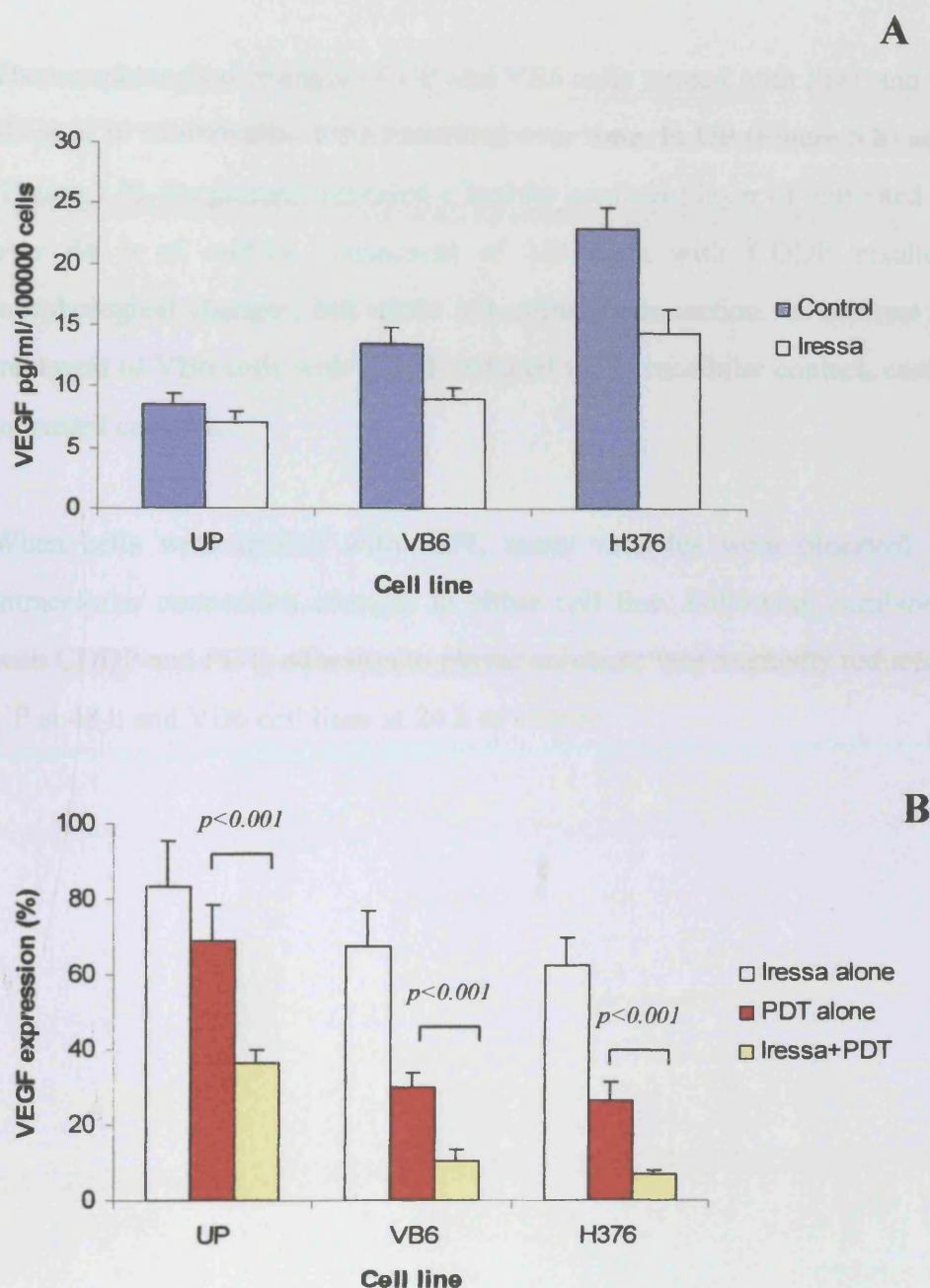


Figure 5.7 ELISA assay of VEGF activity on UP, VB6 and H376 cells. After treatment with Iressa ($0.5\mu\text{M}$ for UP and $0.05\mu\text{M}$ for VB6 and H376 cells) and PDT (Table 3.1), supernatant sampling of cells was collected 48 h after treatment. The amount of secreted VEGF/100000 cells is given in Figure 5.7A. The percentage of secreted VEGF in treated supernatants compared to the untreated control (= 100) is given in Figure 5.7B. Error bar represent standard deviation of triplicate samples. The experiment was repeated twice with similar results.

5.6 Cell morphology

The morphological changes of UP and VB6 cells treated with PDT and CDDP, each alone or in combination were examined over time. In UP (Figure 5.8) and VB6 cells (Figure 5.9), the pictures revealed a healthy confluent layer of untreated control cells over 48 h of culture. Treatment of UP cells with CDDP resulted in wavy morphological changes, but intact intracellular connection. In contrast to UP cells, treatment of VB6 cells with CDDP reduced the intracellular contact, compared to the untreated controls.

When cells were treated with PDT, many vacuoles were observed without any intracellular connection changes in either cell line. Following combined treatment with CDDP and PDT, adhesion to plastic substrate was markedly reduced in both the UP at 48 h and VB6 cell lines at 24 h of culture.

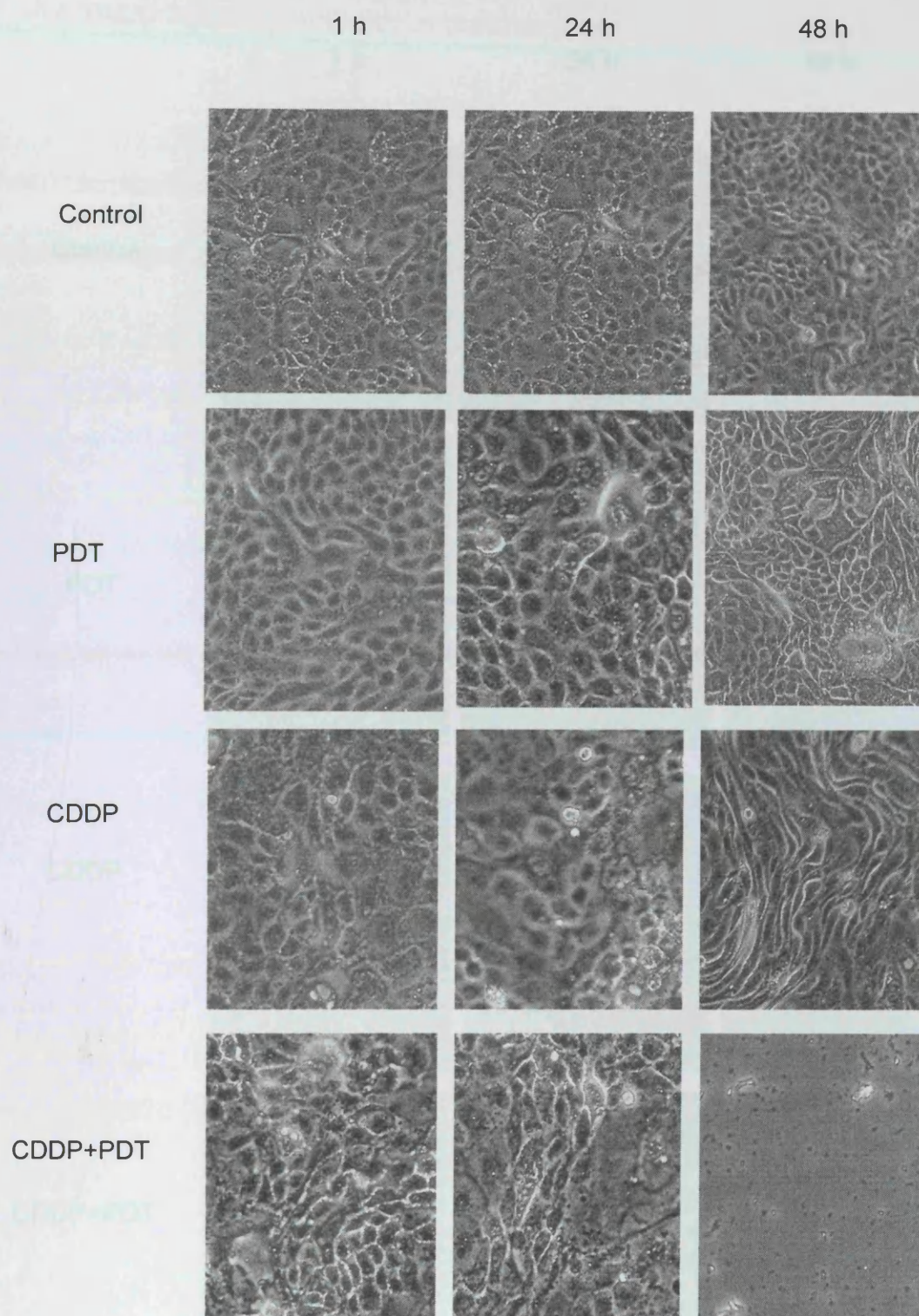


Figure 5.8 Morphology and adhesion of UP cells. Cells were either given no treatment (control) or treated with small dose of CDDP (4 μ g/ml) or PDT (Table 3.1) as a single or in combination. Pictures were taken at 1, 24 or 48h after the treatment.

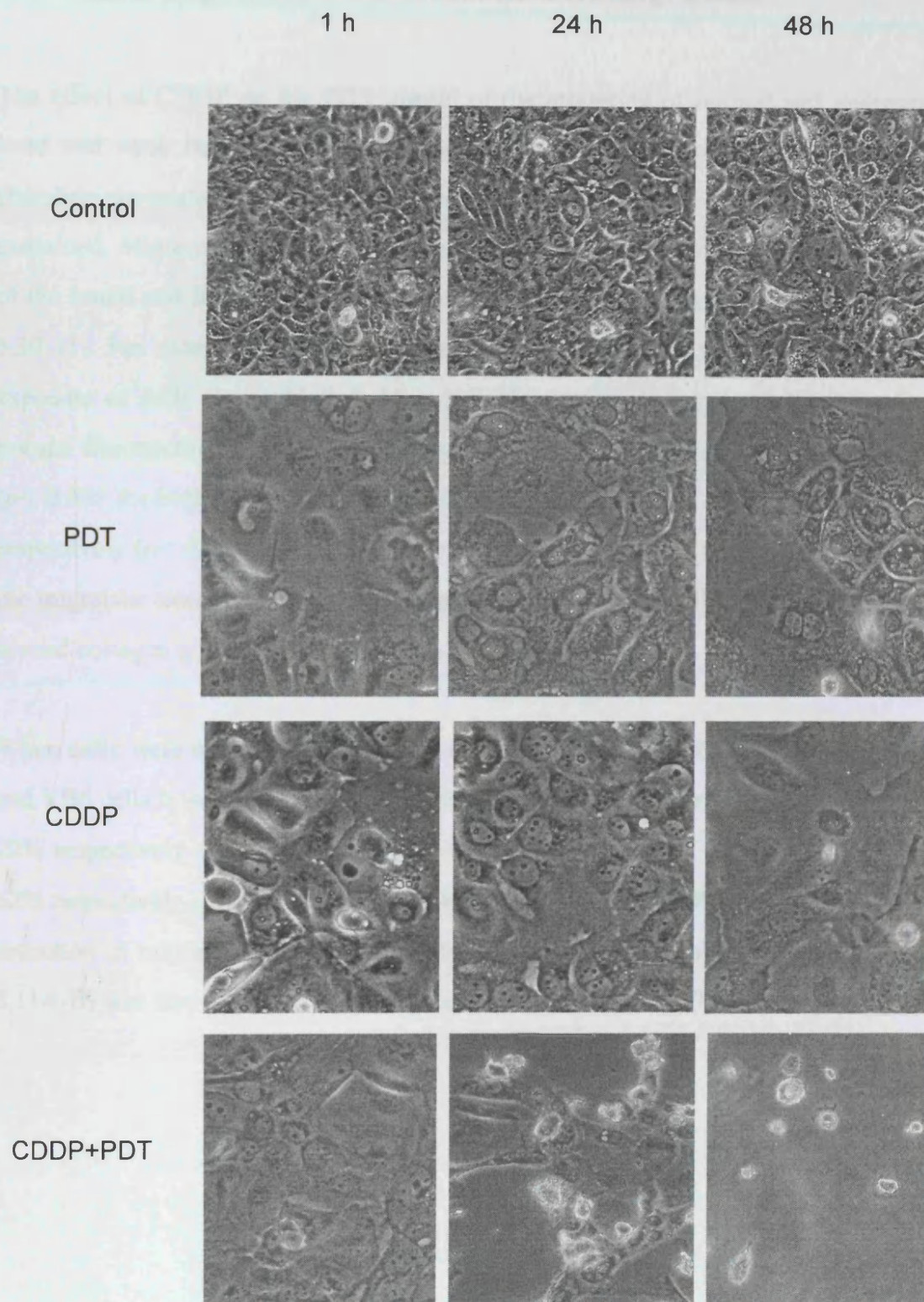


Figure 5.9 Morphology and adhesion of VB6 cells. Cells were either given no treatment (control) or treated with small dose of CDDP ($4\mu\text{g/ml}$) or PDT (Table 3.1) as a single or in combination. Pictures were taken at 1, 24 or 48h after the treatment.

5.7 CDDP regulates PDT effect on cell migration

The effect of CDDP on the PDT impact of the migration of normal and malignant head and neck human cell lines through a 8- μ m pores Transwell® cell culture chamber pre-coated with either fibronectin or collagen type-I ECM protein was examined. Migration experiments revealed that differences in the migration potential of the tested cell lines were dependent on both cell type and matrix proteins (Figure 5.10-11). For example, in UP and VB6 cells in comparison to untreated controls, exposure of cells to a sublethal dose of PDT alone down-regulated the migration toward fibronectin (Figure 5.10A-B) by approximately 56% and 75% respectively ($p < 0.001$ for both), and toward type I collagen (Figure 5.11A-B) by 64% and 67% respectively ($p < 0.001$ for all), whereas treatment of cells with CDDP alone reduced the migration toward fibronectin by approximately 18% and 17% respectively, and toward collagen type-1 by 15% and 20%, respectively.

When cells were exposed to combined doses of CDDP and PDT, migration of UP and VB6 cells toward fibronectin (Figure 5.10A-B) was further reduced by 36% and 22% respectively ($p < 0.001$ for both) in comparison to PDT alone, and 70% and 62% respectively ($p < 0.001$ for both) in comparison to CDDP alone. A significant reduction in migration of UP, VB6 and H376 cells toward collagen type I (Figure 5.11A-B) was also observed following exposure to PDT ($p < 0.05$ for all).

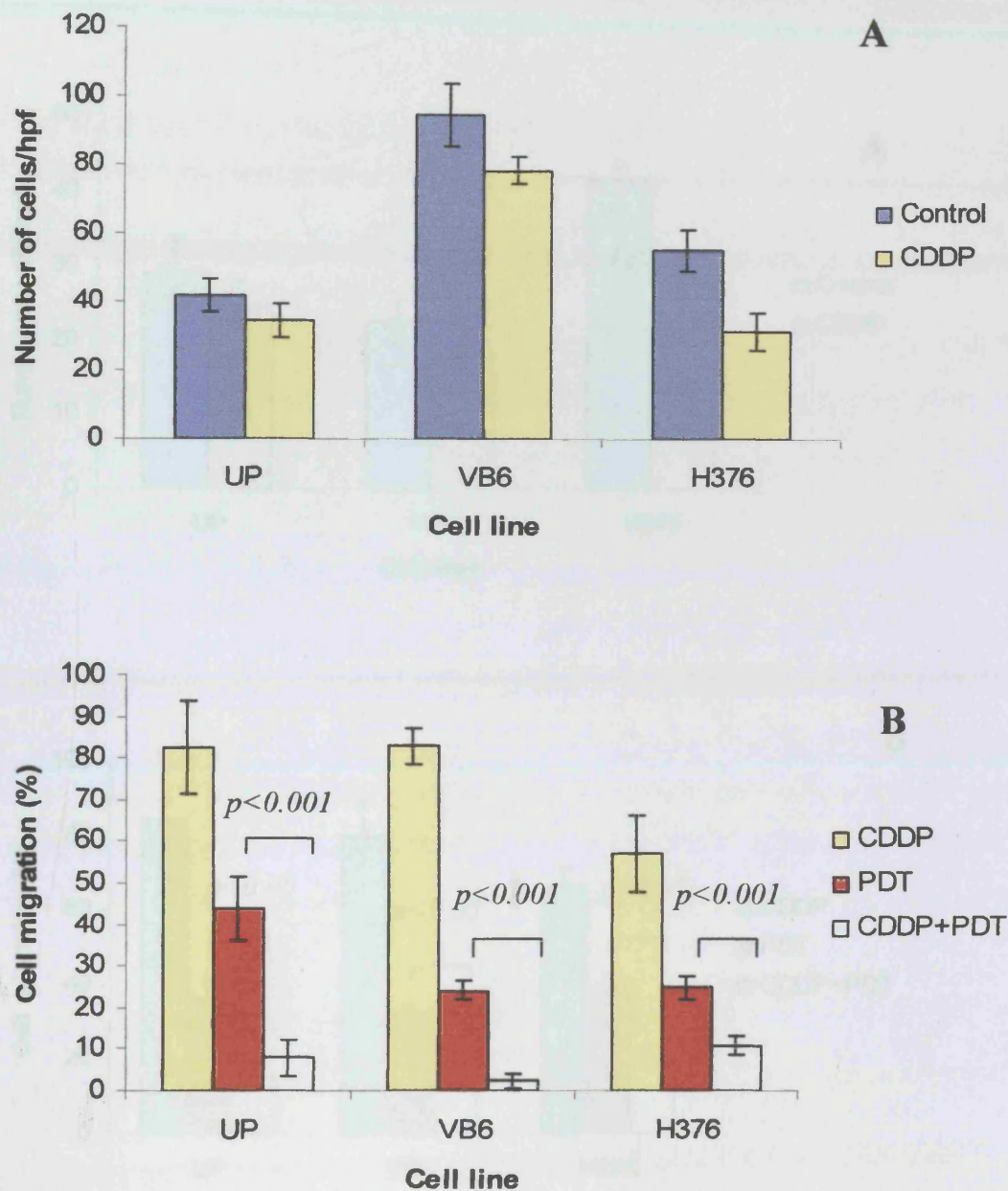


Figure 5.10 Effect of PDT and CDDP on UP, VB6 and H376 cell migration towards fibronectin. After treatment with small dose of CDDP (4 μ g/ml for UP and VB6 cells, and 2 μ g/ml for H376 cells) and PDT (Table 3.1), as single or in combination, cells then were detached and plated on Transwell membranes sub-coated with 10 μ g/ml of fibronectin and allowed to migrate for 4 h. Cells that had migrated and bound to the under-surface of the filter were stained and counted using light microscopy at X40. The number of migrating cells is given in Figure 5.10A. The percent of migrating cells per high power field in each membrane compared to untreated control (= 100) is given in Figure 5.11B. Error bar represent standard deviation of triplicate membranes. The experiment was repeated once with similar results.

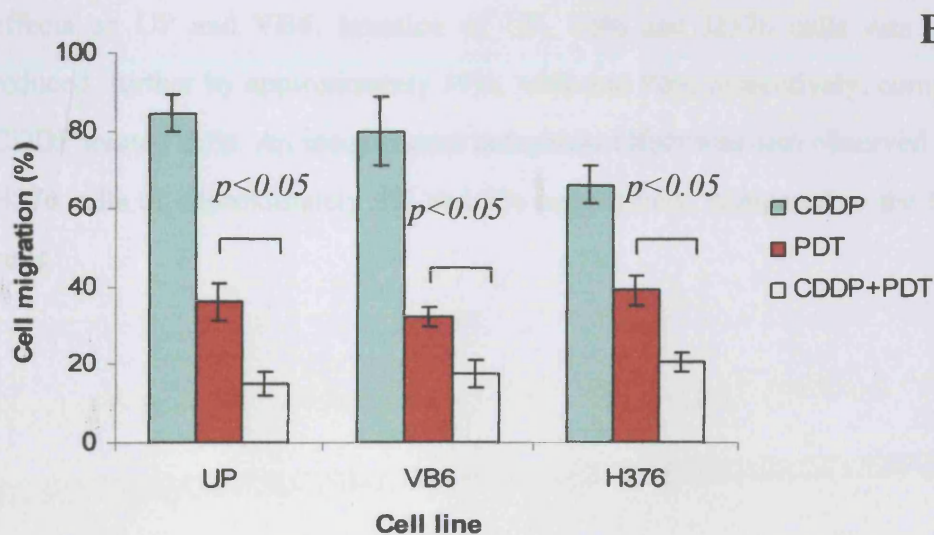
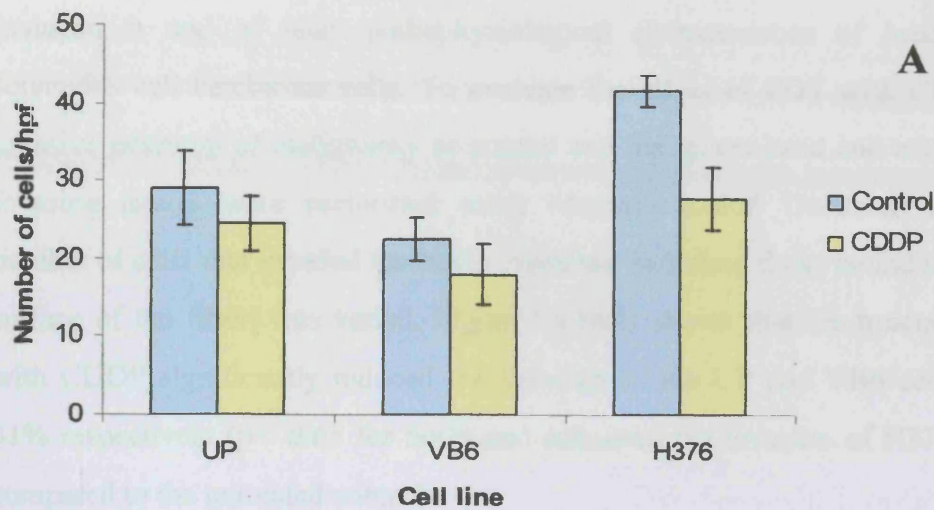


Figure 5.11 Effect of PDT and CDDP on the migration of UP, VB6 and H376 cells towards collagen type-I. After treatment with small dose of CDDP (4 μ g/ml for UP and VB6 cells, and 2 μ g/ml for H376 cells) and PDT (Table 3.1), as single or in combination, cells then were detached and plated on Transwell membranes sub-coated with 10 μ g/ml of collagen type-I and allowed to migrate for 4 h. Cells that had migrated and bound to the under-surface of the filters were stained and counted using light microscopy at X40. The number of migrating cells is given in Figure 5.11A. The percent of migrating cells in each membrane compared to untreated control (= 100) is given in Figure 5.11B. Error bar represent standard deviation of three assays. The experiment was repeated once with similar results.

5.8 CDDP augments PDT invasion inhibition

Invasion is one of main pathophysiological characteristics of head and neck squamous cell carcinoma cells. To evaluate the effect of PDT with CDDP on the invasive potential of malignancy in normal and malignant head and neck cell lines, invasion assays were performed using Matrigel coated Transwell inserts. The number of cells that invaded the lower chamber, including those bound to the under-surface of the filter, was varied. Figure 5.12A-B shows that the treatment of cells with CDDP significantly reduced the invasion of the UP and VB6 cells 28% and 31% respectively ($p < 0.05$ for both) and enhanced the invasion of H376 cells 9%, compared to the untreated controls.

Combined treatment with both CDDP and PDT caused further invasion inhibition effects on UP and VB6. Invasion of UP, VB6 and H376 cells was significantly reduced further by approximately 39%, 40% and 90% respectively, compared to the CDDP treated cells. An insignificant antagonist effect was also observed in VB6 and H376 cells of approximately 9% and 2% respectively, compared to the PDT treated cells.

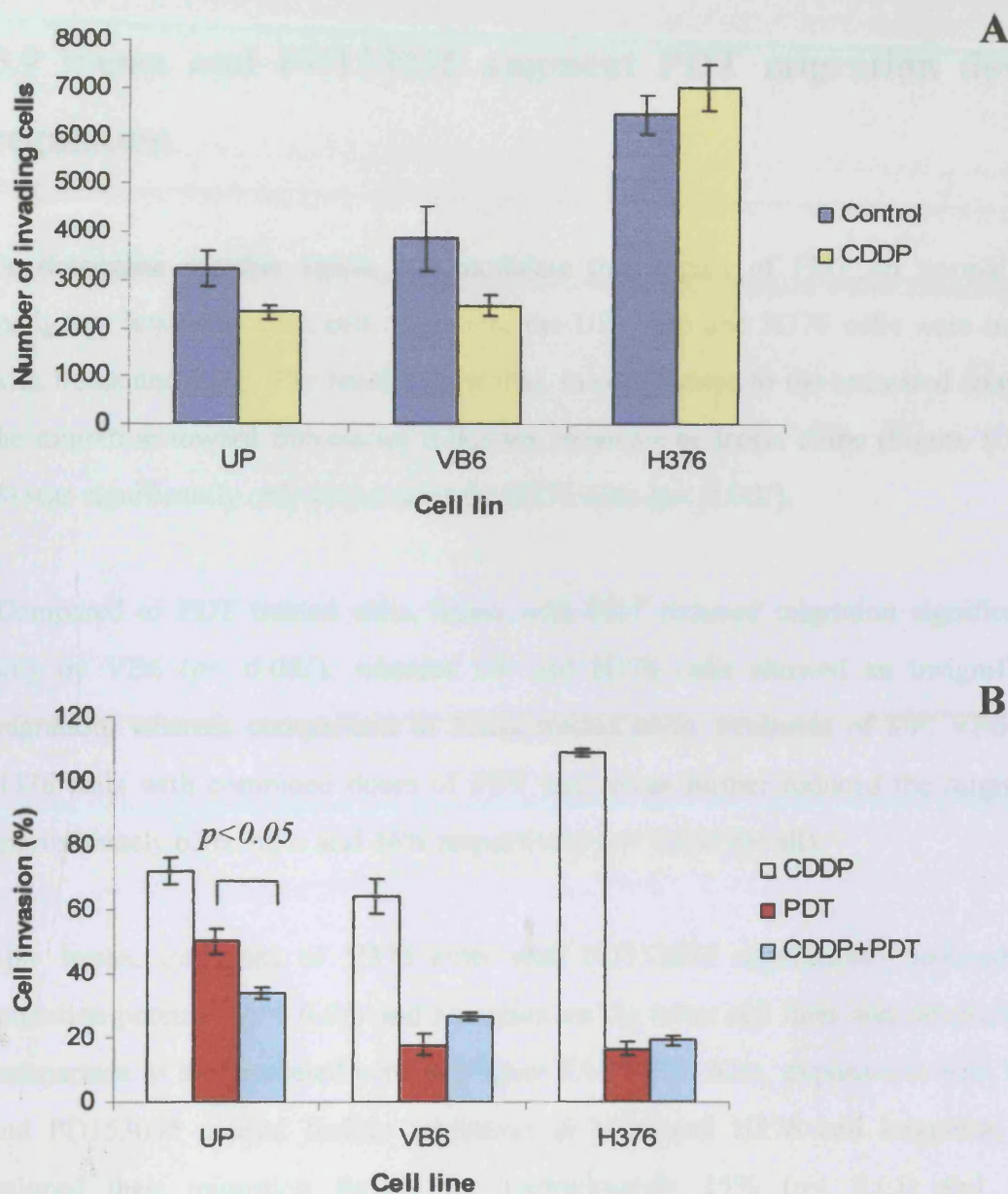


Figure 5.12 Effect of PDT and CDDP chemotherapy on the invasion of UP, VB6 and H376 cells. After treatment with small dose of CDDP (4 μ g/ml for UP and VB6 cells, and 2 μ g/ml for H376 cells) and PDT (Table 3.1), each alone or in combination, cells then were detached and plated on Transwell membranes coated with 40 μ g/cm² of Matrigel diluted in PBS for 72 h. Following incubation, cells that had invaded the lower chamber plus those bound to the under-surface of the filters were trypsinized and counted. The number of invading cells is given in Figure 5.12A. The percent of invading cells compared to untreated control (= 100) is given in Figure 5.12B. Error bar represent standard deviation of three assays. The experiment was repeated once with similar results.

5.9 Iressa and PD153035 augment PDT migration down-regulation

To determine whether Iressa can modulate the impact of PDT on normal and malignant head and neck cell migration, the UP, VB6 and H376 cells were treated with Iressa and PDT. The results show that, in comparison to the untreated controls, the migration toward fibronectin following exposure to Iressa alone (Figure 5.13A-B) was significantly only reduced by the H376 cells ($p < 0.001$).

Compared to PDT treated cells, Iressa with PDT reduced migration significantly only by VB6 ($p < 0.001$), whereas UP and H376 cells showed an insignificant migration, whereas comparison to Iressa treated cells, treatment of UP, VB6 and H376 cells with combined doses of PDT and Iressa further reduced the migration approximately 62%, 66% and 36% respectively ($p < 0.001$ for all).

Like Iressa, treatment of H376 cells with PD153035 significantly reduced the migration potential ($p < 0.01$) and no action on the other cell lines was observed, in comparison to the untreated control (Figure 5.14A-B). Also, exposure to both PDT and PD153035 caused further inhibition in VB6 and H376 cell migration and reduced their migration further by approximately 15% ($p < 0.05$) and 10% respectively, compared to PDT treatment alone (78% and 87% respectively).

Compared to treatment with PD153035 alone, an extreme inhibition was observed in all the three lines tested ($p < 0.001$ for all).

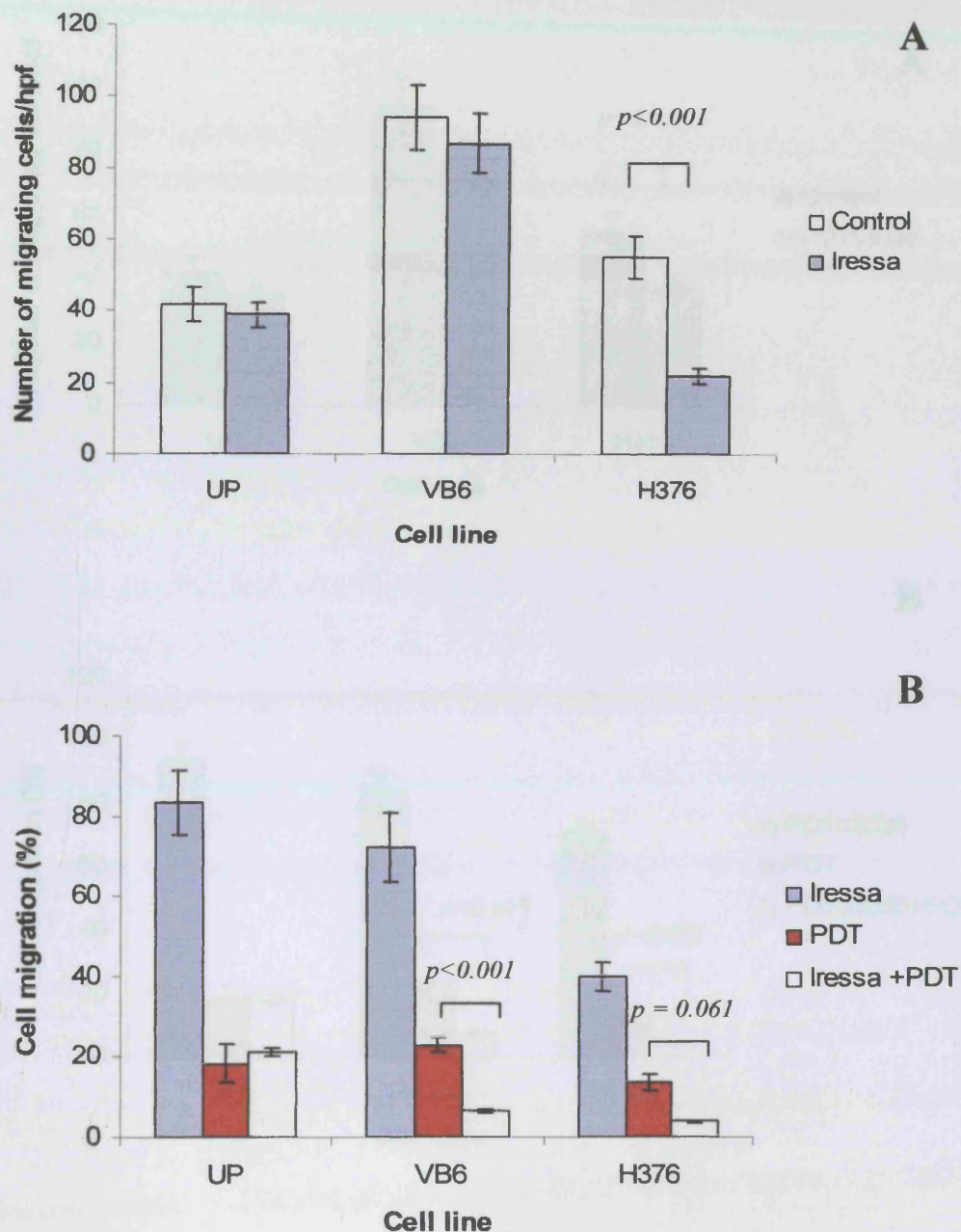


Figure 5.13 Effect of PDT and Iressa on the migration of UP, VB6 and H376 cells towards fibronectin. After treatment with Iressa ($0.5\mu\text{M}$ for UP and $0.05\mu\text{M}$ for VB6 and H376 cells) and PDT (Table 3.1), each alone or in combination, cells then were detached and plated on Transwell membranes sub-coated with $10\mu\text{g/ml}$ of fibronectin and allowed to migrate for 4 h. Cells that had migrated and bound to the under-surface of the filter were stained and counted using light microscopy at X40. The number of migrating cells is given in Figure 5.13A. The percent of migrating cells per high power field in each membrane compared to untreated control (=100) is given in Figure 5.13B. Error bar represent standard deviation of three assays. The experiment was repeated twice with similar results.

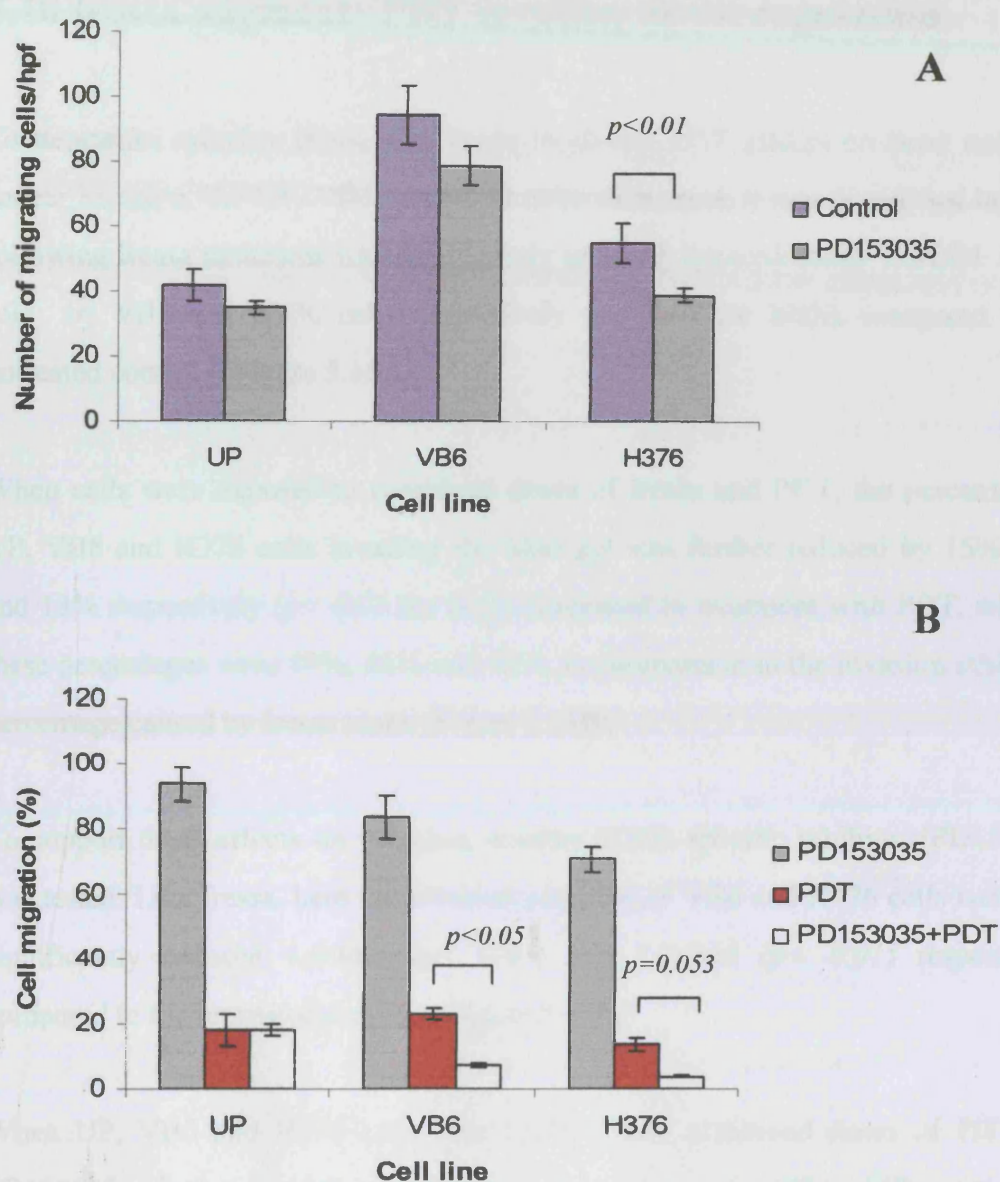


Figure 5.14 Effect of PDT and PD153035 on the migration of UP, VB6 and H376 cells towards fibronectin. After treatment with PD 153035 (1 μ M for UP and 0.5 μ M for VB6 and H376 cells) and PDT (Table 3.1), as single or in combination, cells then were detached and plated on Transwell membranes sub-coated with 10 μ g/ml of fibronectin and allowed to migrate for 4 h. Cells that had migrated and bound to the under-surface of the filter were stained and counted using light microscopy at X40. The number of migrating cells of control and Iressa treated cells is given in Figure 5.14A. The percent of migrating cells in each membrane compared to untreated control (100%) is given in Figure 5.14B. Error bar represent standard deviation of three assays. The experiment was repeated twice with similar results.

5.10 Iressa augments PDT invasion down-regulation

To determine whether Iressa TKI could modulate PDT effects on head and neck cancer invasion, the UP, VB6 and H376 cells were used. It was found that invasion following Iressa treatment was significantly reduced, approximately 1.8-fold and 2-fold by VB6 and H376 cells respectively ($p < 0.01$ for both), compared to the untreated controls (Figure 5.15A).

When cells were exposed to combined doses of Iressa and PDT, the percentage of UP, VB6 and H376 cells invading the Matrigel was further reduced by 15%, 11% and 13% respectively ($p < 0.05$ for both) compared to treatment with PDT, whereas these percentages were 49%, 46% and 44%, in comparison to the invasion inhibition percentage caused by Iressa alone (Figure 5.15B).

To support these effects on invasion, another EGFR-specific inhibitor (PD153035) was tested. Like Iressa, here the invasion potential of VB6 and H376 cells were also significantly reduced 1.6-fold ($p < 0.05$) and 1.8-fold ($p < 0.01$) respectively, compared to the untreated controls (Figure 5.16A).

When UP, VB6 and H376 cells were treated with combined doses of PDT and PD153035, further invasion inhibition was observed, 50%, 56% and 46% respectively, in comparison to PD153035 alone. In comparison to PDT, UP and H376 cells showed significant reduction ($p < 0.05$ and $p < 0.01$), respectively, (Figure 5.16B).

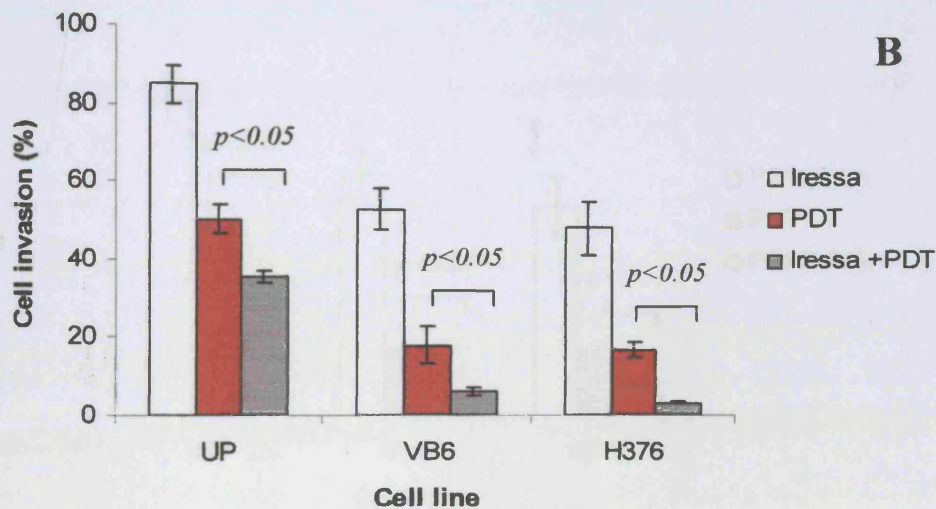
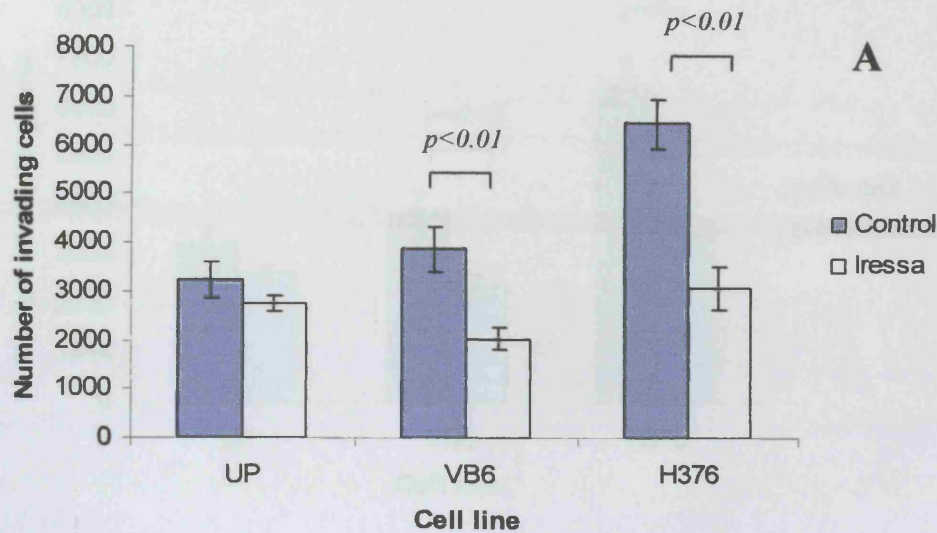


Figure 5.15 Effect of PDT and Iressa on the invasion of UP, VB6 and H376 cells. After treatment with Iressa ($0.5\mu\text{M}$ for UP and $0.05\mu\text{M}$ for VB6 and H376 cells) and PDT (Table 3.1), each alone or in combination, cells then were detached and plated on Transwell membranes coated with $40\mu\text{g}/\text{cm}^2$ of Matrigel diluted in PBS for 72 h. Following incubation, cells that had invaded the lower chamber plus those bound to the under-surface of the filters were trypsinized and counted. The number of invading cells is given in Figure 5.15A. The percent of invading cells compared to untreated control (= 100) is given in Figure 5.15B. Error bar represent standard deviation of three assays. The experiment was repeated twice with similar results.

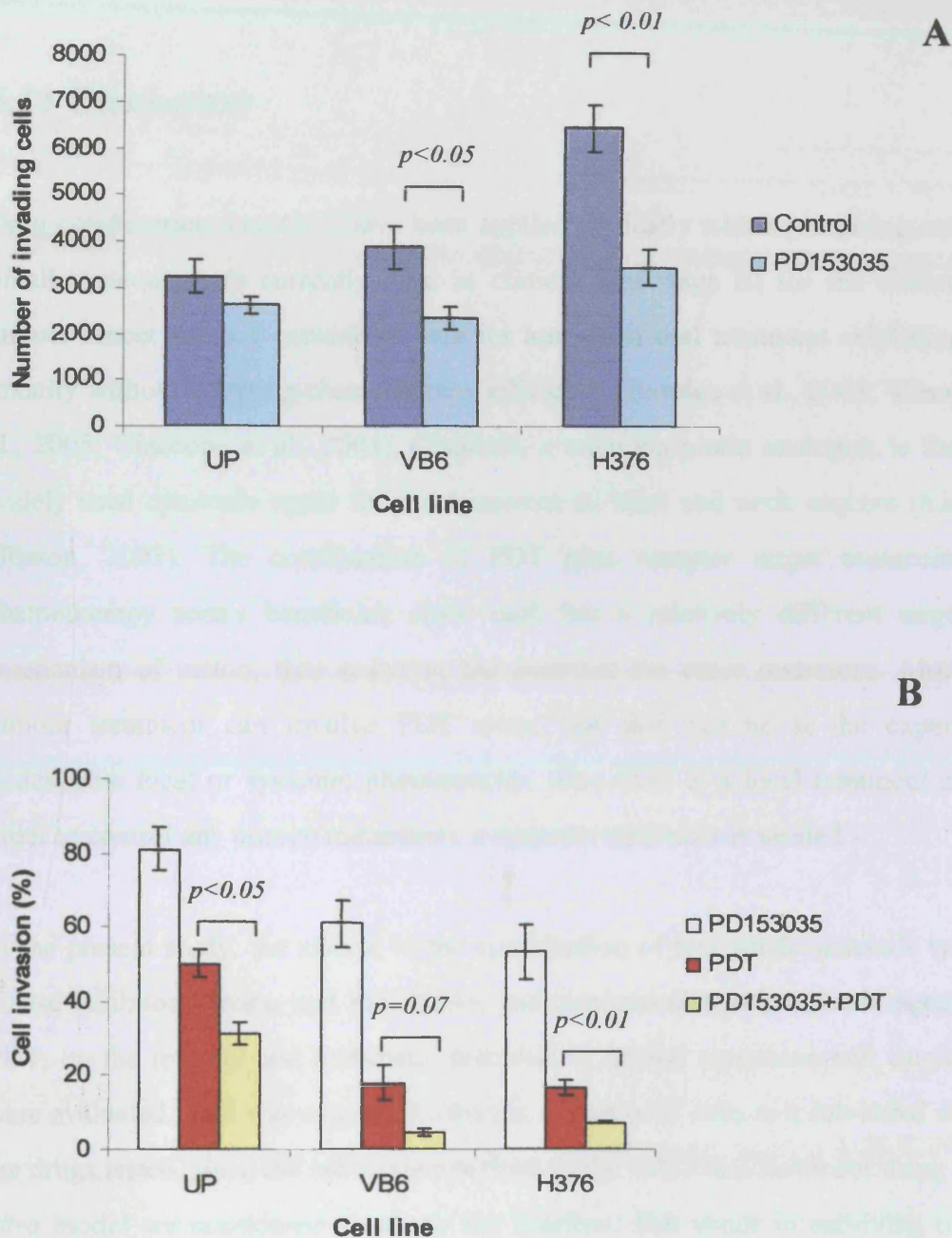


Figure 5.16 Effect of PDT and PD 153035 on the invasion of UP, VB6 and H376 cells. After treatment with PD 153035 (1 μ M for UP and 0.5 μ M for VB6 and H376 cells) and PDT (Table 3.1), each alone or in combination, cells then were detached and plated on Transwell membranes coated with 40 μ g/cm² of Matrigel diluted in PBS for 72 h. Following incubation, cells that had invaded the lower chamber plus those bound to the under-surface of the filters were trypsinized and counted. The number of invading cells is given in Figure 5.16A. The percent of invading cells compared to untreated control (= 100) is given in Figure 5.16B. Error bar represent standard deviation of three assays. The experiment was repeated twice with similar results.

5.11 Discussion

Drug combination strategies have been applied clinically with a promising outcome. Small molecules are currently used in clinical trial stage III for the treatment of human cancer and are considered safe for long-term oral treatment exhibiting mild toxicity without affecting chemotherapy efficiency (Baselga et al., 2005; Veronese et al., 2005; Giaccone et al., 2004). Cisplatin, a common platin analogue, is the most widely used cytotoxic agent for the treatment of head and neck cancers (Kim and Glisson, 2003). The combination of PDT plus receptor target molecules and chemotherapy seems beneficial, since each has a relatively different target and mechanism of action, thus reducing the potential for cross resistance. Moreover, tumour treatment can involve PDT alone, but this can be at the expense of undesirable local or systemic phototoxicity. Also PDT is a local treatment and, in order to control any unseen metastases, a systemic treatment is needed.

In the present study, the effects of the combination of two small molecule tyrosine kinase inhibitors, Iressa and PD153035, and cisplatin chemotherapeutic agent with PDT, on the toxicity and metastatic potential of human squamous cell carcinomas were evaluated. This was examined after the exposure of cells to a sub-lethal dose of the drugs tested, since the sub-toxic reactions to the sub-lethal treatment using the *in vitro* model are considered to mirror the reactions that occur in surviving tumour cells and their surrounding normal tissues at tumour sites in patients.

The results of this study using head and neck squamous cell carcinomas and normal transformed keratinocytes demonstrated that selective tyrosine kinase inhibitors, as a single treatment, reduced cellular viability, and that their combined application with PDT induced a cytotoxic effect. It is difficult to propose a satisfactory explanation for this enhancement, but it may be explained, in part, by an earlier finding of this thesis (reported in Chapter 4), that EGFR expression was reduced following PDT in

the H376 cell line. This is in agreement with EGFR stimulation being lost when human squamous carcinoma cells were treated with PDT (Ahmad et al., 2001). Another possible explanation could be the effect of apoptosis, as reported on several tumours including squamous cell carcinoma cell lines exposed to CDDP (Kuwahara et al., 2000), PD153035 (Faust et al., 1999; Modjtahedi et al., 1998; Mimeault et al., 2003), PDT (Chiu and Oleinick, 2001; Plaetzer et al., 2005) and Iressa (Shintani et al., 2004).

Nonaka et al. demonstrated an additional effect of PDT and CDDP on the survival of lymphoma cells *in vitro* using Photofrin as a photosensitiser (Nonaka et al., 2002). A significant elevation of apoptotic cell numbers compared to CDDP or PDT alone was found, and two apoptotic signal pathways, one for PDT and the other for CDDP, were suggested. Similarly, Canti et al. reported a significantly positive result on combinations of PDT and CDDP in mice bearing tumours (Canti et al., 1998) i.e. enhanced toxicity was evident in combination treatment. Recent data by Crescenzi et al., using breast cancer cells as “targets”, demonstrated that the enhanced cell-killing produced by PDT and CDDP was due to apoptotic effects (Crescenzi et al., 2004). Moreover, this latter group found that PDT mainly killed cells in the G1 phase, whereas CDDP mostly kills in the S-phase of the cell cycle

Several studies on the combination of Iressa with ionizing radiation and chemotherapy have suggested an enhanced cytotoxic effect on tumour cells (Zhu et al., 2005; Raben et al., 2005). The preliminary clinical data suggests that the combination of radiation and PDT is feasible and encourages anti-tumour activity. A pilot study evaluating radiation with PDT has shown that 13 out of 15 patients with locally advanced head and neck cancer experienced a long-lasting and complete response following combined treatment (Suhr et al., 2001). In addition, the authors noted that the anti-tumour effect was dependent on the sequence of treatment.

Another important step during cancer metastasis was investigated in the present Chapter. It is well demonstrated that tumour invasion requires interaction between

invading tumour cells and the ECM, as well as the surrounding microenvironment (Bogenrieder and Herlyn, 2003). Following treatment with CDDP alone, a marked reduction of adhesion and migration of tumour cells was observed. This can be explained as changes in cell morphology and membrane conformation which may have affected the cell attachment, and suggested that further specific studies would be needed to elucidate this. Both small molecules and chemotherapy were able to reduce migration and invasion and their combined application with PDT induced a more inhibitory effect of cell invasion. This inhibition of invasion is in agreement with a previous report on ovarian adenocarcinoma cells, treated with small molecule (ZD1839), where both growth and invasion of cells were inhibited (Fujimura et al., 2002). It is difficult to explain why, but it may be attributed to the observation that stimulation of c-Src tyrosine kinase pathways is the major signal transduction factor involved in growth receptor signals for proliferation and differentiation, and reorganization of the cytoskeleton, which allows increased tumour invasiveness (Irby and Yeatman, 2000). Yang et al. demonstrated that EGFR mediated signalling pathway was a potent inducer of c-Src and Pak1 pathways, and the Iressa drug was able to suppress c-Src, which in turn reduced cancer cell invasion in head and neck cancer cells (Yang et al., 2004). Also they found that the invasion reduction effect was not dependent on EGFR expression and. Invading cells must pass through an extracellular matrix, a process that involves attachment/detachment and enzymatic degradation of the components of the ECM. According to findings of this thesis (demonstrated earlier, in Chapter 4), that $\alpha\text{v}\beta\text{6}$ integrin expression was reduced significantly by the VB6 cell line following PDT which may explain the invasion of VB6 cells following treatment with combined treatment of PDT and TKIs.

The enhanced effect of Iressa on PDT inhibitory effect on the metastatic potential of squamous cell carcinoma cells was accompanied by a reduction in tumour induced angiogenesis, as assessed indirectly by measuring the secreted VEGF. This result indicated that Iressa or PDT, as a single treatment, has reduced the secretion of VEGF, and that combined treatment induced a further reduction of VEGF activity in human head and neck cancers. This result was in agreement with previous work

(Perrotte et al., 1999), which showed that after 48 h of continuous exposure of transitional carcinoma cells to monoclonal antibody C225 (EGFR Ab), VEGF secretion was reduced.

Chapter 6

Results IV

Photodynamic Diagnosis of Oral Tumours

6.1 Introduction

Clinical differentiation of lesions is usually based on morphological changes in tissue. However, this technique is quite difficult to implement and experience is usually considered to be a major factor in its success. However it can be found to be less sensitive in differentiating between lesions with similar clinical and morphological characteristics, e.g. dysplasia and carcinoma *in situ*. Several groups have investigated the use of native tissue fluorescence in the early detection of malignant tissues (de et al., 2005; de et al., 2003; Betz et al., 1999). The results are encouraging, but vary greatly between patients and appear insufficient for others (Betz et al., 1999).

ALA is a precursor of the highly photosensitive PpIX, which can be administered systemically or applied topically to the oral mucosa and facial skin. The principle of ALA induced PpIX is that, in excess, it results in the accumulation of intracellular porphyrins, especially of PpIX, which increase tissue fluorescence (Onizawa et al., 2003). Subsequent irradiation of the lesion with visible light matching the main absorption peak of PpIX, 405 nm, leads to its transfer into an electrically excited molecular state, which rapidly returns to a more stable and less energetic state after the emission of red fluorescent light at around 635 nm.

The difference in fluorescence intensity between normal and premalignant/malignant tissue makes detection and analysis by fluorescent light more applicable (Zheng et al., 2002b). This intensity is governed by many conditions, however, such as

variations in sensitiser rinsing procedure, tumour site and type in each patient undergoing light interrogation (Betz et al., 2002b; Kennedy et al., 1996).

The aim of this clinical study was twofold: to clinically investigate the ability of 5-ALA induced PpIX fluorescence to distinguish between benign and potentially malignant tissues and to develop an applicable algorithm that can be used as a standard for the subsequent analysis of “unknown” lesions.

6.2 Patients

Seventy-one patients (mean age 59 years, range 37-81 years) with clinically suspicious oral lesions took part in this study in the Maxillofacial unit, UCH, London. The 71 biopsies were obtained from various oral sites. The majority came from the tongue, buccal mucosa and floor of the mouth (Table 6.1). These biopsies were examined histopathologically and were found to be either benign or potentially malignant (Table 6.2).

Table 6.1 Number and percentage of surgical biopsies from different anatomical sites

| Site of biopsy | Number of lesions | Percentage |
|----------------|-------------------|------------|
| Tongue | 18 | 25.4% |
| Buccal mucosa | 25 | 35.2% |
| Floor of mouth | 14 | 19.7% |
| Alveolus | 9 | 12.7% |
| Hard palate | 5 | 7.0% |

Table 6.2 Type and percentage of surgical biopsies with different histology

| Histology | Number of biopsies | Percentage |
|--------------------|--------------------|------------|
| Lichen planus | 7 | 9.9% |
| Inflammation | 9 | 12.7% |
| Hyperkeratosis | 22 | 31.0% |
| Mild dysplasia | 14 | 19.7% |
| Moderate dysplasia | 9 | 12.7% |
| Severe dysplasia | 8 | 11.3% |
| Carcinoma in situ | 2 | 2.8% |

6.3 Distance effect on fluorescence ratio

To exclude distance dependence of the fluorescence signals, a spot within normal mucosa was recorded at a different distance and fixed integration time. The data in this experiment showed that the intensity of red (IR) and green (IG) fluorescence was directly related to the distance between the endoscope tip and the tissue surface. Thus, by increasing the distance, the intensity declined, whereas the red-to-green fluorescence ratio remained constant (Figure 6.1).

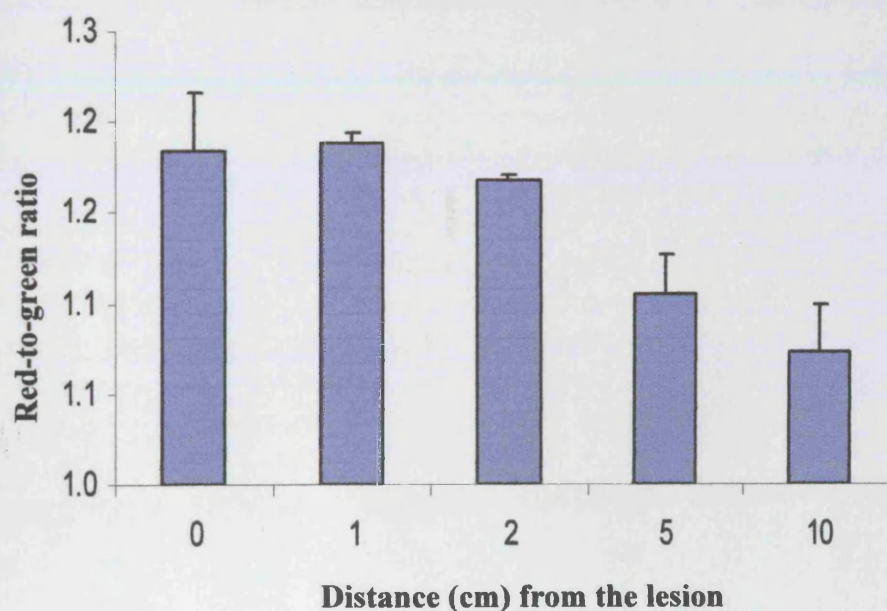


Figure 6.1 The distance dependence of the red-to-green ratio signals evaluated at various observation distances. Error bars represent the standard deviation of three readings.

6.4 Red fluorescence of dysplastic tissue

All of the images were displayed on the system monitor in black and white, and the degree of severity of the lesions was proportional to the brightness of the colour. For example, an increase in brightness suggested the presence of dysplastic lesion (see Figure 2.5). By using the computer programme, a quick analysis of the bright area reproduced the intensities of RGB fluorescence for that area (see Figure 2.6).

When comparing the red PpIX fluorescence to the green tissue fluorescence, a marked increase of the red fluorescence over the green fluorescence in dysplastic lesions and carcinoma in situ was found (Figure 6.2).

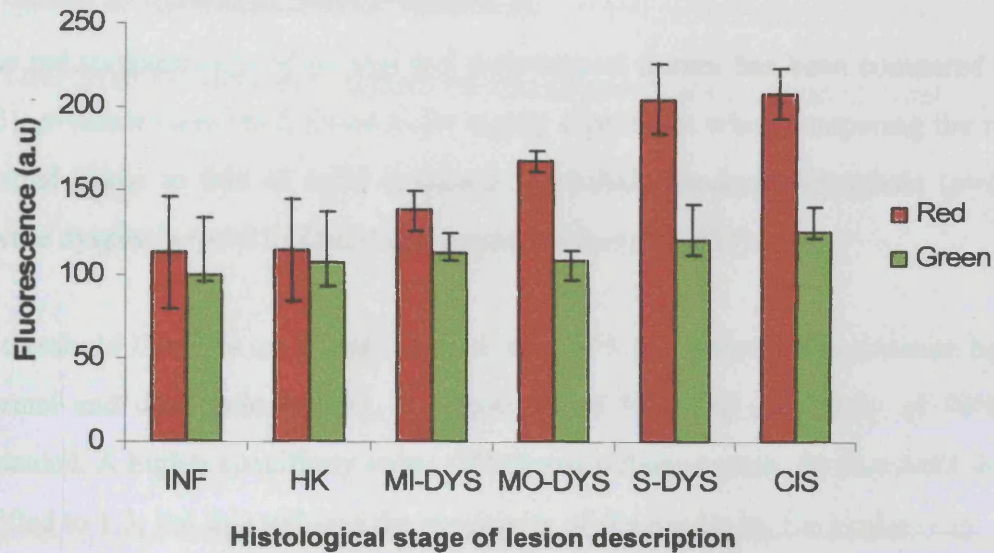


Figure 6.2 Fluorescence intensity versus histopathological stages of oral lesions. Topical ALA was applied on mucosa for 15 min and fluorescence measurements were taken after 2 h. The data represents the % of fluorescence intensity in red and green fluorescence in arbitrary units (a.u). The error bar represents the standard deviation of the same diagnostic group. INF = inflammatory; HK=hyperkeratosis; MI-DYS=mild dysplasia; MO-DYS=moderate dysplasia; S-DYS=severe dysplasia; CIS=carcinoma *in situ*.

6.5 Significant red-to-green ratio

The red-to-green ratio was found to increase when the lesions were identified as dysplastic or carcinoma *in situ* (Figure 6.3).

The red-to-green ratio of normal and pathological tissues has been compared (Table 6.3); p -values have been found to be highly significant when comparing the ratio of normal tissue to that of mild dysplasia ($p=0.002$), moderate dysplasia ($p=0.039$), severe dysplasia ($p=0.018$) and carcinoma *in situ* ($p=0.027$).

A threshold line was set at red-to-green ratio of 1.2 in order to discriminate between normal and dysplastic lesions. A sensitivity of 90% and specificity of 79% were obtained. A higher specificity value (89%) was obtained when the threshold line was shifted to 1.3; but this reduced the sensitivity of the results by 7% (Table 6.3).

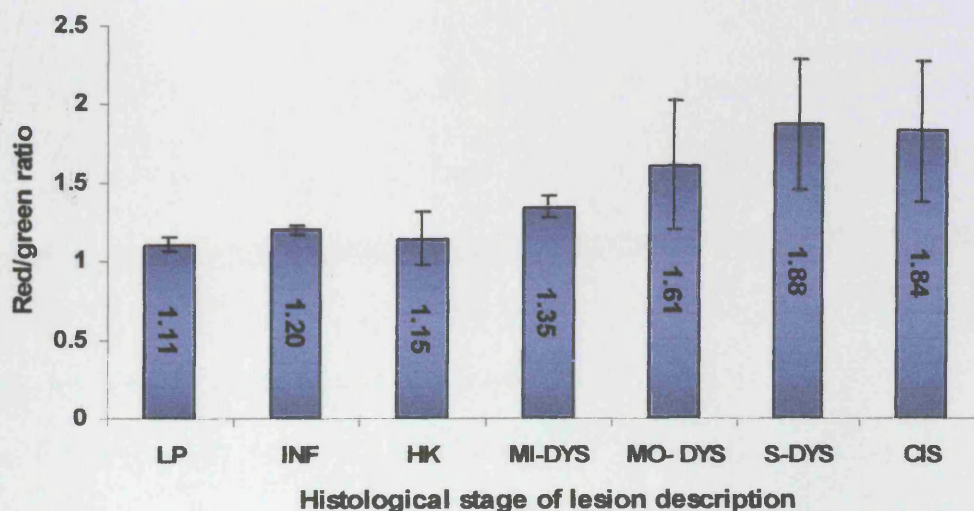


Figure 6.3 Red to green ratio versus histopathological stages of oral lesions. LP=lichen planus; INF=inflammation; HK=hyperkeratosis; MI-DYS=mild dysplasia; MO-DYS=moderate dysplasia; S-DYS=severe dysplasia; CIS=carcinoma *in situ*. The error bar represents the standard deviation of the same diagnostic group.

Table 6.3 Significance of correlation of red-to-green ratio with histopathology of oral lesions. Figures represent *p* values as calculated by student *t*-test

| | LP | INF | HK | MI-DYS | MO- DYS | S-DYS |
|----------------|-----------|------------|-----------|---------------|----------------|--------------|
| LP | - | - | - | - | - | - |
| INF | 0.0207 | - | - | - | - | - |
| HK | NS | NS | - | - | - | - |
| MI-DYS | 0.002 | 0.020 | 0.041 | - | - | - |
| MO- DYS | 0.039 | NS | 0.004 | NS | - | - |
| S-DYS | 0.018 | 0.051 | 0.000 | 0.053 | NS | - |
| CIS | 0.027 | 0.074 | 0.001 | 0.073 | NS | NS |

NS = non significant; LP=lichen planus; INF=inflammation; HK=hyperkeratosis; MI-DYS=mild dysplasia; MO-DYS=moderate dysplasia; S-DYS=sever dysplasia; CIS=carcinoma *in situ*.

Table 6.4 Classification of oral tissue red-to-green fluorescence ratios

| | Red-to-green ratio | |
|--|--------------------|------------|
| | 1.2 | 1.3 |
| Number of biopsies showing dysplasia (confirmed by histology) | 32 | 32 |
| Number of dysplastic sites diagnosed by optical fluorescence ratio as dysplasia (True positive) | 29 | 26 |
| Number of dysplastic sites diagnosed by optical fluorescence ratio as normal (False negative) | 3 | 5 |
| Sensitivity (%) = $\frac{TP}{TP+FN}$ | 90% | 83% |
| Number of biopsies found to be normal histologically | 39 | 39 |
| Number of normal fluorescence ratios found to be normal (True negative) | 31 | 35 |
| Number of normal fluorescence ratios found to be dysplastic (False positive) | 8 | 4 |
| Specificity (%) = $\frac{TN}{TN+FP}$ | 79% | 89% |

* Where TP, TN, FP, FN represent true positives, true negatives, false positives and false negatives respectively

6.5 Discussion

Optical diagnostics have proved to be a reliable source that can be used to give an instant diagnosis of soft and, more interestingly, hard tissues. In the field of head and neck malignancy, most of the experimental spectroscopy work has been performed using fluorescence, Raman, ESS and tri-modal techniques, which involve the combination of these techniques that showed a marked increase in sensitivity and specificity. Currently, there is continued development not only in spectroscopy technology and data acquisition but also in the data analysis methods used. The ultimate aim of all this development is to be able to provide diagnostic algorithms that may be used instantaneously in the clinical setting.

Alfano et al. [1984] first described the use of autofluorescence spectroscopy *in vivo* to differentiate between normal and malignant tissues (Alfano et al., 1984). Since then, several authors have registered their findings with this technique (Gillenwater et al., 1998; Heintzelman et al., 2000; Badizadegan et al., 2004). The technique has also recently been used to map out the individual characteristics of healthy oral mucosa at several anatomical sites within the oral cavity, which can be used as a baseline for further studies (de et al., 2003). Onizawa et al. [1999] examined the usefulness of fluorescence spectroscopy for oral cancer diagnosis. One hundred-thirty oral lesions from 130 patients were subjected to fluorescence spectroscopy; 72/79 (91.1%) and 6/7 (85.7%) of carcinoma and epithelial dysplasia were identified respectively. This suggested that fluorescence spectroscopy was a potentially useful tool in oral tissue pathology diagnosis (Onizawa et al., 1999).

Current routine methods applied for the detection of oral neoplasms are limited to the appearance of the suspected tumour area and it appears difficult for even experienced clinicians to differentiate between different disease stages. Therefore, the development of an enhanced fluorescence imaging system for non-invasive demarcation between normal and altered tissues may revolutionize early clinical

diagnosis. The imaging technique applied in this study was initially developed at the National Laser Centre and a few preliminary tests performed on very few patients.

In the present study, more detailed clinical digital fluorescence images were used, with a correlation to the conventional histological results for different oral anatomical sites following the topical application of an ALA solution. Two channels, red and green, and their ratio diagnostic algorithm were used to quantify the fluorescence intensities.

The clinical data obtained demonstrated that dysplastic positive fluorescence lesions have significantly higher red fluorescence than fluorescence positive benign oral lesions without changes in green autofluorescence. This is in agreement with previous reported studies (Leunig et al., 2000; Zheng et al., 2002b). In clinical trials, a combination of autofluorescence and ALA-induced PpIX fluorescence caused an enhanced demarcation between malignant and healthy tissues (Betz et al., 2002a). Many physiological mechanisms have been proposed in order to explain the enhanced intensity of PpIX in the abnormal tissues, such as deficiency in iron or ferrochelatase (the enzyme required for conversion of PpIX to heme) in tumours results in accumulation of PpIX relative to benign host tissue and the increased percentage of tumour vasculature (Reinhold and Endrich, 1986; Reddi, 1997; Pottier, 1990).

The application of a red-to-green ratio algorithm set to 1.2 cut threshold between normal and abnormal tissues results to 90% sensitivity and 79% specificity, in discriminating between malignant dysplastic lesions and benign lesions. A possible explanation for a slightly low specificity is the number of false positives, probably due to superficial necrotic tissues and porphyrin synthesised by oral microorganisms present in the plaque (Betz et al., 2002a; Leunig et al., 2000). The 10% reduction in sensitivity (90%) could be related to the limited (< 1mm) penetration depth (Leunig et al., 2001), which may have led to poor registration of all cytological and biochemical changes occurring in dysplastic tissues.

The present study supports the data from previous studies. Thus, Zheng et al. investigated ALA induced PpIX fluorescence on 28 patients with suspicious malignant oral lesions, combining both red to green and red to blue ratios, and reported a high sensitivity and specificity of 95% and 97%, respectively (Zheng et al., 2002b). Similarly, others found high specificity by applying a red to blue ratio to discriminate between malignant and pre-malignant bladder lesions, although the red to green ratio was less applicable (Zaak et al., 2001).

In order to enhance specificity, a 1.3 cut threshold between malignant and benign tissues was applied. Nevertheless, there remains the possibility of false negatives, such as insufficient tissue fluorescence due to the improper application of ALA. It is difficult to compare quantitatively the ratio imaging with the other systems due to the inter-system variation in many factors, such as spectral width, background noise and sensitivity. Although the results suggest, that the criteria put forward for the diagnostic purposes described in this chapter, indicate a promising method of distinguishing/clarifying tumour grades.

Chapter 7

Results V

The Scattering Properties of Potentially Malignant Oral Lesions

7.1 Introduction

ESS has been shown to be sensitive to nucleus size, chromatin content and nuclear/cytoplasmic ratio, which are all criteria that the histopathologist looks for when establishing malignancy within a tissue (Mourant et al., 1998; Perelman et al., 1997; Wallace et al., 2000; Mourant et al., 2000; Drezek et al., 2003; Mourant et al., 2000). ESS has, in a number of studies, been combined with extracted intrinsic fluorescence and diffused reflectance forming a “tri-modal spectroscopy” device, which has been shown to have a higher sensitivity and specificity when examining premalignant and malignant lesions (Badizadegan et al., 2004). Therefore, the aim of this clinical trial was to evaluate the ability of the ESS system to discriminate potentially malignant lesions from normal oral tissues and to develop an algorithm for the precise analysis of retrieved tissue signals.

7.2 Patients

Twenty-five patients (17 male and 8 female), mean age 52 years, age range 41-67 years, with clinically suspicious oral leukoplakia took part in this study. Twenty five biopsies were taken from various oral sites (Table 1), and examined histopathologically (Table 2). All types of dysplasia were classified as “malignant”,

whereas all other reports (normal, inflammation and hyperkeratosis) were considered “non-malignant” or “benign” changes.

Table 7.1 The number of biopsies from each region of oral tissue

| Site in oral cavity | No. of biopsies |
|---------------------|-----------------|
| Buccal Mucosa | 9 |
| Floor of Mouth | 3 |
| Sublingual | 2 |
| Tongue | 11 |
| Total | 25 |

Table 7.2 The number of histological grades in the dataset

| Histology | Number of occurrence |
|--------------------------|----------------------|
| Normal | 4 |
| Hyper Keratosis | 10 |
| Mild Dysplasia | 6 |
| Moderate Dysplasia | 3 |
| Severe Dysplasia | 1 |
| Carcinoma <i>in Situ</i> | 1 |
| Total | 25 |

7.3 Elastic spectroscopy detects oral premalignancy

In this study, the aim was to determine the ability of an ESS system to discriminate between benign and dysplastic oral lesions, with the development of the subsequent analysis methods. Results of this study represent the first assessment of the use of ESS for oral tissues classification. A total of 75 spectra (3 for each lesion) were taken. The mean spectra of dysplastic and normal sites are shown in Figure 7.1. Moreover, the standard deviations of the spectra were large and tended to overlap, although differences in the shape of the mean scattered spectra were apparent. The application of the ROC Curve (Receiver-Operator Curves) in Figure 7.2 suggests that the trade-off between optimal sensitivity and specificity is 0.73 and 0.75, respectively. Table 3 shows the true positive, true negative, false positive and false negative values of tissue spectra. A sensitivity of 73% and specificity of 75% to discriminate between normal and dysplastic lesions were obtained.

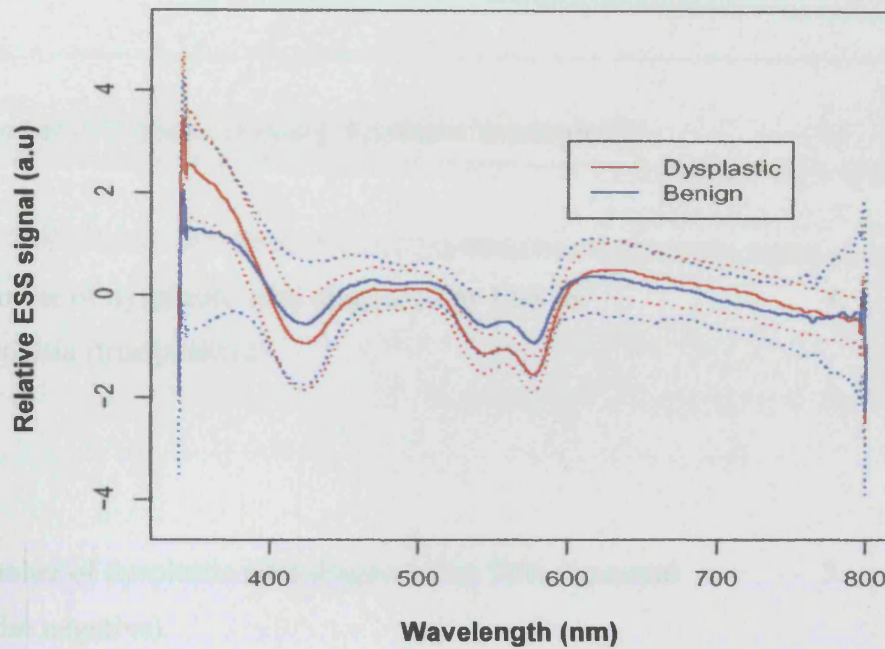


Figure 7.1 A representative ESS spectra plot of the mean dysplastic and benign spectra (solid lines), with one standard deviation plotted either side of the mean (dashed lines).

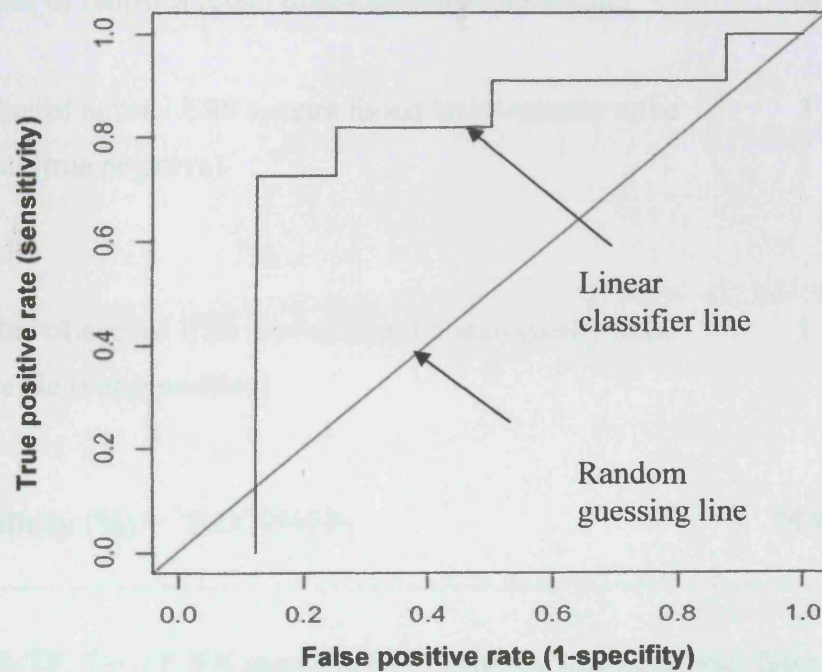


Figure 7.2 A ROC Curve (Receiver-Operator Curve) computed for distinguishing between benign and dysplastic oral lesions by the trade-off between sensitivity and specificity. Optimal sensitivity is (0.727), optimal specificity (0.75).

Table 7.3 Classification of oral tissue spectra (dysplastic vs. normal)

| | |
|---|------------|
| Number of biopsies showing dysplasia histologically | 11 |
| Number of dysplastic sites diagnosed by ESS as dysplasia (true positive) | 8 |
| Number of dysplastic sites diagnosed by ESS as normal (False negative) | 3 |
| Sensitivity (%) = $\frac{*TP}{(TP+FN)}$ | 73% |
| Number of biopsies found histologically to be normal | 14 |
| Number of normal ESS spectra found histologically to be normal (true negative) | 3 |
| Number of normal ESS spectra found histologically to be dysplastic (False positive) | 1 |
| Specificity (%) = $\frac{*TN}{(TN+FP)}$ | 75% |

* Where TP, TN, FP, FN represent true positives, true negatives, false positives and false negatives respectively

7.4 Discussion

The development and use of a new diagnostic instrument for diagnosis of oral dysplasia is a real challenge, particularly as currently there is no database available. The oral tissue, which includes keratinized, non-keratinized, glandular and fatty tissue, results in variable signals when measured by ESS. These render the plotting and correlation of the obtained data sets more complicated. In this study, ESS spectra were combined together, although they originated from geographically and therefore histologically different oral sites (floor of mouth, tongue, cheek). However, prior to combining spectra, each acquired spectrum from a particular site was compared to a spectrum acquired from a histologically-similar normal oral site; the intention here was to reduce discrepancies in the readings.

Recently, there has been increasing interest in the use of optical spectroscopy systems to be able to provide tissue diagnosis in real-time, non-invasively. These systems rely on the fact that the optical spectrum derived from any tissue will contain information about the histological and biochemical make up of that tissue. The technique has not only been shown to have a role in the detection of dysplasia and malignancy but also in performing guided biopsies, monitoring of haemoglobin tissue perfusion in free-flaps and therapeutic drug levels during chemo- and photodynamic therapy (Mourant et al., 1999; Bigio et al., 1999; Johnson et al., 2004).

Epithelial dysplasia in the gastrointestinal tract, in particular Barrett's esophagus, is an important disease state, which is currently being investigated by ESS (Lovat and Bown, 2004). A number of promising clinical studies have shown some unequivocal results, suggesting that this technique can be used as an adjunct to histopathology since it is a cheap, simple-to-use tool and can give rapid and accurate diagnoses (Bohorfoush, 1996; Geboes et al., 1999; Van Veen et al., 2002; Badizadegan et al., 2004; Lovat and Bown, 2004; Badizadegan et al., 2004; Lin et al., 2001).

Georgakoudi and Feld (2004) used tri-modal spectroscopy in patients with Barrett's esophagus and obtained higher sensitivity and specificity when compared with one of the combined techniques (Georgakoudi and Feld, 2004). Work by Haringsma (2002), on Barrett's oesophagus found that ESS was superior to other optical diagnostics in terms of early detection of low-grade dysplasia, based on structural information of the mucosa, in which the size and crowding of nuclei in the epithelial layer play a key role (Haringsma, 2002).

The study of malignancy and dysplasia of the oral cavity using ESS is in development. Ex-vivo work by Jerjes et al. (2004) used the technique to study formalin-fixed specimens of cervical lymph nodes and bony margins taken from patients with oral squamous cell carcinoma. Using linear discriminant analysis, they showed a sensitivity and specificity of 98% and 68% respectively for the lymph nodes, and 87% and 80% for the bone margins (Jerjes et al., 2004). Jerjes et al. also suggested that ESS had the potential to perform a full optical mapping of the suspicious area, thus eliminating the need for subsequent pathological verification (Jerjes et al., 2005).

Muller et al. used diffuse reflectance spectroscopy to look at normal versus abnormal tissue, and dysplastic versus cancerous lesions in the oral cavity. By comparing spectroscopy to histopathology, the accuracy for normal tissues was 91.6% (22/24), compared to 97% (33/34) for abnormal tissues. These figures fell when examining dysplasia, 64.3% (9/14) and carcinoma 50% (5/10). However, when using tri-modal (fluorescence, diffuse reflectance and light scattering) spectroscopy, they showed a sensitivity and specificity of 96% and 96% respectively. when comparing cancerous/dysplastic tissues from normal tissues, and obtained values of 64% and 90% when comparing dysplastic with cancerous tissues, respectively (Muller et al., 2003).

Compared with previous studies using light to differentiate between normal and benign lesions on other human tissues and despite the small number of cases plus the

heterogeneity of the oral tissues, our results yield a reasonable outcome. A small trial examining the combination of diffuse reflectance spectroscopy with fluorescence spectroscopy for the detection of cervical pre-cancer suggests that the two techniques provide complementary diagnostic information (Nordstrom et al., 2001).

Overall, the results of this study support the hypothesis that ESS was able to provide accurate oral dysplasia demarcation and can potentially be used as an effective tool that may replace invasive surgical biopsy. Although this early result is promising, one must consider when more data is added to the analyses, since in this small dataset, patient, site, and histological grade are significant variable, and it is likely that the high level of discrimination between benign and dysplastic tissues is due to the correlation between histological grade and, for example, patient specificity. Further work is required in the form of the collection of more data sets, and careful analysis using multivariate statistical techniques on all the available spectral information, which can potentially improve the accuracy of detection. This requires multiple samples within each tissue category and a large number of patients before it can be used in routine oral diagnosis. Some of the reduction in the sensitivity (28%) and specificity (25%) from 100% can be accounted for by the possibility of discrepancy occurring from combining spectra from different anatomical sites.

Chapter 8

Results VI

Monitoring Photodynamic Therapy by Fluorescence and Elastic Scattering Spectroscopy

8.1 Introduction

A problem of continuing interest in the study of PDT is the definition and measurement of photodynamic dose. For efficacy of PDT, optimal protocols in terms of sensitizer and light doses have been devised for many tumour types. Nevertheless, the actual amount of sensitizer exists in target tissues is largely variable and could lead to variation in treatment outcome (Amelink et al., 2005). As a consequence, this of course, carries a potentially unfavourable outcome and the patient in some cases may need to undergo further treatment or, excess damage may take place, particularly to surrounding normal tissues. It is believed that the majority of photosensitisers accomplish their cytotoxic effect through the production of $^1\text{O}_2$ and other reactive oxygen species (Dougherty et al., 1998). For ALA, like many other sensitizers, the same or similar mechanism is also responsible for its degradation, which is observable as irreversible photobleaching (Wilson et al., 1997). Therefore a method for real-time monitoring of relevant parameters other than pre-determined sensitizer and light doses would be of great benefit for patients.

It was shown that sensitizer photobleaching process is oxygen-dependent process (Ericson et al., 2003; Mang et al., 1987), mediated predominantly by $^1\text{O}_2$ and the degradation of drug is reflected as the bleaching of the loaded sensitizer (Georgakoudi and Foster, 1998). However, the monitoring of sensitizer photobleaching via fluorescence measurement can therefore provide a means of real-

time dosimetry. This concept was introduced by Wilson et al., and involves measuring sensitiser photobleaching rate to determine the $^1\text{O}_2$ concentration during PDT (Wilson et al., 1997). A number of studies have explored the feasibility of this approach. Robinson et al. demonstrated that the rate of PpIX photobleaching increased with decreasing fluence rate (Robinson et al., 1998). Using m-THPC sensitiser, a positive relationship between fluorescence photobleaching and toxicity during *in vitro* PDT was established, and suggested the usefulness of applying this concept as a predictor of tissue damage (Dysart et al., 2005). However, if photobleaching is to be used as a surrogate measure of damage (i.e. an enhanced tumour response can be reflected by rapid bleaching), which very often can be revealed by fluorescence changes, then by monitoring photobleaching through non-invasive recording of the accumulated PpIX in the target tissue before the exposure to PDT and evaluating the changes occurring during and after PDT, could result in better understanding of the PDT process and increase its effectiveness. The objective of this study, therefore was to investigate the feasibility of using fluorescence and elastic scattering systems as real-time monitors of PDT in patients with BCC lesions.

8.2 Patients

Measurements of PpIX fluorescence and scattering spectra were taken from 14 patients treated with ALA-PDT for BCC located on the facial area, including the scalp. Details of the tumours from these patients are given in Table 8.1. The mean age of the patients was 66 years (range 39-78 years). All of the subjects enrolled in this study were 18 years or older, with histologically confirmed BCC. Excluded from the study were pregnant or breastfeeding women. All of the patients were treated and followed-up at the Maxillofacial Unit, University College London Hospitals, UK. All treatment and measurements were performed under a protocol approved by the Ethical Review Board of University College London Hospitals. All patients received written and oral information about the study, which included the aim of the trial and assurance that the procedure would be non-invasive. A full written informed consent was obtained from each patient who entered the trial. Complete response to PDT was defined as the disappearance of the disease (i.e. treatment site was macroscopically normal with no evidence of tumour). Partial response was defined as a decrease of at least 50% in the total tumour size relative to pre-treatment size.

Table 8.1 The number of BCC lesions from each facial region

| Site | No. of lesions | Percentage |
|--------|----------------|------------|
| Cheek | 4 | 29% |
| Temple | 4 | 29% |
| Nose | 3 | 21% |
| Scalp | 3 | 21% |

8.2 PpIX photobleaching measured by FS

The fluorescence-emission signals of PpIX from BCC lesions before, during, and some time (15 min) after light exposure during PDT treatment were measured in the red zone after excitation with blue light. Figure 8.1 shows that PpIX photobleaching was started immediately after the beginning of exposure to 100 J/cm^2 of red light. At 333 s (partway through treatment) after exposure to red light, PpIX was photobleached in lesions of cheek, temple, nose and scalp approximately by 35%, 36%, 22% and 31%, respectively, in comparison to their initial fluorescence values. At 666 s (end of treatment) of exposure, no further PpIX photobleaching was observed in comparison to fluorescence at 333 s of illumination, whereas at 15 min after the end of light exposure, PpIX fluorescence has partially recovered in cheek, temple, nose, and scalp BCC tumours approximately by 12%, 29%, 30% and 8%, respectively, in comparison to those values obtained at the end of light illumination. This recovery in cheek, temple, nose and scalp represents approximately 28%, 17%, 1% and 26%, respectively, of PpIX initial intensity measured prior to light exposure.

Collectively, when one considers the readings of all BCC lesions together, Figure 8.2 showed that approximately 31% of PpIX had bleached when tumours were illuminated for 333 s ($p = 0.0018$), also and in comparison to the end of light exposure (666 s), approximately 20% ($p < 0.05$) of fluorescence intensity had been restored 15 min after light exposure had ended.

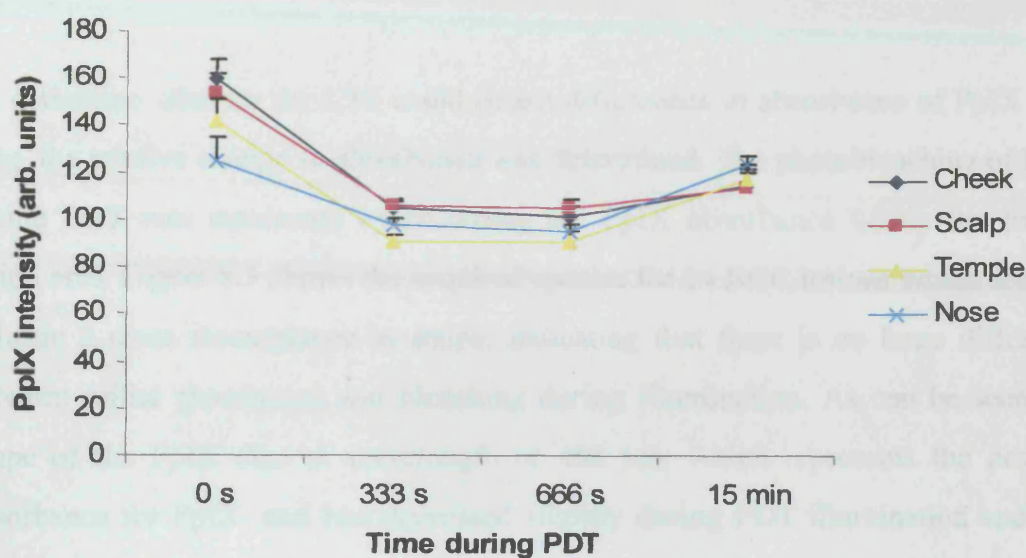


Figure 8.1 PpIX photobleaching and reappearance as function of time during PDT of SCC tumours located in patient's cheek, scalp, temple and nose. Values were calculated from fluorescence images acquired during PDT (333 s), at the end of PDT (666s) and 15 min after the PDT treatment had ended. The control readings were obtained before light illumination (time zero). Data represent the mean fluorescence values \pm SD for each tumour site at different time point during PDT treatment.

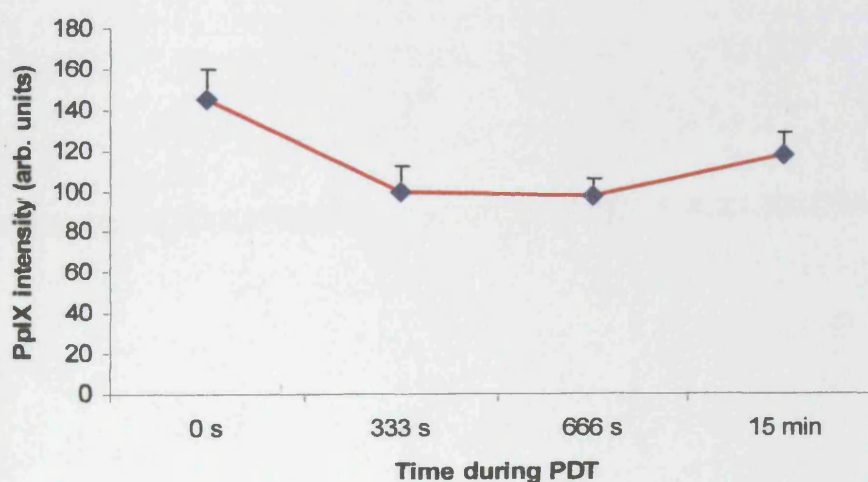


Figure 8.2 PpIX photobleaching and reappearance as function of time during PDT of SCC (n =14). Values were calculated from fluorescence images acquired during PDT (333 s), at the end of PDT (666s) and 15 min after the PDT treatment had ended. The control readings were obtained before light illumination at time zero. Data represents the mean fluorescence values \pm SD at different time point during PDT treatment.

8.3 PpIX photobleaching measured by ESS

To determine whether the ESS could detect differences in absorbance of PpIX over time, the relative change in absorbance was determined. The photobleaching of PpIX during PDT was monitored by recording the PpIX absorbance within the treated lesion area. Figure 8.3 shows the acquired spectra for 14 BCC lesions which seem to indicate a close resemblance in shape, indicating that there is no large difference between initial absorbance and bleaching during illumination. As can be seen, the shape of the PpIX dips at wavelength of 408 nm, which represents the peak of absorbance for PpIX, and had decreased slightly during PDT illumination and was reflected by the increase of the scattering slope. After the PDT illumination is removed, the PpIX absorbance had slightly recovered. When ESS spectra were smoothed and normalized, the photobleaching parameters for all patients were evaluated and absorbance scattering means were determined for all acquired spectra during PDT and compared (Figure 8.4). Using ANOVA test (Appendix 2), only a marginal significant correlation between PpIX photobleaching at the start and during PDT process was found ($p = 0.053$).

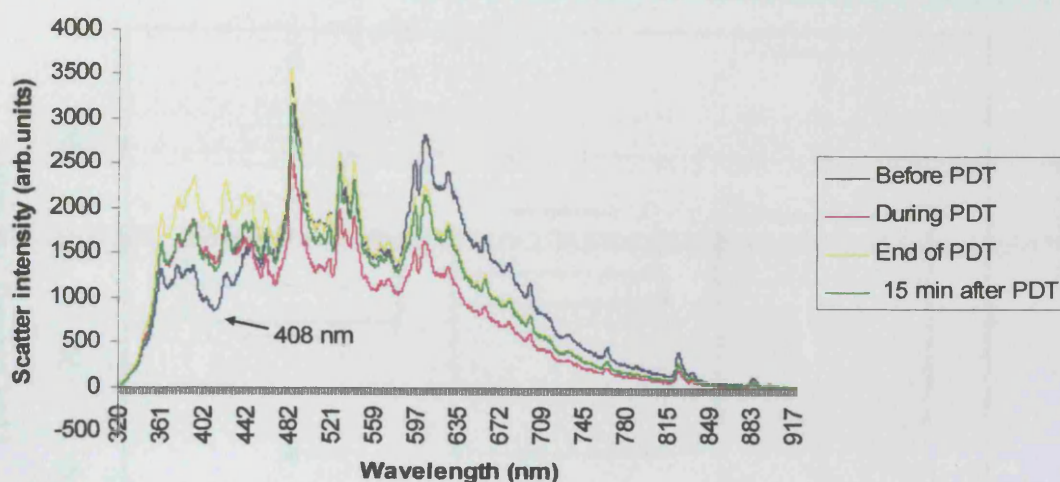


Figure 8.3 Acquired spectra as function of time during PDT shown for SCC lesions ($n = 14$) during PDT. Data shows the absorbance dips and scattering slope for each time point during PDT process over the region of 320- 910 nm. The standard deviation for each spectrum was omitted for clarity. The spectra are coloured according to when they were taken. Blue spectrum was taken at time zero (before the PDT treatment); pink spectrum at 333 s (during PDT); yellow spectrum at 666 s (the end of PDT treatment) and green spectrum at 15 min after the PDT treatment had ended. Arrow indicates PpIX peak absorbance.

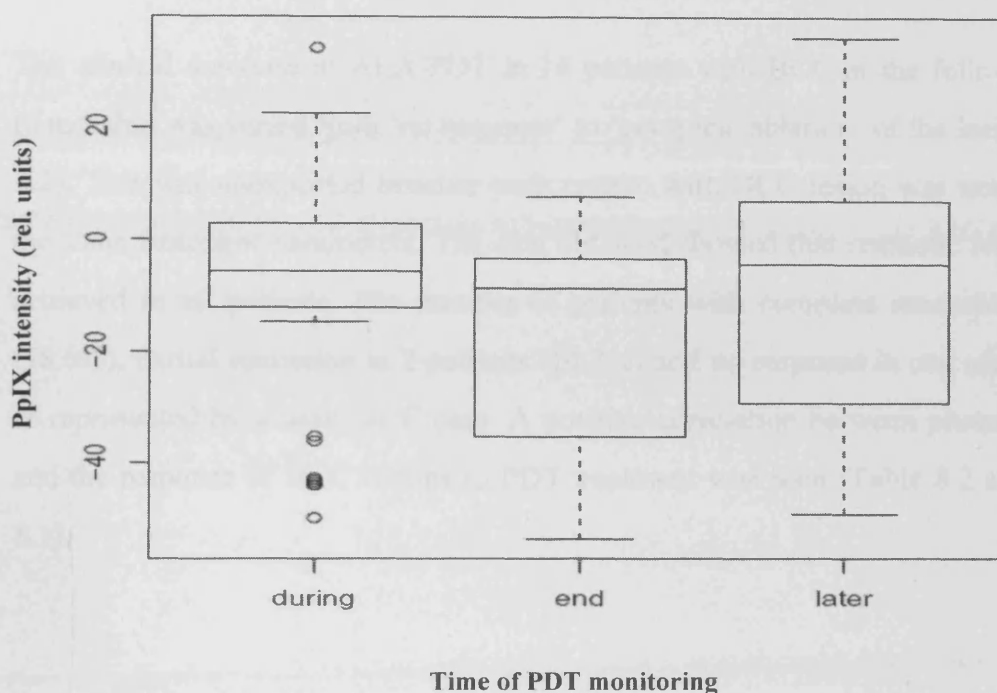


Figure 8.4 Box-plot analysis of results of the fitted spectra as function of time during PDT for SCC lesions shown in Figure 8.3. All spectra underwent smoothing (each intensity point was replaced by the average of the 20 neighbouring points). Each smoothed spectrum was then standardized by subtracting the mean intensity of the spectrum from each data point. Each point was then divided by the standard deviation of the smoothed spectrum; this gave spectra a mean intensity of zero and standard deviation equal to one. The spectra were compared over the region of 408 nm which represents the peak absorbance of PpIX). Data are presented as mean values of PpIX absorbance expressed as relative values to normalized pre-PDT treatment at 408 nm \pm SD (error bars), 25th and 75th quartiles, and circles denoting the outliers/anomalies data. During = at 333 s during PDT; end = end of light exposure (666 s); later = 15 min after PDT had ended (i.e 15 min after red light turned off).

8.4 ALA-PDT

The clinical outcome of ALA-PDT in 14 patients with BCC at the follow-up visit (6 months) was varied from 'no response' to 'complete ablation' of the lesion (Table 8.2). This was unexpected because each patient with BCC lesion was treated using the same treatment parameters. The data obtained showed that cosmetic results were achieved in all patients. The number of patients with complete remission was 11 (78.6%), partial remission in 2 patients (14.3%) and no response in one case (7.1%), as represented by a nasal BCC case. A positive correlation between photobleaching and the response of BCC lesions to PDT treatment was seen (Table 8.2 and Figure 8.1).

Table 8.2 BCC responses to ALA-PDT

| Site | CR* (n) | PR* (n) | NR* (n) | % of CR |
|--------|---------|---------|---------|---------|
| Cheek | 4 | - | - | 100% |
| Nose | 1 | 1 | 1 | 33% |
| Temple | 3 | 1 | - | 75% |
| Scalp | 3 | - | - | 100% |

* Where CR, PR, NR, represent complete response, partial response and no response, respectively.

8.6 Discussion

PDT is an important treatment method for skin lesions such as superficial BCC and AK. Monitoring the relevant parameters, such as sensitiser photobleaching rate or decay time, to determine the concentration of $^1\text{O}_2$ formed during PDT and comparing them to the treatment response. An optimal and reproducible treatment outcome then may be achieved. It has previously been shown that PpIX fluorescence spectroscopy is a useful tool for monitoring PDT dose and determining the lesion response to therapy (Rhodes et al., 1997).

A study by Ericson et al. included 37 patients undergoing PDT for AK of the head, neck and upper chest and aimed to investigate the impact of fluence rate and spectral range on primary treatment outcome and bleaching rate when ALA was used as a photosensitiser. They concluded that both photobleaching rate and primary treatment outcome were dependent on fluence rate. They also suggested that low fluence rate appeared preferable when performing PDT on AK using non-coherent light sources (Ericson et al., 2004).

Amelink et al. (2005) correlated changes in the local tissue optical properties (absorption and scattering coefficients) during ALA-PDT and changes in PpIX fluorescence by using superficial reflectance spectroscopy, which employed a single fibre for the delivery and collection of white light to and from the tissue (Amelink et al., 2005). The spectra acquired were modulated with blood saturation, relative blood volume fraction, scattering intensity and wavelength dependence of the scattering. Except for blood volume, the study showed a marked correlation between the other parameters and photobleaching of PpIX. This suggests that these parameters can predict PDT-response.

In the present study, the red PpIX fluorescence signals were detected after the topical application of PDT. These signals were lost over time during PDT, which may be due to the fact that most PpIX was photobleached. After a cumulative time of 333 s with fixed fluence of 100 J/cm^2 and fluence rate of 150 mW/cm^2 , no significant additional

photobleaching was recorded. This may indicate that current PDT time was excessive, since slow bleaching may result in higher oxygen levels in tissues during treatment, which in turn results in a better treatment response. Numerous studies have demonstrated that the amount of PpIX synthesised after ALA administration is proportional to its emitted fluorescence, as a prediction of PDT success (Jeffes et al., 1997; Mang et al., 1987; Spikes, 1992; Calin et al., 2004). Another study by Fijan et al found no significant correlation between fluorescence intensity and response to PDT (Fijan et al., 1995). This is perhaps not surprising as no two studies using PDT are currently comparable with respect to patient selection, drug/light doses, equipments etc.

Since PpIX is manufactured by tumour cells and surroundings normal tissue cells, ALA cream was applied to the target area with extended margins that were partially shielded during PDT. This may explain the post-PDT re-fluorescence. In the present study, a difference between the PpIX fluorescence at the beginning of PDT and response to PDT was found. However, the amount of PpIX photobleaching was observed in tumours that showed complete response rate; less bleaching was seen in tumours that showed no response. Several studies have shown a positive relation between both PDT-induced damage and PpIX photobleaching rate and the concentration of sensitiser and oxygen availability during exposure to PDT light (Georgakoudi and Foster, 1998; Georgakoudi and Foster, 1998; Langmack et al., 2001).

ESS was applied to clinically presented lesions in order to discover whether there was a significant difference in the absorbance of the active form of ALA (PpIX), which has a relatively sharp absorbance peak at 408 nm (Georgakoudi and Foster, 1998; DaCosta et al., 2003). This latter study did not have spectra taken prior to the drug being administered, so the degree of intensity in this region in the absence of PpIX could not be reconstructed. What could be examined, however, were the changes in absorbance over time as the treatment progressed. If photobleaching occurred, then it might be expected that there may have been more absorbance at the start of the treatment and less absorbance at the end. The outcome was approaching significance, which could be due to the small cohort of patients and different

measurement sites and different lesion types, thus, future studies should consider the control of these variables.

The PDT response was achieved in most tumours, since the same dose of PDT was applied with the same fluence and fluence rate. This agrees with a previous clinical study (Svanberg et al., 1994). The small percentage with no response, or a partial response, could be due to the limited depth of ALA penetration and the nature of the tumours. A similar finding was reported in relation to oesophagus tumours (Boere et al., 2003), and the incorporation of iron chelator to enhance the production of PpIX and subsequently enhanced PDT, was suggested (Curnow et al., 1998).

This study has explored the feasibility of using ESS and FS, as monitors of PpIX photobleaching during PDT. It was found that red fluorescence value decreased markedly during PDT, and was considered to be significant when compared to pre-PDT. The PpIX photobleaching was higher in lesions with high response rate, and less in those with low response rate to PDT; this may be useful indicative of the response rate of tissue to therapy.

Chapter 9

General Discussion

The research presented in this thesis explored the use of light techniques with regard to the control of head and neck cancers at the cellular and clinical levels. It was a unique opportunity to compare both scenarios. Surprisingly, little is known about the relationship between PDT and distant metastases, a consequence that may not be explored for years after the primary treatment. The motivation for such a study emanated from the fact that PDT is mainly indicated for tumour lesion without metastasis. However, it is important to establish what the effects of PDT might be on metastasis. Therefore, the primary aim of the present study was to explore some of the metastasis related biological consequences of PDT at the cellular and molecular levels using OSCC cells as an appropriate *in vitro* model. The second aim was to evaluate, clinically, the ability of an optical system based on fluorescence and elastic scattering spectroscopy, to distinguish between normal, potentially malignant and malignant tissues and to develop an applicable algorithm that may be used as a standard for the subsequent analysis of 'unknown lesions'; in an attempt to control head and neck squamous cell carcinoma (HNSCC) recurrence and established an early detection before spread of tumour cells. The failure to achieve complete ablation of tumours that were previously treated with PDT might be a leading cause of their recurrence and distance metastases. Thus, in order to fill this gap in the knowledge and, in order to ensure complete removal of tumour, a sufficient dose of PDT must be delivered. Therefore, this study also explored the applicability of fluorescence and elastic scattering spectroscopy systems for monitoring PDT in patients with superficial BCC, and to compare this to treatment outcome. To this end, several experiments were conducted to determine the applicability of '*optical biopsy*' and '*optical monitoring*'.

Throughout of this thesis, both *in vitro* and *in vivo* studies have been considered in their own right.

9.1 The *in vitro* studies

The biochemistry of tumour cell biology covers a vast area, and tumour invasion is a complex process that requires interactions between the invading tumour cells and the ECM, as well as the surrounding microenvironment beyond the ECM. This study found that PDT has the capacity to regulate the behaviour of squamous cell carcinomas, and reduce their metastases phenotype. The human oral SCC cell lines were H376 and VB6. The VB6 cell line was transfected with a $\beta 6$ integrin subunit and expressed predominantly $\alpha \nu \beta 6$ integrin receptor. The control cell line used was represented by UP cells (human papilloma virus 16-transformed skin keratinocytes), which are not a cancer line. They are however, more “normal” than the SCC lines. Nevertheless, this research focuses on comparing the influence of PDT in various scenarios, and the same cell line may fulfil this purpose.

Foscan-PDT is currently in clinical use for the treatment of head and neck cancers. In the 1990s, the published research misled the clinicians regarding the photosensitiser selectivity of tumour cells. It was thought that the sensitivity to PDT is related to the cell type, and malignant cells are more sensitive to this than normal keratinocytes (Dougherty et al., 1998). This concept has now been changed, since both malignant and normal cells can retain the sensitiser, and the present study findings support this. The UP cells used in this study were a transformed skin keratinocyte cell line, and not SCC, and were less sensitive to Foscan possibly because of their larger size, compared to H376 and VB6 SCC, which may need a longer time to take up/saturate Foscan *in vitro*. This was clearly explained by this study which found that UP cells sensitiser take-up was less compared to the other OSCC lines. Therefore, in order to examine this concept more fully, two types of cells (normal vs. malignant) with relatively equal size, might be used.

This thesis found that the PDT toxic effect on cells was dependent on both Foscan concentrations and light intensity. It is well known that efficient cell death following PDT requires light, oxygen and photosensitiser quantity not to be limited. When one

of these components is limited, most of the cells do not immediately undergo apoptosis/necrosis, and rather than their growth being arrested, causes activation of several transduction pathways. However, in this study it was possible to achieve lethal effects on cell survival by increasing the light dose rather than sensitiser concentration. This may be of clinical value, since decreasing the sensitiser dose clinically means reduction of adverse effects of sensitiser e.g. patients' long time shielding from sunlight and also treatment costs will be reduced. Nevertheless, using a high dose of sensitiser can also activate anti-apoptotic signalling, e.g. eukaryotic transcription factor (NF- κ B) dependant pathway (Granville et al., 2000).

As discussed in Chapters 4 and 5, the observed suppressive effect of PDT on cellular behaviour towards malignancy was reflected by a decreased affinity of cells to migrate towards extracellular proteins. The reason behind this reduction is not clear, but according to the findings in this thesis, activities of the tumour promoting factors MMP-2, -9 and -13, uPA and the VEGF were significantly reduced in some of the cell lines tested. At the time of writing, this is the first report to explore the effects of Foscan-PDT on MMP-2, -9, and -13, uPA and VEGF activities in head and neck carcinomas. In addition, the present data showed for the first time that cell surface integrin α 5 β 1 and α v β 6 expression were enhanced by Foscan-PDT, especially α 5 β 1 receptor which was significantly increased by PDT in UP and H376 cells.

It was reported that migration of human keratinocytes is mediated by specific integrins (Pilcher et al., 1997; Lange et al., 1995), growth factor receptors and MMPs. In this study, PDT had suppressed migration in UP and H376 cells with decreased secretion of MMP-9, MMP-13, VEGF, increased expression of α 5 β 1 and α v β 6 integrin and decreased expression of EGFR receptors. MMP-2 was significantly activated by H376 cells following PDT, this activation may explain the recurrence in some cases treated here at UCH, London. MMP-2 was reported to be related to the HNSCC tumour metastases to the lymph nodes, while MMP-9 was not. Therefore, MMP-2 was considered as a useful marker for the degrees of tumour invasion and metastases (Kawata et al., 2002). Accordingly, in those tumours, the

administration of anti MMP-2 might enhance the clinical outcome. Moreover, it is not fully understood whether the integrins, $\alpha 5 \beta 1$ and $\alpha v \beta 6$, are implicated in cell migration. In VB6 cells (which expressed high levels of $\alpha v \beta 6$), expression was reduced after PDT. However, investigating the effect of PDT on integrin expressing cells using a range of PDT doses rather than sublethal doses (as used in this study), might answer the latter question. It seems that other mediators or pathways are involved. Expression of $\alpha v \beta 6$ leads to a phenotype which is more migratory, less differentiated and upregulated expression of MMP-2 and MMP-9 (Thomas et al., 2001b). However, it is not hard to imagine how these processes could contribute to invasion of tumour cells *in vivo*. Therefore, further studies would be required to elucidate these mechanisms involved in cell migration.

By combining PDT with chemotherapy (cisplatin) and small molecules (Iressa and PD153035; further enhancement of PDT antimetastatic effects were achieved. At the time of writing, no published reports on the combination of PDT with small molecules could be found, and only a few recent reports on the combination of PDT with chemotherapy and radiation therapy effects on toxicity. The expression of EGFR by flow cytometry revealed an obvious suppression with enhanced anti-tumour PDT activity when small molecules were added. On the immunohistochemical study of HNSCC cases, EGFR was significantly correlated with the lymph node metastasis; this was connected to MMP-2 and MMP-9 (Do et al., 2004). Accordingly, correlation between invasiveness of HNSCC and overexpression of both EGFR and MMP-9 was reported using an *in vitro* Matrigel invasion model (charoenrat et al., 2000). In combination, these findings are important when looking for PDT as an early treatment of cancer lesions that do not lead to established metastases. Also, these observations may help to enhance the prognosis of head and neck carcinoma patients undergoing surgical resection of large tumour masses where at times it is difficult to discern the safe margins. By combining surgery and illumination of the margins with PDT, this may lead to a decrease in, or may even prevent, recurrence and metastases forming.

9.2 Clinical studies

The results of this study represent the first assessment of the use of ESS in the classification of oral tissues. Optical biopsy techniques are based on the idea of light being used for illumination. In biological tissues, the light may both be absorbed with fluorescence emission and subsequently scattered, either elastically or inelastically. The intensity of these events depends on the type of the tissue under investigation. Tools that are sensitive to these changes could therefore have the potential to classify each lesion with a high degree of accuracy, which, if validated, can contribute positively to cancer management. Optical biopsies can be useful not only for oral malignancy, but also for other clinical applications, such as dermatological conditions, breast cancer, and cervical dysplasia. In addition, it is possible that optical biopsies may be applicable anywhere in the body where other image guidance techniques are applied.

There is currently no database relating to optical biopsies in oral tissues, which makes the precise correlation of the obtained samples more difficult. In the clinical trial described in this thesis, optical biopsies were taken from specific tissue areas and the acquired spectra were derived from different anatomical sites in the oral cavity with different structures and volume thicknesses; this highlights the necessity for close co-operation between the clinicians, pathologists and the data interpreter. In addition, little is known by patients and GPs concerning these optical processes, and this may have contributed to the low cohort of patients in this study. In order to help in establishing appropriate controls and the characteristics of the normal spectra, and make the true differences in the ESS spectra, several normal acquired spectra were obtained from different oral anatomical sites. Nevertheless, the FS obtained data were presented with a great degree of accuracy regarding calculated red-to-green diagnostic ratios/algorithms, since the captured images were analysed and the intensity of emitted red and green fluorescence obtained immediately in real time by the PC. Thus, the clinician was able to decide which areas of mucosa were to be captured.

In this study, the application of a red-to-green ratio algorithm set to 1.2 actually reduced thresholds between normal and abnormal tissues and resulted in 90% sensitivity and 79% specificity in discriminating between malignant dysplastic lesions and benign lesions. By implicating the 1.3 threshold, the number of false positive results were reduced by 50% with 10% increase in specificity and only 7% reduction in sensitivity; this indicates the advantages these algorithms.

The ESS results of this study support the hypothesis that ESS was able to provide accurate oral dysplasia demarcation and can be used as an effective tool that may replace the invasive surgical biopsy. Although this early result was promising, more data from different tissues are needed for validation, since in this small dataset the patient, site, and histological grade are limited. For monitoring, ESS was also applied and closely correlated, although results were obtained were not significant; sparseness of the data, the tissue heterogeneity and the absence of any previous databases all may have contributed towards this insignificant outcome.

Current protocol demands that PDT doses are tailored to suit the patient's weight, which may result in either over/or under treatment with subsequent complications. Monitoring the relevant parameters during PDT and comparing them to the treatment response allows the achievement of optimal and reproducible treatment outcomes. The employment of a PpIX fluorescence spectroscopy as a tool for monitoring PDT treatment, and the expected response to therapy is widely reported (Pottier, 1990; Boere et al., 2003; Calin et al., 2004). Monitoring the bleaching of PpIX fluorescence during photodynamic therapy in human BCC skin tumours was investigated in the present study. The response of lesions to PDT was lower in those slow bleaching.

9.3 Conclusions

The research presented in this thesis demonstrates that PDT and its related optical spectroscopy tools may prove beneficial in terms of cancer diagnosis and treatment.

At the cellular level, PDT using m-THPC as a photosensitive agent, either alone or in combination with other anti-cancer agents (cisplatin and small molecules), was found to be an effective antitumour regime. This involved the control, not only of tumour growth, but also some metastatic activities. Despite the difficulty of determining the precise mechanisms behind this suppression of metastasis, this study provides evidence that PDT can, at least partly, regulate many of the processes that are known to be associated with malignancy. This effect may prove of clinical value in the treatment of head and neck cancers, since PDT is applied as a treatment for early cancer without metastasis.

Clinically, PDT has shown to be an efficient treatment for BCC cancer treatment that can be applied with acceptable cosmetic outcome. For diagnosis of early lesions, FS and ESS are shown to be able to identify malignant changes in oral tissues and act as a screening tool for the detection of subsequent primary lesions with the advantages over other non-optical techniques of providing real-time, cost effective and pain-free biopsy methods, unlike surgical biopsies. In this study, FS also demonstrated the great feasibility of simultaneously monitoring 5-ALA induced PpIX fluorescence bleaching during PDT which predicted the outcome of BCC tumours. In order to validate all the observations presented in this thesis, larger patient populations plus increasing the number in each category are needed.

These experiments and results presented here offer a feasible and promising technology which, it is hoped, will lead to an important contribution in the advancements of the diagnosis and treatment of head and neck cancers.

9.4 Future work

The use of light techniques in head and neck oncology is increasing, not only to treat dysplasia and malignancy but also for the purposes of the identification, monitoring and detection of potential complications. Further research is required both at the clinical and *in vitro* levels. At the cell level, further studies are needed to elucidate the molecular events behind the different effects of PDT on the invasive behaviour of oral cancer and to clarify these relationships by carefully designed *in vitro* and subsequent, *in vivo* animal studies. In clinical terms, large multi-centre trials are vital in order to determine the sensitivity and specificity of the individual and combined techniques, as well as to assess and improve their ability in terms of the early detection and management of head and neck oncology. This will help to determine the optimal approach for tumour growth, recurrence and metastasis. Once a more sound knowledge of cancer biology has been established, it may be possible to attach specific markers with specific optical characteristics directly to cancer cells, which will facilitate the tracing of suspicious areas with high sensitivity.

To expand the current knowledge about the biological basis of PDT and according to the findings presented here, using ELISA and zymograms which showed that some MMP protein levels were reduced following exposure to PDT, further studies would elucidate whether Foscan-PDT might have suppressed specific mRNA translation of distinct MMPs as this was subsequently reflected in MMP expression by reduced secretion into the culture supernatants. Thus, future work at the gene level is needed to ascertain whether the suppressive effect of PDT on MMPs and other tumour promoting factors including VEGF and plasminogen activator are true and not just a failure of the cells to secrete the manufactured protein. Also, the mechanisms of MMPs and other tumour promoting factors' down regulation following PDT remain to be elucidated.

Overall, it would be more relevant if all biological molecules investigated in this thesis could be evaluated in animal models before translating the acquired data to the clinical setting.

The FS method applied in this study was adequate, but lacked the capability of providing optical images of large areas of oral lesions and the need for point by point scanning of tissues to be interrogated with the tip of an endoscope to assess the oral tissue mucosa and find the points of high fluorescence. This procedure was, on reflection, perhaps time consuming and PpIX photobleaching might have occurred. Therefore, a tool or system with the ability to switch from endoscope to complete image with wide angle lens in a short time may enhance the detection technique. Furthermore, it has been demonstrated that certain cancers at an early stage of development overexpress certain molecules e.g. EGFR, however, by linking those ligands to long-wavelength-absorbing molecules that can both fluoresce and photosensitise may increase the sensitivity and specificity. This may be investigated for early detection and the simultaneous destruction of target cancers.

Appendix 1

Media and Solutions

Keratinocyte growth medium (KGM) 500ml

| | |
|-----------------------------------|-------|
| 64% DMEM | 320ml |
| 22% Ham's F12 | 112ml |
| 10% FCS | 50ml |
| 1.8 x 10 ⁻⁴ M Adenine | 5ml |
| 0.5 µg/ml Insulin | 250µl |
| 0.4 µg/ml Hydrocortisone | 2ml |
| 10 ng/ml Epidermal growth factor | 0.5ml |
| 1% Penicillin/streptomycin | 5ml |
| 10 ⁻¹⁰ M Cholera toxin | 500µl |
| 2.5 µg/ml Fungizone | 5ml |

Serum free medium (SFM) 500ml

| | |
|----------------------------|-------|
| 99% DMEM | 495ml |
| 1% Penicillin/Streptomycin | 5ml |

Additive free medium (AFM) 500ml

| | |
|----------------------------|-------|
| 67% DMEM | 325ml |
| 22% F-12 | 120ml |
| 10% FCS | 50ml |
| 1% Penicillin/Streptomycin | 5ml |

Freezing medium Per ml

| | |
|----------|--------|
| 90% FCS | 900 µl |
| 10% DMSO | 100 µl |

12% Acrylamide resolving gel ~10ml

| | |
|----------------------------|-------|
| Distilled H ₂ O | 3.3ml |
| 30% Acrylamide mix | 4.0ml |
| 1.5M Tris (pH 8.8) | 2.5ml |
| 1.5M Tris (pH 6.8) | 0.1ml |
| 10% Gelatin | 0.1ml |
| 10% Ammonium persulphate | 0.1ml |
| TEMED | 4µl |

Stacking gel 5ml

| | |
|----------------------------|---------|
| Distilled H ₂ O | 3.0 ml |
| 30% Acrylamide mix | 0.7 ml |
| 1.5M Tris (pH 8.8) | 1.25 ml |
| 1.5M Tris (pH 8.8) | 0.05 ml |
| 10% Ammonium persulphate | 0.02 ml |
| TEMED | 0.01 ml |

1.5M Tris-HCl 50ml

| | |
|--|-------|
| 1.5M Tris-Cl pH 8.8 dH ₂ O to 50ml | 9.75g |
|--|-------|

10% SDS 50ml

| | |
|----------------------------------|----|
| SDS dH ₂ O to 50ml | 5g |
|----------------------------------|----|

0.5M Tris-HCl 50ml

| | |
|--|----|
| 0.5M Tris-Cl pH 6.8 dH ₂ O to 50ml | 3g |
|--|----|

| | |
|-----------------------------------|--------------|
| Sample loading buffer (5X) | 10 ml |
| 1M Tris (pH 6.8) | 3.125 ml |
| 50% Glycerol | 5.0 ml |
| SDS | 1 g |
| 1% Bromophenol blue | 1 ml |
| dH ₂ O | 0.875 ml |

| | |
|------------------------------|---------------|
| Running buffer (10x) | 1000ml |
| Tris base | 29 g |
| Glycine | 144 g |
| SDS | 10 g |
| dH ₂ O to 1 litre | |

| | |
|----------------------------|--------------|
| Renaturing buffer | 500ml |
| Triton X-100 | 12.5 ml |
| Distilled H ₂ O | 487.5 ml |

| | |
|--------------------------|---------------|
| Developing buffer | 200 ml |
| 1M Tris (pH 7.5) | 10 ml |
| 5M NaCl | 8 ml |
| 1M CaCl ₂ | 1.0 ml |
| 2.5% Triton X-100 | 1.6 ml |

| | |
|-----------------------------|---------------|
| Coomassie blue stain | 500 ml |
| Methanol | 150 ml |
| Acetic acid | 50 ml |
| Coomassie Brilliant Blue R | 2.5 g |
| Distilled H ₂ O | 300 ml |

| | |
|----------------------------|---------------|
| Coomassie destain | 500 ml |
| Methanol | 150 ml |
| Acetic acid | 50 ml |
| Distilled H ₂ O | 300 ml |

Appendix 2

Data from Results Chapters

Figure 4.14

Geometric mean fluorescence of flow cytometry ($\alpha 5\beta 1$)

| | Control | Foscan | Light | PDT |
|------|---------|--------|-------|-------|
| UP | 2.19 | 2.75 | 203 | 14.33 |
| VB6 | 5.03 | 5.35 | 4.37 | 9.01 |
| H376 | 6.06 | 9.12 | 7.64 | 34.21 |

Figure 4.16

Geometric mean fluorescence of flow cytometry ($\alpha v\beta 6$)

| | Control | Foscan | Light | PDT |
|------|---------|--------|-------|-------|
| UP | 34.64 | 32.43 | 33.65 | 27.61 |
| VB6 | 74.64 | 77.16 | 75.02 | 59.47 |
| H376 | 2.27 | 3.1 | 2.89 | 19.48 |

Figure 5.18

Geometric mean fluorescence of flow cytometry (EGFR)

| | Control | Foscan | Light | PDT |
|------|---------|--------|-------|-------|
| UP | 6.06 | 6.05 | 6.25 | 18.96 |
| VB6 | 3.25 | ND | ND | 3.48 |
| H376 | 33.29 | 29.16 | 30.67 | 5.66 |

Figure 5.20

Geometric mean fluorescence of flow cytometry (HGFR)

| | Control | Foscan | Light | PDT |
|------|---------|--------|-------|-----|
| UP | 2 | 1.65 | 2.5 | 2.9 |
| VB7 | 1 | 0.026 | 0.45 | 1.4 |
| H376 | 0.7 | 0.9 | 0.6 | 1.3 |

Figure 8.4

The results of an ANOVA where the area under the peak is explained by the time at which the spectrum was taken

| | Degrees of freedom (df) | Sum Sq | Mean Sq | <i>F</i> value | <i>p</i> -value |
|------------------|-------------------------|----------|---------|----------------|-----------------|
| Times | 2 | 2571.49 | 1285.75 | 3.04 | 0.0522 |
| Residuals | 108 | 45740.91 | 423.53 | | |

References

Reference List

- Ackermann,G., Abels,C., Baumler,W., Langer,S., Landthaler,M., Lang,E.W., and Szeimies,R.M. (1998). Simulations on the selectivity of 5-aminolaevulinic acid-induced fluorescence in vivo. *J Photochem. Photobiol. B* 47, 121-128.
- Ackroyd,R., Kelty,C., Brown,N., and Reed,M. (2001). The history of photodetection and photodynamic therapy. *Photochem. Photobiol.* 74, 656-669.
- Agarwal,M.L., Clay,M.E., Harvey,E.J., Evans,H.H., Antunez,A.R., and Oleinick,N.L. (1991). Photodynamic therapy induces rapid cell death by apoptosis in L5178Y mouse lymphoma cells. *Cancer Res.* 51, 5993-5996.
- Agostinis,P., Buytaert,E., Breyssens,H., and Hendrickx,N. (2004). Regulatory pathways in photodynamic therapy induced apoptosis. *Photochem. Photobiol. Sci.* 3, 721-729.
- Agostinis,P., Vandenbogaerde,A., Donella-Deana,A., Pinna,L.A., Lee,K.T., Goris,J., Merlevede,W., Vandenheede,J.R., and De,W.P. (1995). Photosensitized inhibition of growth factor-regulated protein kinases by hypericin. *Biochem. Pharmacol.* 49, 1615-1622.
- Ahmad,N., Kalka,K., and Mukhtar,H. (2001). In vitro and in vivo inhibition of epidermal growth factor receptor-tyrosine kinase pathway by photodynamic therapy. *Oncogene* 20, 2314-2317.
- Al-Hazzaa,A., Bowen,I.D., Randerson,P., and Birchall,M.A. (2005). The effect of ZD1839 (Iressa), an epidermal growth factor receptor tyrosine kinase inhibitor, in combination with cisplatin, on apoptosis in SCC-15 cells. *Cell Prolif.* 38, 77-86.
- Alfano,R.R.T.D., Cordero,J., Tomashefsky,P., Longo,F.W., and Alfano,M.A. (1984). Laser induced fluorescence spectroscopy from native cancerous and normal tissue. *IEEE J Quant Elect* 20, 1507-1511.
- Allison,R., Mang,T., Hewson,G., Snider,W., and Dougherty,D. (2001). Photodynamic therapy for chest wall progression from breast carcinoma is an underutilized treatment modality. *Cancer* 91, 1-8.
- Almeida,R.D., Manadas,B.J., Carvalho,A.P., and Duarte,C.B. (2004). Intracellular signaling mechanisms in photodynamic therapy. *Biochim. Biophys. Acta* 1704, 59-86.
- Amelink,A., van der Ploeg van den Heuvel, de Wolf,W.J., Robinson,D.J., and Sterenberg,H.J. (2005). Monitoring PDT by means of superficial reflectance spectroscopy. *J Photochem. Photobiol. B* 79, 243-251.
- Andersson-Engels,S., Klinteberg,C., Svanberg,K., and Svanberg,S. (1997). In vivo fluorescence imaging for tissue diagnostics. *Phys. Med. Biol.* 42, 815-824.

- Babilas,P., Schacht,V., Liebsch,G., Wolfbeis,O.S., Landthaler,M., Szeimies,R.M., and Abels,C. (2003). Effects of light fractionation and different fluence rates on photodynamic therapy with 5-aminolaevulinic acid in vivo. *Br. J. Cancer* 88, 1462-1469.
- Badizadegan,K., Backman,V., Boone,C.W., Crum,C.P., Dasari,R.R., Georgakoudi,I., Keefe,K., Munger,K., Shapshay,S.M., Sheetse,E.E., and Feld,M.S. (2004). Spectroscopic diagnosis and imaging of invisible pre-cancer. *Faraday Discuss.* 126, 265-279.
- Ball,D.J., Mayhew,S., Vernon,D.I., Griffin,M., and Brown,S.B. (2001). Decreased efficiency of trypsinization of cells following photodynamic therapy: evaluation of a role for tissue transglutaminase. *Photochem. Photobiol.* 73, 47-53.
- Barr,H., MacRobert,A.J., Tralau,C.J., Boulos,P.B., and Bown,S.G. (1990). The significance of the nature of the photosensitizer for photodynamic therapy: quantitative and biological studies in the colon. *Br. J Cancer* 62, 730-735.
- Baselga,J., Albanell,J., Ruiz,A., Lluch,A., Gascon,P., Guillem,V., Gonzalez,S., Sauleda,S., Marimon,I., Tabernero,J.M., Koehler,M.T., and Rojo,F. (2005). Phase II and tumor pharmacodynamic study of gefitinib in patients with advanced breast cancer. *J Clin. Oncol.* 23, 5323-5333.
- Benefield,J., Petruzzelli,G.J., Fowler,S., Taitz,A., Kalkanis,J., and Young,M.R. (1996). Regulation of the steps of angiogenesis by human head and neck squamous cell carcinomas. *Invasion Metastasis* 16, 291-301.
- Bennett,J.H., Morgan,M.J., Whawell,S.A., Atkin,P., Roblin,P., Furness,J., and Speight,P.M. (2000). Metalloproteinase expression in normal and malignant oral keratinocytes: stimulation of MMP-2 and -9 by scatter factor. *Eur. J Oral Sci.* 108, 281-291.
- Betz,C.S., Lai,J.P., Xiang,W., Janda,P., Heinrich,P., Stepp,H., Baumgartner,R., and Leunig,A. (2002a). In vitro photodynamic therapy of nasopharyngeal carcinoma using 5-aminolevulinic acid. *Photochem. Photobiol. Sci.* 1, 315-319.
- Betz,C.S., Mehlmann,M., Rick,K., Stepp,H., Grevers,G., Baumgartner,R., and Leunig,A. (1999). Autofluorescence imaging and spectroscopy of normal and malignant mucosa in patients with head and neck cancer. *Lasers Surg. Med.* 25, 323-334.
- Betz,C.S., Stepp,H., Janda,P., Arbogast,S., Grevers,G., Baumgartner,R., and Leunig,A. (2002b). A comparative study of normal inspection, autofluorescence and 5-ALA-induced PPIX fluorescence for oral cancer diagnosis. *Int. J. Cancer* 97, 245-252.
- Bhushan,M., Young,H.S., Brenchley,P.E., and Griffiths,C.E. (2002). Recent advances in cutaneous angiogenesis. *Br. J. Dermatol.* 147, 418-425.
- Biel,M.A. (1995). Photodynamic therapy of head and neck cancers. *Semin. Surg. Oncol.* 11, 355-359.

- Biel, M.A. (1998). Photodynamic therapy and the treatment of head and neck neoplasia. *Laryngoscope* 108, 1259-1268.
- Bigio, I.J., Bown, S.G., Briggs, G., Kelley, C., Lakhani, S., Pickard, D., Ripley, P.M., Rose, I.G., and Saunders, C. (2000). Diagnosis of breast cancer using elastic-scattering spectroscopy: preliminary clinical results. *J. Biomed. Opt.* 5, 221-228.
- Bigio, I.J. and Mourant, J.R. (1997). Ultraviolet and visible spectroscopies for tissue diagnostics: fluorescence spectroscopy and elastic-scattering spectroscopy. *Phys. Med. Biol.* 42, 803-814.
- Bigio, I.J., Mourant, J.R., and Los, G. (1999). Noninvasive, in-situ measurement of drug concentrations in tissue using optical spectroscopy. *J. Gravit. Physiol* 6, 173-175.
- Boere, I.A., Robinson, D.J., de Bruijn, H.S., van den, B.J., Tilanus, H.W., Sterenborg, H.J., and de Bruin, R.W. (2003). Monitoring in situ dosimetry and protoporphyrin IX fluorescence photobleaching in the normal rat esophagus during 5-aminolevulinic acid photodynamic therapy. *Photochem. Photobiol.* 78, 271-277.
- Bogenrieder, T. and Herlyn, M. (2003). Axis of evil: molecular mechanisms of cancer metastasis. *Oncogene* 22, 6524-6536.
- Bohorfoush, A.G. (1996). Tissue spectroscopy for gastrointestinal diseases. *Endoscopy* 28, 372-380.
- Bonnett, R. (1999). Photodynamic therapy in historical perspective. *Rev. Contemp. Pharmacother.* 10, 1-17.
- Bown, S.G., Tralau, C.J., Smith, P.D., Akdemir, D., and Wieman, T.J. (1986). Photodynamic therapy with porphyrin and phthalocyanine sensitisation: quantitative studies in normal rat liver. *Br. J. Cancer* 54, 43-52.
- Bradley, J.D., Scott, C.B., Paris, K.J., Demas, W.F., Machtay, M., Komaki, R., Movsas, B., Rubin, P., and Sause, W.T. (2002). A phase III comparison of radiation therapy with or without recombinant beta-interferon for poor-risk patients with locally advanced non-small-cell lung cancer (RTOG 93-04). *Int. J. Radiat. Oncol. Biol. Phys.* 52, 1173-1179.
- Braichotte, D.R., Wagnieres, G.A., Bays, R., Monnier, P., and van den Bergh, H.E. (1995). Clinical pharmacokinetic studies of photofrin by fluorescence spectroscopy in the oral cavity, the esophagus, and the bronchi. *Cancer* 75, 2768-2778.
- Brancalion, L. and Moseley, H. (2002). Laser and non-laser light sources for photodynamic therapy. *Lasers Med. Sci.* 17, 173-186.
- Brenneisen, P., Sies, H., and Scharffetter-Kochanek, K. (2002). Ultraviolet-B irradiation and matrix metalloproteinases: from induction via signaling to initial events. *Ann. N. Y. Acad. Sci.* 973, 31-43.

- Calin, M.A., Gruia, M., Herascu, N., and Coman, T. (2004). The monitoring of the accumulation of protoporphyrin IX in Walker tumours by subcutaneous administration of delta-aminolevulinic acid. *J Exp. Ther. Oncol.* 4, 247-251.
- Canti, G., Nicolin, A., Cubeddu, R., Taroni, P., Bandieramonte, G., and Valentini, G. (1998). Antitumor efficacy of the combination of photodynamic therapy and chemotherapy in murine tumors. *Cancer Lett.* 125, 39-44.
- charoenrat, P., Rhys-Evans, P., Modjtahedi, H., Court, W., Box, G., and Eccles, S. (2000). Overexpression of epidermal growth factor receptor in human head and neck squamous carcinoma cell lines correlates with matrix metalloproteinase-9 expression and in vitro invasion. *Int. J. Cancer* 86, 307-317.
- Chin, D., Boyle, G.M., Kane, A.J., Theile, D.R., Hayward, N.K., Parson, P.G., and Coman, W.B. (2005). Invasion and metastasis markers in cancers. *Br. J Plast. Surg.* 58, 466-474.
- Chiu, S.M. and Oleinick, N.L. (2001). Dissociation of mitochondrial depolarization from cytochrome c release during apoptosis induced by photodynamic therapy. *Br. J Cancer* 84, 1099-1106.
- Christofori, G. and Semb, H. (1999). The role of the cell-adhesion molecule E-cadherin as a tumour-suppressor gene. *Trends Biochem. Sci.* 24, 73-76.
- Ciardiello, F., Bianco, R., Damiano, V., Fontanini, G., Caputo, R., Pomatice, G., De, P.S., Bianco, A.R., Mendelsohn, J., and Tortora, G. (2000). Antiangiogenic and antitumor activity of anti-epidermal growth factor receptor C225 monoclonal antibody in combination with vascular endothelial growth factor antisense oligonucleotide in human GEO colon cancer cells. *Clin. Cancer Res.* 6, 3739-3747.
- Clayman, G., Wang, S.W., Nicolson, G.L., El-Naggar, A., Mazar, A., Henkin, J., Blasi, F., Goepfert, H., and Boyd, D.D. (1993). Regulation of urokinase-type plasminogen activator expression in squamous-cell carcinoma of the oral cavity. *Int. J. Cancer* 54, 73-80.
- Copper, M.P., Tan, I.B., Oppelaar, H., Ruevekamp, M.C., and Stewart, F.A. (2003). Meta-tetra(hydroxyphenyl)chlorin photodynamic therapy in early-stage squamous cell carcinoma of the head and neck. *Arch. Otolaryngol. Head Neck Surg.* 129, 709-711.
- Cordes, N. and Meineke, V. (2004). Integrin signalling and the cellular response to ionizing radiation. *J Mol. Histol.* 35, 327-337.
- Cramers, P., Ruevekamp, M., Oppelaar, H., Dalesio, O., Baas, P., and Stewart, F.A. (2003). Foscan uptake and tissue distribution in relation to photodynamic efficacy. *Br. J Cancer* 88, 283-290.
- Crescenzi, E., Varriale, L., Iovino, M., Chiaviello, A., Veneziani, B.M., and Palumbo, G. (2004). Photodynamic therapy with indocyanine green complements and enhances low-dose cisplatin cytotoxicity in MCF-7 breast cancer cells. *Mol. Cancer Ther.* 3, 537-544.

- Culhaci,N., Metin,K., Copcu,E., and Dikicioglu,E. (2004). Elevated expression of MMP-13 and TIMP-1 in head and neck squamous cell carcinomas may reflect increased tumor invasiveness. *BMC. Cancer* 4, 42.
- Curnow,A., Haller,J.C., and Bown,S.G. (2000). Oxygen monitoring during 5-aminolaevulinic acid induced photodynamic therapy in normal rat colon. Comparison of continuous and fractionated light regimes. *J. Photochem. Photobiol. B* 58, 149-155.
- Curnow,A., McIlroy,B.W., Postle-Hacon,M.J., Porter,J.B., MacRobert,A.J., and Bown,S.G. (1998). Enhancement of 5-aminolaevulinic acid-induced photodynamic therapy in normal rat colon using hydroxypyridinone iron-chelating agents. *Br. J Cancer* 78, 1278-1282.
- Curran,S. and Murray,G.I. (1999). Matrix metalloproteinases in tumour invasion and metastasis. *J. Pathol.* 189, 300-308.
- D'Cruz,A.K., Robinson,M.H., and Biel,M.A. (2004). mTHPC-mediated photodynamic therapy in patients with advanced, incurable head and neck cancer: a multicenter study of 128 patients. *Head Neck* 26, 232-240.
- DaCosta,R.S., Andersson,H., and Wilson,B.C. (2003). Molecular fluorescence excitation-emission matrices relevant to tissue spectroscopy. *Photochem. Photobiol.* 78, 384-392.
- Danen,E.H. (2005). Integrins: regulators of tissue function and cancer progression. *Curr. Pharm. Des* 11, 881-891.
- Dano,K., Behrendt,N., Hoyer-Hansen,G., Johnsen,M., Lund,L.R., Ploug,M., and Romer,J. (2005). Plasminogen activation and cancer. *Thromb. Haemost.* 93, 676-681.
- Datta,S.N., Allman,R., Loh,C., Mason,M., and Matthews,P.N. (1997). Effect of photodynamic therapy in combination with mitomycin C on a mitomycin-resistant bladder cancer cell line. *Br. J Cancer* 76, 312-317.
- de Vicente,J.C., Fresno,M.F., Villalain,L., Vega,J.A., and Hernandez,V.G. (2005). Expression and clinical significance of matrix metalloproteinase-2 and matrix metalloproteinase-9 in oral squamous cell carcinoma. *Oral Oncol.* 41, 283-293.
- de,V., Bakker Schut,T.C., Skurichina,M., Witjes,M.J., Van der Wal,J.E., Roodenburg,J.L., and Sterenberg,H.J. (2005). Autofluorescence and Raman microspectroscopy of tissue sections of oral lesions. *Lasers Med Sci* 19, 203-209.
- de,V., Skurichina,M., Witjes,M.J., Duin,R.P., Sterenberg,D.J., Star,W.M., and Roodenburg,J.L. (2003). Autofluorescence characteristics of healthy oral mucosa at different anatomical sites. *Lasers Surg. Med.* 32, 367-376.
- del Carmen,M.G., Rizvi,I., Chang,Y., Moor,A.C., Oliva,E., Sherwood,M., Pogue,B., and Hasan,T. (2005). Synergism of epidermal growth factor receptor-targeted immunotherapy with photodynamic treatment of ovarian cancer in vivo. *J. Natl. Cancer Inst.* 97, 1516-1524.

- Detty, M.R., Gibson, S.L., and Wagner, S.J. (2004). Current clinical and preclinical photosensitizers for use in photodynamic therapy. *J. Med. Chem.* 47, 3897-3915.
- Dilkes, M.G., Benjamin, E., Ovaisi, S., and Banerjee, A.S. (2003). Treatment of primary mucosal head and neck squamous cell carcinoma using photodynamic therapy: results after 25 treated cases. *J. Laryngol. Otol.* 117, 713-717.
- Dima, V.F., Mihailescu, I.N., Dima, S.V., Chivu, L., Stirbet, M., Udrea, M., and Popa, A. (1990). Studies of the effects of associated photodynamic therapy and drugs on macromolecular synthesis of tumoral cells grown in vitro. *Arch. Roum. Pathol. Exp. Microbiol.* 49, 155-175.
- Do, N.Y., Lim, S.C., and Im, T.S. (2004). Expression of c-erbB receptors, MMPs and VEGF in squamous cell carcinoma of the head and neck. *Oncol. Rep.* 12, 229-237.
- Dolmans, D.E., Fukumura, D., and Jain, R.K. (2003). Photodynamic therapy for cancer. *Nat. Rev. Cancer* 3, 380-387.
- Dougherty, T.J. (1996). A brief history of clinical photodynamic therapy development at Roswell Park Cancer Institute. *J. Clin. Laser Med. Surg.* 14, 219-221.
- Dougherty, T.J. (2002). An update on photodynamic therapy applications. *J. Clin. Laser Med. Surg.* 20, 3-7.
- Dougherty, T.J., Gomer, C.J., Henderson, B.W., Jori, G., Kessel, D., Korbélik, M., Moan, J., and Peng, Q. (1998). Photodynamic therapy. *J. Natl. Cancer Inst.* 90, 889-905.
- Drezek, R.A., Richards-Kortum, R., Brewer, M.A., Feld, M.S., Pitris, C., Ferenczy, A., Faupel, M.L., and Follen, M. (2003). Optical imaging of the cervix. *Cancer* 98, 2015-2027.
- Du, H., Olivo, M., Mahendran, R., and Bay, B.H. (2004). Modulation of Matrix metalloproteinase-1 in nasopharyngeal cancer cells by photoactivation of hypericin. *Int. J. Oncol.* 24, 657-662.
- Dysart, J.S., Singh, G., and Patterson, M.S. (2005). Calculation of singlet oxygen dose from photosensitizer fluorescence and photobleaching during mTHPC photodynamic therapy of MLL cells. *Photochem. Photobiol.* 81, 196-205.
- el-Sharabasy, M.M. (1992). Porphyrin studies in chronic renal failure and renal transplantation. *Acta Med. Hung.* 49, 219-223.
- Endlicher, E., Rummele, P., Hausmann, F., Krieg, R., Knuchel, R., Rath, H.C., Scholmerich, J., and Messmann, H. (2001). Protoporphyrin IX distribution following local application of 5-aminolevulinic acid and its esterified derivatives in the tissue layers of the normal rat colon. *Br. J. Cancer* 85, 1572-1576.
- Ericson, M.B., Grapengiesser, S., Gudmundson, F., Wennberg, A.M., Larko, O., Moan, J., and Rosen, A. (2003). A spectroscopic study of the photobleaching of protoporphyrin IX in solution. *Lasers Med. Sci.* 18, 56-62.

Ericson,M.B., Sandberg,C., Stenquist,B., Gudmundson,F., Karlsson,M., Ros,A.M., Rosen,A., Larko,O., Wennberg,A.M., and Rosdahl,I. (2004). Photodynamic therapy of actinic keratosis at varying fluence rates: assessment of photobleaching, pain and primary clinical outcome. *Br. J Dermatol.* 151, 1204-1212.

Fabris,C., Valduga,G., Miotto,G., Borsetto,L., Jori,G., Garbisa,S., and Reddi,E. (2001). Photosensitization with zinc (II) phthalocyanine as a switch in the decision between apoptosis and necrosis. *Cancer Res.* 61, 7495-7500.

Fassina,G., Ferrari,N., Brigati,C., Benelli,R., Santi,L., Noonan,D.M., and Albini,A. (2000). Tissue inhibitors of metalloproteases: regulation and biological activities. *Clin. Exp. Metastasis* 18, 111-120.

Faust,R.A., Tawfic,S., Davis,A.T., and Ahmed,K. (1999). Apoptosis and growth inhibition of head and neck tumor cell line induced by epidermal growth factor receptor tyrosine kinase inhibitor. *Oral Oncol.* 35, 290-295.

Ferley, J., Bray, F., Pisan, P. R., and Parkin, D. M. GLOBOCAN 2000: Cancer incidence, Mortality and prevalence worldwide, version 1.0.2001. Limited version available from [URL:http://www-dep-iarc.fr/globocan/globocan.htm](http://www-dep-iarc.fr/globocan/globocan.htm). Last updated on 18 November 2002. 2000.

Ref Type: Internet Communication

Ferrario,A., Chantrain,C.F., von Tiehl,K., Buckley,S., Rucker,N., Shalinsky,D.R., Shimada,H., DeClerck,Y.A., and Gomer,C.J. (2004). The matrix metalloproteinase inhibitor prinomastat enhances photodynamic therapy responsiveness in a mouse tumor model. *Cancer Res.* 64, 2328-2332.

Fijan,S., Honigsmann,H., and Ortel,B. (1995). Photodynamic therapy of epithelial skin tumours using delta-aminolaevulinic acid and desferrioxamine. *Br. J Dermatol.* 133, 282-288.

Fingar,V.H., Kik,P.K., Haydon,P.S., Cerrito,P.B., Tseng,M., Abang,E., and Wieman,T.J. (1999). Analysis of acute vascular damage after photodynamic therapy using benzoporphyrin derivative (BPD). *Br. J. Cancer* 79, 1702-1708.

Forastiere,A., Koch,W., Trotti,A., and Sidransky,D. (2001). Head and neck cancer. *N. Engl. J. Med.* 345, 1890-1900.

Foultier,M.T., Vonarx-Coinsmann,V., Cordel,S., Combre,A., and Patrice,T. (1994). Modulation of colonic cancer cell adhesiveness by haematoporphyrin derivative photodynamic therapy. *J Photochem. Photobiol. B* 23, 9-17.

Franchi,A., Santucci,M., Masini,E., Sardi,I., Paglierani,M., and Gallo,O. (2002). Expression of matrix metalloproteinase 1, matrix metalloproteinase 2, and matrix metalloproteinase 9 in carcinoma of the head and neck. *Cancer* 95, 1902-1910.

Fujimura,M., Hidaka,T., and Saito,S. (2002). Selective inhibition of the epidermal growth factor receptor by ZD1839 decreases the growth and invasion of ovarian clear cell adenocarcinoma cells. *Clin. Cancer Res.* 8, 2448-2454.

- Gantchev, T.G., Brasseur, N., and van Lier, J.E. (1996). Combination toxicity of etoposide (VP-16) and photosensitisation with a water-soluble aluminium phthalocyanine in K562 human leukaemic cells. *Br. J Cancer* 74, 1570-1577.
- Gath, H.J. and Brakenhoff, R.H. (1999). Minimal residual disease in head and neck cancer. *Cancer Metastasis Rev.* 18, 109-126.
- Geboes, K., Desreumaux, P., Jouret, A., Ectors, N., Rutgeerts, P., and Colombel, J.F. (1999). [Histopathologic diagnosis of the activity of chronic inflammatory bowel disease. Evaluation of the effect of drug treatment. Use of histological scores]. *Gastroenterol. Clin. Biol.* 23, 1062-1073.
- Gelse, K., Poschl, E., and Aigner, T. (2003). Collagens--structure, function, and biosynthesis. *Adv. Drug Deliv. Rev.* 55, 1531-1546.
- Georgakoudi, I. and Feld, M.S. (2004). The combined use of fluorescence, reflectance, and light-scattering spectroscopy for evaluating dysplasia in Barrett's esophagus. *Gastrointest. Endosc. Clin. N. Am.* 14, 519-37, ix.
- Georgakoudi, I. and Foster, T.H. (1998). Singlet oxygen- versus nonsinglet oxygen-mediated mechanisms of sensitizer photobleaching and their effects on photodynamic dosimetry. *Photochem. Photobiol.* 67, 612-625.
- Georgakoudi, I., Jacobson, B.C., Van, D.J., Backman, V., Wallace, M.B., Muller, M.G., Zhang, Q., Badizadegan, K., Sun, D., Thomas, G.A., Perelman, L.T., and Feld, M.S. (2001). Fluorescence, reflectance, and light-scattering spectroscopy for evaluating dysplasia in patients with Barrett's esophagus. *Gastroenterology* 120, 1620-1629.
- Ghosh, S., Munshi, H.G., Sen, R., Linz-McGillem, L.A., Goldman, R.D., Lorch, J., Green, K.J., Jones, J.C., and Stack, M.S. (2002). Loss of adhesion-regulated proteinase production is correlated with invasive activity in oral squamous cell carcinoma. *Cancer* 95, 2524-2533.
- Giaccone, G., Gonzalez-Larriba, J.L., van Oosterom, A.T., Alfonso, R., Smit, E.F., Martens, M., Peters, G.J., van, d., V, Smith, R., Averbuch, S., and Fandi, A. (2004). Combination therapy with gefitinib, an epidermal growth factor receptor tyrosine kinase inhibitor, gemcitabine and cisplatin in patients with advanced solid tumors. *Ann. Oncol.* 15, 831-838.
- Giancotti, F.G. and Ruoslahti, E. (1999). Integrin signaling. *Science* 285, 1028-1032.
- Giannelli, G., Milillo, L., Marinosci, F., Lo, M.L., Serpico, R., and Antonaci, S. (2001). Altered expression of integrins and basement membrane proteins in malignant and pre-malignant lesions of oral mucosa. *J. Biol. Regul. Homeost. Agents* 15, 375-380.
- Gillenwater, A., Jacob, R., Ganeshappa, R., Kemp, B., El-Naggar, A.K., Palmer, J.L., Clayman, G., Mitchell, M.F., and Richards-Kortum, R. (1998). Noninvasive diagnosis of oral neoplasia based on fluorescence spectroscopy and native tissue autofluorescence. *Arch. Otolaryngol. Head Neck Surg.* 124, 1251-1258.
- Ginos, M.A., Page, G.P., Michalowicz, B.S., Patel, K.J., Volker, S.E., Pambuccian, S.E., Ondrey, F.G., Adams, G.L., and Gaffney, P.M. (2004). Identification of a gene

expression signature associated with recurrent disease in squamous cell carcinoma of the head and neck. *Cancer Res.* 64, 55-63.

Gollnick,S.O., Lee,B.Y., Vaughan,L., Owczarczak,B., and Henderson,B.W. (2001). Activation of the IL-10 gene promoter following photodynamic therapy of murine keratinocytes. *Photochem. Photobiol.* 73, 170-177.

Gomer,C.J., Doiron,D.R., Rucker,N., Razum,N.J., and Fountain,S.W. (1984). Examination of action spectrum, dose rate and mutagenic properties of hematoporphyrin derivative photoradiation therapy. *Prog. Clin. Biol. Res.* 170, 459-469.

Granville,D.J., Carthy,C.M., Jiang,H., Levy,J.G., McManus,B.M., Matroule,J.Y., Piette,J., and Hunt,D.W. (2000). Nuclear factor-kappaB activation by the photochemotherapeutic agent verteporfin. *Blood* 95, 256-262.

Granville,D.J., Levy,J.G., and Hunt,D.W. (1998). Photodynamic treatment with benzoporphyrin derivative monoacid ring A produces protein tyrosine phosphorylation events and DNA fragmentation in murine P815 cells. *Photochem. Photobiol.* 67, 358-362.

Greenblatt,M.S., Beaudet,J.G., Gump,J.R., Godin,K.S., Trombley,L., Koh,J., and Bond,J.P. (2003). Detailed computational study of p53 and p16: using evolutionary sequence analysis and disease-associated mutations to predict the functional consequences of allelic variants. *Oncogene* 22, 1150-1163.

Greenlee,R.T., Hill-Harmon,M.B., Murray,T., and Thun,M. (2001). Cancer statistics, 2001. *CA Cancer J Clin.* 51, 15-36.

Hammes,G.G. (2005). *Spectroscopy for the Biological Sciences*. Wiley-Interscience.

Hanahan,D. and Weinberg,R.A. (2000). The hallmarks of cancer. *Cell* 100, 57-70.

Hanlon,E.B., Manoharan,R., Koo,T.W., Shafer,K.E., Motz,J.T., Fitzmaurice,M., Kramer,J.R., Itzkan,I., Dasari,R.R., and Feld,M.S. (2000). Prospects for in vivo Raman spectroscopy. *Phys. Med. Biol.* 45, R1-59.

Haringsma,J. (2002). Barrett's oesophagus: new diagnostic and therapeutic techniques. *Scand. J Gastroenterol. Suppl* 9-14.

Heintzelman,D.L., Lotan,R., and Richards-Kortum,R.R. (2000). Characterization of the autofluorescence of polymorphonuclear leukocytes, mononuclear leukocytes and cervical epithelial cancer cells for improved spectroscopic discrimination of inflammation from dysplasia. *Photochem. Photobiol.* 71, 327-332.

Herbst,R.S. (2004). Review of epidermal growth factor receptor biology. *Int. J. Radiat. Oncol. Biol. Phys.* 59, 21-26.

Hopper,C., Kubler,A., Lewis,H., Tan,I.B., and Putnam,G. (2004a). mTHPC-mediated photodynamic therapy for early oral squamous cell carcinoma. *Int. J. Cancer* 111, 138-146.

- Hopper,C., Niziol,C., and Sidhu,M. (2004b). The cost-effectiveness of Foscan mediated photodynamic therapy (Foscan-PDT) compared with extensive palliative surgery and palliative chemotherapy for patients with advanced head and neck cancer in the UK. *Oral Oncol.* 40, 372-382.
- Hornung,R., Jentsch,B., Crompton,N.E., Haller,U., and Walt,H. (1997). In vitro effects and localisation of the photosensitizers m-THPC and m-THPC MD on carcinoma cells of the human breast (MCF-7) and Chinese hamster fibroblasts (V-79). *Lasers Surg. Med.* 20, 443-450.
- Huang,Z., Chen,Q., Shakil,A., Chen,H., Beckers,J., Shapiro,H., and Hetzel,F.W. (2003). Hyperoxygenation enhances the tumor cell killing of photofrin-mediated photodynamic therapy. *Photochem. Photobiol.* 78, 496-502.
- Humphries,M.J., Matsumoto,K., White,S.L., and Olden,K. (1986). Inhibition of experimental metastasis by castanospermine in mice: blockage of two distinct stages of tumor colonization by oligosaccharide processing inhibitors. *Cancer Res.* 46, 5215-5222.
- Hundsdoerfer,B., Zeilhofer,H.F., Bock,K.P., Dettmar,P., Schmitt,M., Kolk,A., Pautke,C., and Horch,H.H. (2005). Tumour-associated urokinase-type plasminogen activator (uPA) and its inhibitor PAI-1 in normal and neoplastic tissues of patients with squamous cell cancer of the oral cavity - clinical relevance and prognostic value. *J. Craniomaxillofac. Surg.* 33, 191-196.
- Hynes,R.O. (2002). A reevaluation of integrins as regulators of angiogenesis. *Nat. Med.* 8, 918-921.
- Irby,R.B. and Yeatman,T.J. (2000). Role of Src expression and activation in human cancer. *Oncogene* 19, 5636-5642.
- Jeffes,E.W., McCullough,J.L., Weinstein,G.D., Fergin,P.E., Nelson,J.S., Shull,T.F., Simpson,K.R., Bukaty,L.M., Hoffman,W.L., and Fong,N.L. (1997). Photodynamic therapy of actinic keratosis with topical 5-aminolevulinic acid. A pilot dose-ranging study. *Arch. Dermatol.* 133, 727-732.
- Jeon,G.A., Lee,J.S., Patel,V., Gutkind,J.S., Thorgeirsson,S.S., Kim,E.C., Chu,I.S., Amornphimoltham,P., and Park,M.H. (2004). Global gene expression profiles of human head and neck squamous carcinoma cell lines. *Int. J. Cancer* 112, 249-258.
- Jerjes,W., Swinson,B., Johnson,K.S., Thomas,G.J., and Hopper,C. (2005). Assessment of bony resection margins in oral cancer using elastic scattering spectroscopy: a study on archival material. *Arch. Oral Biol.* 50, 361-366.
- Jerjes,W., Swinson,B., Pickard,D., Thomas,G.J., and Hopper,C. (2004). Detection of cervical intranodal metastasis in oral cancer using elastic scattering spectroscopy. *Oral Oncol.* 40, 673-678.
- Jiang,F., Chopp,M., Katakowski,M., Cho,K.K., Yang,X., Hochbaum,N., Tong,L., and Mikkelsen,T. (2002). Photodynamic therapy with photofrin reduces invasiveness of malignant human glioma cells. *Lasers Med. Sci.* 17, 280-288.

- Jiang,F., Zhang,Z.G., Katakowski,M., Robin,A.M., Faber,M., Zhang,F., and Chopp,M. (2004). Angiogenesis induced by photodynamic therapy in normal rat brains. *Photochem. Photobiol.* 79, 494-498.
- Johnson,K.S., Chicken,D.W., Pickard,D.C., Lee,A.C., Briggs,G., Falzon,M., Bigio,I.J., Keshtgar,M.R., and Bown,S.G. (2004). Elastic scattering spectroscopy for intraoperative determination of sentinel lymph node status in the breast. *J. Biomed. Opt.* 9, 1122-1128.
- Jones,H.J., Vernon,D.I., and Brown,S.B. (2003). Photodynamic therapy effect of m-THPC (Foscan) in vivo: correlation with pharmacokinetics. *Br. J Cancer* 89, 398-404.
- Juliano,R.L. (2002). Signal transduction by cell adhesion receptors and the cytoskeleton: functions of integrins, cadherins, selectins, and immunoglobulin-superfamily members. *Annu. Rev. Pharmacol. Toxicol.* 42, 283-323.
- Karrer,S., Bosserhoff,A.K., Weiderer,P., Landthaler,M., and Szeimies,R.M. (2003). Influence of 5-aminolevulinic acid and red light on collagen metabolism of human dermal fibroblasts. *J Invest Dermatol.* 120, 325-331.
- Karrer,S., Bosserhoff,A.K., Weiderer,P., Landthaler,M., and Szeimies,R.M. (2004). Keratinocyte-derived cytokines after photodynamic therapy and their paracrine induction of matrix metalloproteinases in fibroblasts. *Br. J Dermatol.* 151, 776-783.
- Kawahara,E., Okada,Y., Nakanishi,I., Iwata,K., Kojima,S., Kumagai,S., and Yamamoto,E. (1993). The expression of invasive behavior of differentiated squamous carcinoma cell line evaluated by an in vitro invasion model. *Jpn. J. Cancer Res.* 84, 409-418.
- Kawata,R., Shimada,T., Maruyama,S., Hisa,Y., Takenaka,H., and Murakami,Y. (2002). Enhanced production of matrix metalloproteinase-2 in human head and neck carcinomas is correlated with lymph node metastasis. *Acta Otolaryngol.* 122, 101-106.
- Kelly,J.F. and Snell,M.E. (1976). Hematoporphyrin derivative: a possible aid in the diagnosis and therapy of carcinoma of the bladder. *J. Urol.* 115, 150-151.
- Kennedy,J.C., Marcus,S.L., and Pottier,R.H. (1996). Photodynamic therapy (PDT) and photodiagnosis (PD) using endogenous photosensitization induced by 5-aminolevulinic acid (ALA): mechanisms and clinical results. *J. Clin. Laser Med. Surg.* 14, 289-304.
- Kennedy,J.C., Pottier,R.H., and Pross,D.C. (1990). Photodynamic therapy with endogenous protoporphyrin IX: basic principles and present clinical experience. *J. Photochem. Photobiol. B* 6, 143-148.
- Kerkela,E. and Saarialho-Kere,U. (2003). Matrix metalloproteinases in tumor progression: focus on basal and squamous cell skin cancer. *Exp. Dermatol.* 12, 109-125.

- Kessel,D. and Luo,Y. (1999). Photodynamic therapy: a mitochondrial inducer of apoptosis. *Cell Death. Differ.* 6, 28-35.
- Kim,E.S. and Glisson,B.S. (2003). Treatment of metastatic head and neck cancer: chemotherapy and novel agents. *Cancer Treat. Res.* 114, 295-314.
- Kleiner,D.E. and Stetler-Stevenson,W.G. (1999). Matrix metalloproteinases and metastasis. *Cancer Chemother. Pharmacol.* 43 *Suppl.*, S42-S51.
- Kovacs,A.F., Landes,C.A., Hamscho,N., Risse,J.H., Berner,U., and Menzel,C. (2005). Sentinel node biopsy as staging tool in a multimodality treatment approach to cancer of the oral cavity and the oropharynx. *Otolaryngol. Head Neck Surg.* 132, 570-576.
- Kramer,R.H., Shen,X., and Zhou,H. (2005). Tumor cell invasion and survival in head and neck cancer. *Cancer Metastasis Rev.* 24, 35-45.
- Krueger,T., Altermatt,H.J., Mettler,D., Scholl,B., Magnusson,L., and Ris,H.B. (2003). Experimental photodynamic therapy for malignant pleural mesothelioma with pegylated mTHPC. *Lasers Surg. Med.* 32, 61-68.
- Kubler,A.C., de,C.J., Hopper,C., Leonard,A.G., and Putnam,G. (2001). Treatment of squamous cell carcinoma of the lip using Foscan-mediated photodynamic therapy. *Int. J Oral Maxillofac. Surg.* 30, 504-509.
- Kurahara,S., Shinohara,M., Ikebe,T., Nakamura,S., Beppu,M., Hiraki,A., Takeuchi,H., and Shirasuna,K. (1999). Expression of MMPS, MT-MMP, and TIMPs in squamous cell carcinoma of the oral cavity: correlations with tumor invasion and metastasis. *Head Neck* 21, 627-638.
- Kurita,H. and Kurashina,K. (1996). Vital staining with iodine solution in delineating the border of oral dysplastic lesions. *Oral Surg. Oral Med. Oral Pathol. Oral Radiol. Endod.* 81, 275-280.
- Kuwahara,D., Tsutsumi,K., Kobayashi,T., Hasunuma,T., and Nishioka,K. (2000). Caspase-9 regulates cisplatin-induced apoptosis in human head and neck squamous cell carcinoma cells. *Cancer Lett.* 148, 65-71.
- Lange,T.S., Kirchberg,J., Bielinsky,A.K., Leuker,A., Bank,I., Ruzicka,T., and Scharffetter-Kochanek,K. (1995). Divalent cations (Mg²⁺, Ca²⁺) differentially influence the beta 1 integrin-mediated migration of human fibroblasts and keratinocytes to different extracellular matrix proteins. *Exp. Dermatol.* 4, 130-137.
- Langmack,K., Mehta,R., Twyman,P., and Norris,P. (2001). Topical photodynamic therapy at low fluence rates--theory and practice. *J Photochem. Photobiol. B* 60, 37-43.
- Laughner,E., Taghavi,P., Chiles,K., Mahon,P.C., and Semenza,G.L. (2001). HER2 (neu) signaling increases the rate of hypoxia-inducible factor 1alpha (HIF-1alpha) synthesis: novel mechanism for HIF-1-mediated vascular endothelial growth factor expression. *Mol. Cell Biol.* 21, 3995-4004.

- Lejbkiewicz,F. and Salzberg,S. (1992). Biological effects of photoactivated-HPD and cholesteryl hemisuccinate on erythroid differentiation. *Biomater. Artif. Cells Immobilization Biotechnol.* 20, 1111-1120.
- Leunig,A., Betz,C.S., Mehlmann,M., Stepp,H., Arbogast,S., Grevers,G., and Baumgartner,R. (2000). Detection of squamous cell carcinoma of the oral cavity by imaging 5-aminolevulinic acid-induced protoporphyrin IX fluorescence. *Laryngoscope* 110, 78-83.
- Leunig,A., Mehlmann,M., Betz,C., Stepp,H., Arbogast,S., Grevers,G., and Baumgartner,R. (2001). Fluorescence staining of oral cancer using a topical application of 5-aminolevulinic acid: fluorescence microscopic studies. *J. Photochem. Photobiol. B* 60, 44-49.
- Leunig,A., Rick,K., Stepp,H., Goetz,A., Baumgartner,R., and Feyh,J. (1996). [Photodynamic diagnosis of neoplasms of the mouth cavity after local administration of 5-aminolevulinic acid]. *Laryngorhinootologie* 75, 459-464.
- Li,X., Yang,Y., Hu,Y., Dang,D., Regezi,J., Schmidt,B.L., Atakilit,A., Chen,B., Ellis,D., and Ramos,D.M. (2003). Alphasbeta6-Fyn signaling promotes oral cancer progression. *J. Biol. Chem.* 278, 41646-41653.
- Lilge,L. and Wilson,B.C. (1998). Photodynamic therapy of intracranial tissues: a preclinical comparative study of four different photosensitizers. *J Clin. Laser Med. Surg.* 16, 81-91.
- Lin,W.C., Toms,S.A., Johnson,M., Jansen,E.D., and Mahadevan-Jansen,A. (2001). In vivo brain tumor demarcation using optical spectroscopy. *Photochem. Photobiol.* 73, 396-402.
- Liotta,L.A., Thorgeirsson,U.P., and Garbisa,S. (1982). Role of collagenases in tumor cell invasion. *Cancer Metastasis Rev.* 1, 277-288.
- Lisnjak,I.O., Kutsenok,V.V., Polyschuk,L.Z., Gorobets,O.B., and Gamaleia,N.F. (2005). Effect of photodynamic therapy on tumor angiogenesis and metastasis in mice bearing Lewis lung carcinoma. *Exp. Oncol.* 27, 333-335.
- Liu,D., Aguirre,G.J., Estrada,Y., and Ossowski,L. (2002). EGFR is a transducer of the urokinase receptor initiated signal that is required for in vivo growth of a human carcinoma. *Cancer Cell* 1, 445-457.
- Lovat,L. and Bown,S. (2004). Elastic scattering spectroscopy for detection of dysplasia in Barrett's esophagus. *Gastrointest. Endosc. Clin. N. Am.* 14, 507-17, ix.
- Luo,J., Lubaroff,D.M., and Hendrix,M.J. (1999). Suppression of prostate cancer invasive potential and matrix metalloproteinase activity by E-cadherin transfection. *Cancer Res.* 59, 3552-3556.
- Ma,L.W., Moan,J., Berg,K., Peng,Q., and Steen,H.B. (1993). Potentiation of photodynamic therapy by mitomycin C in cultured human colon adenocarcinoma cells. *Radiat. Res.* 134, 22-28.

- Ma,L.W., Steen,H.B., Moan,J., Berg,K., Peng,Q., Saether,H., and Rimington,C. (1992). Cytotoxicity and cytokinetic effects of mitomycin C and/or photochemotherapy in a human colon adenocarcinoma cell line. *Int. J Biochem.* 24, 1807-1813.
- Maeda,T., Matsumura,S., Hiranuma,H., Jikko,A., Furukawa,S., Ishida,T., and Fuchihata,H. (1998). Expression of vascular endothelial growth factor in human oral squamous cell carcinoma: its association with tumour progression and p53 gene status. *J. Clin. Pathol.* 51, 771-775.
- Magne,N., Fischel,J.L., Dubreuil,A., Formento,P., Marcie,S., Lagrange,J.L., and Milano,G. (2002). Sequence-dependent effects of ZD1839 ('Iressa') in combination with cytotoxic treatment in human head and neck cancer. *Br. J. Cancer* 86, 819-827.
- Maier,A., Anegg,U., Tomaselli,F., Rehak,P., Sankin,O., Fell,B., Renner,H., Pinter,H., Smolle-Juttner,F.M., and Friehs,G.B. (2000). Does hyperbaric oxygen enhance the effect of photodynamic therapy in patients with advanced esophageal carcinoma? A clinical pilot study. *Endoscopy* 32, 42-48.
- Mandy,F.F., Bergeron,M., and Minkus,T. (1995). Principles of flow cytometry. *Transfus. Sci.* 16, 303-314.
- Mang,T.S., Dougherty,T.J., Potter,W.R., Boyle,D.G., Somer,S., and Moan,J. (1987). Photobleaching of porphyrins used in photodynamic therapy and implications for therapy. *Photochem. Photobiol.* 45, 501-506.
- Maragou,P., Bazopoulou-Kyrkanidou,E., Panotopoulou,E., Kakarantza-Angelopoulou,E., Sklavounou-Andrikopoulou,A., and Kotaridis,S. (1999). Alteration of integrin expression in oral squamous cell carcinomas. *Oral Dis.* 5, 20-26.
- Marchal,S., Fadloun,A., Maugain,E., D'Hallewin,M.A., Guillemin,F., and Bezdetnaya,L. (2005). Necrotic and apoptotic features of cell death in response to Foscan photosensitization of HT29 monolayer and multicell spheroids. *Biochem. Pharmacol.* 69, 1167-1176.
- Margaron,P., Sorrenti,R., and Levy,J.G. (1997). Photodynamic therapy inhibits cell adhesion without altering integrin expression. *Biochim. Biophys. Acta* 1359, 200-210.
- Maulik,G., Shrikhande,A., Kijima,T., Ma,P.C., Morrison,P.T., and Salgia,R. (2002). Role of the hepatocyte growth factor receptor, c-Met, in oncogenesis and potential for therapeutic inhibition. *Cytokine Growth Factor Rev.* 13, 41-59.
- Melnikova,V.O., Bezdetnaya,L.N., Bour,C., Festor,E., Gramain,M.P., Merlin,J.L., Potapenko,A.Y., and Guillemin,F. (1999). Subcellular localization of meta-tetra (hydroxyphenyl) chlorin in human tumor cells subjected to photodynamic treatment. *J Photochem. Photobiol. B* 49, 96-103.

- Messmann,H., Szeimies,R.M., Baumler,W., Knuchel,R., Zirngibl,H., Scholmerich,J., and Holstege,A. (1997). Enhanced effectiveness of photodynamic therapy with laser light fractionation in patients with esophageal cancer. *Endoscopy* 29, 275-280.
- Mimeault,M., Pommery,N., and Henichart,J.P. (2003). Synergistic antiproliferative and apoptotic effects induced by epidermal growth factor receptor and protein kinase a inhibitors in human prostatic cancer cell lines. *Int. J Cancer* 106, 116-124.
- Mitra,S., Goren,E.M., Frelinger,J.G., and Foster,T.H. (2003). Activation of heat shock protein 70 promoter with meso-tetrahydroxyphenyl chlorin photodynamic therapy reported by green fluorescent protein in vitro and in vivo. *Photochem. Photobiol.* 78, 615-622.
- Mizejewski,G.J. (1999). Role of integrins in cancer: survey of expression patterns. *Proc. Soc. Exp. Biol. Med.* 222, 124-138.
- Moan,J. (1986). Effect of bleaching of porphyrin sensitizers during photodynamic therapy. *Cancer Lett.* 33, 45-53.
- Moan,J. and Berg,K. (1991). The photodegradation of porphyrins in cells can be used to estimate the lifetime of singlet oxygen. *Photochem. Photobiol.* 53, 549-553.
- Moan,J., Berg,K., Bommer,J.C., and Western,A. (1992). Action spectra of phthalocyanines with respect to photosensitization of cells. *Photochem. Photobiol.* 56, 171-175.
- Modjtahedi,H., Affleck,K., Stubberfield,C., and Dean,C. (1998). EGFR blockade by tyrosine kinase inhibitor or monoclonal antibody inhibits growth, directs terminal differentiation and induces apoptosis in the human squamous cell carcinoma HN5. *Int. J Oncol.* 13, 335-342.
- Mourant,J.R., Canpolat,M., Brocker,C., Esponda-Ramos,O., Johnson,T.M., Matanock,A., Stetter,K., and Freyer,J.P. (2000). Light scattering from cells: the contribution of the nucleus and the effects of proliferative status. *J Biomed. Opt.* 5, 131-137.
- Mourant,J.R., Hielscher,A.H., Eick,A.A., Johnson,T.M., and Freyer,J.P. (1998). Evidence of intrinsic differences in the light scattering properties of tumorigenic and nontumorigenic cells. *Cancer* 84, 366-374.
- Mourant,J.R., Johnson,T.M., Los,G., and Bigio,I.J. (1999). Non-invasive measurement of chemotherapy drug concentrations in tissue: preliminary demonstrations of in vivo measurements. *Phys. Med. Biol.* 44, 1397-1417.
- Muller,M.G., Valdez,T.A., Georgakoudi,I., Backman,V., Fuentes,C., Kabani,S., Laver,N., Wang,Z., Boone,C.W., Dasari,R.R., Shapshay,S.M., and Feld,M.S. (2003). Spectroscopic detection and evaluation of morphologic and biochemical changes in early human oral carcinoma. *Cancer* 97, 1681-1692.
- Myoung,H., Kim,M.J., Hong,S.D., Lee,J.I., Lim,C.Y., and Hong,S.P. (2002). Expression of membrane type I-matrix metalloproteinase in oral squamous cell carcinoma. *Cancer Lett.* 185, 201-209.

- Niedre, M.J., Secord, A.J., Patterson, M.S., and Wilson, B.C. (2003). In vitro tests of the validity of singlet oxygen luminescence measurements as a dose metric in photodynamic therapy. *Cancer Res.* 63, 7986-7994.
- Nonaka, M., Ikeda, H., and Inokuchi, T. (2002). Effect of combined photodynamic and chemotherapeutic treatment on lymphoma cells in vitro. *Cancer Lett.* 184, 171-178.
- Nordstrom, R.J., Burke, L., Niloff, J.M., and Myrtle, J.F. (2001). Identification of cervical intraepithelial neoplasia (CIN) using UV-excited fluorescence and diffuse-reflectance tissue spectroscopy. *Lasers Surg. Med.* 29, 118-127.
- Novo, M., Huttmann, G., and Diddens, H. (1996). Chemical instability of 5-aminolevulinic acid used in the fluorescence diagnosis of bladder tumours. *J. Photochem. Photobiol. B* 34, 143-148.
- Nozaki, S., Endo, Y., Nakahara, H., Yoshizawa, K., Hashiba, Y., Kawashiri, S., Tanaka, A., Nakagawa, K., Matsuoka, Y., Kogo, M., and Yamamoto, E. (2005). Inhibition of invasion and metastasis in oral cancer by targeting urokinase-type plasminogen activator receptor. *Oral Oncol.* 41, 971-977.
- Nyberg, P., Moilanen, M., Paju, A., Sarin, A., Stenman, U.H., Sorsa, T., and Salo, T. (2002). MMP-9 activation by tumor trypsin-2 enhances in vivo invasion of human tongue carcinoma cells. *J. Dent. Res.* 81, 831-835.
- O'Toole, E.A. (2001). Extracellular matrix and keratinocyte migration. *Clin. Exp. Dermatol.* 26, 525-530.
- Oleinick, N.L., Morris, R.L., and Belichenko, I. (2002). The role of apoptosis in response to photodynamic therapy: what, where, why, and how. *Photochem. Photobiol. Sci.* 1, 1-21.
- Onizawa, K., Okamura, N., Saginoya, H., and Yoshida, H. (2003). Characterization of autofluorescence in oral squamous cell carcinoma. *Oral Oncol.* 39, 150-156.
- Onizawa, K., Saginoya, H., Furuya, Y., and Yoshida, H. (1996). Fluorescence photography as a diagnostic method for oral cancer. *Cancer Lett.* 108, 61-66.
- Onizawa, K., Saginoya, H., Furuya, Y., Yoshida, H., and Fukuda, H. (1999). Usefulness of fluorescence photography for diagnosis of oral cancer. *Int. J. Oral Maxillofac. Surg.* 28, 206-210.
- Osiecka, B.J., Ziolkowski, P., Gamian, E., Lis-Nawara, A., White, S.G., and Bonnett, R. (2003). Determination of vascular-endothelial growth factor levels in serum from tumor-bearing BALB/c mice treated with photodynamic therapy. *Med. Sci. Monit.* 9, BR110-BR114.
- Pacheco, M.M., Kowalski, L.P., Nishimoto, I.N., and Brentani, M.M. (2002). Differential expression of c-jun and c-fos mRNAs in squamous cell carcinoma of the head and neck: associations with uPA, gelatinase B, and matrilysin mRNAs. *Head Neck* 24, 24-32.

- Pankov,R. and Yamada,K.M. (2002). Fibronectin at a glance. *J. Cell Sci.* *115*, 3861-3863.
- Payoux,P., Dekeister,C., Lopez,R., Lauwers,F., Esquerre,J.P., and Paoli,J.R. (2005). Effectiveness of lymphoscintigraphic sentinel node detection for cervical staging of patients with squamous cell carcinoma of the head and neck. *J. Oral Maxillofac. Surg.* *63*, 1091-1095.
- Pe,M.B., Ikeda,H., and Inokuchi,T. (1994). Tumour destruction and proliferation kinetics following periodic, low power light, haematoporphyrin oligomers mediated photodynamic therapy in the mouse tongue. *Eur. J. Cancer B Oral Oncol.* *30B*, 174-178.
- Pei,X.F., Gorman,P.A., and Watt,F.M. (1991). Two strains of human keratinocytes transfected with HPV16 DNA: comparison with the normal parental cells. *Carcinogenesis* *12*, 277-284.
- Peng,Q., Warloe,T., Berg,K., Moan,J., Kongshaug,M., Giercksky,K.E., and Nesland,J.M. (1997). 5-Aminolevulinic acid-based photodynamic therapy. Clinical research and future challenges. *Cancer* *79*, 2282-2308.
- Pereira,D.B., Carvalho,A.P., and Duarte,C.B. (2003). Genistein inhibits Ca²⁺ influx and glutamate release from hippocampal synaptosomes: putative non-specific effects. *Neurochem. Int.* *42*, 179-188.
- Perelman,L.T., Winn,J., Wu,J., Dasari,R.R., and Feld,M.S. (1997). Photon migration of near-diffusive photons in turbid media: a Lagrangian-based approach. *J Opt. Soc. Am. A Opt. Image Sci. Vis.* *14*, 224-229.
- Perrotte,P., Matsumoto,T., Inoue,K., Kuniyasu,H., Eve,B.Y., Hicklin,D.J., Radinsky,R., and Dinney,C.P. (1999). Anti-epidermal growth factor receptor antibody C225 inhibits angiogenesis in human transitional cell carcinoma growing orthotopically in nude mice. *Clin. Cancer Res.* *5*, 257-265.
- Pilcher,B.K., Dumin,J.A., Sudbeck,B.D., Krane,S.M., Welgus,H.G., and Parks,W.C. (1997). The activity of collagenase-1 is required for keratinocyte migration on a type I collagen matrix. *J. Cell Biol.* *137*, 1445-1457.
- Plaetzer,K., Kiesslich,T., Oberdanner,C.B., and Krammer,B. (2005). Apoptosis following photodynamic tumor therapy: induction, mechanisms and detection. *Curr. Pharm. Des* *11*, 1151-1165.
- Pogue,B.W., O'Hara,J.A., Goodwin,I.A., Wilmot,C.J., Fournier,G.P., Akay,A.R., and Swartz,H. (2002). Tumor PO(2) changes during photodynamic therapy depend upon photosensitizer type and time after injection. *Comp Biochem. Physiol A Mol. Integr. Physiol* *132*, 177-184.
- Pottier,R. (1990). In vitro and in vivo fluorescence monitoring of photosensitizers. *J. Photochem. Photobiol. B* *6*, 103-109.

- Prenzel,N., Zwick,E., Daub,H., Leserer,M., Abraham,R., Wallasch,C., and Ullrich,A. (1999). EGF receptor transactivation by G-protein-coupled receptors requires metalloproteinase cleavage of proHB-EGF. *Nature* 402, 884-888.
- Prime,S.S., Nixon,S.V., Crane,I.J., Stone,A., Matthews,J.B., Maitland,N.J., Remnant,L., Powell,S.K., Game,S.M., and Scully,C. (1990). The behaviour of human oral squamous cell carcinoma in cell culture. *J Pathol.* 160, 259-269.
- Raben,D., Helfrich,B., Chan,D.C., Ciardiello,F., Zhao,L., Franklin,W., Baron,A.E., Zeng,C., Johnson,T.K., and Bunn,P.A., Jr. (2005). The effects of cetuximab alone and in combination with radiation and/or chemotherapy in lung cancer. *Clin. Cancer Res.* 11, 795-805.
- Ramos,D.M., But,M., Regezi,J., Schmidt,B.L., Atakilit,A., Dang,D., Ellis,D., Jordan,R., and Li,X. (2002). Expression of integrin beta 6 enhances invasive behavior in oral squamous cell carcinoma. *Matrix Biol.* 21, 297-307.
- Ramos,M.C., Steinbrenner,H., Stuhlmann,D., Sies,H., and Brenneisen,P. (2004). Induction of MMP-10 and MMP-1 in a squamous cell carcinoma cell line by ultraviolet radiation. *Biol. Chem.* 385, 75-86.
- Reddi,E. (1997). Role of delivery vehicles for photosensitizers in the photodynamic therapy of tumours. *J. Photochem. Photobiol. B* 37, 189-195.
- Regezi,J.A., Ramos,D.M., Pytela,R., Dekker,N.P., and Jordan,R.C. (2002). Tenascin and beta 6 integrin are overexpressed in floor of mouth in situ carcinomas and invasive squamous cell carcinomas. *Oral Oncol.* 38, 332-336.
- Reinhold,H.S. and Endrich,B. (1986). Tumour microcirculation as a target for hyperthermia. *Int. J. Hyperthermia* 2, 111-137.
- Rhodes,L.E. and Diffey,B.L. (1997). Fluorescence spectroscopy: a rapid, noninvasive method for measurement of skin surface thickness of topical agents. *Br. J Dermatol.* 136, 12-17.
- Rhodes,L.E., Tsoukas,M.M., Anderson,R.R., and Kollias,N. (1997). Iontophoretic delivery of ALA provides a quantitative model for ALA pharmacokinetics and PpIX phototoxicity in human skin. *J Invest Dermatol.* 108, 87-91.
- Richards-Kortum,R. and Sevick-Muraca,E. (1996). Quantitative optical spectroscopy for tissue diagnosis. *Annu. Rev. Phys. Chem.* 47, 555-606.
- Rittenhouse-Diakun,K., Van,L.H., Morgan,J., Hryhorenko,E., Paszkiewicz,G., Whitaker,J.E., and Oseroff,A.R. (1995). The role of transferrin receptor (CD71) in photodynamic therapy of activated and malignant lymphocytes using the heme precursor delta-aminolevulinic acid (ALA). *Photochem. Photobiol.* 61, 523-528.
- Robbins,K.T., Doweck,I., Samant,S., and Vieira,F. (2005). Effectiveness of superselective and selective neck dissection for advanced nodal metastases after chemoradiation. *Arch. Otolaryngol. Head Neck Surg.* 131, 965-969.

- Robinson,C.M., Stone,A.M., Shields,J.D., Huntley,S., Paterson,I.C., and Prime,S.S. (2003). Functional significance of MMP-2 and MMP-9 expression by human malignant oral keratinocyte cell lines. *Arch. Oral Biol.* 48, 779-786.
- Robinson,D.J., de Bruijn,H.S., van,d., V, Stringer,M.R., Brown,S.B., and Star,W.M. (1998). Fluorescence photobleaching of ALA-induced protoporphyrin IX during photodynamic therapy of normal hairless mouse skin: the effect of light dose and irradiance and the resulting biological effect. *Photochem. Photobiol.* 67, 140-149.
- Rousset,N., Vonarx,V., Eleouet,S., Carre,J., Kerninon,E., Lajat,Y., and Patrice,T. (1999). Effects of photodynamic therapy on adhesion molecules and metastasis. *J. Photochem. Photobiol. B* 52, 65-73.
- Rundhaug,J.E. (2005). Matrix metalloproteinases and angiogenesis. *J Cell Mol. Med.* 9, 267-285.
- Runnels,J.M., Chen,N., Ortel,B., Kato,D., and Hasan,T. (1999). BPD-MA-mediated photosensitization in vitro and in vivo: cellular adhesion and beta1 integrin expression in ovarian cancer cells. *Br. J Cancer* 80, 946-953.
- Salomon,D.S., Brandt,R., Ciardiello,F., and Normanno,N. (1995). Epidermal growth factor-related peptides and their receptors in human malignancies. *Crit Rev. Oncol. Hematol.* 19, 183-232.
- Sauter,E.R., Nesbit,M., Watson,J.C., Klein-Szanto,A., Litwin,S., and Herlyn,M. (1999). Vascular endothelial growth factor is a marker of tumor invasion and metastasis in squamous cell carcinomas of the head and neck. *Clin. Cancer Res.* 5, 775-782.
- Scott,M.A., Hopper,C., Sahota,M., cllroy,B.W., Bown,S.G., and MacRobert,A.J. (2000). Fluorescence Photodiagnostics and Photobleaching Studies of Cancerous Lesions using Ratio Imaging and Spectroscopic Techniques. *Lasers Med Sci* 15, 63-72.
- Sharman,W.M., van Lier,J.E., and Allen,C.M. (2004). Targeted photodynamic therapy via receptor mediated delivery systems. *Adv. Drug Deliv. Rev.* 56, 53-76.
- Shintani,S., Li,C., Mihara,M., Yano,J., Terakado,N., Nakashiro,K., and Hamakawa,H. (2004). Gefitinib ('Iressa', ZD1839), an epidermal growth factor receptor tyrosine kinase inhibitor, up-regulates p27KIP1 and induces G1 arrest in oral squamous cell carcinoma cell lines. *Oral Oncol.* 40, 43-51.
- Smith,E.M., Ritchie,J.M., Summersgill,K.F., Hoffman,H.T., Wang,D.H., Haugen,T.H., and Turek,L.P. (2004). Human papillomavirus in oral exfoliated cells and risk of head and neck cancer. *J. Natl. Cancer Inst.* 96, 449-455.
- Sokolov,K., Follen,M., and Richards-Kortum,R. (2002). Optical spectroscopy for detection of neoplasia. *Curr. Opin. Chem. Biol.* 6, 651-658.
- Spikes,J.D. (1992). Quantum yields and kinetics of the photobleaching of hematoporphyrin, Photofrin II, tetra(4-sulfonatophenyl)-porphine and uroporphyrin. *Photochem. Photobiol.* 55, 797-808.

- Stone,N., Stavroulaki,P., Kendall,C., Birchall,M., and Barr,H. (2000). Raman spectroscopy for early detection of laryngeal malignancy: preliminary results. *Laryngoscope* 110, 1756-1763.
- Suhr,M.A., Hopper,C., MacRobert,A.J., Speight,P.M., Kubler,A.C., and Kunz,L. (2001). [Clinical pilot study of interstitial photodynamic therapy for treatment of advanced head and neck tumors]. *Mund Kiefer Gesichtschir.* 5, 277-282.
- Sundelin,K., Roberg,K., Grenman,R., and Hakansson,L. (2005). Effects of cytokines on matrix metalloproteinase expression in oral squamous cell carcinoma in vitro. *Acta Otolaryngol.* 125, 765-773.
- Svanberg,K., Andersson,T., Killander,D., Wang,I., Stenram,U., andersson-Engels,S., Berg,R., Johansson,J., and Svanberg,S. (1994). Photodynamic therapy of non-melanoma malignant tumours of the skin using topical delta-amino levulinic acid sensitization and laser irradiation. *Br. J Dermatol.* 130, 743-751.
- Taber,S.W., Fingar,V.H., Coots,C.T., and Wieman,T.J. (1998). Photodynamic therapy using mono-L-aspartyl chlorin e6 (Npe6) for the treatment of cutaneous disease: a Phase I clinical study. *Clin. Cancer Res.* 4, 2741-2746.
- Teiten,M.H., Bezdetnaya,L., Merlin,J.L., Bour-Dill,C., Pauly,M.E., Dicato,M., and Guillemin,F. (2001). Effect of meta-tetra(hydroxyphenyl)chlorin (mTHPC)-mediated photodynamic therapy on sensitive and multidrug-resistant human breast cancer cells. *J Photochem. Photobiol. B* 62, 146-152.
- Teiten,M.H., Marchal,S., D'Hallewin,M.A., Guillemin,F., and Bezdetnaya,L. (2003). Primary photodamage sites and mitochondrial events after Foscan photosensitization of MCF-7 human breast cancer cells. *Photochem. Photobiol.* 78, 9-14.
- Thomas,G.J., Jones,J., and Speight,P.M. (1997). Integrins and oral cancer. *Oral Oncol.* 33, 381-388.
- Thomas,G.J., Lewis,M.P., Whawell,S.A., Russell,A., Sheppard,D., Hart,I.R., Speight,P.M., and Marshall,J.F. (2001a). Expression of the alphavbeta6 integrin promotes migration and invasion in squamous carcinoma cells. *J Invest Dermatol.* 117, 67-73.
- Thomas,G.J., Poomsawat,S., Lewis,M.P., Hart,I.R., Speight,P.M., and Marshall,J.F. (2001b). alpha v beta 6 Integrin upregulates matrix metalloproteinase 9 and promotes migration of normal oral keratinocytes. *J Invest Dermatol.* 116, 898-904.
- Togashi,H., Uehara,M., Ikeda,H., and Inokuchi,T. (2006b). Fractionated photodynamic therapy for a human oral squamous cell carcinoma xenograft. *Oral Oncol.*
- Togashi,H., Uehara,M., Ikeda,H., and Inokuchi,T. (2006a). Fractionated photodynamic therapy for a human oral squamous cell carcinoma xenograft. *Oral Oncol.*
- Tomaselli,F., Maier,A., Sankin,O., Anegg,U., Stranzl,U., Pinter,H., Kapp,K., and Smolle-Juttner,F.M. (2001). Acute effects of combined photodynamic therapy and

hyperbaric oxygenation in lung cancer--a clinical pilot study. *Lasers Surg. Med.* 28, 399-403.

Triesscheijn,M., Ruevekamp,M., Aalders,M., Baas,P., and Stewart,F.A. (2005). Outcome of mTHPC Mediated Photodynamic Therapy is Primarily Determined by the Vascular Response. *Photochem. Photobiol.*

Uehara,M., Inokuchi,T., Sano,K., and ZuoLin,W. (2001). Expression of vascular endothelial growth factor in mouse tumours subjected to photodynamic therapy. *Eur. J Cancer* 37, 2111-2115.

Uehara,M., Sano,K., Ikeda,H., Sekine,J., Irie,A., Yokota,T., Tobita,T., Ohba,S., and Inokuchi,T. (2004). Expression of vascular endothelial growth factor and prognosis of oral squamous cell carcinoma. *Oral Oncol.* 40, 321-325.

Uzdensky,A.B., Juzeniene,A., Kolpakova,E., Hjortland,G.O., Juzenas,P., and Moan,J. (2004). Photosensitization with protoporphyrin IX inhibits attachment of cancer cells to a substratum. *Biochem. Biophys. Res. Commun.* 322, 452-457.

Van Veen,R.L., Aalders,M.C., Pasma,K.L., Siersema,P.D., Haringsma,J., Van,D., V, Gabeler,E.E., Robinson,D.J., and Sterenborg,H.J. (2002). In situ light dosimetry during photodynamic therapy of Barrett's esophagus with 5-aminolevulinic acid. *Lasers Surg. Med.* 31, 299-304.

Venables, W. N. and Ripley, B. D. **Modern applied statistics.** 4th Edition.Springer.ISBN 0-387-95457-0. 2002.
Ref Type: Journal (Full)

Veronese,M.L., Sun,W., Giantonio,B., Berlin,J., Shults,J., Davis,L., Haller,D.G., and O'Dwyer,P.J. (2005). A phase II trial of gefitinib with 5-fluorouracil, leucovorin, and irinotecan in patients with colorectal cancer. *Br. J Cancer* 92, 1846-1849.

Vokes,E.E., Ki Hong,W., Lippman,S.M., and Weichselbaum,R.R. (1993). Head and neck cancer. *N Engl J Med* 328, 184-194.

Vollmers,H.P., Imhof,B.A., Braun,S., Waller,C.A., Schirmacher,V., and Birchmeier,W. (1984). Monoclonal antibodies which prevent experimental lung metastases. Interference with the adhesion of tumour cells to laminin. *FEBS Lett.* 172, 17-20.

Vonarx,V., Foultier,M.T., Xavier de,B.L., Anasagasti,L., Morlet,L., and Patrice,T. (1995). Photodynamic therapy decreases cancer colonic cell adhesiveness and metastatic potential. *Res. Exp. Med. (Berl)* 195, 101-116.

Wallace,M.B., Perelman,L.T., Backman,V., Crawford,J.M., Fitzmaurice,M., Seiler,M., Badizadegan,K., Shields,S.J., Itzkan,I., Dasari,R.R., Van,D.J., and Feld,M.S. (2000). Endoscopic detection of dysplasia in patients with Barrett's esophagus using light-scattering spectroscopy. *Gastroenterology* 119, 677-682.

Werner,J.A., Rathcke,I.O., and Mandic,R. (2002). The role of matrix metalloproteinases in squamous cell carcinomas of the head and neck. *Clin. Exp. Metastasis* 19, 275-282.

- West,C.M. and Moore,J.V. (1992). Mechanisms behind the resistance of spheroids to photodynamic treatment: a flow cytometry study. *Photochem. Photobiol.* 55, 425-430.
- Wilson,B.C., Olivo,M., and Singh,G. (1997). Subcellular localization of Photofrin and aminolevulinic acid and photodynamic cross-resistance in vitro in radiation-induced fibrosarcoma cells sensitive or resistant to photofrin-mediated photodynamic therapy. *Photochem. Photobiol.* 65, 166-176.
- Xue,H., Atakilit,A., Zhu,W., Li,X., Ramos,D.M., and Pytela,R. (2001). Role of the $\alpha(v)\beta6$ integrin in human oral squamous cell carcinoma growth in vivo and in vitro. *Biochem. Biophys. Res. Commun.* 288, 610-618.
- Xue,L.Y., He,J., and Oleinick,N.L. (1997). Rapid tyrosine phosphorylation of HS1 in the response of mouse lymphoma L5178Y-R cells to photodynamic treatment sensitized by the phthalocyanine Pc 4. *Photochem. Photobiol.* 66, 105-113.
- Yang,Z., Bagheri-Yarmand,R., Wang,R.A., Adam,L., Papadimitrakopoulou,V.V., Clayman,G.L., El-Naggar,A., Lotan,R., Barnes,C.J., Hong,W.K., and Kumar,R. (2004). The epidermal growth factor receptor tyrosine kinase inhibitor ZD1839 (Iressa) suppresses c-Src and Pak1 pathways and invasiveness of human cancer cells. *Clin. Cancer Res.* 10, 658-667.
- Yarden,Y. (2001). The EGFR family and its ligands in human cancer. signalling mechanisms and therapeutic opportunities. *Eur. J. Cancer* 37 *Suppl* 4, S3-S8.
- Yasuda,T., Sakata,Y., Kitamura,K., Morita,M., and Ishida,T. (1997). Localization of plasminogen activators and their inhibitor in squamous cell carcinomas of the head and neck. *Head Neck* 19, 611-616.
- Ylipalosaari,M., Thomas,G.J., Nystrom,M., Salhimi,S., Marshall,J.F., Huotari,V., Tervahartiala,T., Sorsa,T., and Salo,T. (2005). $\alpha v\beta 6$ integrin down-regulates the MMP-13 expression in oral squamous cell carcinoma cells. *Exp. Cell Res.* 309, 273-283.
- Yoshizaki,T., Maruyama,Y., Sato,H., and Furukawa,M. (2001). Expression of tissue inhibitor of matrix metalloproteinase-2 correlates with activation of matrix metalloproteinase-2 and predicts poor prognosis in tongue squamous cell carcinoma. *Int. J. Cancer* 95, 44-50.
- Yow,C.M., Chen,J.Y., Mak,N.K., Cheung,N.H., and Leung,A.W. (2000). Cellular uptake, subcellular localization and photodamaging effect of temoporfin (mTHPC) in nasopharyngeal carcinoma cells: comparison with hematoporphyrin derivative. *Cancer Lett.* 157, 123-131.
- Zaak,D., Frimberger,D., Stepp,H., Wagner,S., Baumgartner,R., Schneede,P., Siebels,M., Knuchel,R., Kriegmair,M., and Hofstetter,A. (2001). Quantification of 5-aminolevulinic acid induced fluorescence improves the specificity of bladder cancer detection. *J. Urol.* 166, 1665-1668.

- Zavras,A.I., Douglass,C.W., Joshipura,K., Wu,T., Laskaris,G., Petridou,E., Dokianakis,G., Segas,J., Lefantzis,D., Nomikos,P., Wang,Y.F., and Diehl,S.R. (2001). Smoking and alcohol in the etiology of oral cancer: gender-specific risk profiles in the south of Greece. *Oral Oncol.* 37, 28-35.
- Zemzoum,I., Kates,R.E., Ross,J.S., Dettmar,P., Dutta,M., Henrichs,C., Yurdseven,S., Hofler,H., Kiechle,M., Schmitt,M., and Harbeck,N. (2003). Invasion factors uPA/PAI-1 and HER2 status provide independent and complementary information on patient outcome in node-negative breast cancer. *J. Clin. Oncol.* 21, 1022-1028.
- Zheng,W., Soo,K.C., Sivanandan,R., and Olivo,M. (2002b). Detection of neoplasms in the oral cavity by digitized endoscopic imaging of 5-aminolevulinic acid-induced protoporphyrin IX fluorescence. *Int. J. Oncol.* 21, 763-768.
- Zheng,W., Soo,K.C., Sivanandan,R., and Olivo,M. (2002a). Detection of squamous cell carcinomas and pre-cancerous lesions in the oral cavity by quantification of 5-aminolevulinic acid induced fluorescence endoscopic images. *Lasers Surg. Med.* 31, 151-157.
- Zhu,B.D., Yuan,S.J., Zhao,Q.C., Li,X., Li,Y., and Lu,Q.Y. (2005). Antitumor effect of Gefitinib, an epidermal growth factor receptor tyrosine kinase inhibitor, combined with cytotoxic agent on murine hepatocellular carcinoma. *World J Gastroenterol.* 11, 1382-1386.

List of Publications

Published Papers

I. Assessment of Oral Premalignancy Using Elastic Scattering Spectroscopy

Sharwani A, Jerjes W, Salih V., Swinson B, Bigio IJ, Hopper C.
Oral Oncology (2006) 42,343-349

II. Fluorescence Spectroscopy Combined with 5-Aminolevulinic acid Induced Protoporphyrin IX fluorescence in Detecting Oral Premalignancy

Sharwani A, Jerjes W, Salih V., MacRobert AJ, El-Maaytah M, Hopper C
Journal of Photochemistry and Photobiology: B. Biology 83(2006) 27-33

Papers currently submitted for publication

Photodynamic Therapy Down-regulated the Invasion Promoting Factors in Human oral Cancer

Sharwani A, Lewis M, Swinson B, Bigio IJ, Hopper C, Salih V
Archives of Oral Biology. *In press*

Published abstracts

I. cellular uptake and toxicity of meta-tetrahydroxyphenyl chlorin (m-THPC; Foscan) mediated photodynamic therapy on oral carcinoma cells.

Sharwani A., Salih V, Hopper C.
British Medical Laser Association, Annual Autumn Meeting. The UCL Eastman Dental Institute for Oral Health Care Sciences, London (9-10 September 2004)

II. Effects of meta-tetrahydroxyphenyl chlorin (m-THPC; Foscan) mediated PDT on invasion and metastasis of head and neck carcinomas

Sharwani A., Salih V., Hopper C.
10th World Congress of the International Photodynamic Association, Munich, Germany, 22-25 June 2005.

III. Fluorescence spectroscopy combined with 5-aminolevulinic acid induced protoporphyrin IX fluorescence in detecting oral premalignancy

Sharwani A, Jerjes W, Salih V, Hopper C
Lasers in Medical Science, volume 20: S12 (2005).

IV. Assessment of oral premalignancy using elastic scattering spectroscopy

Sharwani A, Jerjes W, Salih V, Hopper C
Lasers in Medical Science, volume 20: S34 (2005).

V. Monitoring of photobleaching in photodynamic therapy using fluorescence spectroscopy: assessment of the clinical outcome

Sharwani A, Jerjes W, Salih V, Hopper C

Lasers in Medical Science, volume 20: S38 (2005).

Poster presentation

I. Effects of meta-tetrahydroxyphenyl chlorin (m-THPC; Foscan) on head and neck carcinomas.

Sharwani A., Hopper C., Olsen I.

British Society for Dental Research, Annual Scientific Meeting, 6-8 April 2004, Birmingham, UK

II Monitoring of photobleaching in photodynamic therapy using fluorescence spectroscopy

Sharwani A, Jerjes W, Salih V, Hopper C

20th International Congress Laser Medicine, International Academy Laser Medicine and Surgery, 12th Nov 2005, Florence, Italy

Oral presentations

I. Photodynamic effects of meta-tetrahydroxyphenyl chlorin (m-THPC; Foscan) on invasion and metastasis of head and neck carcinomas

10th World Congress International Photodynamic Association, 22-25th June 2005, Munich, Germany.

II. Fluorescence spectroscopy combined with 5-aminolevulinic acid induced protoporphyrin IX fluorescence in detecting oral premalignancy

20th International Congress Laser Medicine, International Academy Laser Medicine and Surgery, 10th November 2005, Florence, Italy

III. Assessment of oral premalignancy using elastic scattering spectroscopy

20th International Congress Laser Medicine, International Academy Laser Medicine and Surgery, 12th November 2005, Florence, Italy

Oral Oncology (2006) 42, 343–349



ORAL
ONCOLOGY

<http://intl.elsevierhealth.com/journals/oron/>

Assessment of oral premalignancy using elastic scattering spectroscopy

A. Sharwani ^a, W. Jerjes ^a, V. Salih ^b, B. Swinson ^a, I.J. Bigio ^c,
M. El-Maaytah ^a, C. Hopper ^{a,d,e}



Available online at www.sciencedirect.com

SCIENCE @ DIRECT®

Journal of Photochemistry and Photobiology B: Biology 83 (2006) 27–33

Journal of
Photochemistry
and
Photobiology
B: Biology

www.elsevier.com/locate/jphotobiol

Fluorescence spectroscopy combined with 5-aminolevulinic acid-induced protoporphyrin IX fluorescence in detecting oral premalignancy

A. Sharwani ^a, W. Jerjes ^{a,1}, V. Salih ^b, A.J. MacRobert ^c, M. El-Maaytah ^a,
H.S.M. Khalil ^d, C. Hopper ^{a,c,*}



